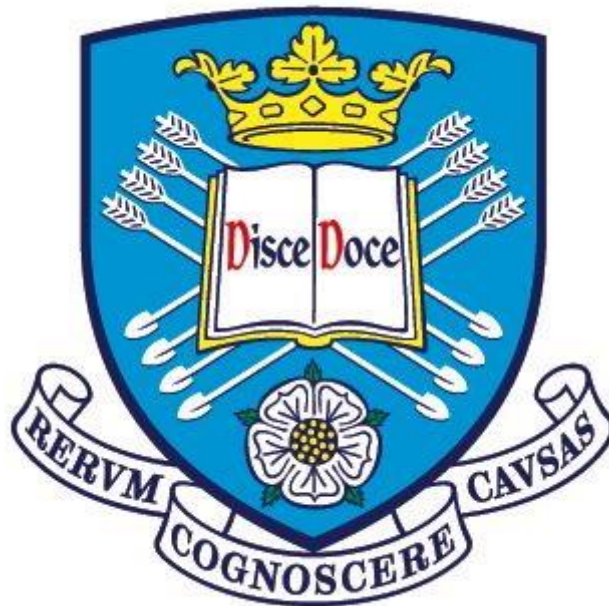


**The University of Sheffield**



**Direct Torque Control of Dual Three-phase  
Permanent Magnet Synchronous Machine Drives**

**Yuan Ren**

**A thesis submitted for the degree of Doctor of Philosophy**

Department of Electronic and Electrical Engineering

The University of Sheffield

Mapping Street, Sheffield, S1 3JD, UK

**February 2016**

## ABSTRACT

This thesis focuses on the direct torque control (DTC) of single and dual three-phase permanent magnet synchronous machine (PMSM) drives, with particular reference to the reduction of steady-state errors, torque ripple, and current harmonics in switching-table-based DTC (ST-DTC).

Due to its simple structure, excellent transient response and robustness against rotor parameters, DTC has become a powerful control scheme for AC motor drives. However, PMSM drives using ST-DTC usually suffer from steady-state error and ripple of torque. Based on the analysis of the instantaneous variation rates of stator flux and torque of each converter output voltage vector, the steady-state error of torque can be minimized by properly shifting the bands of the torque hysteresis regulator. The existing methods of torque ripple reduction can be regarded as optimization methods with different duty ratios of the active vectors, which are usually complicated and parameter dependent. Since the machine speed is the dominant factor determining the instantaneous torque variation rate, a simple and effective method can be developed to obtain the duty ratio by considering the effect of machine angular velocity. This method is parameter independent and easy to implement.

Dual three-phase drive systems have been widely investigated. Besides the aforementioned two problems associated with ST-DTC of a single three-phase system, i.e. steady-state error and ripple of torque, harmonic currents inevitably occur, which can be regarded as a third problem. The harmonic currents lead to increased losses. Using the vector space decomposition technique (VSD), the dual three-phase drive system consists of two subspaces. One of the subspaces is related to torque production; the other is responsible for the harmonic currents. Therefore, the harmonic currents can be reduced if the flux in the additional subspace is minimized; this can be achieved by optimizing the switching table or replacing the conventional vectors with synthetic vectors. Synthetic vectors are the concept inspired by space vector pulse width modulation (SVPWM) for dual three-phase machine drives. Synthetic vectors can minimize the voltage components in the additional subspace within one control period.

To ameliorate the three problems, two types of synthetic vectors are introduced which can reduce the harmonic currents effectively when used, together with the most suitable switching sequences. The two types of synthetic vectors have a substantially different influence on the variation rate of

torque. Therefore both are used simultaneously to improve the torque performance. A modified five-level torque regulator is proposed to improve the torque performance. With the proposed method harmonic currents have been greatly reduced, the steady-state error and the ripple of torque can be considerably reduced, while preserving the simple structure and excellent dynamic performance.

The modified ST-DTC strategies are suitable for most applications for their desirable torque and current performance. However, for some applications, a constant switching frequency is required. Therefore, PWM-DTC are also discussed in this thesis. The steady-state torque and current performance can be further improved by use of PWM techniques specific to three-phase machines. PWM-DTC often increase the computational burden of the control algorithm on the processor and can lead to deterioration of the dynamic performance or machine parameter dependence. For example, dynamic performance is affected strongly when PI regulators are used in the torque control loop. Similarly, the performance are heavily influenced by the machine parameters when a machine-model based reference voltage calculator is used.

## **ACKNOWLEDGEMENTS**

I would like to express my deep gratitude to my supervisor Professor Z.Q. Zhu for his patient guidance, enthusiastic encouragement and constructive suggestions during the whole PhD research process.

I am very grateful to Dr. Zhan-Yuan Wu, Dr. Jiaming Liu and Dr. Kan Liu for their technical assistance on many topics. Discussions with Mr. Ali H Almarhoon, Mr. Peilin Xu, Dr. Yashan Hu, and Mr Hanlin Zhan were also helpful.

Further thanks for the support provided by the technical staff in the Electrical Machines and Drives Group at the University of Sheffield.

Finally, I warmly thank my family for their love and encouragement.

# CONTENT

ABSTRACT.....	I
ACKNOWLEDGEMENTS.....	III
CONTENT.....	IV
NOMENCLATURE.....	IX
ACRONYMS.....	XII
1. General Introduction.....	1
1.1. Introduction.....	1
1.2. Direct Torque Control of the Three-phase PMSM.....	2
1.2.1. SVPWM-based Direct Torque Control.....	6
1.2.2. Duty-ratio-based Direct Torque Control.....	8
1.3. Control of Dual Three-phase PMSM.....	10
1.3.1. Modelling of Dual Three-phase PMSM.....	11
1.3.2. Current Control of Dual Three-phase PMSM.....	13
1.3.3. PWM Techniques of Dual Three-phase PMSM.....	16
1.3.4. Direct Torque Control of Dual Three-phase PMSM.....	20
1.4. Scope of Research and Contributions.....	24
1.4.1. Scope of Research.....	24
1.4.2. Contributions.....	26
2. Experimental Systems.....	29
2.1. Introduction.....	29
2.2. dSPACE Based Control System and Software Environment.....	29
2.2.1. A/D Board DS2004.....	30
2.2.2. Encoder Board DS3001.....	30
2.2.3. Processor Board DS1006.....	31

2.2.4.	PWM Board DS5101 .....	31
2.3.	Test Rigs Employed for Research .....	32
2.3.1.	Test Rig for Machine I .....	32
2.3.2.	Test Rig for Machine II .....	32
2.4.	Conclusions .....	35
3.	Improved Torque Regulator to Reduce Steady-state Error of Torque Response for Direct Torque Control of Permanent Magnet Synchronous Machine Drives .....	36
3.1.	Introduction .....	36
3.2.	Analysis of Steady-state Torque Response Error in PMSM DTC .....	37
3.2.1.	Machine Equations .....	37
3.2.2.	Effect of Inverter Voltage Vectors on Torque and Stator Flux Variations .....	37
3.2.3.	Steady-state Error of Torque Response .....	40
3.3.	New ST-DTC Method Using Proposed Band-shifted Torque Regulator .....	43
3.4.	Experimental Results .....	47
3.4.1.	Steady-state Performance of the New DTC Method Using the Proposed Band-Shifted Torque Regulator .....	48
3.4.2.	Steady-state and Dynamic Performance of Inner Torque Loop Control .....	51
3.4.3.	Dynamic Responses to External Load Disturbance .....	53
3.4.4.	Conclusions .....	53
4.	Direct Torque Control of Permanent Magnet Synchronous Machine Drives with a Simple Duty Ratio Regulator .....	55
4.1.	Introduction .....	55
4.2.	Analysis of Steady-State Performance in PMSM DTC .....	56
4.2.1.	Direct Torque Control Principle .....	56
4.2.2.	Analysis of Torque and Stator Flux Variations .....	58
4.2.3.	Reasons for Deterioration of Steady-state Performance of Torque .....	59

4.3.	New DTC Methods to Improve the Torque Performance.....	60
4.4.	Experimental Results.....	67
4.4.1.	Comparison of Steady Performance of Different ST-DTC Methods .....	67
4.4.2.	Dynamic Performance of Inner Torque Loop Control without Outer Speed Loop	73
4.4.3.	Dynamic and Steady-state Performance with Outer Speed Loop When Machine Operates on Opposite Direction of Rotation.....	74
4.4.4.	Sensitivity of System Performance to Control Parameter Variation .....	75
4.5.	Conclusion.....	76
5.	Modified Switching-table Strategy for Reduction of Current Harmonics in Direct Torque Controlled Dual Three-phase Permanent Magnet Synchronous Machine Drives .....	78
5.1.	Introduction .....	78
5.2.	Machine Model and Analysis of Inverter Voltage Vectors.....	79
5.2.1.	Machine Model .....	79
5.2.2.	Analysis of the Inverter Voltage Vectors.....	80
5.3.	Classical ST-DTC Scheme.....	80
5.4.	Proposed DTC Scheme .....	82
5.5.	Experimental Results.....	87
5.5.1.	Steady-state Performance of Different ST-DTC Strategies.....	87
5.5.2.	Dynamic Performance of Inner Torque Loop Control for Conventional and Proposed DTC	91
5.5.3.	Dynamic Response to External Load Disturbance for Proposed DTC Strategy ....	91
5.6.	Conclusion.....	93
6.	Enhancement of Steady-state Performance in Direct Torque Controlled Dual Three-phase Permanent Magnet Synchronous Machine Drives with Modified Switching Table .....	94
6.1.	Introduction .....	94
6.2.	Proposed ST-DTC Strategy.....	94

6.2.1.	Principle of Proposed ST-DTC Strategy.....	94
6.2.2.	Switching Sequence and Implementation.....	98
6.2.3.	Modification of Torque Regulator to Improve the Steady-state Performance of Torque Response.....	103
6.3.	Experimental Results.....	105
6.3.1.	Steady-state Performance of Different ST-DTC Strategies.....	105
6.3.2.	Dynamic Performance of Speed Response.....	115
6.3.3.	Dynamic Response to External Load Disturbance for the Proposed DTC Strategy	117
6.4.	Conclusion.....	118
7.	Reduction of Harmonic Current and Torque Ripple for Dual Three-phase Permanent Magnet Synchronous Machines Using a Modified Switching-table-based Direct Torque Controller ....	120
7.1.	Introduction .....	120
7.2.	Proposed ST-DTC Strategy of DTP PMSM System .....	121
7.2.1.	Selection of Applied Vectors.....	121
7.2.2.	Switching Sequence and Implementation.....	123
7.2.3.	Design of Torque Regulator to Enhance the Steady-state Performance of Torque Response .....	128
7.2.4.	Compensation of Inverter Non-linearity.....	135
7.3.	Experimental Results.....	135
7.3.1.	Performance of Dead-time Compensator.....	136
7.3.2.	Steady-state Performance of Different ST-DTC Strategies.....	139
7.3.3.	Dynamic performance of Different ST-DTC Strategies.....	147
7.3.4.	Dynamic Response to External Load Disturbance for the Proposed DTC Strategy	148
7.4.	Conclusion.....	149

8. Space-vector PWM Based Direct Torque Control of Dual Three-phase Permanent Magnet Synchronous Machine Drives .....	151
8.1. Introduction .....	151
8.2. Deadbeat DTC Algorithm .....	152
8.2.1. Deadbeat Algorithm.....	152
8.2.2. Specific PWM Technique for Dual Three-phase Drives .....	153
8.3. Experimental Results.....	154
8.3.1. Steady-state Performance of Different ST-DTC Strategies.....	155
8.3.2. Dynamic Performance of Different ST-DTC Strategies.....	165
8.4. Conclusion.....	166
9. General Conclusions and Discussions .....	168
9.1. Switching-table-based Direct Torque Control of Three-phase PMSM.....	168
9.2. Switching-table-based Direct Torque Control of Dual Three-phase PMSM.....	169
9.3. PWM-based Direct Torque Control of Dual Three-phase PMSM.....	170
9.4. Future Work .....	171
References.....	174
APPENDICES .....	184
Appendix A: Specification of Prototype Machines .....	184
Appendix B: The stator flux and torque estimators .....	186
Appendix C: The method to identify parameters of the machines .....	189

## NOMENCLATURE

$d$	Duty ratio of active vectors
$d_+, d_-$	Duty ratio of active vectors when $\varepsilon_T$ is 1 and -1
$D_{bs}$	Band-shifted distance
$e_{sMT}$	Back-EMF vector in synchronous reference frame aligned with stator flux vector
$f_{av}$	Average commutation frequency
$f_s$	Sampling frequency
$G_i$	Voltage vector group
$H_\psi, H_T$	Stator flux and torque hysteresis bands
$i_{a\_THD}$	THD of phase-a current
$I_s$	Phase stator currents
$I_{s\alpha\beta}$	Stator current vector in $\alpha\beta$ reference frame/subspace
$I_{sz1z2}$	Stator current vector in $z_1z_2$ subspace
$I_{so1o2}$	Stator current vector in $o_1o_2$ subspace
$L_s$	$\alpha$ and $\beta$ axis inductance
$L_{ls}$	Stator leakage inductance
$L_m$	Magnetizing inductance in $\alpha\beta$ subspace
$N_{EL}$	The number of encoder lines
$O_{ED}$	The scaled output of the encoder
$P$	Number of pole pairs
$\sigma$	Absolute value of variation of torque
$R_s$	Stator resistance

$T_e$	Electromagnetic torque
$T_{e0}$	Torque value at current instant
$T_{e\_min}, T_{e\_max}$	Minimum and maximum value of torques
$T_s$	Sampling period
$U_{comp}$	Compensation phase voltages
$V_{s\alpha\beta}$	Stator voltage vector in $\alpha\beta$ reference frame/subspace
$V_{sz1z2}$	Stator voltage vector in $z1z2$ subspace
$V_{so1o2}$	Stator voltage vector in $o1o2$ subspace
$\delta$	Angle between stator flux and rotor flux
$\theta_r$	Electrical rotor position
$\theta_{s\alpha\beta}$	Position of stator flux vector in $\alpha\beta$ subspace
$\theta_{sz1z2}$	Position of stator flux vector in $z1z2$ subspace
$\psi_{s\alpha\beta}$	Stator flux vector in $\alpha\beta$ reference frame/ subspace
$\psi_{r\alpha\beta}$	Rotor flux vector in $\alpha\beta$ reference frame/ subspace
$\psi_{sz1z2}$	Stator flux vector in $z1z2$ subspace
$\psi_{so1o2}$	Stator flux vector in $o1o2$ subspace
$\psi_f$	Permanent magnet flux
$\psi_s$	Amplitude of stator flux
$\psi_r$	Amplitude of rotor flux
$\psi_{s\_ripple}, T_{e\_ripple}$	Ripples of stator flux and torque
$\omega_1 (\omega_N)$	Electrical rotor angular velocity (rated value)
$\Delta\psi_s, \Delta T_e$	Steady-state errors of stator flux and torque responses

$\varepsilon_T, \varepsilon_\psi$	Torque and stator flux control signals
$\times$	Cross-product
$\cdot$	Dot-product
*	Reference value

## ACRONYMS

AC	Alternating current
DC	Direct current
DPC	Direct power control
DTC	Direct torque control
FOC	Field oriented control
P-DTC	Predictive direct torque control
PHS	Peripheral high-speed
PI	Proportional-integral
PMSM	Permanent magnet synchronous machine
PWM	Pulse width modulation
ST-DTC	Switching-table-based direct torque control
SVPWM	Space vector pulse width modulation
THD	Total harmonic distortion
VSD	Vector space decomposition
VSI	Voltage-source-inverter

# 1. General Introduction

## 1.1. Introduction

Three-phase electric drives have dominated the industrial drives market for decades. However, for high-power and/or high-current applications such as electric/hybrid vehicles, renewable energy generation, aerospace applications, and ship propulsion, high power and high switching frequency semiconductor devices are usually very expensive or not available [BOJ03]. Recently, multiphase drives have been receiving a great deal of interest, due to their advantages in power segmentation, lower torque pulsation, high reliability at the system level, and lower dc-link voltage requirement [BOJ05], [HAD06], [LEV08a], [ZHA95]. Among the various kinds of multiphase machines, one type of six-phase machine called dual three-phase machine, is one of the most interesting and widely-discussed types. Dual three-phase machine has two sets of three-phase windings spatially shifted by 30 electrical degrees and, hence, sixth harmonic torque pulsation can be inherently suppressed [GOP84].

Nowadays, scalar control methods such as constant volt/hertz (V/f) control is still used for applications like pumps and fans, where high dynamic performance is not a demand. However, for high-performance motion control applications like servo applications, the closed-loop control such as field oriented control (FOC) and direct torque control (DTC) are commonly used for alternating current (AC) machine drives [PER03]. Compared with FOC, DTC is well known for its simple structure, excellent transient response and good robustness against machine parameter variations. However, since the classical switching-table-based DTC (ST-DTC) only employs two hysteresis regulators and one switching table to choose the proper vectors to adjust the torque and stator flux, large steady-state error and ripple of torque always occur in the real-time system.

In a dual three-phase drive system there are harmonic components of current in the stator windings [ZHA95]. These harmonic currents inevitably result in increased losses and should be suppressed. This loss mechanism, the reduction of the steady-state error and ripple of torque are the main challenges facing ST-DTC when used in dual three-phase drives.

This thesis will focus on the reduction of steady-state error and ripple of torque, and the suppression of current harmonics in single and dual three-phase permanent magnet synchronous

machine (PMSM) drives. This chapter will firstly introduce the existing DTC methods for three-phase drives. Secondly, a brief introduction of multiphase machines and their control methods, especially for dual three-phase machines, will be given. Lastly, the main content and contributions of the thesis are presented.

### 1.2. Direct Torque Control of the Three-phase PMSM

Since its introduction by Takahashi [TAK86] and Depenbrock [DEP88] for induction machine drives, DTC has become a powerful control scheme for three-phase AC machine drives, and has also been extended to PMSM drives [CAS04], [GEY09], [LAS04a], [REN14], [XIA14], [XU14], [ZHA11a], [ZHA11c], [ZHA12]. PMSM has several advantages including: high power density, high efficiency, ease of maintenance and excellent control performance. In this thesis, the research is based on PMSM drives. A voltage-source-inverter-fed (VSI-fed) PMSM drive system is shown in Fig. 1.1.

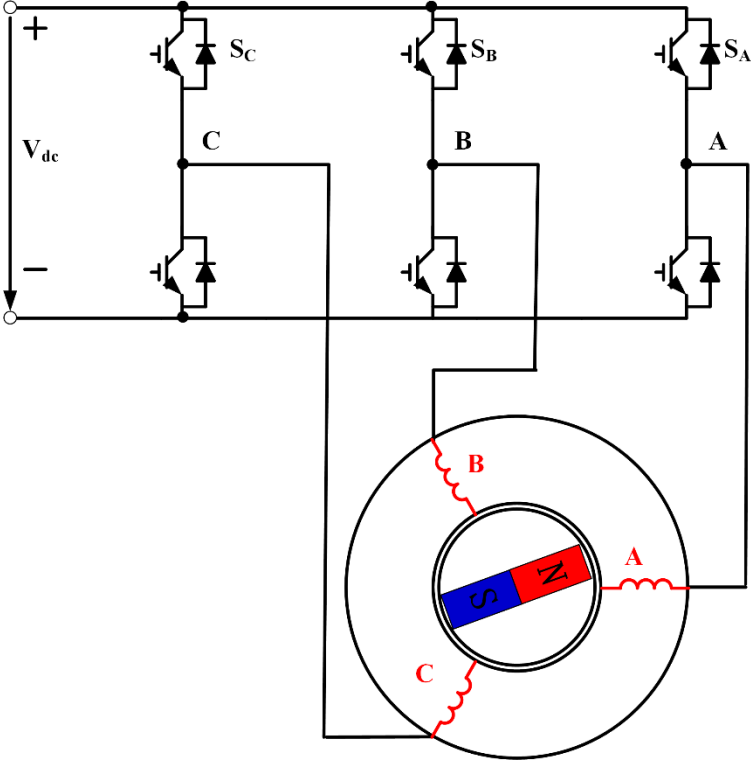


Fig. 1.1. VSI-fed three-phase PMSM.

For the control of AC machines drives, scalar control methods such as V/f control are the simplest methods which are still suitable for the applications where high dynamic performance is not necessary such as pumps and fans applications. In the V/f control, the machine is assumed to be driven by a sinusoidal voltage source of adjustable amplitude and frequency [JUN04]. The typical control diagram of V/f control is shown in Fig. 1.2. The block abs is used to obtain the absolute value of reference speed, then the permanent magnet flux is multiplied with the absolute value to get the amplitude of voltage command  $V_s^*$ . At the same time, the angle of voltage command is obtained by an angle generator with the input of reference speed. Then the command voltage vector  $V_{s\alpha\beta}^*$  can be obtained and will input to the PWM generator to generate the gate signals.

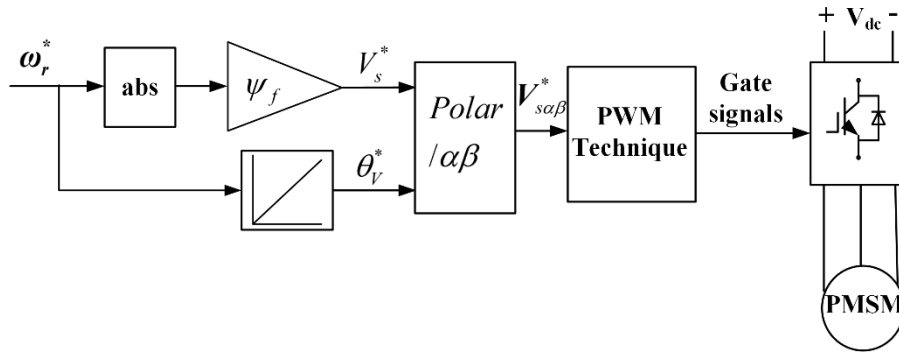


Fig. 1.2. V/f of PMSM drive.

The V/f control method is easy to implement, and the steady-state performance is acceptable for many applications. However, for the high-performance applications, especially when the transient torque response is vital, the V/f control is not competent anymore [TAN16]. In that case, FOC or DTC usually be employed.

The main idea of FOC is to considering the AC machine as a DC machine by employing coordinate transformations. Then the current component related to flux generation and the current component in charge of torque generation can be controlled independently. The surface-mounted PMSM (SPMSM) mathematical model in  $dq$  rotor reference frame is given by

$$\begin{cases} V_d = R_s I_d + p\psi_d - \omega_l \psi_q \\ V_q = R_s I_q + p\psi_q + \omega_l \psi_d \end{cases} \quad (1.1)$$

$$\begin{cases} \psi_d = LI_d + \psi_f \\ \psi_q = LI_q \end{cases} \quad (1.2)$$

$$T_e = \frac{3}{2} P \psi_f I_q \quad (1.3)$$

where  $V_d$ ,  $V_q$  are the stator voltage components,  $I_d$ ,  $I_q$  are the current components,  $L$  is the synchronous inductance.

It can be seen from (1.1) - (1.3) that  $I_q$  is the current component related to torque, and  $I_d$  is the current component related to stator flux, and they can be controlled separately. The classical control diagrams of FOC of PMSMs are given in Fig. 1.3. The control of stator flux and torque are achieved by controlling two current components  $I_d$  and  $I_q$  in a rotor flux reference frame. Coordinate transformations and two PI regulators are required. Proper pulse width modulation (PWM) strategies such as carrier-based PWM or space vector pulse width modulation (SVPWM) are often employed to implement the voltage vector references.

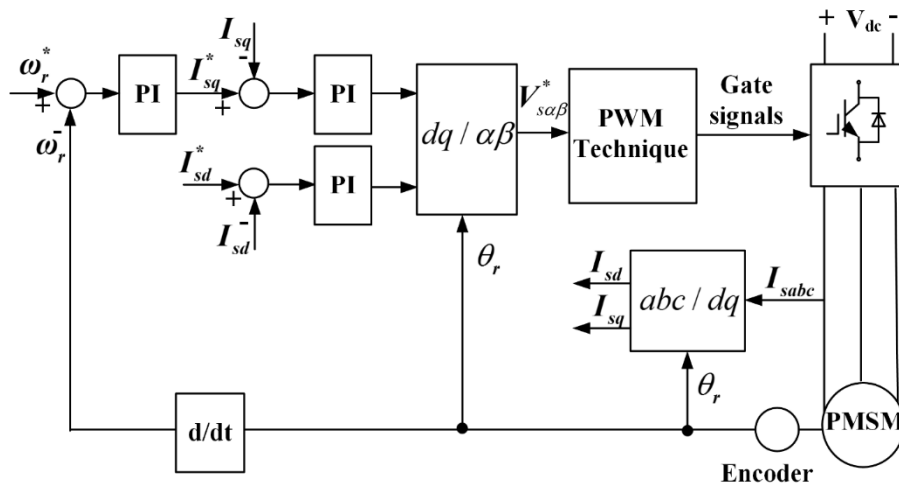


Fig. 1.3. FOC of PMSM drive.

Compared to the FOC scheme, the structure of DTC is much simpler. The classical control diagrams of DTC of PMSMs are given in Fig. 1.4. In DTC the stator flux and torque can be controlled directly by properly selecting the inverter voltage vectors from a switching table. The errors of stator flux and torque are regulated by flux and torque hysteresis regulators, respectively. The selection of voltage vectors is based on the output of two hysteresis regulators and the location

of stator flux. The locations of eight voltage vectors and the basic principle of ST-DTC are depicted in Fig. 1.5. When the stator flux vector is located in sector 1 and rotates anticlockwise, if voltage vectors with positive quadrature component are applied ( $V_2$  or  $V_3$ ), torque increases, and if vectors with negative quadrature component are applied ( $V_5$  or  $V_6$ ), torque decreases. At the same time, the magnitude of stator flux increases if vectors with positive direct component are applied ( $V_2$  or  $V_6$ ), and decreases if vectors with negative direct component are applied ( $V_3$  or  $V_5$ ). Therefore, if both the torque and flux need to be increased,  $V_2$  should be employed. Similarly, in other situations, the most suitable voltage vectors can be obtained.

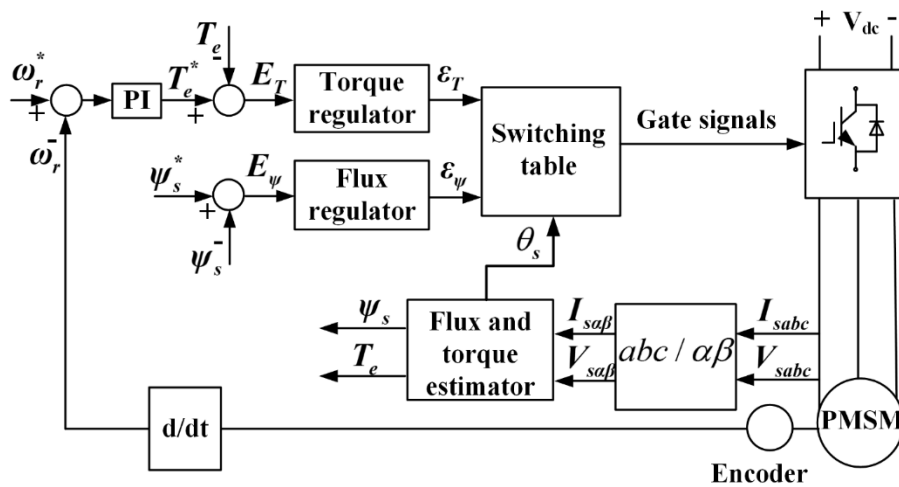


Fig. 1.4. DTC of PMSM drive.

DTC does not require current regulators, nor coordinate transformations or specific modulation. Consequently the algorithm is much simpler, and the transient torque control performance is significantly improved compared to FOC. However, the operation of the hysteresis regulator implemented in a digital signal processor (DSP or dSPACE) is quite different from that of the ideal condition. Since only one vector is applied during the whole sampling period, both torque and stator flux will exceed their predefined hysteresis bands due to the fixed sampling frequency and the time delay caused by the data processing. Therefore, undesired torque and stator flux ripples will occur, as well as the steady-state torque error [AMB04], [KAN01].

Various modified DTC schemes have been proposed to solve the aforementioned problems. The modified DTC schemes can be divided into two categories according to their basic principle of operation: SVPWM-based DTC and duty-ratio-based DTC, as shown in Fig. 1.6. The PWM

modulator in Fig. 1.6 can be either SVPWM or carried-based PWM.

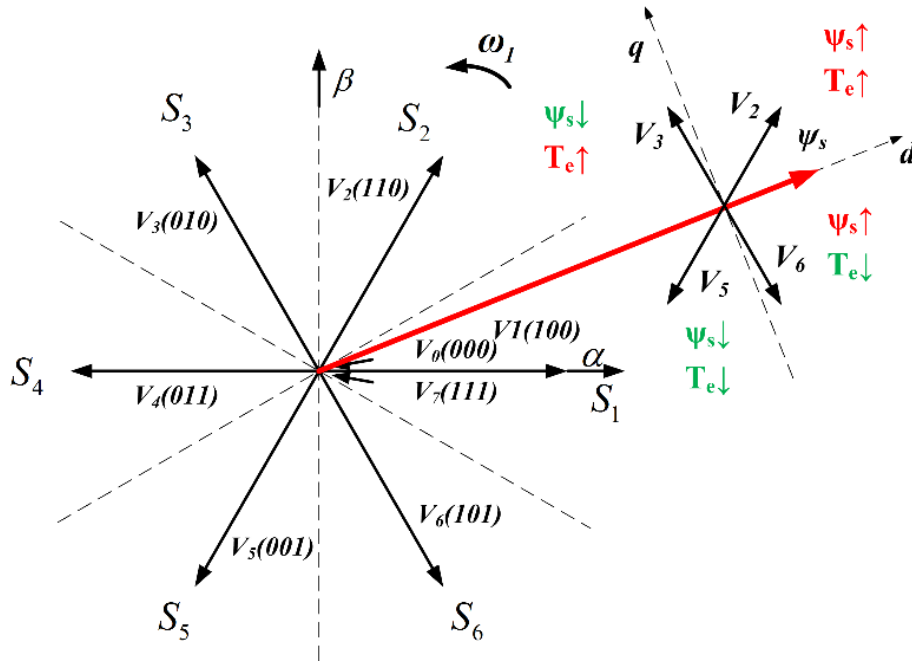


Fig. 1.5. Conventional DTC operating principle.

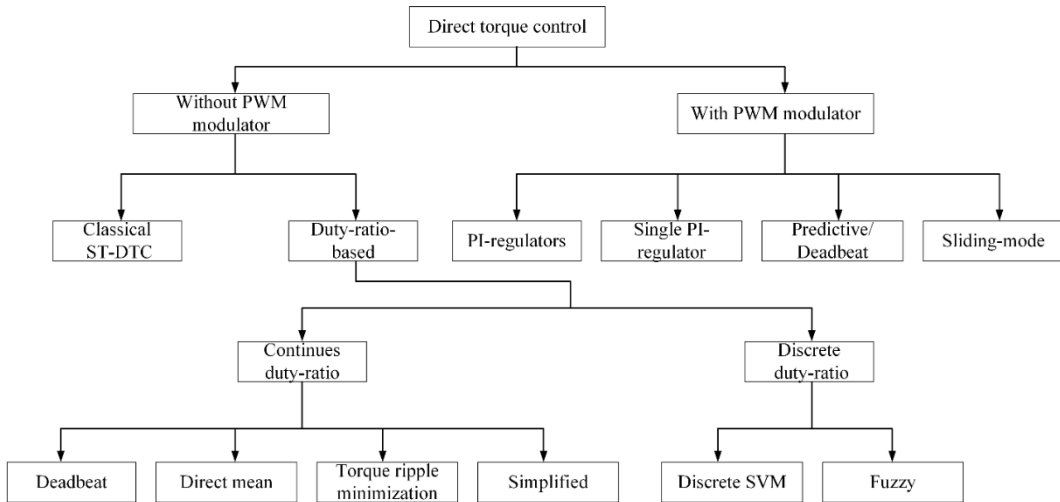


Fig. 1.6. Summary of DTC methods for three-phase machine drives.

### 1.2.1. SVPWM-based Direct Torque Control

The DTC with incorporation space vector modulation (SVM-DTC) has proved to be an effective scheme to reduce torque ripple. In SVM-DTC, the switching table is replaced by the SVPWM to

implement the command reference voltage vectors. The most commonly used SVM-DTC schemes employ two PI regulators instead of hysteresis regulators to regulate the flux and torque [LAI01]. The outputs of these PI regulators are the voltage commands in the stator flux-aligned synchronous reference frame, Fig. 1.7. After the coordinate transformation, the SVPWM technique is adopted to implement the voltage reference command in the stationary reference frame, as shown in Fig. 1.8. Other methods can also be employed to obtain the command voltage vector, for instance, a single PI controller [TAN04], deadbeat control [HAB92], [WES09], [XU14], sliding mode control [LAS04a], [LAS04b], torque predictive scheme [HAO12]. Among them, the single PI controller method and sliding mode control method employ controllers to generate the command voltage vector, while the deadbeat control methods and torque predictive scheme methods use the machine model to generate the command voltage vector.

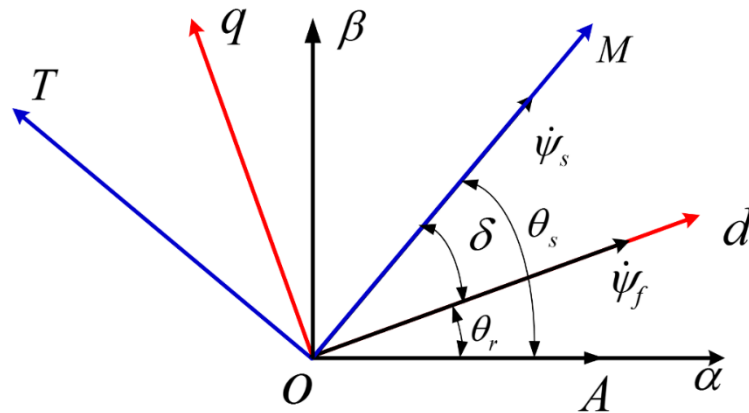


Fig. 1.7. Different types of reference frames of PMSM.

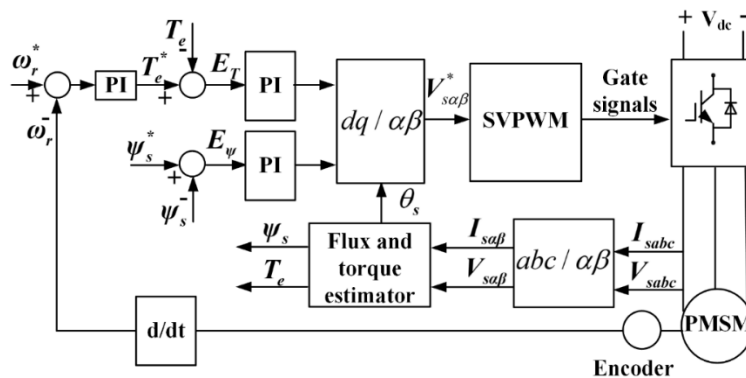


Fig. 1.8. Classical SVM-DTC of PMSM.

All the SVM-DTC methods can adjust the torque and flux more accurately, and hence, the torque and flux ripples are reduced while with a fixed switching frequency. However, due to the use of a rotational coordinate transformation and SVPWM, the system complexity and computational burden are inevitably increased. Furthermore, the excellent dynamic torque performance is impaired if PI regulators are used. The DTC schemes are machine parameter dependent if machine-model-based reference voltage calculators are used instead of PI regulators.

### 1.2.2. Duty-ratio-based Direct Torque Control

Another sort of modified DTC scheme, which does not incorporate a transformation to a rotating reference frame, operates by dividing one sampling period into several intervals [CAS00], [KAN99], [KEN03], [PAC05], [ROM03], [SHY10], [ZHA11a], [ZHA11b]. This type of duty-ratio-based DTC method still use two hysteresis regulators. The switching table is usually modified so that more than one vector is utilized within one sampling period to reduce flux and torque ripples. This type of method can be regarded as a combination of classical ST-DTC and SVM-DTC. It is expected to inherit the merits of both methods, i.e., simple structure, reduced torque ripple, and excellent dynamic torque performance.

The methods to obtain the duty ratio of the active vector can be classified into two categories: continuous duty ratio methods and discrete duty ratio methods, Fig. 1.6. For the former method, the duty ratios of active vectors are obtained by various optimizations. It is expected that by introducing the zero vectors, the torque performance will be improved since the zero vectors have the smaller absolute value of torque variation rate, as shown in Fig. 1.9.

The three typical optimizations are as follows:

The first method is to control the instantaneous torque such that it is equal to the reference value at the end of the cycle [KEN03], called deadbeat method, i.e.

$$T_e(k+1) = T_e^*(k) \quad (1.4)$$

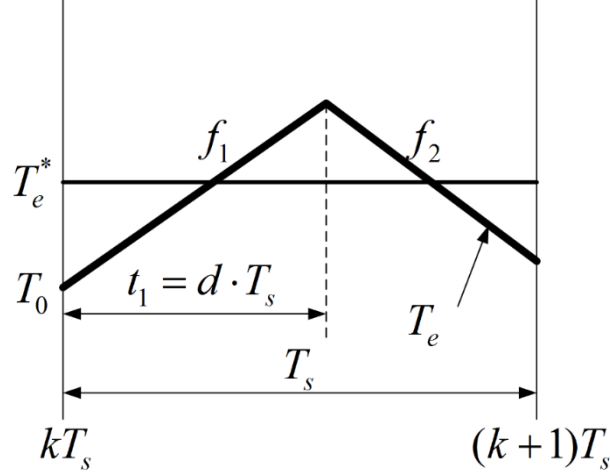


Fig. 1.9. Typical method of duty ratio determination.

The second method is to equalize the mean torque with its reference value over one sampling period [PAC05], called direct mean control method, i.e.

$$\frac{1}{T_s} \int_{kT_s}^{(k+1)T_s} (T_e^*(k) - T_e) dt = 0 \quad (1.5)$$

The third method is to minimize the torque ripple over one sampling period, called torque ripple method [KAN99], i.e.

$$\frac{1}{T_s} \int_{kT_s}^{(k+1)T_s} (T_e^*(k) - T_e)^2 dt \rightarrow \min \quad (1.6)$$

Taking PMSM as an example, the torque variation rate is as follows [REN14]

$$\frac{dT_e}{dt} = -\frac{R_s}{L_s} T_{e0} + \frac{3P}{2L_s} (-\psi_{r\beta} V_{s\alpha} + \psi_{r\alpha} V_{s\beta} - \omega_1 |\psi_{r\alpha\beta}| |\psi_{s\alpha\beta}| \cos \delta) \quad (1.7)$$

Consequently, the duty ratio value of active vectors can be obtained from (1.4)-(1.7). However, it can be seen from (1.7) that the torque variation is parameter dependent, which makes the three methods strongly dependent on the motor parameters, and also time-consuming.

The other category is the discrete duty ratio method since only a finite number of duty-ratio values are available. For instance, the concept of discrete space vector modulation is introduced in [CAS00], and the fuzzy-logic adaptation is utilized in [ROM03]. For these types of methods, more

than one switching table is required, while the speed information is employed as the third input for the modified switching tables. 5-level torque regulators are used instead of the classical 2-level or 3-level regulators. These improved methods achieve better steady-state performance compared to the conventional ST-DTC without involving additional machine parameters. However, since more switching tables are utilized, the algorithm is still complicated. Furthermore, the design of torque regulators is not deeply discussed.

A simple duty determination method which does not use the complicated torque variation equation was also proposed to reduce the torque and stator flux ripples [ZHA11a], [ZHA11b], as shown in(1.8). This method is easy to implement. However, due to only one duty determination being used under different speed and torque conditions, significant steady-state error of torque always exists, and there is no simple analytical solution to obtain the key control parameters.

$$d = \left| \frac{T_e^* - T_e}{C_T} \right| + \left| \frac{\psi_s^* - \psi_s}{C_\psi} \right| \quad (1.8)$$

### 1.3. Control of Dual Three-phase PMSM

Among the various kinds of multiphase machines such as five-phase [GAO11], [PAR07], [ZHE11], six-phase [BOJ05], [CHE14], [DUR11], [GOP93], [HAD06], [HAT05], [ZHA95], seven-phase [LEV08b], and nine-phase [KEL03], one type of six-phase machine called dual three-phase machine is one of the most interesting and commonly-discussed types. Dual three-phase machine has two sets of three-phase windings spatially shifted by 30 electrical degrees, as shown in Fig. 1.10. Hence, it has the inherent advantage of suppression of the sixth harmonic torque pulsation [GOP84].

However, significant stator harmonic currents are usually observed in the voltage-source-inverter fed dual three-phase machine [KLI83], [ZHA95]. These harmonic currents will cause extra losses and require higher semiconductor device ratings [DUR11]. For high-power and/or high-current applications, such as electric/hybrid vehicles, renewable energy generation, aerospace applications, and ship propulsion, the efficiency of the machine is very important. Therefore, the harmonic currents should be reduced to as small as possible [BOJ03].

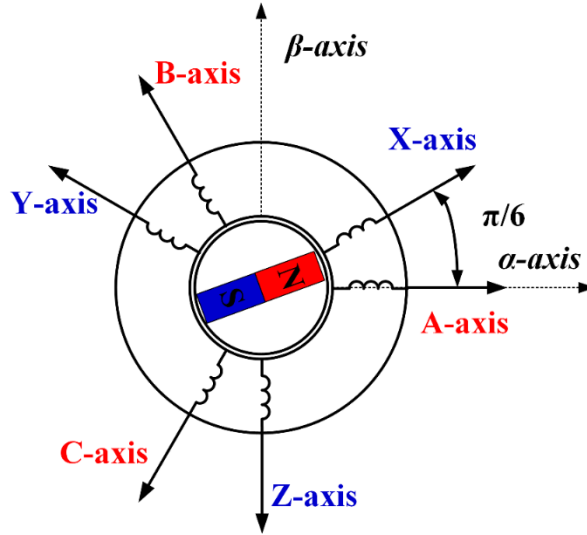


Fig. 1.10. Dual three-phase PMSM.

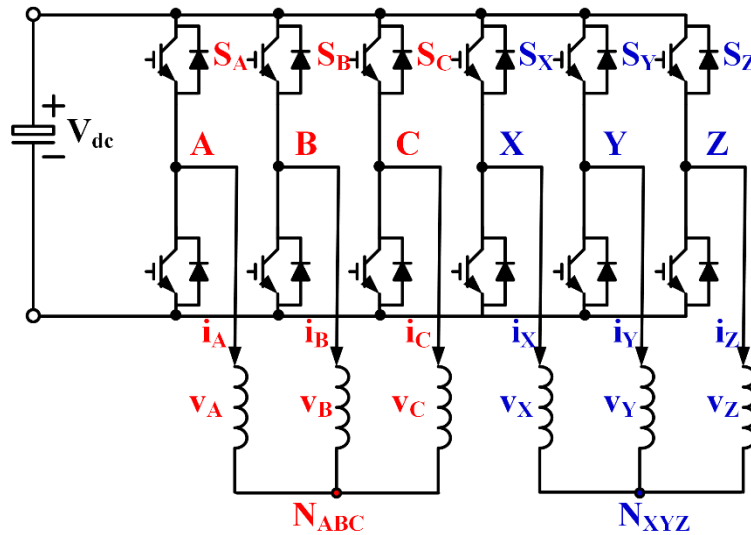


Fig. 1.11. Voltage-source-inverter-fed (VSI) dual three-phase PMSM and drive.

### 1.3.1. Modelling of Dual Three-phase PMSM

The dual three-phase machine model is a complex six-dimensional electromechanical system, which makes the modelling and control of the dual three-phase machine very difficult. Therefore, the vector space decomposition approach (VSD) is proposed in [ZHA95], which transforms the conventional six-dimensional system to a new six-dimensional composed of three mutually orthogonal subspaces, by using a transformation matrix. The transformation matrix is as follows

$$[T_6] = \frac{1}{3} \begin{bmatrix} 1 & \cos \frac{4\pi}{6} & \cos \frac{8\pi}{6} & \cos \frac{\pi}{6} & \cos \frac{5\pi}{6} & \cos \frac{9\pi}{6} \\ 0 & \sin \frac{4\pi}{6} & \sin \frac{8\pi}{6} & \sin \frac{\pi}{6} & \sin \frac{5\pi}{6} & \sin \frac{9\pi}{6} \\ 1 & \cos \frac{8\pi}{6} & \cos \frac{4\pi}{6} & \cos \frac{5\pi}{6} & \cos \frac{\pi}{6} & \cos \frac{9\pi}{6} \\ 0 & \sin \frac{8\pi}{6} & \sin \frac{4\pi}{6} & \sin \frac{5\pi}{6} & \sin \frac{\pi}{6} & \sin \frac{9\pi}{6} \\ 1 & 1 & 1 & 0 & 0 & 0 \\ 0 & 0 & 0 & 1 & 1 & 1 \end{bmatrix} \quad (1.9)$$

By employing the VSD technique, the fundamental components of the machine variables and the harmonics of order  $k=12m \pm 1$  ( $m=1, 2, 3, \dots$ ) are transformed into the  $\alpha\beta$  subspace, whilst the harmonics of order  $k=6m \pm 1$ , ( $m=1, 3, 5, \dots$ ) are mapped into the  $z_1z_2$  subspace. The zero-sequences of order  $k=3m$ , ( $m=1, 3, 5, \dots$ ) are located in the  $o_1o_2$  subspace, which disappear when the neutral points are isolated, Fig. 1.11.

Then the final model of dual three-phase surface mounted PMSM, under the assumption of sinusoidally distributed windings and neglecting mutual leakage inductance, magnetic saturation and core losses, can be described in a stationary reference frame as [ZHA95]

$$V_{s\alpha\beta} = R_s I_{s\alpha\beta} + p\psi_{s\alpha\beta} \quad (1.10)$$

$$\psi_{s\alpha\beta} = L_s I_{s\alpha\beta} + \psi_{r\alpha\beta} \quad (1.11)$$

$$\psi_{r\alpha\beta} = \psi_f e^{j\theta_r} \quad (1.12)$$

$$V_{sz_1z_2} = R_s I_{sz_1z_2} + p\psi_{sz_1z_2} \quad (1.13)$$

$$\psi_{sz_1z_2} = L_{ls} I_{sz_1z_2} \quad (1.14)$$

$$T_e = 3P(\psi_{s\alpha} i_{s\beta} - \psi_{s\beta} i_{s\alpha}) \quad (1.15)$$

where,  $L_s = L_{ls} + 3L_m$  is the stator inductance.



Since the neutral points are isolated, it is natural that the dual three-phase PMSM can be considered as two three-phase systems. Therefore, the current control method employs a double  $dq$  synchronous reference frame approach, where two sets of three-phase PMSMs are controlled independently. The reference currents both in  $d$ - and  $q$ -axis are shared by two individual current controllers that correspond to the two three-phase sets. The double  $dq$  current control method uses four simple PI current regulators. The diagram of the double  $dq$  method is shown in Fig. 1.13. To improve the control performance, the speed-dependent decoupling terms between the two sets are derived and added to the reference voltages [BOJ03C]. Although this method can provide excellent performance for current imbalance compensation between the two sets, it cannot compensate for the current imbalance between phase windings in each set.

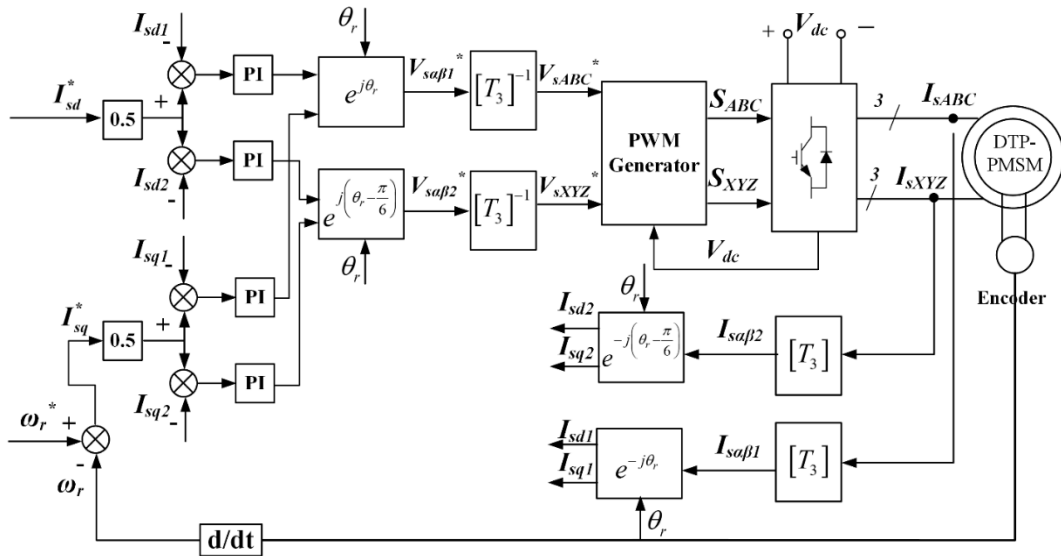


Fig. 1.13. Double  $dq$  current control for dual three-phase PMSM drives.

The VSD technique provides an alternative method to describe the machine model, which is more straightforward since different harmonic components are located in different subspaces. Unlike the double  $dq$  current control method which are only suitable for the dual three-phase machine, the VSD technique can be applied to multiphase machines with any phase number. For the methods based on the VSD model, proper PWM technique is required to ensure that the voltage components in different subspaces are properly controlled. This is discussed in next section.

Controlling only the  $\alpha\beta$  subspace is insufficient for adequate performance of dual three-phase machines. The current control method in a stationary reference frame is presented in [BOJ06],

where the modified PI regulators are employed in the  $\alpha\beta$  subspace and resonant regulators are adopted in  $z_1z_2$  subspace, all the current controllers are dependent on the electrical angular speed, therefore, this method is complicated to implement. The currents in the  $z_1z_2$  subspace are controlled by PI regulators for five-phase machines in [JON09]. By applying a rotational transformation, the transformed  $z_1z_2$  currents will appear as DC and AC components. The PI regulators can fully compensate the DC components, while the AC components only can be reduced to some extent restricted by the PI controllers' bandwidth. In [CHE14], it is proved that the currents in  $z_1z_2$  subspace can be considered as circulating currents between the two three-phase sets. Using this approach, the characteristics of currents in the  $z_1z_2$  subspace, due to the machine/inverter asymmetries, are analysed in detail, Fig. 1.14. Consequently, dual-PI controllers (synchronous and anti-synchronous PI controllers) are employed for the control of currents in the  $z_1z_2$  subspace, which are proved to be capable of eliminating harmonic currents in  $z_1z_2$  subspace caused by machine/inverter asymmetries, Fig. 1.15.

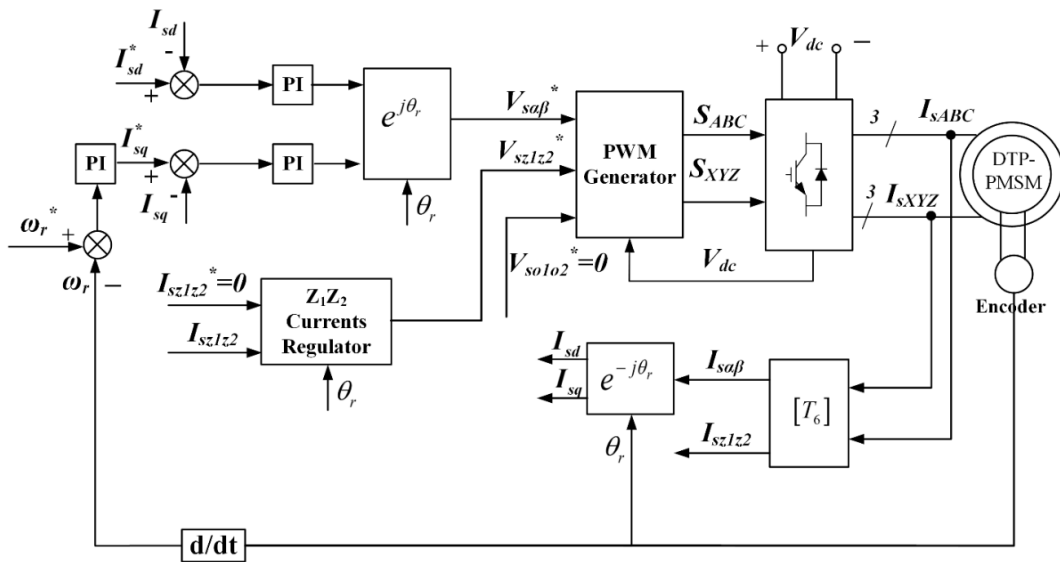


Fig. 1.14. Current control based on VSD for dual three-phase PMSM drives.

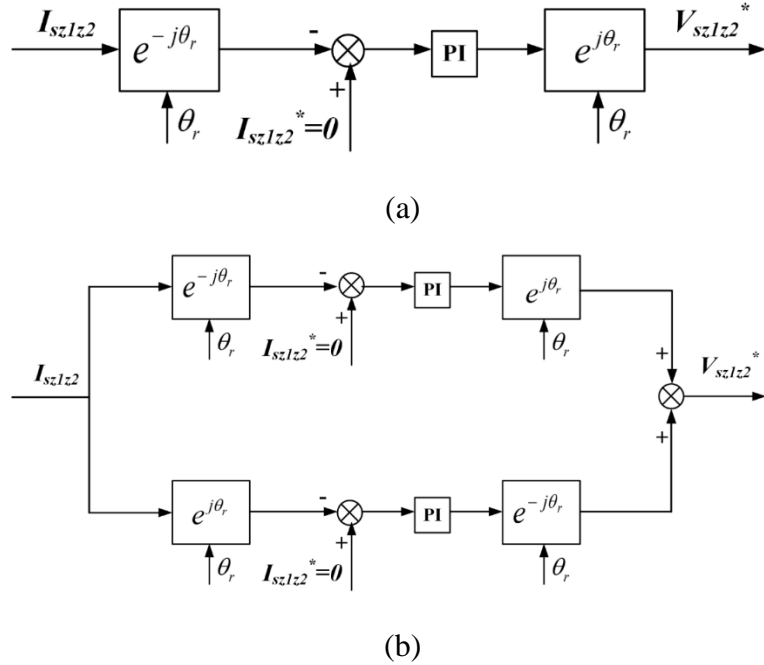


Fig. 1.15. Two types of current controllers in  $z1z2$  subspace. (a) Single PI regulators (b) Dual-PI regulators.

Although the stator current harmonics can be reduced, the methods employed usually use coordinate transformations, current control loops and complicated PWM strategies to impose the desired flux and torque, thus time-consuming calculations are required.

### 1.3.3. PWM Techniques of Dual Three-phase PMSM

Similar to three-phase machine drives, the most popular PWM strategies for the two-level VSI-fed dual three-phase machine drives are carrier-based PWM and SVPWM techniques.

Carrier-based PWM methods are the most straightforward approach due to the simple structure. In principle, the carrier-based PWM methods can be easily extended from three-phase drives to any multiphase drive. In three-phase drives, since the total number of voltage vectors is only  $2^3=8$ , the implementation of space vector PWM is not appreciably more difficult than carrier-based PWM. However, as the phase number increases, the number of voltage vectors grows at an exponential rate, making it harder to implement a suitable SVPWM scheme. For instance, for a 15-phase drive, there are  $2^{15} = 32,768$  voltage vectors. The SVPWM scheme for online implementation would be impractical, while implementation of carrier-based PWM it is comparatively quite straightforward [HOU03C].

For the carrier-based PWM for three-phase drives, the main disadvantage is the lower DC link voltage utilization; hence, a zero-sequence injection technique is usually employed. For the case of dual three-phase drives with isolated neutral points, a double zero-sequence injection is adopted for the carrier-based PWM. The zero-sequence components are injected in each of the three-phase set as shown in Fig. 1.16.

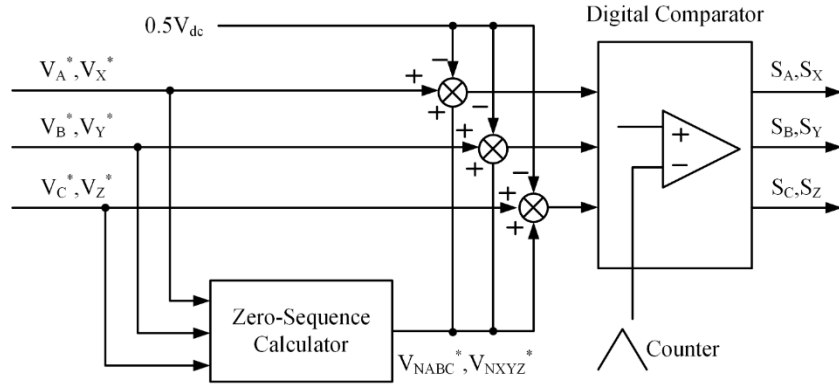


Fig. 1.16. Double zero-sequence injection for carrier-based PWM.

The specific SVPWM schemes are based on the VSD technique which constructs three subspaces to analyse the dual three-phase system. As the three subspaces are mutually perpendicular, no coupling occurs between any two of them, and the specific harmonics can be exclusively assigned to a single subspace. The fundamental components of the machine variables and the harmonics of order  $k=12m \pm 1$  ( $m=1, 2, 3, \dots$ ) are transformed into the  $\alpha\beta$  subspace. These harmonics are responsible for torque production, whilst the harmonics of order  $k=6m \pm 1$ , ( $m=1, 3, 5, \dots$ ) are mapped into the  $z_1z_2$  subspace. These harmonics should be minimized since the impedance in the  $z_1z_2$  subspace is quite small such that moderate amplitude harmonics can lead to the large harmonic currents. The zero-sequences of order  $k=3m$ , ( $m=1, 3, 5, \dots$ ) are located in the  $o1o2$  subspace, which disappears when the neutral points are isolated. Therefore, the aim of the specific SVPWM for dual three-phase drives is to minimize the harmonic current within one switching period.

Dual three-phase machine is an asymmetric six phase machine, hence, there are  $2^6 = 64$  voltage vectors. The voltage vector number is named based on a binary value of  $V_i = S_Z S_Y S_X S_C S_B S_A$  considering  $V_i$  as a 6-digit binary number, where value of each phase switching component  $S_i$  is set as “1” when its equivalent stator terminal is connected to DC link voltage rail and “0” if it is

linked to negative DC voltage rail. For instance,  $V_9$  (001001) means phases X and A are connected to DC link voltage rail, and phases Z, Y, C, B are connected to negative DC voltage rail. Since there are 64 vectors in a dual three-phase drive, there are many SVPWM strategies can be designed by choosing different vectors. By utilizing VSD technique, all the 64 vectors can be transformed into three subspaces: When the neutral points of two three-phase sets are isolated as shown Fig. 1.11, subspaces  $o_1o_2$  disappears. The 64 voltage vectors can be presented in  $\alpha\beta$  and  $z_1z_2$  subspace is shown in Fig. 1.17.

To gain the maximum DC link voltage utilization, the employment of the outermost 12 vectors is the most common approach, as shown in Fig. 1.18.

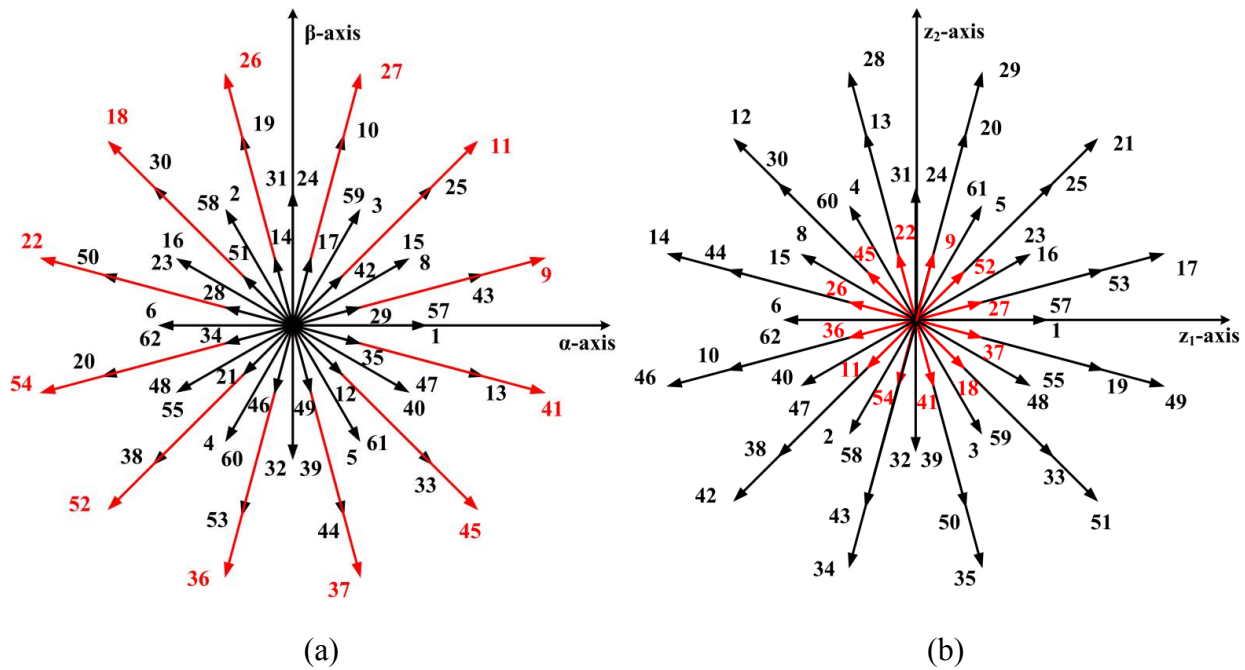


Fig. 1.17. Voltage vectors in different subspaces. (a)  $\alpha\beta$  subspace, (b)  $z_1z_2$  subspace

For each reference vector, the four nearest vectors out of the outermost 12 vectors in  $\alpha\beta$  subspace will be selected along with the zero vectors, where the dwell time of each vector meets the following set of equations [ZHA95], where  $V_{\alpha k}$ ,  $V_{\beta k}$ ,  $V_{z_1 k}$ ,  $V_{z_2 k}$  represent the projections of the voltage vector  $V_k$  on  $\alpha$ ,  $\beta$ ,  $z_1$ ,  $z_2$  axes, respectively, while  $T_k$  indicates the dwell time of the voltage vector  $V_k$ .

$$\left\{ \begin{array}{l} \sum_{k=1}^5 V_{\alpha k} \cdot T_k = v_{\alpha}^* \cdot T_s \\ \sum_{k=1}^5 V_{\beta k} \cdot T_k = v_{\beta}^* \cdot T_s \\ \sum_{k=1}^5 V_{z1k} \cdot T_k = v_{z1}^* \cdot T_s \\ \sum_{k=1}^5 V_{z2k} \cdot T_k = v_{z2}^* \cdot T_s \\ \sum_{k=1}^5 T_k = T_s \end{array} \right. \quad (1.16)$$

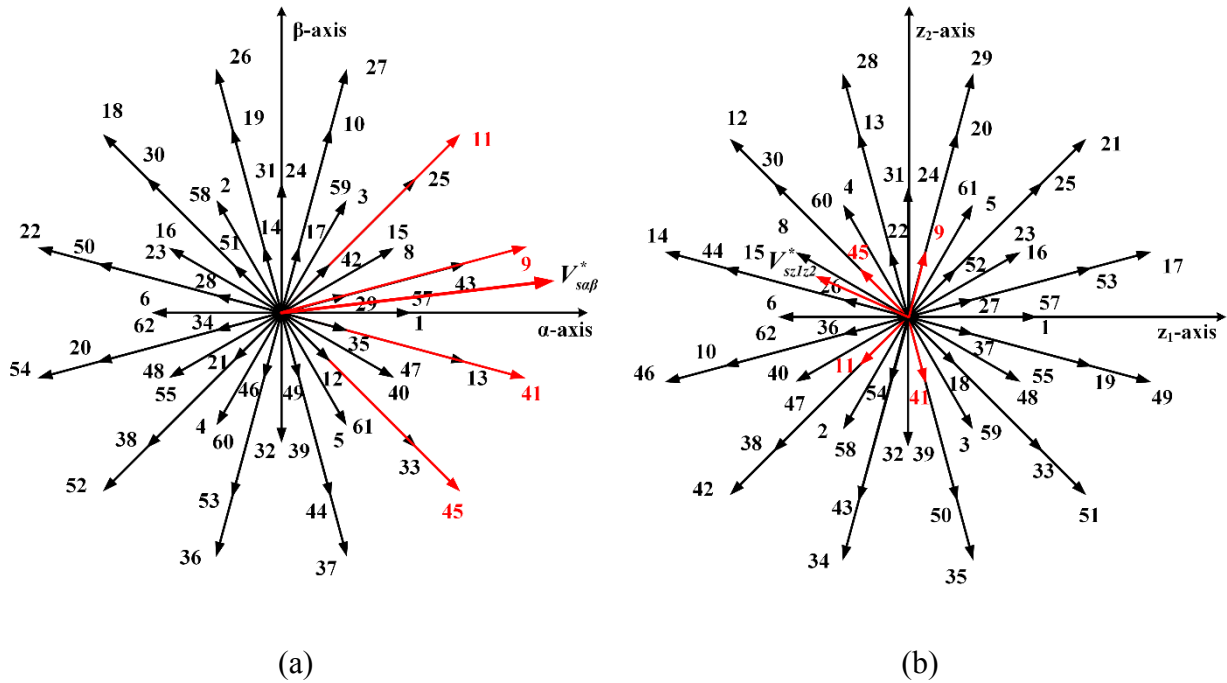


Fig. 1.18. SVPWM technique for dual three-phase drives. (a)  $\alpha\beta$  subspace. (b)  $z_1z_2$  subspace.

Therefore, the dwell time of each vector can be calculated from

$$\begin{cases} \begin{bmatrix} T_1 \\ T_2 \\ T_3 \\ T_4 \end{bmatrix} = \begin{bmatrix} V_{\alpha 1} & V_{\alpha 2} & V_{\alpha 3} & V_{\alpha 4} \\ V_{\beta 1} & V_{\beta 2} & V_{\beta 3} & V_{\beta 4} \\ V_{z_1 1} & V_{z_1 2} & V_{z_1 3} & V_{z_1 4} \\ V_{z_2 1} & V_{z_2 2} & V_{z_2 3} & V_{z_2 3} \end{bmatrix}^{-1} \cdot \begin{bmatrix} v_{\alpha}^* \cdot T_s \\ v_{\beta}^* \cdot T_s \\ v_{z_1}^* \cdot T_s \\ v_{z_2}^* \cdot T_s \end{bmatrix} \\ T_5 = T_s - T_1 - T_2 - T_3 - T_4 \end{cases} \quad (1.17)$$

The calculation of dwell times using (1.17) for online implementation is very time-consuming. A simplified implementation is presented in [HAD06], where the dwell times of the active vectors can be obtained from an offline table, as shown in Table 1.1, and  $T_a$  to  $T_f$  can be easily obtained as

$$\begin{bmatrix} T_a \\ T_b \\ T_c \\ T_d \\ T_e \\ T_f \end{bmatrix} = \frac{T_s}{2V_{dc}} \cdot \begin{bmatrix} 2-\sqrt{3} & -1 & -2-\sqrt{3} & 1 \\ \sqrt{3}-1 & 1-\sqrt{3} & 1+\sqrt{3} & -1-\sqrt{3} \\ 1 & \sqrt{3}-2 & -1 & 2+\sqrt{3} \\ 1 & 2-\sqrt{3} & -1 & -2-\sqrt{3} \\ \sqrt{3}-1 & \sqrt{3}-1 & 1+\sqrt{3} & 1+\sqrt{3} \\ 2-\sqrt{3} & 1 & -2-\sqrt{3} & -1 \end{bmatrix} \cdot \begin{bmatrix} v_{\alpha}^* \\ v_{\beta}^* \\ v_{z_1}^* \\ v_{z_2}^* \end{bmatrix} \quad (1.18)$$

Table 1.1 Offline Table of Dwell Times of Active Vectors

	S1	S2	S3	S4	S5	S6	S7	S8	S9	S10	S11	S12
$T_1$	$T_a$	$T_b$	$T_c$	$T_d$	$T_e$	$T_f$	$-T_a$	$-T_b$	$-T_c$	$-T_d$	$-T_e$	$-T_f$
$T_2$	$T_b$	$T_c$	$T_d$	$T_e$	$T_f$	$-T_a$	$-T_b$	$-T_c$	$-T_d$	$-T_e$	$-T_f$	$T_a$
$T_3$	$T_e$	$T_f$	$-T_a$	$-T_b$	$-T_c$	$-T_d$	$-T_e$	$-T_f$	$T_a$	$T_b$	$T_c$	$T_d$
$T_4$	$T_f$	$-T_a$	$-T_b$	$-T_c$	$-T_d$	$-T_e$	$-T_f$	$T_a$	$T_b$	$T_c$	$T_d$	$T_e$

This SVPWM scheme has been extended to 24 sectors [MAR08], where further improvement of performance has been claimed. However, the computational burden is commensurately increased.

### 1.3.4. Direct Torque Control of Dual Three-phase PMSM

A DTC strategy, which has been successfully employed for three-phase drives, is also investigated in this work and has been extrapolated to dual-three-phase drives. It is an alternative solution to current control methods lauded for its simple structure, excellent transient response and good robustness [BOJ05], [HAT05].

Based on the VSD technique, only the variables in the  $\alpha\beta$  subspace in the dual three-phase system are related to the torque production. Therefore, it is easy to extend the classical ST-DTC of three-phase drives to dual three-phase drives, as depicted in Fig. 1.19. Based on the estimated stator flux position, a flux hysteresis regulator and a torque hysteresis regulator are used to generate the switching states according to a switching table. However, due to lack of control of harmonic components in the  $z_1z_2$  subspace, the classical ST-DTC strategy inevitably suffers from the large stator current harmonics [BOJ05]. For dual three-phase drive systems, the additional inverter vectors permit greater flexibility in vector selection compared to a single three-phase drive. Having more vectors to select from requires a more elaborate selection criterion.

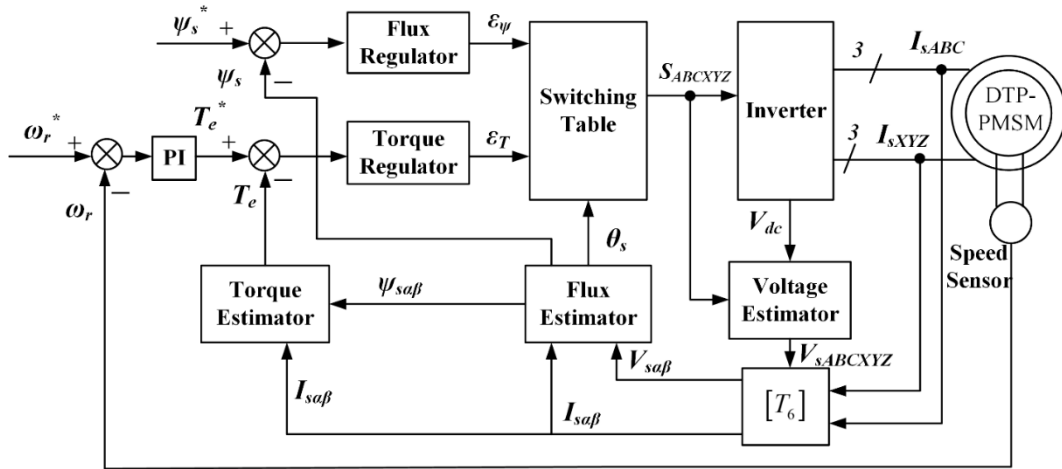
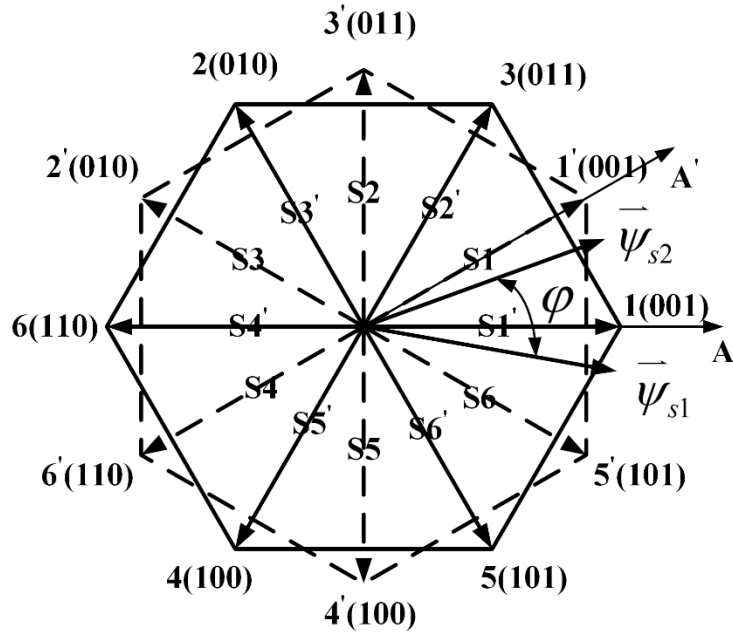
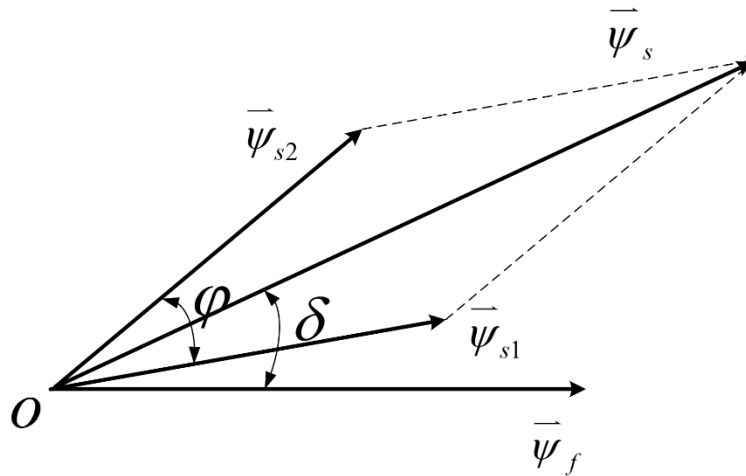


Fig. 1.19. Conventional ST-DTC of dual three-phase PMSM drives.

Considering that the dual three-phase machine can be regarded as two sets of three-phase machines when the neutral points are isolated, Hatua [HAT05] proposes a modified ST-DTC technique called individual flux control method where both inverters are switched from their respective hexagonal space vector locations to maintain the individual and resultant flux magnitudes constant at their respective reference values, as shown Fig. 1.20(a). Set 1 consists of phase A, B, C, and set 2 consists of phase D, E, F. Three different algorithms are proposed to ensure that the flux of set2 leads the flux of set1 by 30 degrees in phase, Fig. 1.20(b). These methods can improve flux and torque performance to some extent. However, the structure of the ST-DTC method becomes complicated and the problem of phase current harmonics remains.



(a)



(b)

Fig. 1.20. The modified ST-DTC based on individual flux control. (a) Individual hexagonal space vector. (b) Description of different fluxes.

Another modified ST-DTC method for dual three-phase drives is to employ another 12 active vectors having the second greatest amplitude in the  $\alpha\beta$  subspace [HAO12C]. These 12 active vectors have a similar effect on flux and torque in  $\alpha\beta$  subspace but opposite influence on flux in



## 1.4. Scope of Research and Contributions

### 1.4.1. Scope of Research

This thesis is focused on ST-DTC of three-phase and dual three-phase PMSM drives. The modified ST-DTC strategies are proposed to improve the steady-state performance of torque and currents, while still maintaining the merits of classical ST-DTC, such as excellent dynamic performance and machine parameter independence. PWM-based DTC strategies are also discussed for the dual three-phase PMSM drives which can achieve a constant switching frequency.

The remainder of thesis chapters are summarized as follows:

**Chapter 2:** The experimental platform based on a dSPACE control system is described. This includes the hardware setup and software environment, as well as the single and dual three-phase PM machines which are tested in the later chapters.

**Chapter 3:** A novel and simple on-line band-shifted torque regulator is described based on the analysis of torque variation of each voltage vector. This is designed to reduce the steady-state torque response error in the classical ST-DTC strategy. The main results of this chapter have been published in the following paper:

- [1]. Z. Q. Zhu, Y. Ren, and J. M. Liu, "Improved torque regulator to reduce steady-state error of torque response for direct torque control of permanent magnet synchronous machine drives," *IET, Electr. Power Appl.*, vol. 8, no. 3, pp. 108-116, 2014.

**Chapter 4:** A simple and effective method to obtain the duty ratio is presented. This is achieved by considering the effect of the machine angular velocity, which can significantly reduce the torque ripple. Existing methods to optimize the duty ratio of the active vector are usually complicated and parameter dependent by comparison. They are often based on the analysis of instantaneous variation rates of stator flux and torque of each converter output voltage vector. The main results of this chapter have been published in the following paper:

- [2]. Y. Ren, Z. Q. Zhu, and J. M. Liu, "Direct torque control of permanent-magnet synchronous machine drives with a simple duty ratio regulator," *IEEE Trans. Ind. Electron.*, vol. 61, no. 10, pp. 5249-5258, Oct. 2014.

**Chapter 5:** Detailed modelling of a dual three-phase PMSM and the analysis of the effect of various voltage vectors on torque and flux variation and harmonic currents are described. Then, an optimized ST-DTC strategy is proposed. This strategy consists of a two-step process to determine the most appropriate inverter voltage vector with the objective of reducing harmonic currents in the stator. The main results of this chapter have been published in the following paper:

- [3]. K. D. Hoang, Y. Ren, Z. Zhu, and M. Foster, "Modified switching-table strategy for reduction of current harmonics in direct torque controlled dual three-phase permanent magnet synchronous machine drives," *IET, Electr. Power Appl.*, vol. 9, no. 1, pp. 10-19, Jan. 2015.

**Chapter 6:** A modified switching table comprised of 12 new synthetic voltage vectors is proposed for ST-DTC strategy of a dual three-phase PMSM. With this new switching table the variables relating to the torque production are well controlled and the variables contributing to the current harmonics are eliminated within one sampling period. Furthermore, a simple modified torque regulator is proposed to reduce the torque ripple and the steady-state error of torque often observed in real-time systems. An optimal switching sequence for implementation in a real-time system is described which minimizes the computation burden. The main results of this chapter have been published in the following paper:

- [4]. Y. Ren and Z. Q. Zhu, "Enhancement of steady-state performance in direct-torque-controlled dual three-phase permanent-magnet synchronous machine drives with modified switching table," *IEEE Trans. Ind. Electron.*, vol. 62, no. 6, pp. 3338-3350, Jun. 2015.

**Chapter 7:** Two types of synthetic vectors which can reduce the harmonic currents effectively are introduced for VSI-fed dual three-phase drive. The most suitable switching sequences are described. A modified five-level torque regulator is proposed to improve the torque performance. With this method harmonic currents have been suppressed and the steady-state error and ripple of torque can be considerably reduced. The merits of classical ST-DTC such as simple structure and excellent dynamic performance are preserved. The main results of this chapter have been published in the following paper:

- [5]. Y. Ren and Z. Q. Zhu, "Reduction of both harmonic current and torque ripple for dual three-phase permanent-magnet synchronous machine using modified switching-table-based direct torque control," *IEEE Trans. Ind. Electron.*, vol. 62, no. 11, pp. 6671-6683, Nov. 2015.

**Chapter 8:** Some applications require a constant switching frequency. Therefore, a modified deadbeat-based PWM-DTC strategy for dual three-phase machine drives is proposed in this chapter. The PI controllers in the synchronous reference frame for currents in the  $z_1z_2$  subspace are employed together with the deadbeat-based reference voltage calculator. Then specific SVPWM techniques are adopted to implement the reference voltage vectors. A simple dead-time compensator is utilized to reduce the effect of inverter non-linearity on harmonic currents.

**Chapter 9:** This chapter concludes the work, and some related future work is discussed.

The story line of the whole thesis is described as shown in Fig. 1.22.

### 1.4.2. Contributions

The major contributions of this thesis are as follows:

- By analysing the instantaneous variation rates of stator flux and torque of each converter output voltage vector, a novel and simple on-line band-shifted torque regulator is proposed to minimize this steady-state error of torque response, which is very effective whilst preserves the merits of the conventional direct torque control, i.e. simple structure, good robustness, and excellent transient response.
- Based on the analysis of the instantaneous variation rates of torque, a simple and effective method for determining the appropriate duty ratio in DTC three-phase PMSM drives to reduce the torque ripple, accounting for the influence of machine angular velocity, is proposed, which is parameter independent and much simpler than the existing duty-ratio-based DTC.

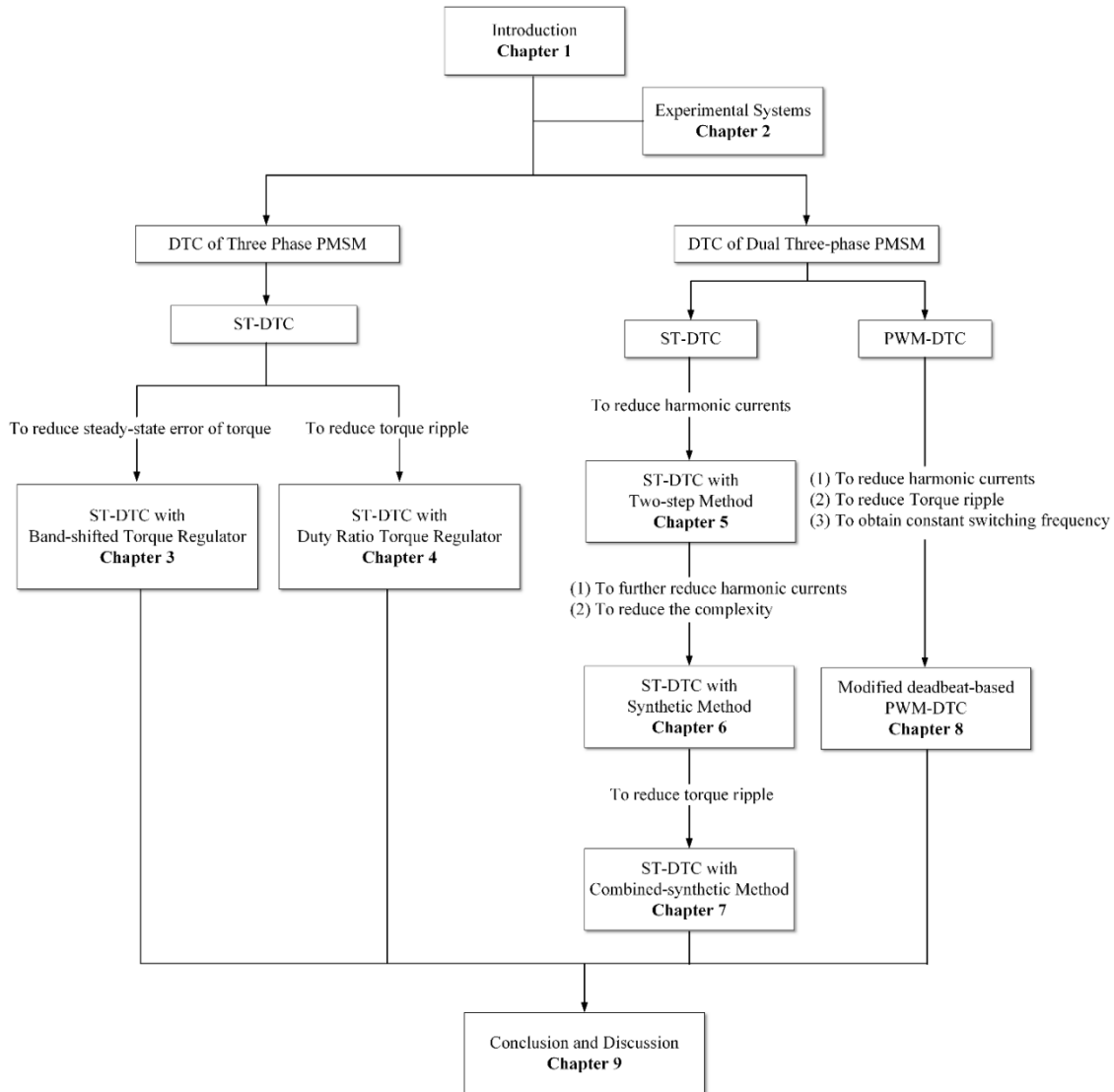


Fig. 1.22. The story line of the whole thesis.

- A two-step process voltage vector selection scheme for modified ST-DTC strategy is presented, which not only controls the variables in the  $\alpha\beta$  subspace to meet the requirement of torque production, but also significantly reduces the magnitude of the flux space vector in the  $z_1z_2$  subspace, which results in considerably lower harmonics in stator currents.
- To reduce the harmonic current whilst keep the simple structure of ST-DTC method, a modified switching table consisting of 12 new synthetic voltage vectors is proposed. The switching sequences have been discussed, and the most suitable one for the

implementation of real-time system has been proposed to minimize the computation burden. Considering the difference of decreasing and increasing variation and the influence of one-step delay in real-time system, a simply modified torque regulator is proposed to improve the performance of torque response.

- To deal with all of the three issues related to ST-DTC of dual three-phase drives, two groups of synthetic vectors which can minimize the harmonic currents within one sampling period are firstly introduced, along with their most appropriate switching sequences for real-time system to implement with minimized computation burden. Then, based on the analysis of the torque variations for both large and small synthetic vectors and zero vectors in different operating regions, as well as the discussion of the function of outer and inner bands of torque regulator, a simple modified torque regulator is proposed to further improve the steady-state performance of torque. By the employment of the proposed strategy, not only harmonic currents are significantly suppressed but also steady-state error and ripple of torque are considerably reduced, without deteriorating simplicity of structure and excellent dynamic performance.
- To achieve the constant switching frequency, a modified deadbeat-based PWM-DTC strategy for dual three-phase machine drives is proposed. Considering that the harmonic currents cannot be minimized in the conventional deadbeat-PWM-DTC since only the variables in  $\alpha\beta$  subspace are controlled, two PI controllers in synchronous reference frame for currents in  $z_1z_2$  subspace are employed together with the deadbeat-based reference voltage calculator, and then specific SVPWM technique are adopted to implement the reference voltage vectors. After that, the simple dead-time compensator is utilized to reduce the effect of inverter non-linearity on harmonic currents. The proposed deadbeat-PWM-DTC has achieved considerable reduction of steady-state error and ripple of torque, as well as the harmonic currents, while keeping the merit of excellent dynamic performance of ST-DTC.

## 2. Experimental Systems

### 2.1. Introduction

In this chapter, the experimental platforms for the control of three-phase PM machines and dual three-phase PM machines is described. The experimental systems are based on a dSPACE control system which can be program automatically from a Matlab/Simulink model. The three-phase systems and dual three-phase systems share the same machine drive platform where two sets of three-phase inverters are fed from one DC power supply. For the three-phase system, only one three-phase inverter is enabled. In the practical implementation, two versions of the dSPACE system are utilized. A dSPACE DS1006 is employed for the three-phase drive system, while a dSPACE DS1005 is adopted for the dual three-phase drive system. Since there is little difference between these two versions, only the dSPACE DS1006 is introduced in this chapter.

The experimental test system is illustrated in Fig. 2.1.

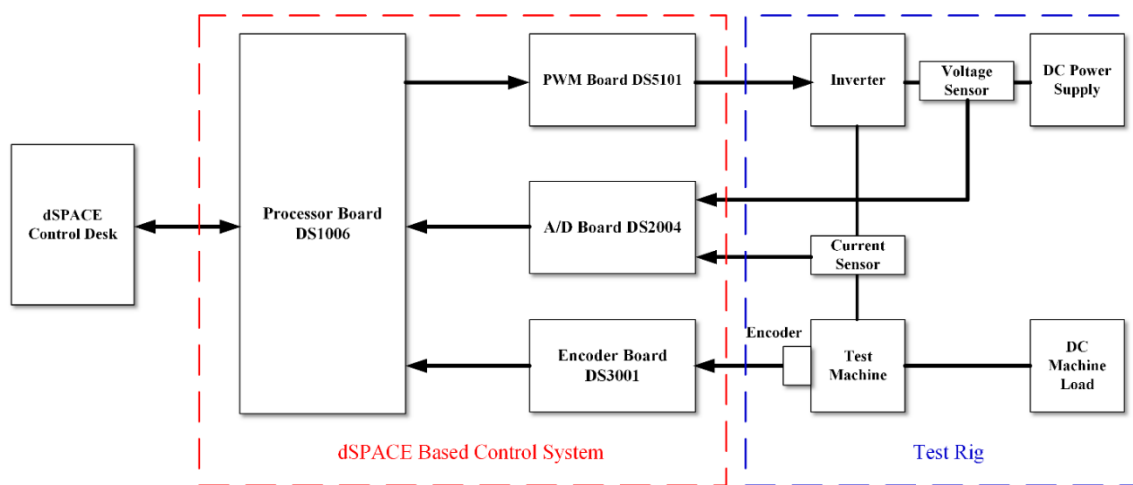


Fig. 2.1. Setup of experimental system

### 2.2. dSPACE Based Control System and Software Environment

Like other digital systems such as DSP-based control systems, the dSPACE based control system consists of several circuit boards and corresponding development software. As can be seen from Fig. 2.1, the circuit boards utilized in this thesis include A/D board DS2004, Encoder Board DS3001, Processor Board DS1006 and PWM Board DS5101, which will be introduced briefly later in this chapter. Unlike other digital systems, the program writing and debugging which are

time-consuming, are not necessary in the dSPACE system. The dSPACE offers a package of modules for Matlab/Simulink which provides an interactive environment for algorithm development and data analysis. The program can be automatically generated from the Matlab/Simulink model, which saves time and cost.

The dSPACE hardware is connected to the host PC by an optical fibre cable, which provides high communication speed (up to 100 MB/s) for the transmission of real-time data. All the data generated in the Matlab/Simulink model can be captured and monitored during the operation by the dSPACE control desk. Therefore, it is easy to debug and optimize the program. Furthermore, since enormous volumes of data can be captured and saved, Matlab/Simulink is very convenient to display and analyse the experimental performance.

The hardware boards of dSPACE are introduced briefly as follows [DSP10]:

### **2.2.1. A/D Board DS2004**

The quality of input signals is vital for any control system. For the dSPACE system utilized in this thesis, high-speed A/D Board DS2004 is employed to digitize analogue input signals at high sampling rate. The DS2004 has 16 independent A/D conversion channels, each having a separate A/D converter equipped with differential inputs. The conversion time is 800 ns per channel (1.25 MS/s/ch). The DS2004 board provides many different hardware and software-based triggering mechanisms as well as data buffers for burst data transfer. The measurement modes plus 4 external trigger inputs and extensive trigger functions enable the conversion of both single measurement values and whole sample bursts. The board buffers up to 16,384 values per channel and then transfers them to the processor board as a burst. This reduces the communication overhead and improves the overall system performance.

### **2.2.2. Encoder Board DS3001**

The DS3001 incremental encoder interface has been designed to provide precise position measurement with sensors providing digital phase information. The board comprises five independent channels each providing everything needed to connect an incremental encoder and process its output signals: a regulated encoder power supply with sense lines, differential or single-ended inputs for the encoder's two phase lines, and an index input. The signals can be either

differential RS422 or single-ended TTL.

The radian position angle can be obtained from the scaled output signal by Simulink model as follows:

$$\theta_r = 2^{21} \cdot \frac{2\pi}{N_{EL}} \cdot O_{EN} \quad (2.1)$$

Then the speed can be obtained by differentiating the position angle,

$$\omega_r = \frac{\theta_r(k) - \theta_r(k-1)}{T_s} \quad (2.2)$$

Although the rotor position is not required in the DTC methods, and both the position angle and rotor speed can be obtained by sensorless techniques, an encoder is still employed in this thesis since this research is focused on the main principles of ST-DTC and its potential improvement. No sensorless techniques are employed in this work.

### **2.2.3. Processor Board DS1006**

The DS1006 processor board is the heart of dSPACE modular hardware, which is designed for very complex, large, and processing-intensive models in high-end real-time applications. It provides the computing power for real-time system and also functions as an interface to the I/O boards and the host PC. The DS1006 is directly connectable to all dSPACE I/O boards via a Peripheral high-speed (PHS) bus. The board is built around the AMD Opteron, x86-compatible 64-bit server multi-core processor. It provides 512 kB of L2 cache per core and 6 MB of shared L3 cache. The operating frequency of the each core is 2.4 GHz. The DS1006 also has 1 GB of local memory for executing real-time models, 128 MB of global memory per core for exchanging data with the host PC, and 2 MB of on-board boot flash memory, plus an optional application flash memory on a compact flash card for automatic, host-independent, booting of real-time applications.

### **2.2.4. PWM Board DS5101**

The demands of PWM resolution and flexibility are very high in machine drive control. The DS5101 Digital Waveform Output Board can generate pulse-width modulation waveforms at

various frequencies. The DS5101 autonomously generates any TTL pulse patterns on up to 16 channels with a time resolution of 25 ns.

The output of DS5101 can be categorized as 1-phase PWM signal generation (PWM1), 3-phase PWM signal generation (PWM3), and 3-phase PWM signal generation with inverted and non-inverted outputs (PWM6). For machine drive control PWM6 is usually utilized. Two sets of PWM6 can be implemented on two three-phase drives or one dual three-phase drive.

### **2.3. Test Rigs Employed for Research**

Two PMSMs are employed for the experimental investigation. The three-phase PMSM (machine I) is used for the experimental verification in Chapters 3 and 4, while the dual three-phase PMSM (machine II) is employed in Chapters 5 to 8. The two test rigs are described in the next section. Note that they are not specially designed for the experiments implemented in this thesis. However, they are suitable for the verification of effectiveness of the proposed strategies.

#### **2.3.1. Test Rig for Machine I**

The experimental test setup consists of a DC power supply, a three-phase inverter, a dSPACE DS1006 digital controller, and a laboratory prototype of the PMSM which is intended for the safety critical applications [ISH05]. The three-phase PMSM drive system and dual three-phase drive system share the same dSPACE control system. The photo of machine I is shown in Fig. 2.2 and its parameters are given in Appendix A.

#### **2.3.2. Test Rig for Machine II**

The experimental setup consists of a DC power supply, a dual three-phase inverter, a dSPACE DS1005 digital controller, and a laboratory prototype of the dual three-phase PMSM intended for wind generation application [HU14]. The specification of machine II is given in Appendix A. The method to identify parameters of the machines is given in Appendix C. The experimental test-rig is shown in Fig. 2.3. A permanent magnet DC motor connected to an adjustable power resistor is used as a load machine coupled with the prototype dual three-phase PMSM.

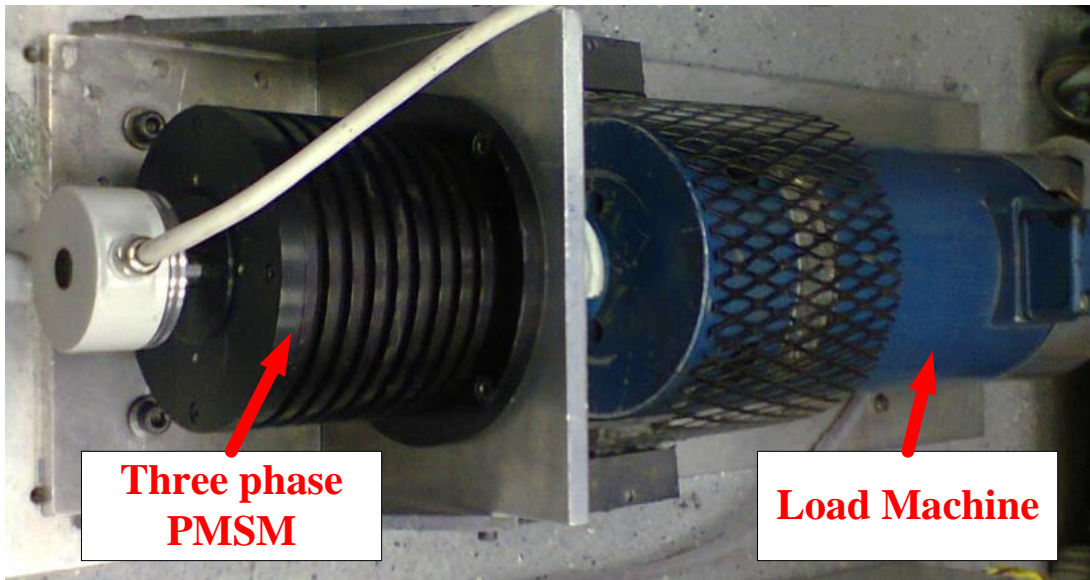
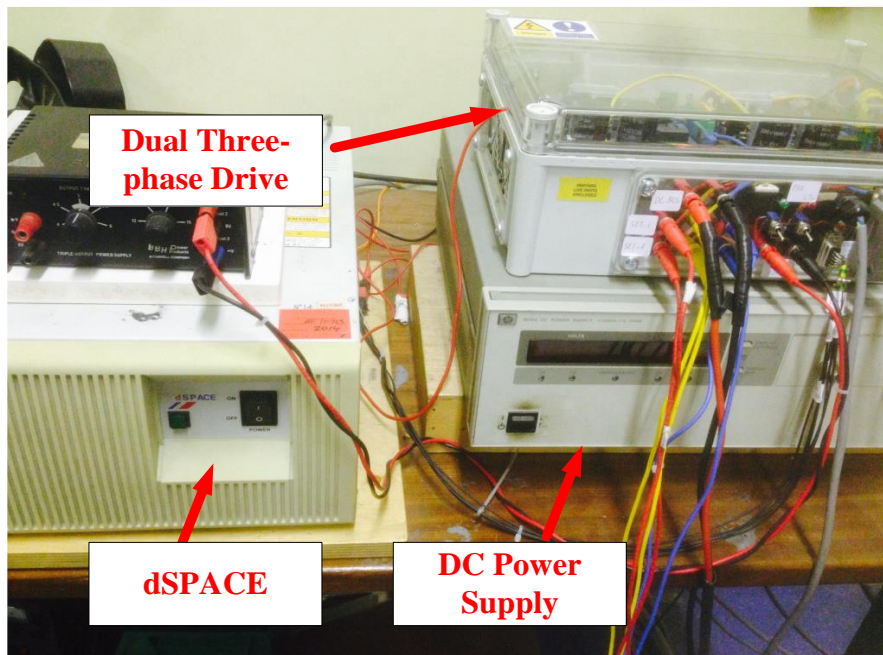
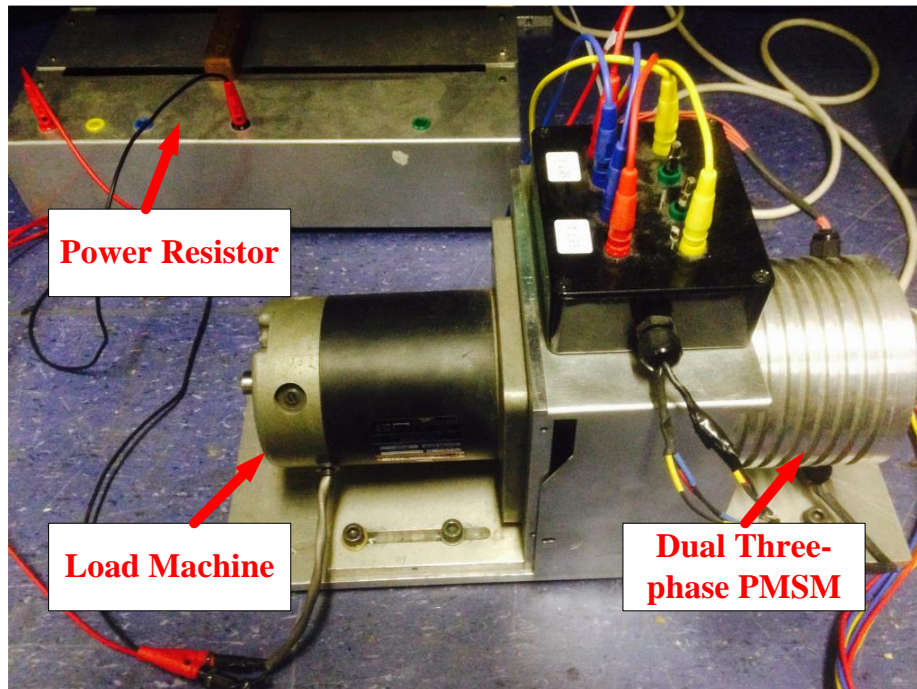


Fig. 2.2. Three-phase PMSM machine I and load machine.



(a)



(b)

Fig. 2.3. Photos of experimental test-rig: (a) Machine drive system. (b) Dual three-phase machine and load.

The dual three-phase machine drive shown in Fig. 2.4 is based on a STEVAL-IHM027V1, a 1 kW, three-phase machine control demonstration board produced by STMicroelectronics. The power module of the board is the STGIPS10K60A featuring a 600 V, 10 A IGBT intelligent power module. An interface board is used to pass the gate drive signals from the DS5101 digital waveform output board to the power inverter and to measure DC voltage and phase current and feedback the measured signals to the DS2004 high-Speed A/D board.

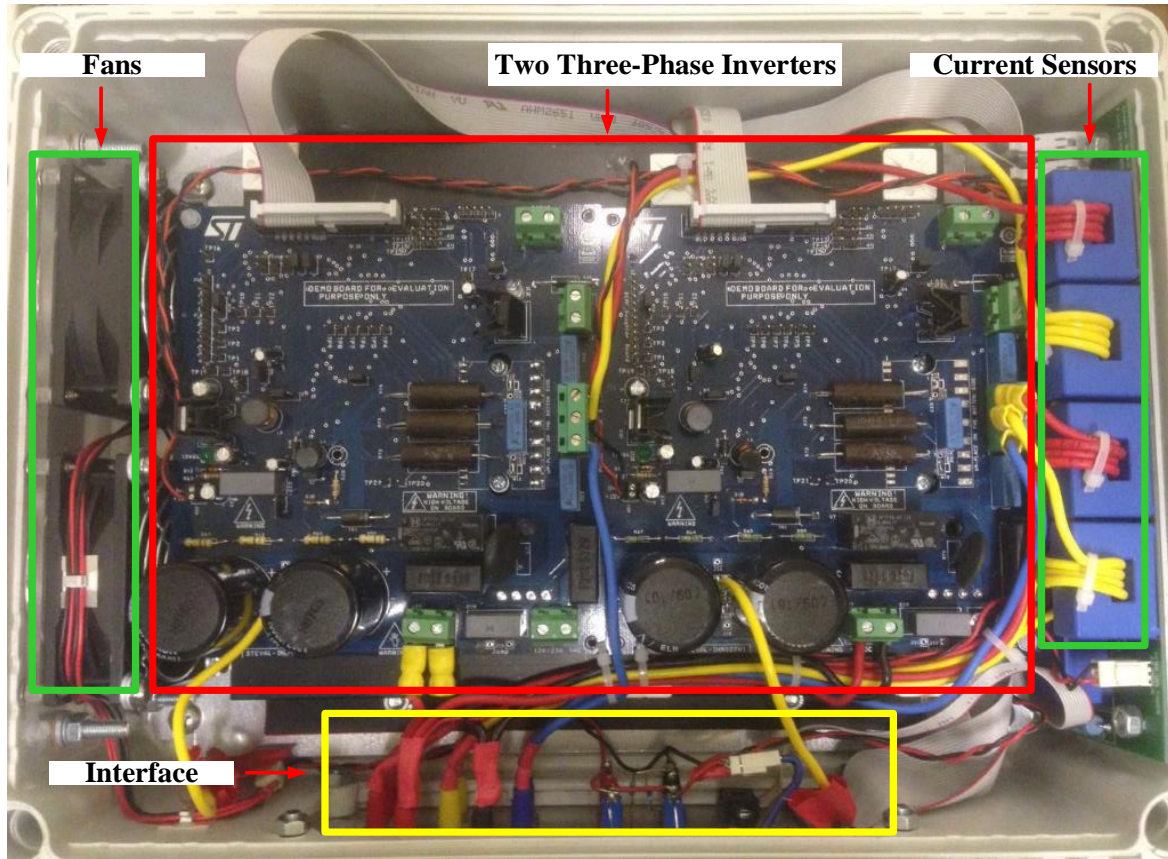


Fig. 2.4. Dual three-phase power inverters.

## 2.4. Conclusions

In this chapter, the experimental platforms for the control of three-phase PM machine and dual three-phase PM machine are briefly described.

### **3. Improved Torque Regulator to Reduce Steady-state Error of Torque Response for Direct Torque Control of Permanent Magnet Synchronous Machine Drives**

#### **3.1. Introduction**

DTC has become a powerful control scheme for AC motor drives due to its simple structure, excellent transient response and good robustness in the face of uncertain or changing rotor parameters. Hysteresis regulators are implemented in the conventional switching-table based DTC method for the regulation of both electromagnetic torque and stator flux. Compared to FOC techniques, coordinate transformations and specific modulations are not required in the DTC method. Hence, the transient torque control performance can be significantly improved [CAS02]. However, in a digital signal processor (DSP or dSPACE), no matter how advanced they are, the response of both torque and stator flux controllers will exceed the predefined hysteresis bands because of the time delay and the fixed sampling frequency leading to large torque and stator flux ripple. Furthermore, steady-state errors of torque and stator flux responses will occur as well, due to the difference between the decreasing and increasing variation rates, particularly in the torque response, as shown in this chapter. Although the steady state torque error is irrelevant in drives with closed-loop speed control. Since the motor torque must be equal to the load torque in steady state performance, then the reference for the torque will be higher. However, the error is important in torque drives that operate in torque control mode, without closed-speed speed control, such as the electric vehicle or hybrid electric vehicle applications.

Various modified DTC-based strategies which incorporate SVPWM [LAI01], [LAS04a], [TAN04], [WES09], [XU14], [ZHA11a], or divide one sampling period into several intervals have proved to be effective in improving the torque performance [CAS00], [KAN99], [KEN03], [PAC05], [ROM03], [SHY10],[ZHA11a], [ZHA11b]. However, these methods either increase the system complexity, parameter dependence and computational burden or still incur the steady-state torque error. Hu [HU11] proposed a specific asymmetric hysteresis regulator based on the power variation rate to reduce the steady-state error of active power in the direct power control method (DPC) for grid-connected DC-AC converters. However, the method is only suitable for this specific case, and a common method for general use is not given.

With the development of power electronics, fast switching devices may be employed to reduce the steady-state torque response error. However, reduction of steady-state error in torque response without increasing the switching frequency is still desirable, particularly when the operating speed and/or pole number of the machine is high (i.e. the number of switching events per electric cycle is relatively low), and/or when the power rating of the machine drive system is high and relatively low switching frequency needs to be employed in order to reduce the switching losses.

This chapter will focus on minimising the steady-state error of torque in the ST-DTC of a PMSM, but will not specifically address the torque ripple, which is reserved for the next chapter. Based on detailed analysis of the steady-state torque response error in a PMSM, a novel band-shifted torque regulator is proposed to reduce the steady-state torque response error on-line by shifting the bands of the torque regulator. An improved ST-DTC method with a band-shifted torque regulator is proposed and compared with the conventional ST-DTC under different operating conditions. This experiment is based on a dSPACE platform with a laboratory prototype of the PMSM. The experimental results validate the effectiveness of the proposed method.

## 3.2. Analysis of Steady-state Torque Response Error in PMSM DTC

### 3.2.1. Machine Equations

The surface-mounted PMSM can be modelled in a stationary reference frame as

$$\mathbf{V}_{s\alpha\beta} = R_s \mathbf{I}_{s\alpha\beta} + \frac{d\boldsymbol{\psi}_{s\alpha\beta}}{dt} \quad (3.1)$$

$$\boldsymbol{\psi}_{s\alpha\beta} = L_s \mathbf{I}_{s\alpha\beta} + \boldsymbol{\psi}_{r\alpha\beta} \quad (3.2)$$

$$\boldsymbol{\psi}_{r\alpha\beta} = \psi_f e^{j\theta_r} \quad (3.3)$$

$$T_e = \frac{3}{2} P \boldsymbol{\psi}_{s\alpha\beta} \times \mathbf{I}_{s\alpha\beta} \quad (3.4)$$

### 3.2.2. Effect of Inverter Voltage Vectors on Torque and Stator Flux Variations

Based on (3.4), the instantaneous torque variation can be expressed as

$$\frac{dT_e}{dt} = \frac{3}{2} P \left( \frac{d\psi_{s\alpha\beta}}{dt} \times I_{s\alpha\beta} + \psi_{s\alpha\beta} \times \frac{dI_{s\alpha\beta}}{dt} \right) \quad (3.5)$$

Substituting (3.1), (3.2) and (3.3) into (3.5) yields the torque variation

$$\frac{dT_e}{dt} = -\frac{R_s}{L_s} T_{e0} + \frac{3}{2} \frac{P}{L_s} (-V_{s\alpha\beta} \times \psi_{r\alpha\beta} - \psi_{s\alpha\beta} \times j\omega_1 \psi_{r\alpha\beta}) \quad (3.6)$$

Since

$$\psi_{s\alpha\beta} \times j\omega_1 \psi_{r\alpha\beta} = \omega_1 \psi_{s\alpha\beta} \cdot \psi_{r\alpha\beta} \quad (3.7)$$

The torque variation can be transposed to give

$$\frac{dT_e}{dt} = -\frac{R_s}{L_s} T_e + \frac{3}{2} \frac{P}{L_s} (-\psi_{r\beta} V_{s\alpha} + \psi_{r\alpha} V_{s\beta} - \omega_1 |\psi_{r\alpha\beta}| |\psi_{s\alpha\beta}| \cos \delta) \quad (3.8)$$

Whilst the amplitude of stator flux can be obtained as

$$\psi_s = \sqrt{\psi_{s\alpha}^2 + \psi_{s\beta}^2} \quad (3.9)$$

Differentiation of (3.9) results in the instantaneous stator flux variation as

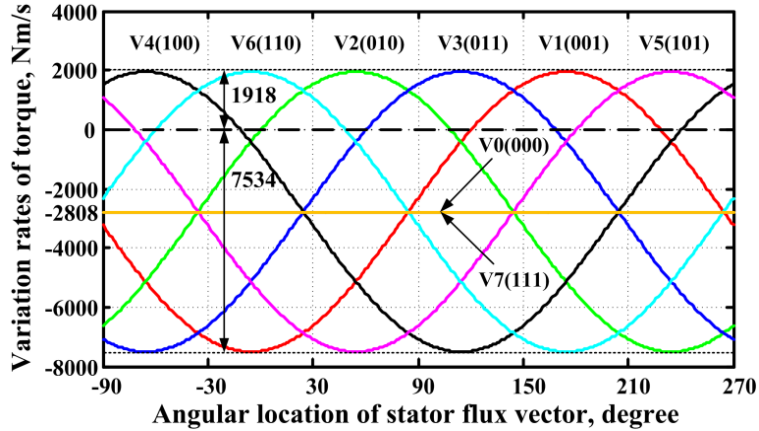
$$\frac{d\psi_s}{dt} = \frac{1}{\sqrt{\psi_{s\alpha}^2 + \psi_{s\beta}^2}} \left( \psi_{s\alpha} \frac{d\psi_{s\alpha}}{dt} + \psi_{s\beta} \frac{d\psi_{s\beta}}{dt} \right) \quad (3.10)$$

Then, by substitution of (3.1) and (3.2) into (3.10) provides the stator flux variation without the differential terms in the right hand side

$$\frac{d\psi_s}{dt} = -\frac{R_s}{L_s} |\psi_{s\alpha\beta}| + \frac{R_s}{L_s} |\psi_{r\alpha\beta}| \cos \delta + \frac{1}{|\psi_{s\alpha\beta}|} (V_{s\alpha} \psi_{s\alpha} + V_{s\beta} \psi_{s\beta}) \quad (3.11)$$

Fig. 3.1 graphically illustrates the variation rates of instantaneous torque and flux for each inverter voltage vector in six sectors which are defined in Fig. 3.1(a). The test machine parameters and control parameters are given in Appendix A.





(c)

Fig. 3.1. Stator flux and torque variation rate due to each inverter voltage vector over a range of angular locations of stator flux vector. Rated speed: 400 rpm, rated torque: 5 Nm. (a) Voltage vectors and sector division in the  $\alpha\beta$  reference frame. (b) Variation rates of stator flux. (c) Variation rates of torque.

In Fig. 3.1(b) and (c), each sine curve or straight line represents one active vector or one zero vector, respectively. When the variation rate of one vector is positive (i.e. increasing variation rate), it means that once this vector is applied, the stator flux or the torque will increase, but will decrease while the vector with decreasing variation rate is applied.

It can be seen from Fig. 3.1(b) that for the stator flux, the zero voltages can almost maintain a constant stator flux, and the increasing and decreasing variation rates of the active vectors are almost the same. However, for the torque as shown in Fig. 3.1(c), the variation rates of zero voltage vectors are -2808 Nm/s which will always decrease the torque, whilst the absolute value of maximum decreasing variation rate of the active vectors (which is 7534 Nm/s) is much larger than the maximum increasing rate (which is 1918 Nm/s).

### 3.2.3. Steady-state Error of Torque Response

The operation of the hysteresis regulator implemented in a digital signal processor is quite different from that under ideal conditions. Typical operation of the ideal hysteresis regulator and a practical discrete hysteresis regulator are illustrated in Fig. 3.2(a) and (b) respectively. In an ideal implementation, the control action is triggered immediately whenever the controlled variable

exceeds the bands. Hence, the torque ripple can be kept exactly within the hysteresis band. However, the control action in a practical discrete digital hysteresis regulator can only be applied at specific sampling instants (denoted by  $\circ$  in Fig. 3.2) due to the fixed sampling time  $T_s$ . Therefore, the controlled variable in a discrete time system will always exceed the predefined hysteresis bands where  $\blacktriangle$  denotes the band limits in Fig. 3.2. This will result in higher flux and torque ripple than in the ideal case. Since the decreasing variation rate is higher than the increasing variation rate, a steady-state error exists between the reference and the response, particularly in the torque response. Fig. 3.3 presents the experimental results of the stator flux and torque using conventional regulator, when the rotor speed reference and the stator flux reference are set to the rated speed 400 rpm, and 0.0775 Wb, respectively, and the reference torque is set as 5 Nm. The torque and flux hysteresis bands are set as  $\pm 0.0005$  Wb, and  $\pm 0.1$  Nm, respectively.

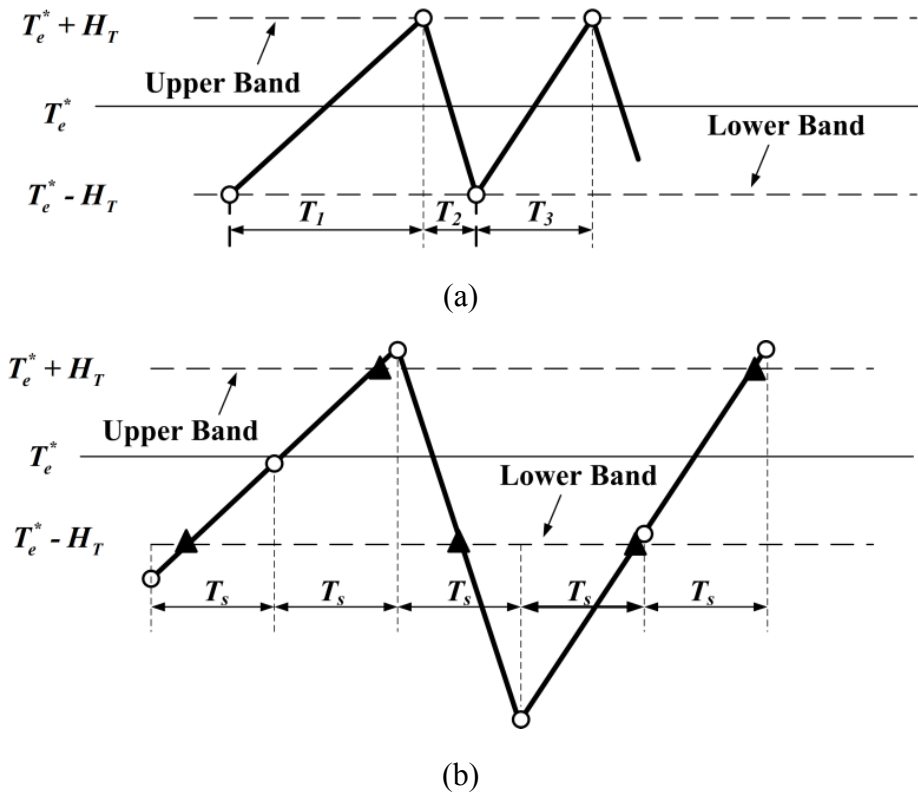
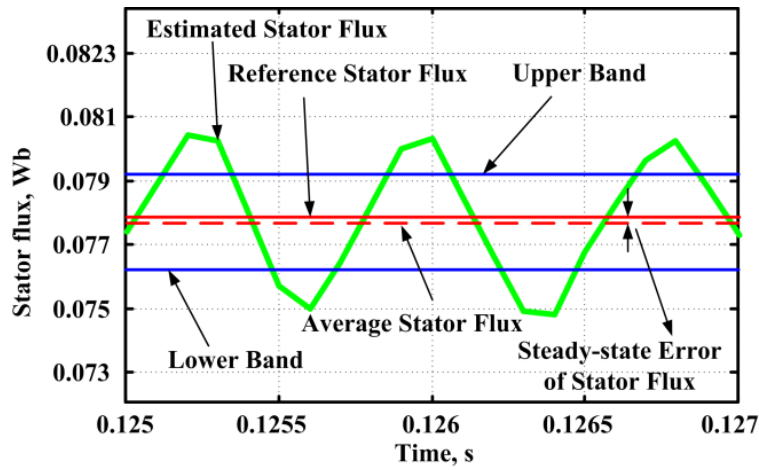
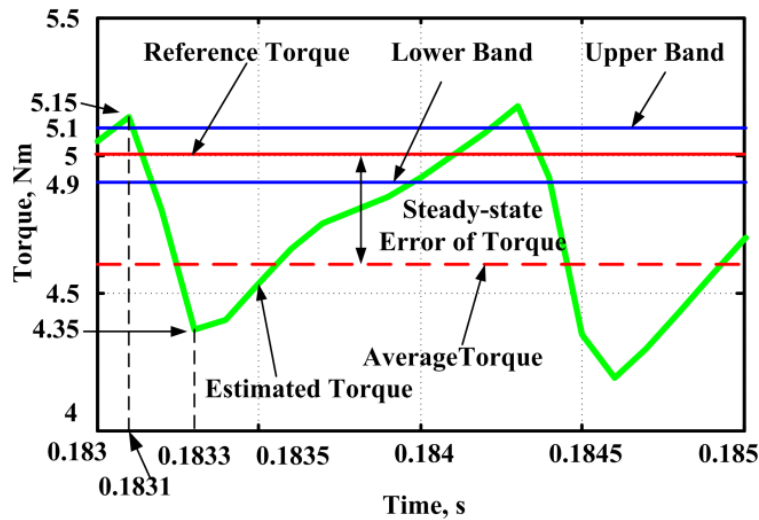


Fig. 3.2. Operation of the ideal and discrete hysteresis regulator ( $\circ$ : the instant when new sample time starts;  $\blacktriangle$ : the instant when torque hits the bands). (a) Ideal hysteresis regulator. (b) Discrete hysteresis regulator.



(a)



(b)

Fig. 3.3. Experimental results of stator flux and torque using conventional regulator. (a) Stator flux response. (b) Torque response.

For the torque response shown in Fig. 3.3(b), the torque response exceeds the lower band of hysteresis regulator much more than the upper one due to the much larger decreasing variation rate than the increasing variation rate and due to the fixed sampling time. For example, the estimated torque exceeds the upper band slightly (around 0.05 Nm) at 0.1831 s. At 0.1833 s the torque exceeds the lower band by approximately 0.55 Nm due to its larger torque decreasing variation rate as shown in Fig. 3.1(c). The variation rate is much larger than the upper case resulting in significant steady-state error in the torque response.

For the flux response shown in Fig. 3.3(a), although the instantaneous flux also exceeds its hysteresis bands due to the fixed sampling time, the average flux can still follow its reference with a small steady-state error because of similar decreasing and increasing variation rates of the vectors for stator flux.

If the sampling frequency is large enough, the performance of a discrete hysteresis regulator will approach the ideal performance. However, this requires an expensive high speed digital processor and A/D converter. Limitations may also be imposed by switching losses and the maximum switching frequency of the power semiconductors. Therefore, reduction of steady-state error in torque response without increasing the switching frequency is also desirable.

This chapter aims to minimize the steady-state error of torque response. The steady-state error of the flux is usually not a problem, as confirmed by experimental results. Therefore, the control method of flux in the new controller is the same to that of the conventional ST-DTC. An improved voltage model based on a low-pass filter [HIN03], [ZHA11a] is employed to estimate the stator flux and torque.

### 3.3. New ST-DTC Method Using Proposed Band-shifted Torque Regulator

The steady-state torque response error always exists in the conventional ST-DTC method implemented in a digital signal processor. Since the only variable that can be adjusted is the bands, it is meaningful to investigate the effect of the bands on the performance of conventional ST-DTC method.

From (3.8), it can be seen that the derivation of torque in one sampling period consists of three parts:

$$\frac{dT_e}{dt} = K_1 + K_2 + K_3 \quad (3.12)$$

where

$$K_1 = -\frac{R_s}{L_s} T_e \quad (3.13)$$

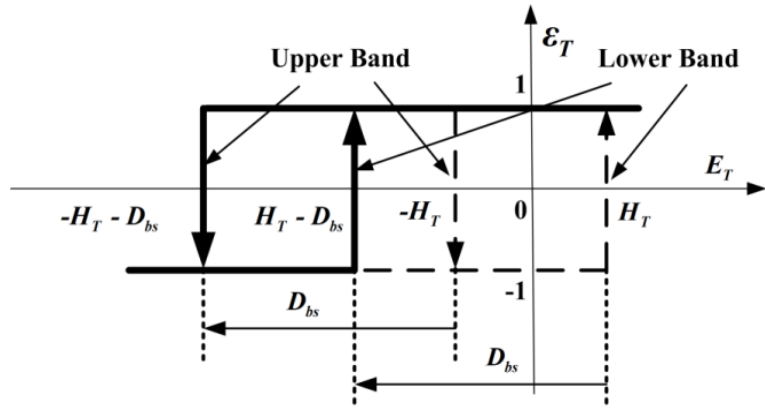
$$K_2 = -\frac{3}{2} \frac{P}{L_s} \omega_1 |\psi_{r\alpha\beta}| |\psi_{s\alpha\beta}| \cos \delta \quad (3.14)$$

$$K_3 = \frac{3}{2} \frac{P}{L_s} (-\psi_{r\beta} V_{s\alpha} + \psi_{r\alpha} V_{s\beta}) \quad (3.15)$$

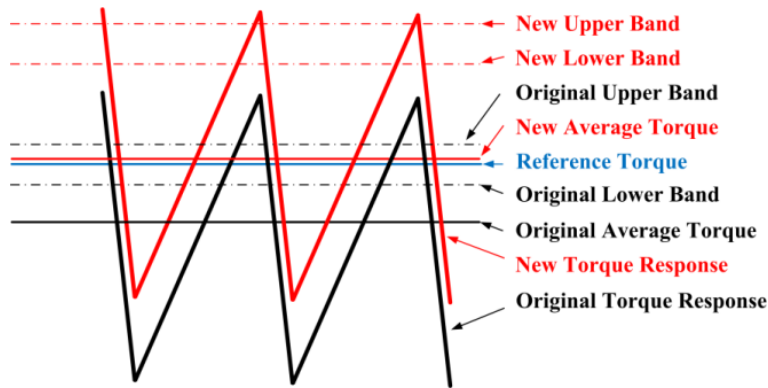
$K_1$  and  $K_2$ , which are proportional to the torque and rotor speed, respectively, are always negative, whereas the third contribution  $K_3$  which reflects the real effect caused by the inverter voltage vector is a sinusoidal component whose average value over one sampling period is zero. Therefore, the average decreasing variation of torque is always larger than the average increasing one.

The output average torque is the average of the effect of all the vectors that are employed in the control process. Hence, when using a conventional symmetrical torque hysteresis regulator, the average output torque is usually smaller than the reference, and the difference depends on the operating conditions. Therefore, shifting both upper and lower bands to raise the average torque is a feasible solution for minimising the steady-state error of torque response, Fig. 3.4(a). The band width is kept the same to keep the same control accuracy. The original upper band,  $-H_T$ , is modified to,  $-H_T - D_{bs}$ , and the lower band is changed from,  $H_T$ , to,  $H_T - D_{bs}$ , as shown in Fig. 3.4(b).

The shifted distance,  $D_{bs}$ , plays a significant role in the performance of the proposed torque regulator and corresponds to the steady-state error of torque response. Owing to the variation of steady-state error of torque response under different operating conditions, the shifted distance,  $D_{bs}$ , cannot be a single value. On the contrary, it should be optimised on-line under continuously varying operating conditions.



(a)



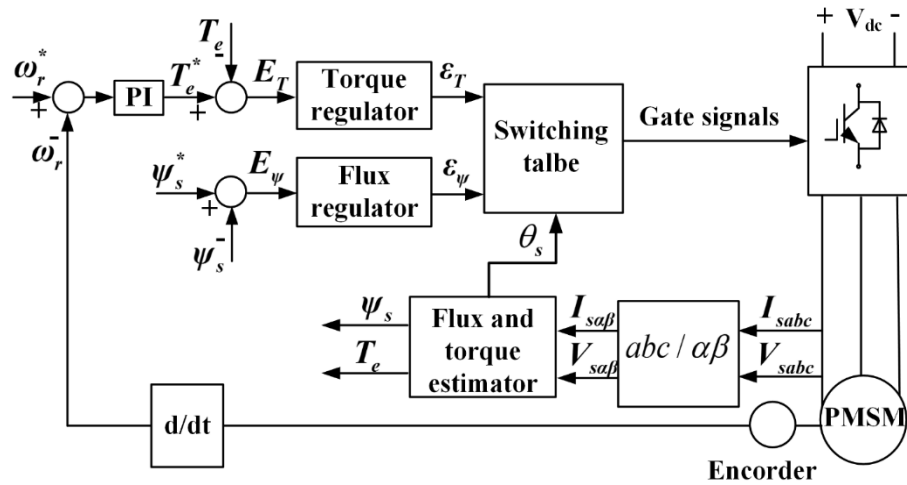
(b)

Fig. 3.4. Illustration of conventional and proposed torque regulator. (a) Band- shifted torque regulator. (b) Improvement by using band shifted torque regulator.

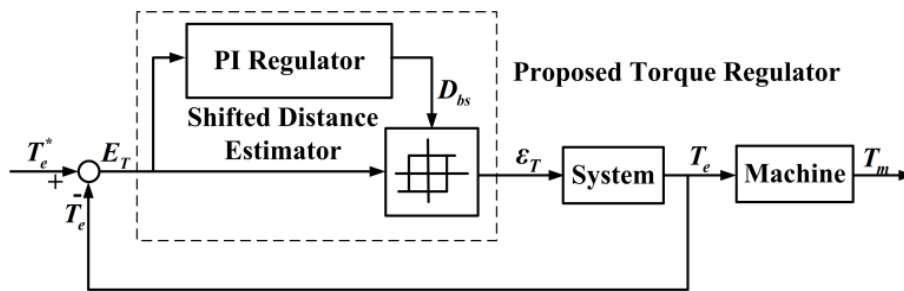
Consequently, a shifted distance estimator is proposed and illustrated in Fig. 3.5. At each sampling instant, the torque difference between the estimated and reference torques can be calculated. Then, the shifted distance,  $D_{bs}$ , which corresponds to the average output torque error can be obtained by the shifted distance estimator. Numerous methods can be adopted to implement the shifted distance estimator and, for simplicity, a PI regulator is adopted here, Fig. 3.5(b). After the band shifted distance estimator reaches to steady-state, the output error could be fully minimised.

Conventional transfer function analysis cannot be applied here due to the non-linearity both in the switching table and the hysteresis regulator. Hence, the PI regulator gains cannot be determined by systematic methods. Since the output of the PI regulator only increases the accuracy of the hysteresis regulator to reduce the steady-state error of torque response, both the steady-state and

dynamic performance of torque response are not be significantly influenced by the parameters of the PI regulator. If the appropriate parameters for the PI regulator are used, the effectiveness of the proposed methods will be improved. On the one hand, since the instantaneous torque error  $E_T = T_e^* - T_e$  is very large,  $K_{p\_SDE}$  should be small enough in order to obtain the nearly constant value of  $D_{bs}$ , to avoid a large peak in torque ripple. On the other hand,  $K_{i\_SDE}$  will influence the tracking rate of the average torque in the torque transient process. Therefore,  $K_{i\_SDE}$  should be large enough while keeping constant  $D_{bs}$ . Once the PI parameters of the shifting distance estimator are adjusted appropriately, the steady-state torque error will approach zero and the tracking rate of the average torque will be maximised. A small improvement in the torque ripple and average commutation frequency are achieved. This is confirmed by the detailed experimental results in section 3.4.



(a)



(b)

Fig. 3.5. Control diagram of proposed ST-DTC method of PMSM. (a) Conventional control diagram of ST-DTC method of PMSM. (b) Proposed torque regulator for ST-DTC.

For this particular improved controller design, the PI controller for band adaptation also suffers

from one-step delay due to the digital implementation. However, the steady-state error of torque response is the important metric, rather than the instantaneous torque error. The steady-state torque response error is almost constant under the same operating conditions. Therefore, the reduction of the steady-state error of torque response in steady-state will not be influenced by the delay. This is shown in Fig. 3.6 and Fig. 3.7 and Table 3.1.

Since the proposed torque regulators only focus on the steady-state error compensation, it will not deteriorate the performance of stator flux, THD, or the dynamic torque response. This will be shown later by experiments. Noted that:

(a) Since the reference torque which is generated by the PI control of speed loop is just an intermediate variable in the practical experimental system, the reference torque in the conventional DTC is slightly larger than that in the proposed method, and the average torque and the fundamental components of currents in the two methods are nearly the same. Therefore, it is still reasonable to do the THD comparison in this chapter.

(b) In DTC strategies, the switching frequency changes with the operating conditions. Therefore, in this chapter the total switching losses are estimated using the average commutation frequency,  $f_{av}$ . The average commutation frequency is calculated by counting the total commutation events of one phase leg during a fixed period, [ZHA11a].

(c) Although the analysis is based on the surface PMSM, the conclusion are also suitable for the interior-PMSM: the decreasing and increasing variations of torque are still significantly different because of the existence of two offsets:  $K_1$  which is proportional to torque and  $K_2$  which is proportional to speed, especially under high speed and heavy load conditions. Therefore, the proposed method is also applicable for the interior PMSM DTC systems.

### **3.4. Experimental Results**

Several experiments have been carried out on a dSPACE platform with the laboratory prototype of the three-phase permanent magnet synchronous machine, machine I. The overall control scheme with conventional and improved torque regulators shown in Fig. 3.5 is implemented in dSPACE. The sampling frequency is 10 kHz, and the DC-Bus voltage is 45 V. The PI parameters of the shifting distance estimator are  $K_{p\_SDE} = 0.1$ ,  $K_{i\_SDE} = 20$ . The one-step delay caused by the digital

implementation in dSPACE is not compensated for the sake of simplicity.

### 3.4.1. Steady-state Performance of the New DTC Method Using the Proposed Band-Shifted Torque Regulator

Fig. 3.6 compares the results of DTC method with the conventional and proposed torque regulators. The rotor speed reference and stator flux reference are set to rated speed 400 rpm, and 0.0775 Wb, respectively, and the reference torque is set as 5 Nm. The torque and flux hysteresis bands are set as

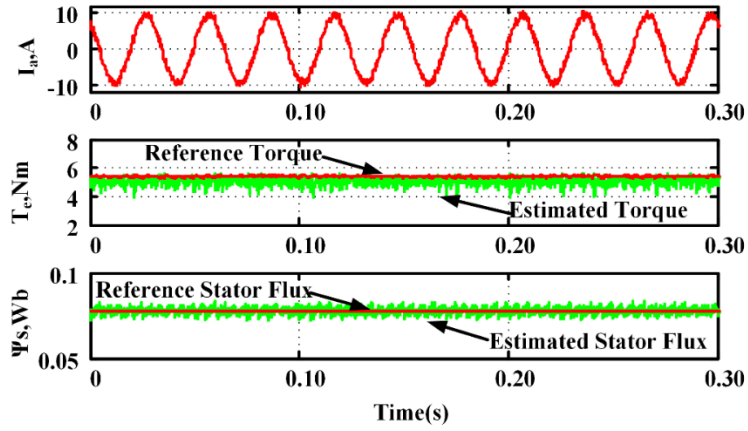
$$\pm H_{\psi} = \pm 0.0005 \text{ Wb}, \pm H_T = \pm 0.1 \text{ Nm} \quad (3.16)$$

As shown in Fig. 3.6, the average stator flux can follow the reference in both conventional and proposed strategies. However, a steady-state error of torque response exists in the DTC using the conventional torque regulator. This error is significantly reduced by using the proposed torque regulator. Detailed quantitative results are given in Table 3.1, where the torque and stator flux ripple is calculated as

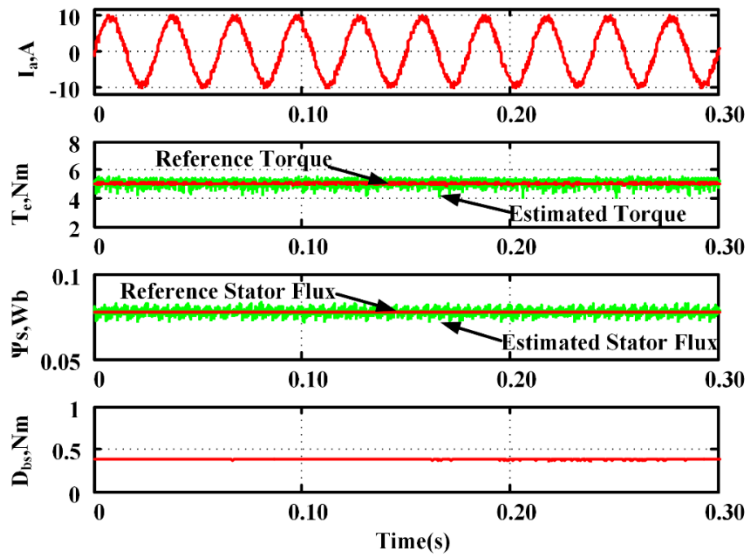
$$T_{e\_ripple} = \sqrt{\frac{1}{n} \sum_{i=1}^n (T_{e\_i} - T_{e\_av})^2} \quad (3.17)$$

$$\psi_{s\_ripple} = \sqrt{\frac{1}{n} \sum_{i=1}^n (\psi_{s\_i} - \psi_{s\_av})^2} \quad (3.18)$$

where  $T_{e\_i}$  and  $\psi_{s\_i}$  are the instant values of torque and stator flux, respectively.  $T_{e\_av}$  and  $\psi_{s\_av}$  are the average values of torque and stator flux, respectively.



(a)



(b)

Fig. 3.6. Steady-state performance of DTC using different torque regulators. (a) Conventional torque regulator. (b) Proposed band-shifted torque regulator.

From Table 3.1, the steady-state error of torque response in the proposed ST-DTC method is less than 0.1%, which is a considerable improvement compared to the conventional ST-DTC method where the error is greater than 7.5%. The ST-DTC method using a band-shifted torque regulator also has small improvement in both the torque ripple and the average commutation frequency compared to the conventional ST-DTC method. There is a slight increase in the THD of stator currents, however. The comparison of minimum and maximum values of torque for the conventional and proposed methods shows that the average torque ripple and the peak-peak torque

ripple have been slightly decreased. For the stator flux, the proposed ST-DTC method has almost the same performance as the conventional ST-DTC method.

Table 3.1 Steady-state Performance of Different DTC Strategies.

400 rpm, 5 Nm	Conventional	Proposed
Steady-state stator flux error, $ \Delta\psi_s $ (%)	0.2361	0.2702
Steady-state torque response error, $ \Delta T_e $ (%)	<b><u>7.5105</u></b>	<b><u>0.0086</u></b>
Stator flux ripple, $\psi_{s\_ripple}$ (Wb)	$20.35 \times 10^{-4}$	$20.56 \times 10^{-4}$
Torque ripple, $T_{e\_ripple}$ (Nm)	0.2649	0.2378
THD of phase-a current, $i_{a\_THD}$ (%)	4.30	4.84
Band-shifted distance, $D_{bs}$ (Nm)	NA	0.3768
Average commutation frequency, $f_{av}$ (kHz)	1.715	1.6304
Minimum torque, $T_{e\_min}$ (Nm)	3.92	4.08
Maximum torque, $T_{e\_max}$ (Nm)	5.65	5.53

The performance of DTC strategies with the conventional and proposed torque regulators are also compared under different operating conditions. Fig. 3.7(a) shows the estimated steady-state torque error and torque ripple and average commutation frequency under the same load torque, 2 Nm, and different rotor speeds from 100 rpm to 400 rpm. Fig. 3.7(b) illustrates these experimental results under the same rotor speed, 400 rpm over a range of load torque from no-load to rated load. The steady-state torque response error can be reduced significantly by the proposed DTC strategy under a wide range of speed and load conditions. The reduction of average commutation frequency is an addition advantage, which results in the similar value of both noise and inverter commutation loss as in conventional DTC. Although the torque ripple is slightly reduced with the proposed strategy, it still leaves a notable torque ripple (approximately 5% of rated torque) especially at the rated load condition. However, it is still desirable to reduce the steady-state torque error without increasing the switching frequency in situation where the torque ripple is not a key design parameter.

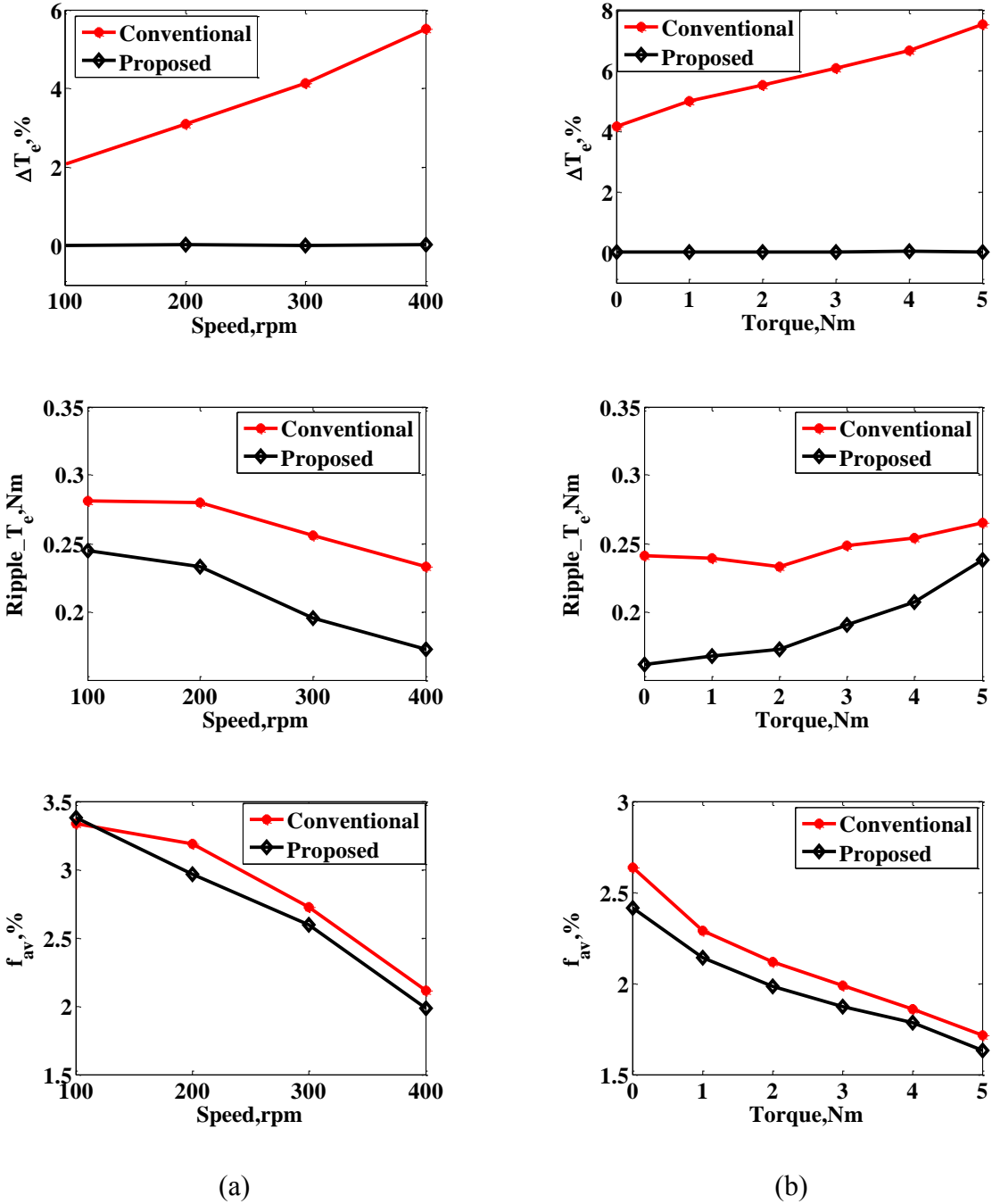


Fig. 3.7. Comparison of steady-state errors of torque, torque ripple and average commutation frequency for different DTC strategies. (a) Under the same load torque (2 Nm) and different rotor speeds. (b) Under the same rotor speed (400 rpm) and different load torque.

### 3.4.2. Steady-state and Dynamic Performance of Inner Torque Loop Control

The band-shifted torque regulator is used to minimise the steady-state error of torque response

on-line. However, the data in Fig. 3.6 and Fig. 3.7 are all obtained with an outer speed control loop. The additional speed controller may disturb the actual performance of the proposed torque regulator. Therefore, the steady-state performance of torque without speed controller, i.e. with torque controller only, for both conventional and proposed ST-DTC strategies is presented in Fig. 3.8. This is even much more important since it has been presented in introduction part of this chapter that, the steady state error of torque is vital in torque drives that operate in torque control mode, without closed-speed speed control. For the conventional ST-DTC method, the average torque is much lower than the reference torque, whereas for the proposed ST-DTC method, the average torque and the reference torque are nearly the same, which means that the steady-state torque response error is significantly reduced by using the proposed torque regulator.

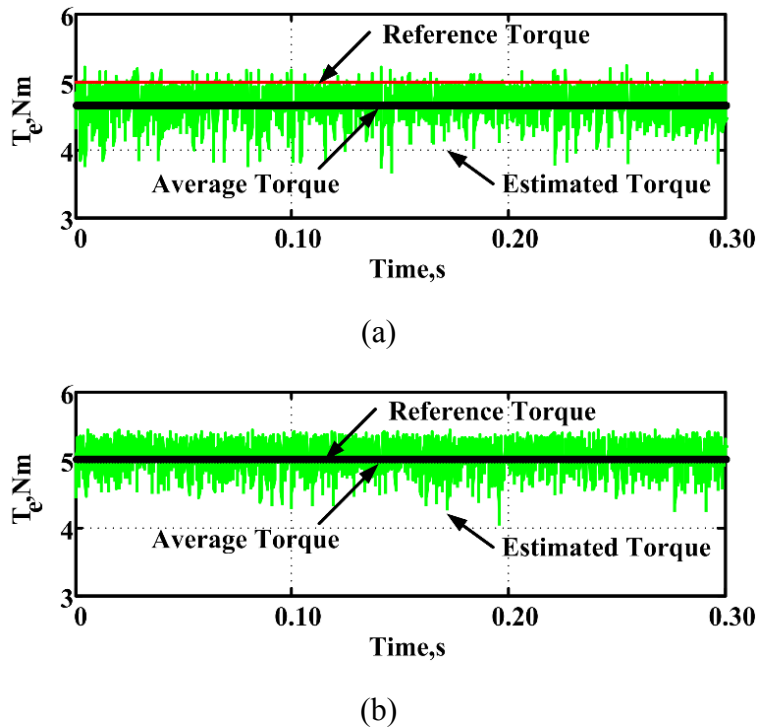


Fig. 3.8. Steady-state performance of inner torque loop control using different torque regulators: reference torque: 5 Nm. (a) Conventional ST-DTC method. (b) Proposed ST-DTC method.

Fig. 3.9 shows the dynamic response of torque when torque reference changes from 2 Nm to -2 Nm, with open-loop speed control. With appropriate values of PI parameters for the shifting distance estimator, the steady-state error of torque response can be reduced to nearly zero in a very short time ( $< 1$  s). The instantaneous torque response fall time is around 0.8 ms under transient

conditions. This is similar to the conventional ST-DTC. Therefore, the proposed torque regulator does not deteriorate the dynamic torque performance.

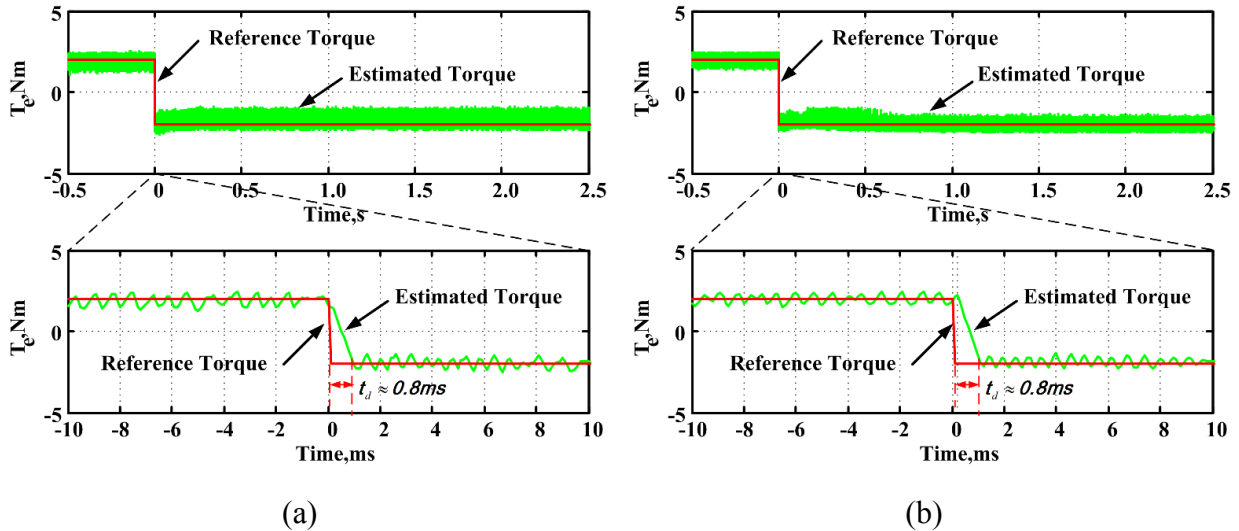


Fig. 3.9. Dynamic performance of inner torque loop control using different torque regulators: reference torque: 2 Nm to -2 Nm. (a) Conventional ST-DTC method. (b) Proposed ST-DTC method.

### 3.4.3. Dynamic Responses to External Load Disturbance

The response to an external load disturbance is compared for the conventional ST-DTC and for the proposed method using the band-shifted torque regulator. The motor is initially operated under steady-state with a speed of 400 rpm and no load. The rated external load is suddenly added at 0.5 s in Fig. 3.10. The torque generated with the new method follows the reference produced by speed regulator as well as the conventional one. The speed in both the conventional and proposed strategy reverts to the set point value in less than 0.2 s. The proposed ST-DTC method preserves the robustness against external load disturbance as well as the conventional ST-DTC.

### 3.4.4. Conclusions

The steady-state error of torque is very important in motor drives especially with only torque controller, without closed-loop speed controller. This chapter analysed the steady-state error of torque in the conventional ST-DTC method for three-phase PMSM drives. A new band-shifted torque regulator has been proposed to minimise the steady-state error of torque response. The

experimental results have verified that the proposed method using the band-shifted torque regulator can significantly reduce the steady-state error of torque response over a wide range of operating conditions. A slight reduction in torque ripple and average commutation frequency is achieved. Average commutation frequency is a metric of switching losses the switching losses. The merits of the conventional ST-DTC including: simple structure and excellent transient response are still preserved.

Although the analyses and experiments in this chapter are based on the DTC of three-phase PMSM drives, the proposed torque regulator can also be extended for general use and could be applied to other fields or machines that would benefit from hysteresis-based direct torque and power control strategies exhibiting the same problem of steady-state error due to the significant difference between the increasing and decreasing variation of the torque/active power.

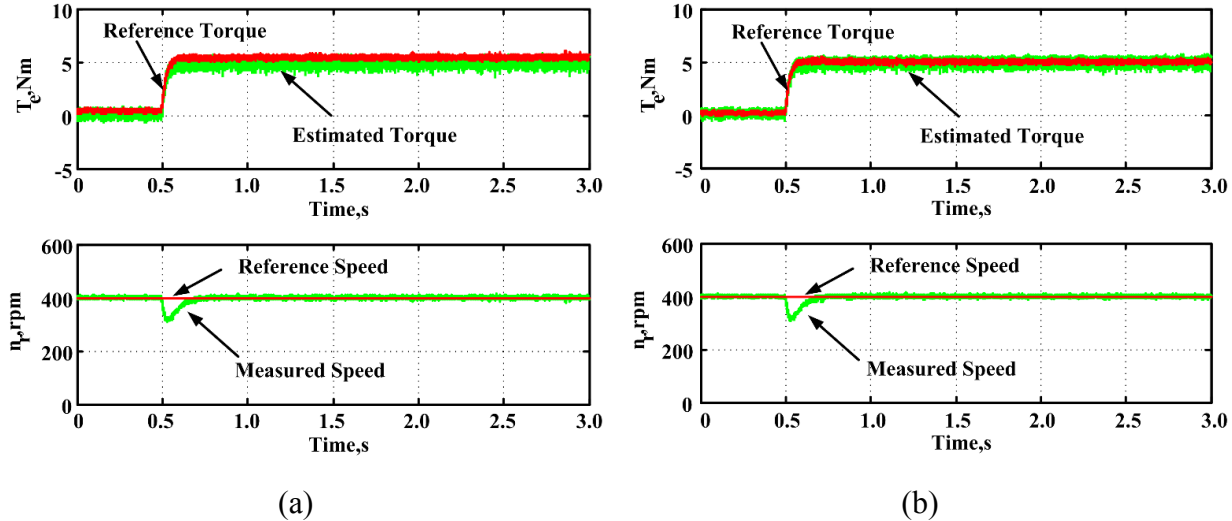


Fig. 3.10. Response to external disturbance for different ST-DTC strategies. (a) Conventional ST-DTC method. (b) Proposed ST-DTC method.

## **4. Direct Torque Control of Permanent Magnet Synchronous Machine Drives with a Simple Duty Ratio Regulator**

### **4.1. Introduction**

The conventional DTC scheme uses hysteresis regulators and a switching table for the control of the stator flux and electromagnetic torque [AMB04], [KAN01], [MAT13]. Compared to the FOC scheme, DTC does not require current regulators, coordinate transformations or specific modulation. Hence, the transient torque control performance of DTC is significantly better than that of FOC. However, the operation of the hysteresis regulator implemented in a digital signal processor (DSP or dSPACE) is quite different from that of the ideal condition -both torque and stator flux will exceed their predefined hysteresis bands due to the fixed sampling frequency and the time delay which is caused by the data processing. Therefore, undesired torque and stator flux ripples will occur, as well as the steady-state error of torque [AMB04], [KAN01].

To solve these problems, various modified DTC-based schemes have been proposed. Among them is the DTC incorporating SVPWM, which has been shown to be an effective scheme for reduction of torque ripple [LAI01], [LAS04a], [LAS04b], [TAN04], [WES09], [XU14]. Another popular method is predictive direct torque control (P-DTC) which calculates the system variables one step in advance to obtain the optimized inverter voltage vectors [BEE10], [CAP13], [HAO12], [MIR09]. Despite the better performance of SVM-DTC and P-DTC, the parameter dependence, system complexity and computational burden are increased. It is desirable to obtain improved performance while maintaining the simplicity and robustness of conventional ST-DTC if possible.

Another sort of modified ST-DTC scheme, is to divide one sampling period into several intervals. This sort of scheme does not incorporate a transformation to a rotating reference frame. The duty ratio of the active vector are obtained based on various optimizations, such as equalizing the mean torque with its reference value over one sampling period [PAC05], torque-ripple minimum [KAN99], [SHY10], fuzzy-logic adaptation [ROM03], and discrete-SVM [CAS00]. These improved methods achieve better steady-state performance, but rely heavily on the motor parameters, and are also complex. A simple duty determination method to reduce the torque and stator flux ripple is proposed. However, due to only one duty determination being used under different speed and torque conditions, a significant steady-state error of torque always exists. There

is no simple, analytical solution to obtain the key control parameters yet [ZHA11a], [ZHA11b], [ZHA11c].

This chapter aims to improve the torque performance in the ST-DTC method, while preserving the merits of conventional ST-DTC, such as simple structure and excellent transient response. Based on the analysis of instantaneous variation rates of stator flux and torque of each converter output voltage vector, a simple and effective method, which takes the effect of machine angular velocity into account, is proposed to obtain the duty ratio. A simple way to select the key control parameters is introduced. Then the operating principle and features of the proposed method will be analysed. This improved ST-DTC method with the proposed duty ratio determination will be compared with the conventional ST-DTC and two existing duty-based ST-DTCs under different operating regions on a dSPACE platform with a prototype PM machine. The experimental results validate the effectiveness of the proposed duty-based ST-DTC method.

## **4.2. Analysis of Steady-State Performance in PMSM DTC**

### **4.2.1. Direct Torque Control Principle**

According to the principle of conventional ST-DTC, the inverter switching signals are generated by using a switching table. Stator flux and torque can be controlled directly and independently by properly selecting the inverter voltage vectors, which can be represented, in the three-phase systems, by six active voltage vectors and two zero voltage vectors, Fig. 4.1.

By way of example, the operating principle of a conventional ST-DTC is presented in Fig. 4.1. When the stator flux vector is located in sector 1 and rotates anticlockwise, torque increases if voltage vectors with positive quadrature component are applied ( $V_2$  or  $V_3$ ), and decreases if vectors with negative quadrature component are applied ( $V_5$  or  $V_6$ ). At the same time, the stator flux magnitude increases if vectors with positive direct component are applied ( $V_2$  or  $V_6$ ), and decreases if vectors with negative direct component are applied ( $V_3$  or  $V_5$ ). A switching table for sector 1 can be deduced as shown in Table 4.1.



torque and stator flux will exceed the predefined hysteresis bands. This results in undesirable torque ripple and stator flux ripple. These vectors only cause partial variation of the torque and stator flux. In a practical system both the machine angular velocity and the load torque will also affect the variation of the torque and stator flux. This effect will be investigated in the following section.

#### 4.2.2. Analysis of Torque and Stator Flux Variations

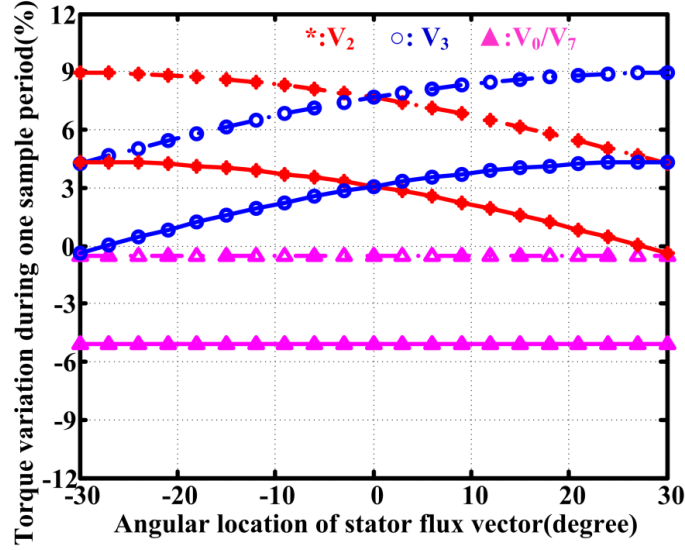
As deduced in chapter 3, for a surface-mounted PMSM, the instantaneous torque variation can be obtained and expressed as

$$\frac{dT_e}{dt} = -\frac{R_s}{L_s} T_{e0} + \frac{3}{2} \frac{P}{L_s} (-\psi_{r\beta} V_{s\alpha} + \psi_{r\alpha} V_{s\beta} - \omega_1 |\psi_{r\alpha\beta}| |\psi_{s\alpha\beta}| \cos \delta) \quad (4.2)$$

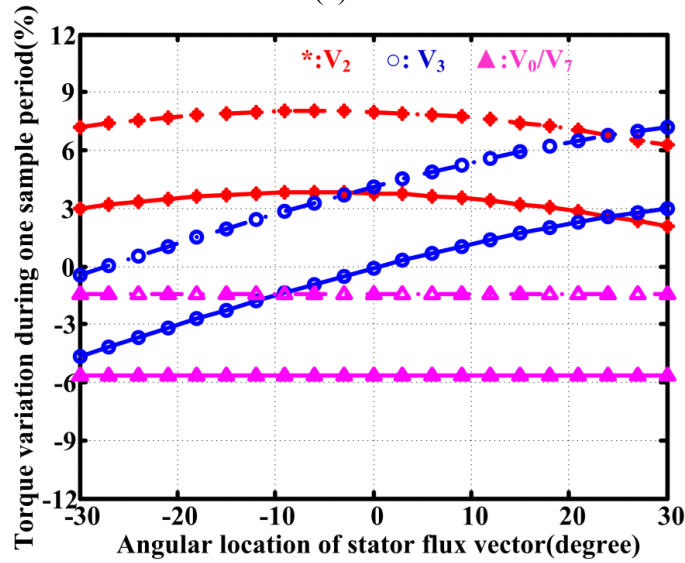
where  $T_{e0}$  is the torque value at current instant.

In order to investigate the torque variation over different operating regions, computation of (4.2) under different stator flux angular velocity, machine angular velocity and load conditions leads to the torque variations of Fig. 4.2 [AMB04], for the stator flux vector in sector 1 and sampling period  $T_s = 100 \mu\text{s}$ . When considering the variation of torque over each sampling period, the change of flux vector position in one sampling period is not considered.

The variations as a percentage of the rated torque, are very large and this partially explains the high torque ripple exhibited by the conventional ST-DTC technique when the voltage vectors operate over the whole sampling period. Fig. 4.2 shows that the torque variations are greatly influenced by the machine angular velocity and, to a lesser extent, by the load torque. In particular, during high speed operation the torque variations are modified substantially compared to their ideal operation. The key modifications are as follows: (a) From -30 degree to 0 degree, the torque variation produced by  $V_3$  is negative instead of positive, i.e., it is opposite to the voltage vector demand; (b) The torque decreasing variation produced by the zero vectors along the entire sector is noticeable.



(a)



(b)

Fig. 4.2. Torque variation versus stator flux vector position at (a) no load, and (b) full load. (dashed line: machine angular velocity  $\omega_l = 10\% \omega_N$ , solid line: machine angular velocity  $\omega_l = 100\% \omega_N$ )

### 4.2.3. Reasons for Deterioration of Steady-state Performance of Torque

Unsatisfactory steady-state performance of torque is influenced by three main factors: (1) the selected voltage vectors are applied during the whole sampling period; (2) the average decreasing

variation rates of the active vectors are much larger than the average increasing variation rates; (3) at some high machine angular velocity and heavy load torque regions, the torque variations caused by the selected voltage vector would be opposite to the voltage demand. An improved DTC should diminish the effects brought by these factors.

The one-step delay and the inherent delay in the dSPACE PWM unit also deteriorates the steady-state response of the torque [AMB04], [HAO12]. However, in the dSPACE DS 1006 used in this chapter, there is only a 25 ns inherent delay and its influence is negligible since it is very small compared to  $1 \times 10^5$  ns for one-step sampling delay. To eliminate the effect of the one-step delay would cause more computational burden and at the same time would make the method machine parameters and control parameters dependent, which should be avoided.

### 4.3. New DTC Methods to Improve the Torque Performance

From the above analyses, the main reasons causing torque ripple is that only one voltage vector is used during one sampling period and the effect of machine angular velocity is neglected. Many modified techniques have been presented to ameliorate this problem [BEE10], [CAP13], [CAS00], [KAN99], [KEN03], [LAI01], [LAS04a], [PAC05], [ROM03], [SHY10], [TAN04], [WES09], [XU14]. However, these methods either increase the system complexity, parameter dependence and computation burden, or cannot achieve desirable performance over the whole operating envelope. In this chapter a simple duty ratio determination method based on the principle of RMS torque ripple [KAN99] is proposed by taking the effect of machine angular velocity into account.

Kang [KAN99] aims to make the RMS torque ripple  $T_{e\_ripple}$  during the sampling period  $T_s$  minimal, as shown in Fig. 4.3.

$$T_{e\_ripple}^2 = \frac{1}{T_s} \int_{kT_s}^{(k+1)T_s} (T_e^* - T_e)^2 dt \rightarrow \min \quad (4.3)$$

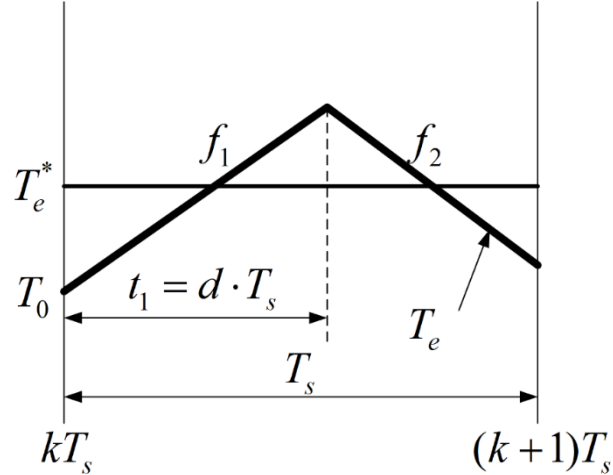


Fig. 4.3. Typical method of duty determination.

With a small  $T_s$ , slopes  $f_1$  and  $f_2$  which represent instantaneous torque variation can be considered to be constant during the duration of  $T_s$  because the dynamics of flux and speed are slow by comparison.

Therefore, the time duration of the active vector can be obtained as

$$t_1 = \frac{2(T_e^* - T_0) - f_2 T_s}{2f_1 - f_2} \quad (4.4)$$

The torque ripple can be reduced by using this accurate duty ratio determination. However, this method will inevitably not only increase the system complexity and computational burden, but also introduce parameter dependence. Furthermore, it is more seriously affected by the one-step delay, due to its parameter dependence, which has been analysed in detail and confirmed by simulation in [ZHA11a].

To suppress these drawbacks, a simpler method is desirable which is robust to parameter variations while taking the effect of machine angular velocity into account.

Fig. 4.2 shows that the torque variation is greatly influenced by the machine angular velocity and to a lesser extent by the load torque. The effect of instantaneous torque on the torque variation is ignored in this chapter for simplicity. The reduction of the torque variations is almost proportional to the increment of the machine angular velocity, which also can be found in (4.2) when the load is kept unchanged.

Therefore, when  $\varepsilon_T = 1$ , which means the torque should be increased, the torque variations of active vector  $f_{1+}$  and zero vector  $f_{2+}$  can be assumed as

$$\begin{cases} f_{1+} = f_0 & , \omega = 0 \\ f_{1+} = k_1 f_0 & , \omega = \omega_N \end{cases} \quad (4.5)$$

$$\begin{cases} f_{2+} = 0 & , \omega = 0 \\ f_{2+} = (k_1 - 1)f_0 & , \omega = \omega_N \end{cases} \quad (4.6)$$

where  $f_0$  is the torque variation when machine angular velocity is zero;  $k_1$  is the ratio of the torque variation at rated machine angular velocity to that at zero speed.

Then, the universal expressions of  $f_{1+}$  and  $f_{2+}$  thus can be obtained as

$$f_{1+} = f_0 + \frac{f_0(k_1 - 1)\omega}{\omega_N} \quad (4.7)$$

$$f_{2+} = \frac{f_0(k_1 - 1)\omega}{\omega_N} \quad (4.8)$$

By substituting (4.7) and (4.8) into (4.4), the time duration of the active vector  $t_{1+}$  when  $\varepsilon_T = 1$  can be found

$$t_{1+} = \frac{2(T_e^* - T_0) - f_{2+}T_s}{2f_{1+} - f_{2+}} = \frac{2(T_e^* - T_0)}{(2 + \frac{(k_1 - 1)\omega}{\omega_N})f_0} - \frac{\frac{(k_1 - 1)\omega}{\omega_N} f_0 T_s}{(2 + \frac{(k_1 - 1)\omega}{\omega_N})f_0} \quad (4.9)$$

While  $\varepsilon_T = -1$ , similar result can be obtained

$$f_{1-} = -f_0 + \frac{f_0(k_1 - 1)\omega}{\omega_N} \quad (4.10)$$

$$f_{2-} = \frac{f_0(k_1 - 1)\omega}{\omega_N} \quad (4.11)$$

where  $f_{1-}$  and  $f_{2-}$  are the torque variations of the active vector and the zero vector, respectively.

By substituting (4.10) and (4.11) into (4.4), the time duration of the active vector  $t_{1-}$  when  $\varepsilon_T = -1$  can be obtained as

$$t_{1-} = \frac{2(T_e^* - T_0) - f_{2-} T_s}{2f_{1-} - f_{2-}} = \frac{2(T_e^* - T_0)}{(-2 + \frac{(k_1 - 1)\omega}{\omega_N})f_0} - \frac{\frac{(k_1 - 1)\omega}{\omega_N} f_0 T_s}{(-2 + \frac{(k_1 - 1)\omega}{\omega_N})f_0} \quad (4.12)$$

Then, the duty ratios of active vector can be expressed as

$$d_+ = \frac{t_{1+}}{T_s} = \frac{2(T_e^* - T_0)}{(2 + \frac{(k_1 - 1)\omega}{\omega_N})f_0 T_s} - \frac{\frac{(k_1 - 1)\omega}{\omega_N} f_0 T_s}{(2 + \frac{(k_1 - 1)\omega}{\omega_N})f_0 T_s}, \varepsilon_T = 1 \quad (4.13)$$

$$d_- = \frac{t_{1-}}{T_s} = \frac{2(T_e^* - T_0)}{(-2 + \frac{(k_1 - 1)\omega}{\omega_N})f_0 T_s} - \frac{\frac{(k_1 - 1)\omega}{\omega_N} f_0 T_s}{(-2 + \frac{(k_1 - 1)\omega}{\omega_N})f_0 T_s}, \varepsilon_T = -1 \quad (4.14)$$

In order to simplify (4.13) and (4.14), which are parameter dependent, they can be rewritten as

$$d = \begin{cases} d_+ = \frac{2\Delta T_e}{K_a - K_b \omega} + \frac{K_b \omega}{K_a - K_b \omega}, & \varepsilon_T = 1 \\ d_- = \frac{2\Delta T_e}{-K_a - K_b \omega} + \frac{K_b \omega}{-K_a - K_b \omega}, & \varepsilon_T = -1 \end{cases} \quad (4.15)$$

where  $\Delta T_e$  is the instantaneous torque error;  $K_a = 2f_0 T_s$ ,  $K_b = (1 - k_1)f_0 T_s / \omega_N$  are two positive constants.

### Analysis of the selection of control parameters $K_a$ and $K_b$

The range of  $K_a$  and  $K_b$  can be estimated from the given parameters. Firstly, there is an inherent relationship between  $K_a$  and  $K_b$ :

$$\frac{K_b}{K_a} = \frac{(1 - k_1)}{2\omega_N} \quad (4.16)$$

Ignoring the effect of torque,  $k_l$  can be estimated from Fig. 4.2 as

$$k_1 \in (0, 0.5) \quad (4.17)$$

Hence, from (4.16) and (4.17), if  $K_a$  is selected,  $K_b$  can be easily determined. On the other hand, according to definition,  $f_0$  can be calculated from (4.2) with  $\omega_l = 0$  and ignoring the effect of torque,

$$f_0 = \frac{3P}{2L_s} (-\psi_{r\beta} V_{s\alpha} + \psi_{r\alpha} V_{s\beta}) \quad (4.18)$$

In the particular system described in chapter 3,  $f_0$  can be obtained from Fig. 3.1 as

$$f_0 = \frac{(1918 + 7534)}{2} \sin(\theta + 60^\circ), \theta \in (-30^\circ, 30^\circ] \quad (4.19)$$

Thus,  $K_a$  can be computed as

$$K_a = 2f_0 T_s = 0.9452 \sin(\theta + 60^\circ), \theta \in (-\pi/6, \pi/6] \quad (4.20)$$

Therefore,

$$K_a \in (0.4726, 0.9452] \text{ Nm} \quad (4.21)$$

Then, according to (4.16), (4.17) and (4.21), appropriate control parameters  $K_a$  and  $K_b$  can be determined.

Of course,  $K_a$  changes with the variation of system parameters, especially inductance and permanent magnet flux linkage. However, according to the foregoing estimated method, it can be found that the new range will not be much different from the proposed range. Therefore, it is not difficult to obtain the appropriate value of control parameters. The experimental results will verify that the system is highly robust in the face of variation of the control parameters.

Once adjusted,  $K_a$  and  $K_b$  are two fixed constants, and then the duty ratio will be automatically adjusted with the instantaneous torque error and the machine angular velocity.

To analyse the effectiveness of the novel duty ratio determination from a theoretical perspective, the operating principles are presented by taking the stator flux in sector 1 as an example.

#### a) Common regulatory mechanism

When the machine angular velocity is constant, the higher the absolute value of torque error is, the larger the duty ratio will be, which therefore guarantees the long duration of active vectors to diminish the torque error as soon as possible. Then, the duty ratio will become smaller, which lets the zero vectors to work for longer time to reduce the torque ripple effectively.

According to the analysis of Fig. 4.2, the torque variation is influenced greatly by the machine angular velocity. Hence, it is necessary to analyse the effectiveness over different speed regions.

#### **b) In low and medium speed regions**

When the speed is not so high, the absolute values of torque variation of active vectors are much higher than that of the zero vectors. Therefore, to apply a zero vector after an active vector during one sampling period is one feasible solution for minimizing the torque ripple as well as keeping the torque tracing well.

#### **c) In high speed region**

At high speed regions, due to the high back EMF, the increasing torque variation of  $V_2$  and  $V_3$  will decrease, even at some high speed and heavy load regions, the torque variation of  $V_3$  will become negative (Fig. 4.2 (b)). Therefore, if the duty ratio of active vector at that time is very small, the torque will grow very slowly, even at some particular conditions, it will remain constant or decrease instead, the obvious steady state error of torque will thus occur. It should be noted that, under some particular conditions, although applying active vector cannot increase the torque effectively (e.g.  $V_3$  in Fig. 4.2(b), where both the active vector  $V_3$  and zero vector  $V_0/V_7$  will decrease the torque when the position of flux from -30 degrees to 0 degree), due to smaller absolute torque variation value compared to zero vectors, active vectors will still be the better choice.

On the other hand, the absolute values of decreasing torque variation of active vectors  $V_5$  and  $V_6$  (even zero vectors  $V_0$  and  $V_7$ ) become very large compared to the increasing torque variation of  $V_2$  and  $V_3$  at the same time. Hence, it is desirable and also possible to apply an active vector ( $V_5$  or  $V_6$ ) for shorter duration and zero vector for longer duration. In existing chapters [KAN99], [ZHA11a], it is suggested that for the case  $\varepsilon_T = -1$  the same method is used to obtain the duty of active vectors as the case when  $\varepsilon_T = 1$ , i.e., active vectors are still considered as the major vectors whilst zero vectors are only considered as auxiliary. However, due to much larger absolute value of decreasing torque variation determined by both active and zero vectors compared to the increasing torque

variation under the same condition, significant torque ripple and steady-state error of torque will occur. In the proposed method, when  $\varepsilon_T = -1$ , due to their considerable value of torque variation, zero vectors will be most frequently used instead of the active vectors whose absolute value of torque variation is much larger.

From (4.15), it can be seen that when  $K_a$  and  $K_b$  keep unchanged,  $d_+$  will increase but  $d_-$  will decrease with the increase of machine angular velocity. Therefore, when the machine angular velocity is large enough,  $d_+$  will approach 1, and set to 1 when it is larger than 1; while for  $d_-$ , it will be set to 0 if it is less than 0. Therefore, both the steady-state error and ripple of torque will be diminished. At the same time, due to the considerable variation of zero vectors, the dynamic performance of system will not be deteriorated.

#### **d) When machine operates on opposite direction of rotation**

When machine operates on opposite direction of rotation, the calculation of duty ratio (4.15) is still tenable. The increasing variation of torque is much larger than the decreasing one, which is opposite to the normal situation. Fortunately, the calculation of duty ratio (4.15) can be rewritten as

$$d = \begin{cases} d_+ = \frac{2\Delta T_e}{K_a - K_b\omega} + \frac{K_b\omega}{K_a - K_b\omega} \\ \quad = \frac{2(-\Delta T_e)}{-K_a - K_b(-\omega)} + \frac{K_b(-\omega)}{-K_a - K_b(-\omega)} & , \varepsilon_T = 1 \\ d_- = \frac{2\Delta T_e}{-K_a - K_b\omega} + \frac{K_b\omega}{-K_a - K_b\omega} \\ \quad = \frac{2(-\Delta T_e)}{K_a - K_b(-\omega)} + \frac{K_b(-\omega)}{K_a - K_b(-\omega)} & , \varepsilon_T = -1 \end{cases} \quad (4.22)$$

It can be seen from (4.22) and (4.15) that,  $d_+$  in (4.22) equals to  $d_-$  in (4.15), and  $d_-$  in (4.22) equals to  $d_+$  in (4.15). Therefore, all the forgoing analyses are valid when machine operates on opposite direction of rotation, which means the proposed methods can still be used even during speed reversal. The experimental results confirm the effectiveness of the proposed method during speed reversal.

#### 4.4. Experimental Results

Detailed experiments have been conducted on the laboratory prototype of the PMSM machine I. Four kinds of ST-DTC methods are compared and analysed: conventional ST-DTC, proposed ST-DTC method, and two existing duty-based ST-DTC methods, designated as M1 in [KAN99] and M2 in [ZHA11a], respectively. M1 is an accurate method, and M2 is a simple duty ratio determination which is parameter independent. These two methods have been introduced in the introduction of this chapter.

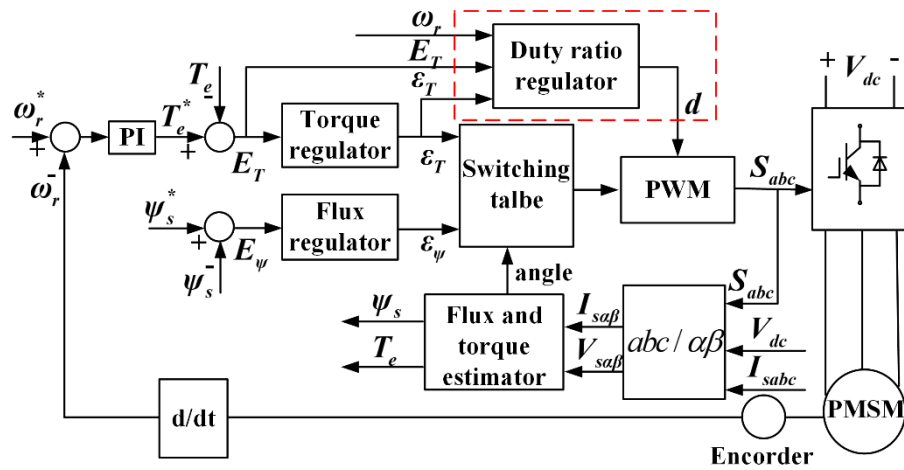


Fig. 4.4. Control diagram of ST-DTC of PMSM.

The overall control scheme with conventional, proposed and two existing ST-DTCs is shown in Fig. 4.4, where the dashed box indicates the duty ratio calculator. The sample frequency is 10 kHz, and the control parameters  $K_a$  and  $K_b$  are set as:  $K_a = 0.945$  Nm,  $K_b = 0.0009$  Nm/(rad/s). All the results were captured using dSPACE software, and then plotted using Matlab.

##### 4.4.1. Comparison of Steady Performance of Different ST-DTC Methods

In order to verify the feasibility of the proposed ST-DTC, Fig. 4.5 compares the measured results for conventional, proposed and two existing ST-DTCs at rated speed and torque: 400 rpm, 5 Nm.

Fig. 4.5, shows no significant difference among the four ST-DTC strategies in the case of both the steady-state error and ripple of stator flux. However, for the torque, there exists large torque ripple in the conventional ST-DTC, Fig. 4.5(a), and can be reduced by M1, M2 and the proposed duty-based ST-DTC at different levels, Fig. 4.5(b)-(d). Detailed quantitative results are given in Table 4.2, where the torque and stator flux ripples are calculated using

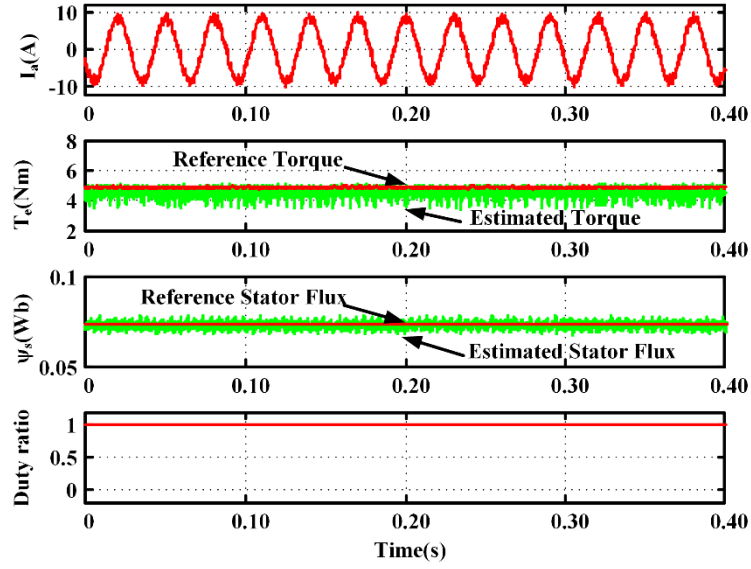
$$\psi_{s\_ripple} = \sqrt{\frac{1}{n} \sum_{i=1}^n (\psi_{s\_i} - \psi_{s\_av})^2} \quad (4.23)$$

$$T_{e\_ripple} = \sqrt{\frac{1}{n} \sum_{i=1}^n (T_{e\_i} - T_{e\_av})^2} \quad (4.24)$$

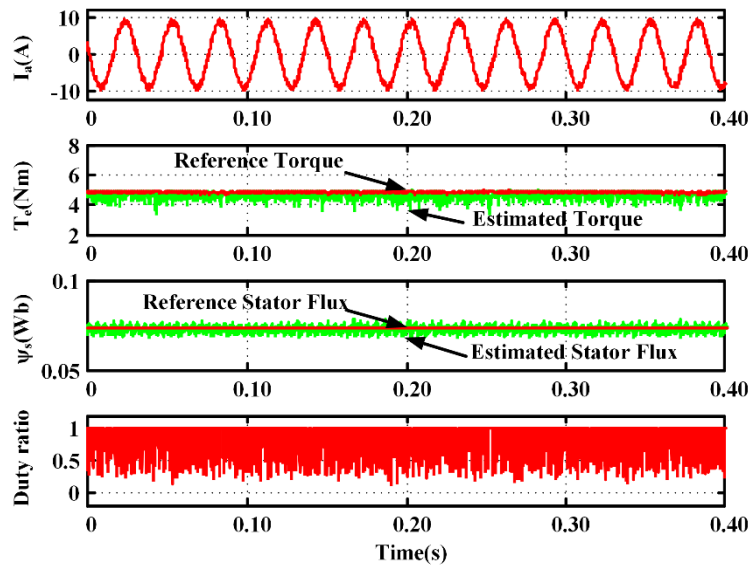
where  $\psi_{s\_i}$  and  $T_{e\_i}$  are the instantaneous value of stator flux and torque, respectively, whilst  $\psi_{s\_av}$  and  $T_{e\_av}$  are the average values of stator flux and torque, respectively. The average commutation frequency,  $f_{av}$ , is calculated by counting the total commutation instants of one phase leg during a fixed period, is used to indicate the switching losses. In calculating the THD of stator current, the maximum frequency is 1000 Hz, in this case when the machine speed is 400 rpm, the maximum harmonic order is 29<sup>th</sup>.

Table 4.2 Steady-state Performance of Different ST-DTC Methods

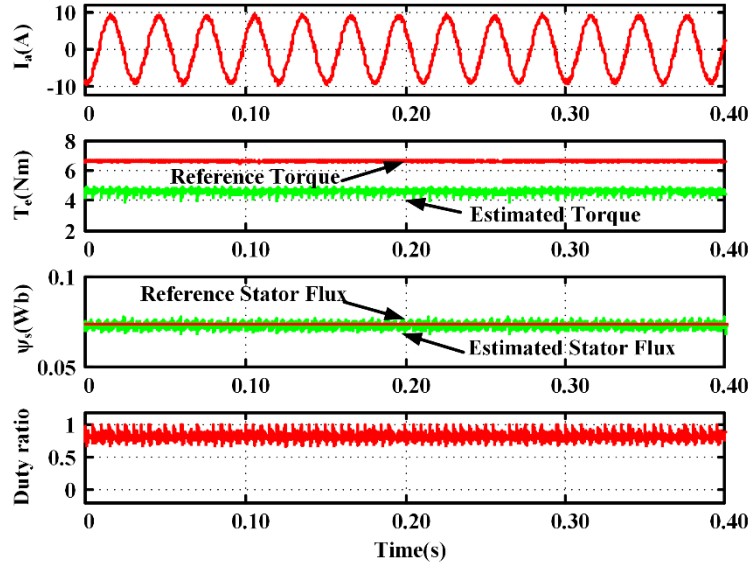
400 rpm, 5 Nm	Conventional	M1	M2	Proposed
$\Delta\psi_s$ (%)	0.1270	0.2254	0.1614	-0.0307
$\Delta T_e$ (%)	7.9810	4.3654	<b><u>40.0712</u></b>	<b><u>3.5538</u></b>
$\psi_{s\_ripple}$ (Wb)	19.78e-4	17.73e-4	16.21e-4	17.15e-4
$T_{e\_ripple}$ (Nm)	0.3504	0.2362	0.1376	<b><u>0.1851</u></b>
THD <sub>I<sub>a</sub></sub> (%)	4.44	3.93	4.09	4.11
$f_{av}$ (kHz)	1.8983	3.6467	5.4313	<b><u>3.2517</u></b>



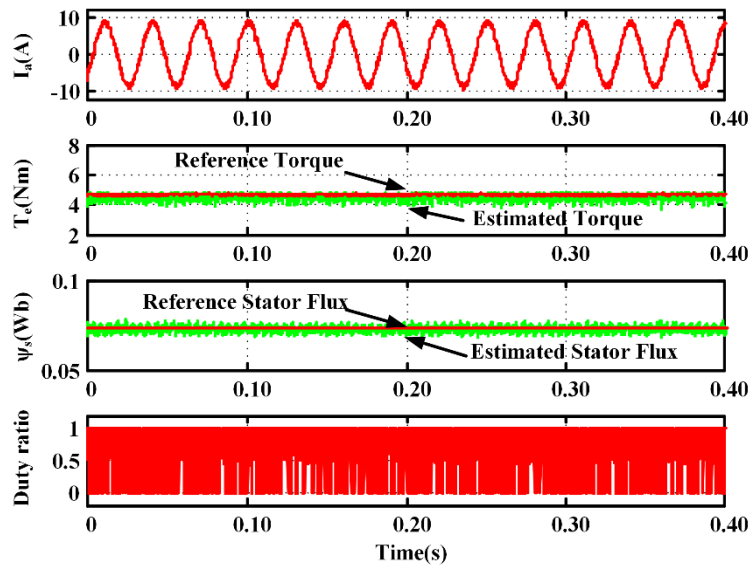
(a)



(b)



(c)



(d)

Fig. 4.5. Comparison of measured steady-state performance of various ST-DTC methods (Rated condition: 400 rpm, 5 Nm) (a) Conventional ST-DTC method (b) M1 (c) M2 (d) Proposed ST-DTC method

According to Table 4.2, M2 achieves the largest torque ripple reduction, which is 60.73% compared to conventional ST-DTC, and then followed by proposed method with 47.14% and M1 with 32.59%. However, a steady-state error of torque exists in M2 of 40.07%, much larger than conventional ST-DTC. In both M1 and the proposed method, the steady-state error of torque is lower than the conventional ST-DTC. The stator flux ripple is slightly reduced in all three duty-based methods. The THD of the stator current is similar to the conventional ST-DTC in all methods.

It should point out that, the methods in Table 3.1 employ the torque regulator with a proper bandwidth, while the methods in Table 4.2 use torque regulator with zero bandwidth for the fair comparison with M1 and M2, since for both M1 and M2, the torque regulator with zero bandwidth is utilized. The methods with proper bandwidth have smaller torque ripples compared to the conventional method, nevertheless, the torque ripple of M1, M2, and proposed methods in Table 4.2 are still smaller than conventional methods whether conventional torque regulator or band-shifted torque regulator is used as shown in Table 3.1.

For M2, in each sector, only the active vectors which increase the torque and the zero vectors is be used. For example, when the stator flux vector lies in sector 1, only  $V_2$ ,  $V_3$ , and  $V_0$ ,  $V_7$  will be employed. Their absolute value of torque variation is much smaller than that of  $V_5$  and  $V_6$ . Hence, smaller ripple but larger steady-state error of torque is produced. As for M1, although it uses an accurate determination of duty ratio, it is seriously affected by the one-step delay due to its parameter dependence. This effect has been analysed in detail and confirmed by simulation results in [ZHA11a]. The proposed method is parameter independent, and the duty ratio can be adjusted automatically according to the change of the speed. Therefore, desirable steady-state performance is achieved.

The average commutation frequency of the three duty-based methods, especially M2, becomes bigger than the conventional one. Due to the principle of the duty-based ST-DTC strategy – employing an active vector and a zero vector together in one sampling period, it is inevitable that average commutation frequency,  $f_{av}$ , will become a little higher. Among the three improved methods, the proposed one achieves the desirable improvement of steady-state torque performance at the lowest cost, of increased average commutation frequency. The duty ratio obtained by the proposed method will approach zero when  $\varepsilon_T = -1$ . Consequently, zero vectors will be most frequently used, resulting in lower steady-state error and torque ripple compared to M1.

The steady-state performance of torque and stator flux with the conventional, improved and two existing duty-based ST-DTC methods are also compared under different speed conditions. Fig. 4.6 shows the steady-state performance of torque and stator flux under the condition of no load and machine speed from 40 rpm to 400 rpm.

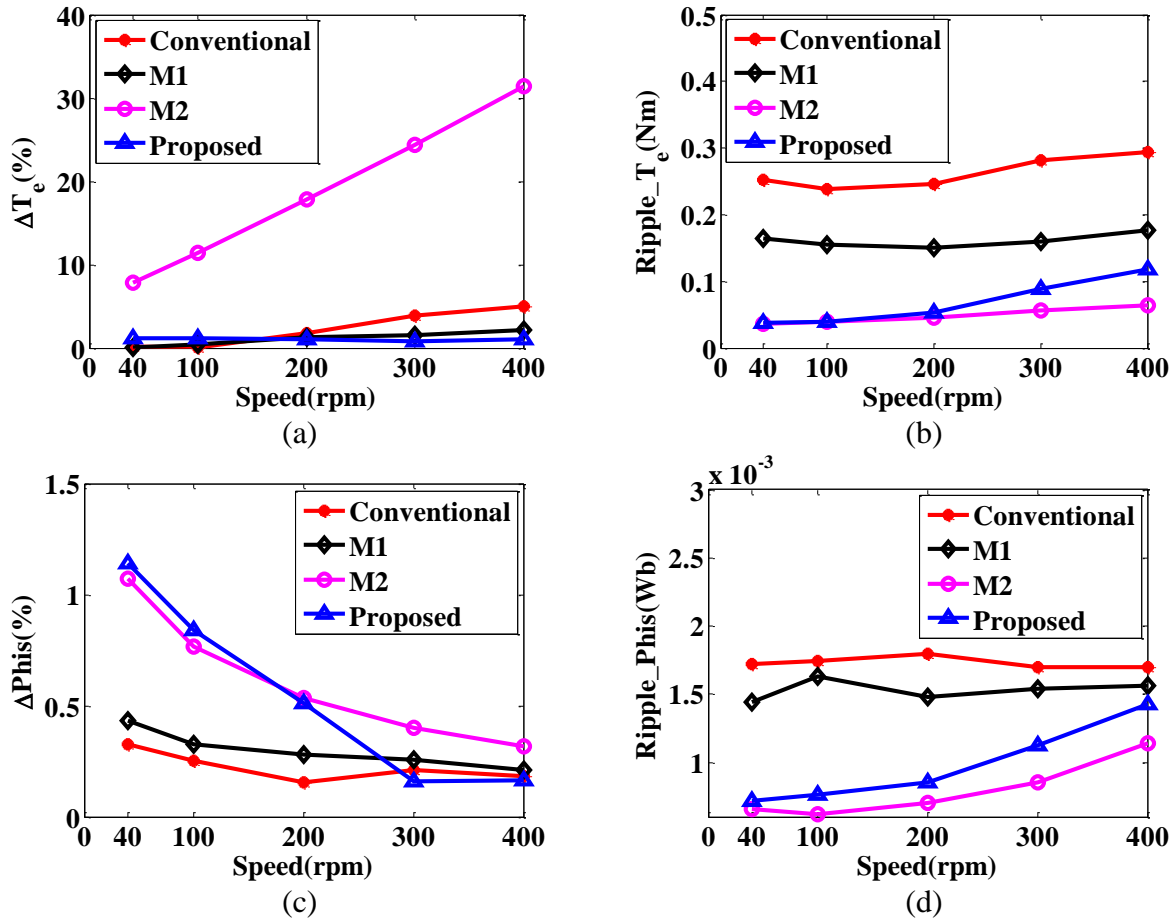


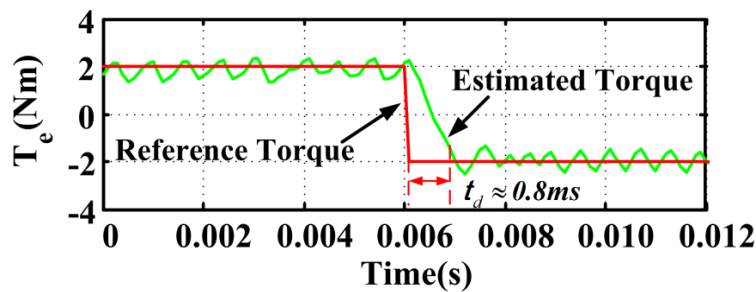
Fig. 4.6. Comparison of measured steady-state performances of torque and stator flux for conventional and improved ST-DTC methods. (a) Steady-state error of torque. (b) Torque ripple. (c) Steady-state error of stator flux. (d) Stator flux ripple.

Fig. 4.6 shows that although M2 achieves the lowest ripple of torque and stator flux, the steady-state error of torque is much larger than that of conventional ST-DTC over a wide range of speed. Both M1 and the proposed ST-DTC methods also obtain better performance of the ripple of torque and stator flux compared to the conventional method, and comparing the two, the proposed method is more effective. From Fig. 4.6, the application of the proposed duty-based ST-DTC can effectively reduce the steady-state torque error and provide a significant reduction in torque and

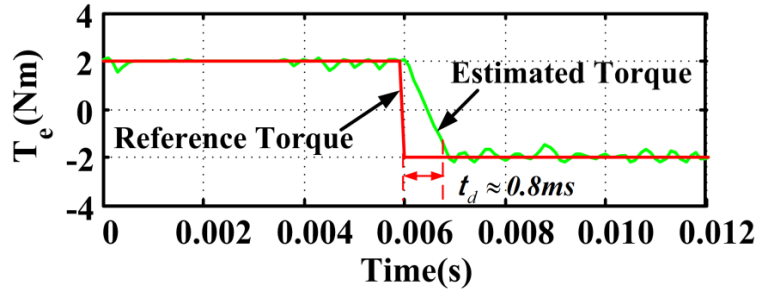
stator flux ripple over a wide range of speed.

#### 4.4.2. Dynamic Performance of Inner Torque Loop Control without Outer Speed Loop

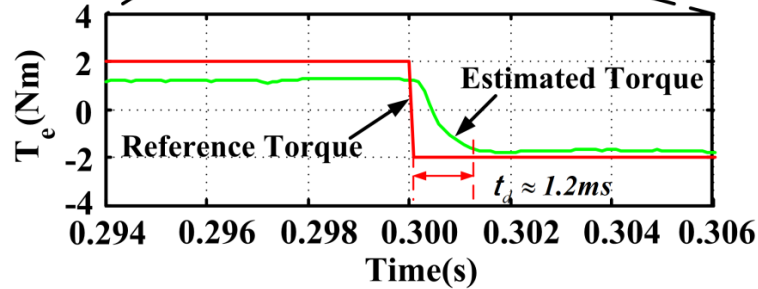
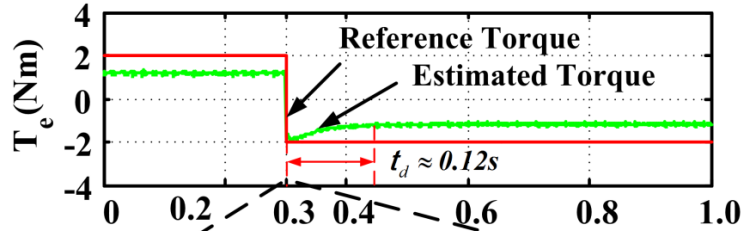
The proposed duty-based ST-DTC method can improve the steady-state performance of both stator flux and torque. In order to verify the dynamic performance of the torque control of the proposed method, the outer speed loop should be removed first, because the additional speed controller may disturb the dynamic performance of the inner torque control loop. Therefore, the dynamic performance of torque without the speed controller, i.e. with inner torque control only, for both conventional and improved ST-DTC methods is presented in Fig. 4.7. In order to also confirm the dynamic performance of low speed and speed reversal, the reference torque is set as 2 Nm to -2 Nm. The torque fall time due to M2 and the proposed method is the same as that of the conventional torque regulator, which is approximately 0.8 ms, as shown in Fig. 4.7(a). Hence, the proposed method will not deteriorate the dynamic torque performance. For M1, due to opposite function of zero and active vectors for applied torque in each sampling period, when speed is reversed and  $\varepsilon_T = -1$ , more settling time (1.2 ms in Fig. 4.7(c)) is needed. Because of the steady-state error of torque, the torque will take a long time (0.12 s in Fig. 4.7(c.)) to stabilise.



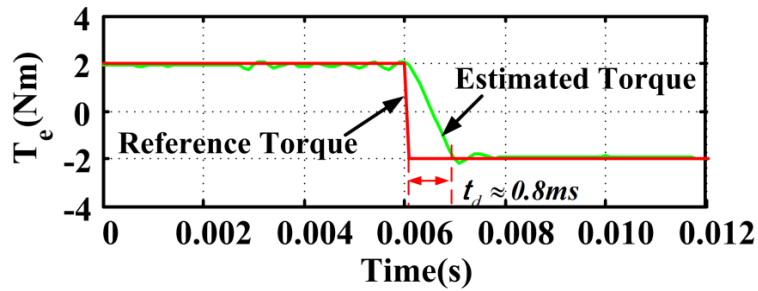
(a)



(b)



(c)



(d)

Fig. 4.7. Dynamic performances of torque response using inner torque loop control only, without an outer speed control loop. Reference torque from 2 Nm to -2 Nm. (a) Conventional ST-DTC method. (b) M1. (c) M2. (d) Proposed ST-DTC method.

#### 4.4.3. Dynamic and Steady-state Performance with Outer Speed Loop When Machine Operates on Opposite Direction of Rotation

Fig. 4.8 shows the dynamic and steady-state performance of the conventional and proposed ST-

DTC methods with an outer speed loop when the reference speed is reversed from 200 rpm to -200 rpm, with no load.

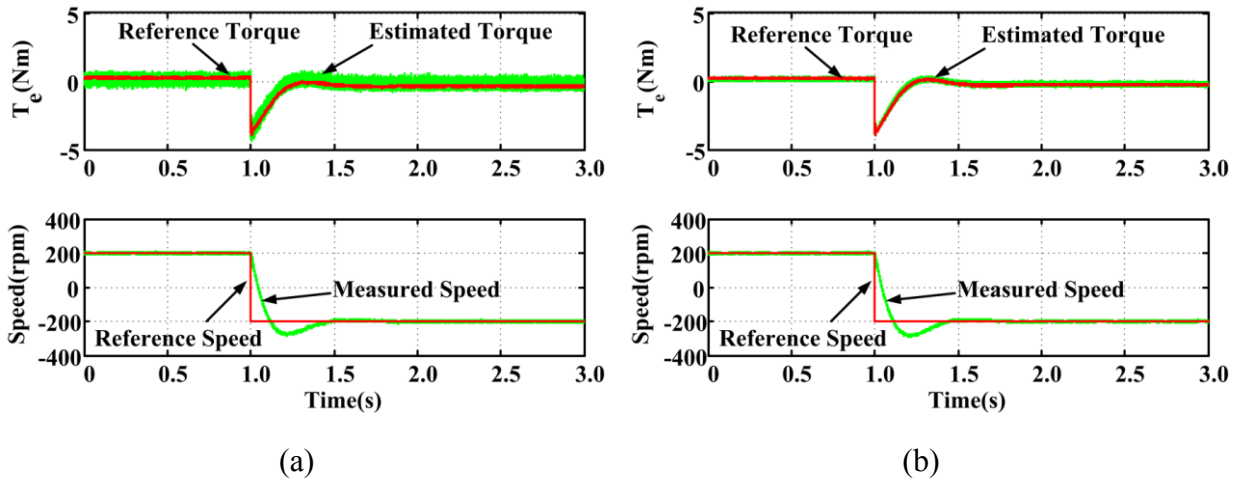


Fig. 4.8. Dynamic and steady-state performances when reference speed changes from 200 rpm to -200 rpm. (a) Conventional ST-DTC. (b) Proposed ST-DTC.

Fig. 4.8 shows the proposed strategy has similar dynamic performance to conventional ST-DTC when the reference speed is reversed.

#### 4.4.4. Sensitivity of System Performance to Control Parameter Variation

The above experiment is carried out with specific control parameters, e.g.  $K_a = 0.945$  Nm,  $K_b = 0.0009$  Nm/(rad/s). The prior analysis provides the region from which  $K_a$  and  $K_b$  can be selected. In order to analyse the sensitivity of system performance to control parameter variation, Fig. 4.9 presents the steady-state performance of the proposed ST-DTC method under rated load conditions when control parameters are  $K_a = 0.7$  Nm,  $K_b = 0.0005$  Nm/(rad/s). Compared with Fig. 4.5(d), there is no significant difference between the two sets of results. The steady-state error and ripple of torque in Fig. 4.9 is 4.2037% and 0.1751 Nm, respectively, very close to that of Fig. 4.5(d), which are 3.5538% and 0.1851 Nm, respectively. This confirms that the proposed ST-DTC method is robust against variation in control parameters.

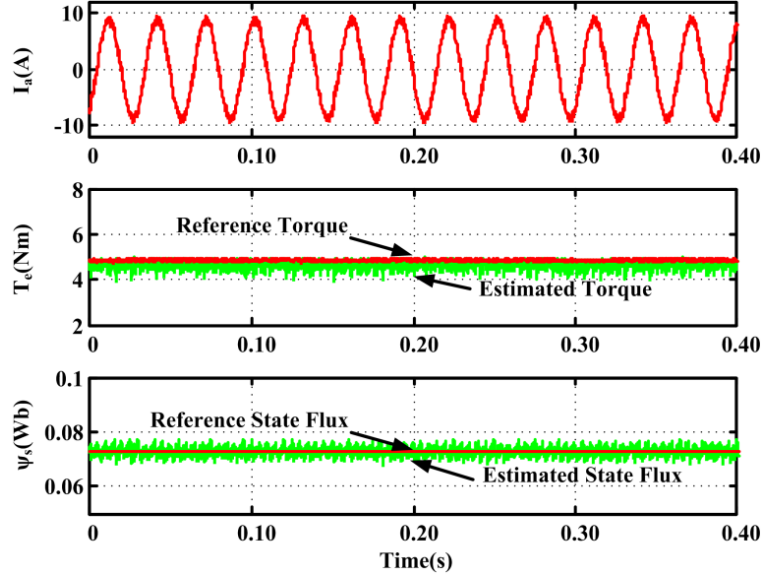


Fig. 4.9. Steady-state performance of proposed ST-DTC method with different control parameters:  $K_a = 0.7 \text{ Nm}$ ,  $K_b = 0.0005 \text{ Nm/(rad/s)}$  (rated condition: 400 rpm, 5 Nm).

#### 4.5. Conclusion

This chapter has proposed, analysed and experimentally verified a simple and effective method for determining the appropriate duty ratio in ST-DTC three-phase PMSM drives to reduce the torque ripple and steady-state error of torque, accounting for the influence of machine angular velocity. A simple estimated method is proposed to obtain the range of the key control parameters. Compared to the existing duty-based ST-DTC methods, the proposed method can achieve good torque and flux performance at the lower cost of increased average communication frequency.

The proposed duty ratio determination method has the following features:

- (1) Simple structure. Compared to conventional ST-DTC, just a duty ratio regulator is added.
- (2) Parameter independent. Unlike the previous duty-based methods, where many parameters such as stator inductance and permanent magnet flux are required, in the proposed ST-DTC method, only the torque error and speed is needed to compute the duty ratio, which makes it robust to parameter variation.
- (3) Desirable steady-state performance over a wide range of operating speed regions, even when the machine operates on opposite direction of rotation.

(4) Similar, desirable, transient response to the conventional ST-DTC.

Although the analyses and experiments in this chapter are based on the ST-DTC of three-phase PMSM drives, the proposed duty ratio determination can also be extended for general use and applied to the other machines utilising switching table-based direct torque and power control methods, when the machine exhibits similar problems to the machine in this chapter i.e. ripple and/or steady-state error.

## **5. Modified Switching-table Strategy for Reduction of Current Harmonics in Direct Torque Controlled Dual Three-phase Permanent Magnet Synchronous Machine Drives**

### **5.1. Introduction**

Recently, interest in multiphase machine drives has increased considerably, especially for high-power and/or high-current applications such as aerospace applications, ship propulsion, electric/hybrid vehicles, and renewable energy generation. In these applications, the controlled power can be shared by more inverter legs to reduce the current stress on each semiconductor device compared to three-phase converters [BOJ03]. Other potential advantages of the multiphase machine drives are higher reliability at the system level, lower torque pulsations, and lower DC-link voltage requirement [BOJ05], [LEV08a].

A very interesting and widely discussed type of multiphase machine is the dual three-phase machine having two sets of three-phase windings spatially shifted by 30 electrical degrees, as shown in Fig. 1.10(a). In the dual three-phase machine, the sixth harmonic torque pulsation, which is dominant in three-phase systems, will be completely absent because of the opposition of these components produced by two sets of windings [GOP84]. Nevertheless, large stator circulating harmonic currents will occur in the VSI-fed dual three-phase machine since the machine impedance associated with these harmonics is very small - only composed of the stator resistance and leakage inductance, according to the machine model using VSD technique [ZHA95]. These unexpected harmonic currents cause extra losses and require higher semiconductor device ratings [ABB84].

Previous investigations have explored vector control using suitable PWM techniques and to extend this theory for dual three-phase machine drives [BOJ03], [HAD06]. Although unexpected stator harmonic currents can be minimized under these strategies, complicated and time-consuming calculation is required.

A DTC strategy is an applicable alternative because of its simple structure, excellent transient response and robustness against machine parameters. Based on the vector space decomposition technique [ZHA95], only the variables in  $\alpha\beta$  subspace in the dual three-phase system relate to the torque, which is similar to the case in three-phase drives. Therefore, the classical ST-DTC strategy

can be easily extrapolated to dual three-phase drives. However, the classical ST-DTC strategy suffers from the large stator harmonic currents because of a lack of control over the harmonic components in the  $z_1z_2$  subspace. Hatua [HAT05] has developed three individual flux control methods of the ST-DTC technique for the dual three-phase machine drive to reduce the torque ripple. The unexpected stator harmonic currents still exist however so harmonic suppression schemes have been developed and reported for the ST-DTC of five-phase machines [LIL11], [ZHE11].

This chapter aims to reduce the stator harmonic currents in the classical ST-DTC strategy for dual three-phase PMSM drives, while preserving its advantages, such as simple structure and robustness. The remainder of this chapter consists of the following sections. In section 5.2, machine modelling and analysis based on the vector space decomposition technique is described. In section 5.3, the basic principle of switching-table-based DTC strategies for dual three-phase drives is presented. Then a two-step process to select the most appropriate voltage vector is presented in section 5.4. The first step selects the voltage vector group to meet the torque and flux control requirements according to the classical switching table and outputs of the hysteresis regulators. The second step involves choosing the most suitable voltage vector from that group, based on the position of the harmonic stator flux, to reduce the harmonic currents. Experimental results are provided in section 5.5 to demonstrate the validity of the proposed solutions.

## **5.2. Machine Model and Analysis of Inverter Voltage Vectors**

### **5.2.1. Machine Model**

The model of dual three-phase surface-mounted PMSM in a stationary reference frame has been given in (1.10) - (1.15).

Based on (1.15), after using a VSD approach, torque and flux production involves only  $\alpha\beta$  components, which makes the machine control equally simple as for the case of a three-phase machine. However, it also can be seen from (1.13) and (1.14) that the  $z_1z_2$  components are responsible for the large circulating harmonic currents because of the small impedance in the  $z_1z_2$  subspace. Therefore, the applied voltage vectors should contain not only the voltage commands in  $\alpha\beta$  components but also the voltage commands to minimize the average amplitude of  $z_1z_2$  components.

### 5.2.2. Analysis of the Inverter Voltage Vectors

Owing to its six inverter legs, dual three-phase system contains  $2^6 = 64$  inverter voltage vectors, much more than three-phase system. By neglecting the zero voltage vectors, the  $\alpha\beta$  and  $z_1z_2$  subspace voltage vectors can be shown in Fig. 1.17 (a) and (b), respectively.

Fig. 1.17 shows that the outermost voltage vectors in the  $\alpha\beta$  subspace causing highest effect in the torque production are the ones which have the lowest influence in the  $z_1z_2$  subspace - innermost voltage vectors in the  $z_1z_2$  subspace. Therefore, the outermost voltage vectors in the  $\alpha\beta$  subspace are often chosen for controlling dual three-phase machine drive to maximize the efficiency of system and, at the same time, minimize losses because the voltage vector components in the  $z_1z_2$  subspace do not contribute to rotating air gap flux but cause stator harmonic currents and result in losses.

### 5.3. Classical ST-DTC Scheme

The machine model of a dual three-phase PMSM is the same as the single three-phase PMSM from a control perspective. Therefore, the classical ST-DTC strategy for the three-phase system can be easily extrapolated to dual three-phase PMSM systems, as shown in Fig. 1.19. Compared to the ST-DTC for three-phase drives, the only change is that the classical CLARKE transformation ( $abc \rightarrow \alpha\beta 0$ ) is replaced by a new transformation  $[T_6]$  ( $abcxyz \rightarrow \alpha\beta z_1z_2 0 1 0 2$ ) given in (1.9).

Consequently, based on the estimated stator flux position, the  $\alpha\beta$  subspace can be divided into 12 sectors, Fig. 5.1(a). Then, torque and flux regulators are used to generate the inverter vectors by using a switching table, as shown in Fig. 1.19. In order to achieve the best dynamic torque performance, only voltage vectors from the outermost layer of a 12-sided polygon in the  $\alpha\beta$  subspace, together with the zero vectors, will be selected to structure the switching table. Fundamentally, when the stator flux vector  $\psi_{s\alpha\beta}$  lies in sector  $k$ , as shown in Fig. 5.1(b), instantaneous control of stator flux and torque can be achieved by employing appropriate voltage vectors according to Table 5.1, where all the voltage vectors are selected to obtain the fastest torque response.

In Table 5.1, the torque and stator flux control signals  $\varepsilon_T$  and  $\varepsilon_\psi$  are generated by torque and flux

regulators, respectively, which are defined as

$$\varepsilon_T = \begin{cases} 1, & \text{to increase } T_e \\ 0, & \text{to maintain } T_e \\ -1, & \text{to decrease } T_e \end{cases} ; \varepsilon_\psi = \begin{cases} 1, & \text{to increase } \psi_s \\ -1, & \text{to decrease } \psi_s \end{cases} \quad (5.1)$$

The classical ST-DTC strategy is simple to implement. However, since only the  $\alpha\beta$  components associated with torque production are regulated under this control method, although the vectors of outermost layer in the  $\alpha\beta$  subspace has the lowest amplitude in the  $z_1z_2$  subspace, the  $z_1z_2$  components are still freely circulated inside the machine. Large harmonic currents will be observed because the only limitation is the leakage inductance, as shown in (1.14).

Therefore, a DTC technique taking into account the  $z_1z_2$  components to minimize their effects on the harmonic currents is required.

Table 5.1 Switching Table for Classical ST-DTC

$T_e$	$\psi_s$	Vector required
↑	↑	$V_{k+2}$
↑	↓	$V_{k+3}$
↓	↑	$V_{k-3}$
↓	↓	$V_{k-4}$
<b>0</b>		$V_{zero}$

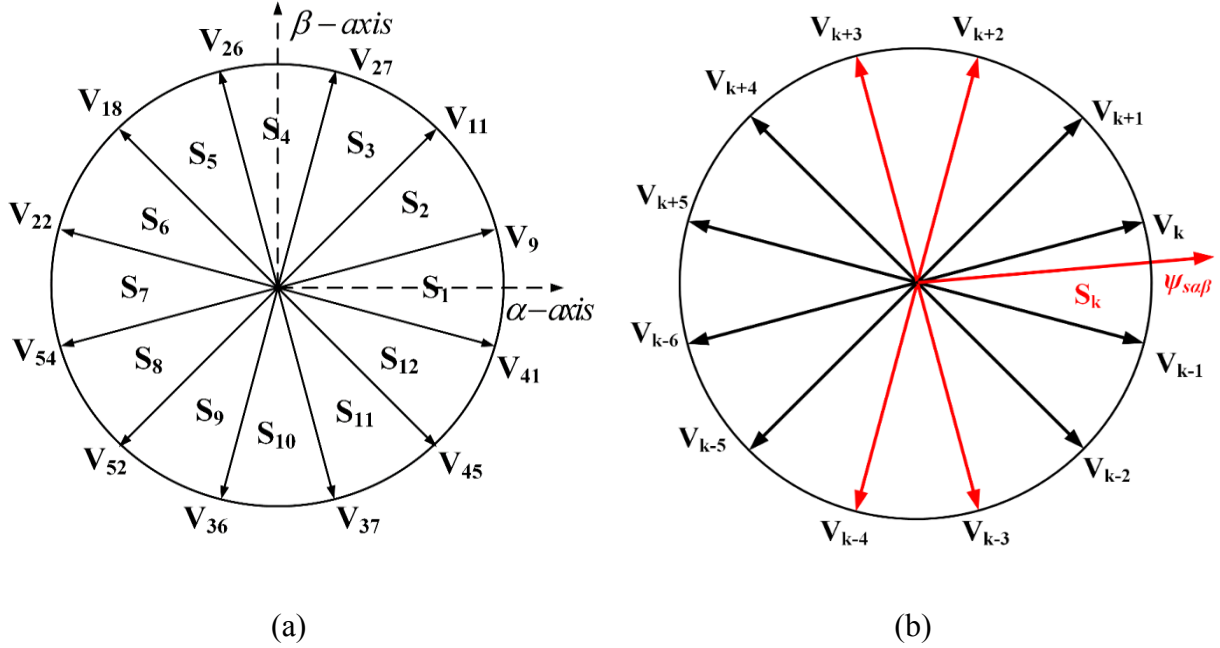


Fig. 5.1. The principle of classical ST-DTC. (a) Definition of 12 sectors in the  $\alpha\beta$  subspace. (b) Selection of voltage vectors when the stator flux lies in sector  $k$ .

#### 5.4. Proposed DTC Scheme

It can be seen from (1.14) that in the  $z_1z_2$  subspace, the undesirable harmonic current is proportional to the stator flux in the  $z_1z_2$  subspace  $\psi_{sz_1z_2}$ . Therefore, minimizing the stator flux  $\psi_{sz_1z_2}$  is an effective way to reduce the harmonic currents  $i_{sz_1z_2}$ .

In the  $\alpha\beta$  subspace, there are three voltage vectors pointing in the same direction, e.g.  $V_9$ ,  $V_{43}$  and  $V_{29}$  in Fig. 5.2, having nearly similar effects on torque and flux control except that the larger vectors provide faster responses. However, in the  $z_1z_2$  subspace,  $V_9$  and  $V_{29}$  still point to the same direction, while  $V_{43}$  points to the oppositional direction compared to  $V_9$  and  $V_{29}$ , and therefore cause oppositional effects on the variation of  $z_1z_2$  flux  $\psi_{sz_1z_2}$ .

In order to facilitate a clearer description, the active vectors in the  $\alpha\beta$  subspace are classified into four layers according to their amplitudes, from innermost to outermost:  $D_1$ ,  $D_2$ ,  $D_3$ ,  $D_4$ , whereas in the  $z_1z_2$  subspace the sequence, from innermost to outermost:  $D_4$ ,  $D_2$ ,  $D_3$ ,  $D_1$ , as shown in Fig. 5.2. Therefore, it can be deduced that the vectors of  $D_1$  and  $D_4$  have the same effect on  $\psi_{sz_1z_2}$ , while vectors in  $D_3$  layer have the opposite effect. Consequently, by introducing the vectors from layer  $D_3$  into the control strategy, it is possible to reduce the amplitude of  $\psi_{sz_1z_2}$ . This should result in

the corresponding harmonic currents decreasing. The  $D_1$  layer vectors are in the same direction as the  $D_4$  layer vectors both in the  $\alpha\beta$  subspace and the  $z_1z_2$  subspace. However the  $D_1$  vectors have much smaller amplitude in the  $\alpha\beta$  subspace and larger in amplitude in the  $z_1z_2$  compared to the  $D_4$  vectors, so they will not be considered further. The vectors of  $D_2$  will not be employed either due to the different direction both in the  $\alpha\beta$  and  $z_1z_2$  subspace compared to  $D_1$ ,  $D_3$  and  $D_4$ .

By dividing the  $z_1z_2$  subspace into two half-subspaces having a diameter orthogonal to  $V_9$  and  $V_{43}$ , Fig. 5.2(b), if the  $z_1z_2$  flux vector is located in one half-subspace, a voltage vector in the other half-subspace should be adopted to minimize the  $z_1z_2$  stator flux magnitude and then reduce the  $z_1z_2$  current harmonic components. For example, if  $\psi_{sz_1z_2}$  is located in sector 2 in the  $z_1z_2$  subspace, as shown in Fig. 5.2(b), then applying  $V_9$  will led to an increase in amplitude of  $\psi_{sz_1z_2}$ , while applying  $V_{43}$  would result in a decrease. This is the key reason why there are large harmonic currents in the classical ST-DTC controlled dual three-phase machines, although the vectors of the outermost layer in the  $\alpha\beta$  subspace have the lowest amplitudes in the  $z_1z_2$  subspace. Hence,  $V_{43}$ , instead of  $V_9$ , should be employed in the classical ST-DTC strategy. Similar results can be extended to other sectors. As shown in Fig. 5.2(b) and Fig. 5.1(a), the definition of the sectors of  $z_1z_2$  subspace is the same as that of  $\alpha\beta$  subspace, i.e.

Sector  $k$ :

$$-\frac{\pi}{12} + \frac{\pi}{6}(k-1) \leq \theta_{s\alpha\beta}, \theta_{sz_1z_2} < \frac{\pi}{12} + \frac{\pi}{6}(k-1), \quad k = 1, 2, \dots, 12 \quad (5.2)$$

Consequently, there are two steps to pick an appropriate voltage vector.

- 1) According to the sector of  $\psi_{s\alpha\beta}$  in the  $\alpha\beta$  subspace and the outputs of hysteresis comparators, one vector in  $D_3$  and one vector in  $D_4$  are chose as candidates. These should have the same direction in the  $\alpha\beta$  subspace and are defined as one group in this chapter.
- 2) Based on the position of  $\psi_{sz_1z_2}$  in the  $z_1z_2$  subspace, the vector which can reduce the amplitude of  $\psi_{sz_1z_2}$  is chosen from the selected group.

The first step is the same as the selection of vectors in the classical ST-DTC, therefore, the vector groups can be chosen from Table 5.1, and the vector group is also named with the vector chosen from Table 5.1. A switching table for the second step is presented in Table 5.2. For example, if the

vector group 9 is selected from Table 5.1 in the first step, only when  $\psi_{sz1z2}$  lies in sectors 1 - 6, will  $V_9$  be employed as in the classical ST-DTC strategy, otherwise,  $V_{43}$  will be adopted to decrease the amplitude of  $\psi_{sz1z2}$ .

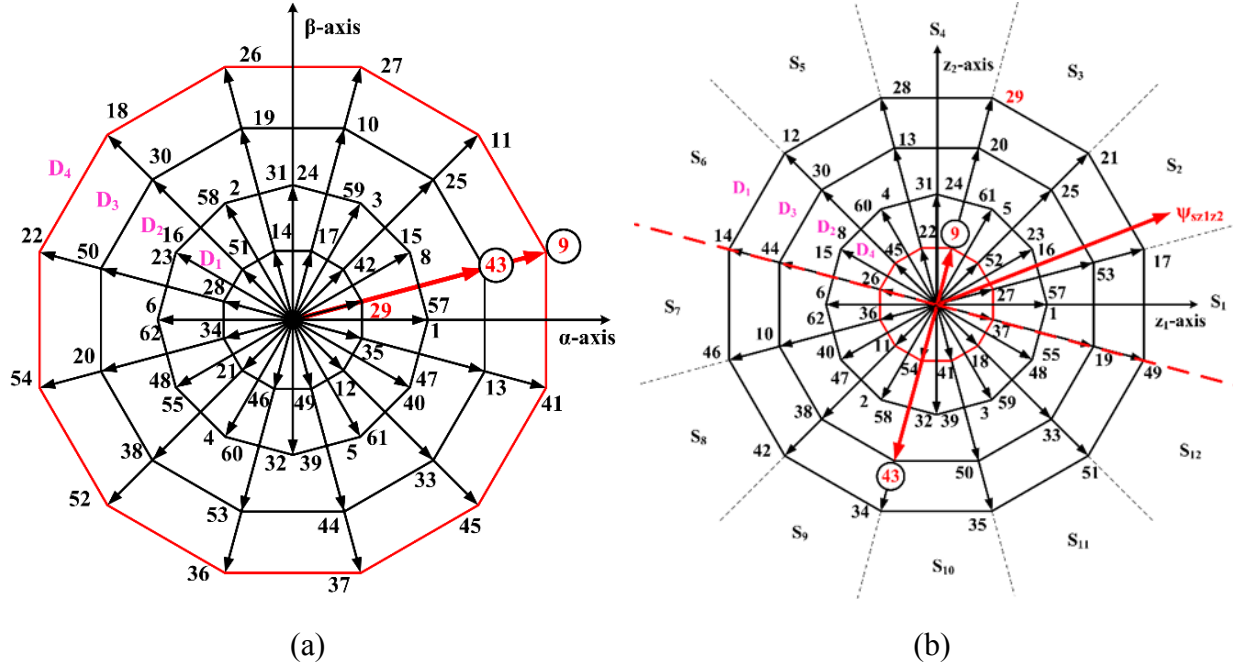


Fig. 5.2. Proposed voltage vector selection strategy in two subspaces. (a)  $\alpha\beta$  subspace. (b)  $z_1z_2$  subspace.

The block diagram of the proposed ST-DTC strategy is illustrated in Fig. 5.3. Compared to the block diagram of classical ST-DTC strategy as shown in Fig. 1.19, only one harmonic suppression module consisting of the flux estimator in the  $z_1z_2$  subspace shown in Appendices B and switching Table 5.2 is added to decrease the stator harmonic currents, therefore, the merits of the classical DTC strategy, i.e. simple structure and good robustness, are still preserved.

Table 5.2 Switching Table for Step Two in the Proposed DTC of Dual Three-phase Drive

Vector group $G_i$	Sector of $\psi_{sz1z2}$	Selected vector	Vector group $G_i$	Sector of $\psi_{sz1z2}$	Selected vector
9	7,8,9,10,11,12	$V_9$	54	1,2,3,4,5,6	$V_{54}$
	1,2,3,4,5,6	$V_{43}$		7,8,9,10,11,12	$V_{20}$
11	12,1,2,3,4,5	$V_{11}$	52	6,7,8,9,10,11	$V_{52}$
	6,7,8,9,10,11	$V_{25}$		12,1,2,3,4,5	$V_{38}$
27	5,6,7,8,9,10	$V_{27}$	36	11,12,1,2,3,4	$V_{36}$
	11,12,1,2,3,4	$V_{10}$		5,6,7,8,9,10	$V_{53}$
26	10,11,12,1,2,3	$V_{26}$	37	4,5,6,7,8,9	$V_{37}$
	4,5,6,7,8,9	$V_{19}$		10,11,12,1,2,3	$V_{44}$
18	3,4,5,6,7,8	$V_{18}$	45	9,10,11,12,1,2	$V_{45}$
	9,10,11,12,1,2	$V_{30}$		3,4,5,6,7,8	$V_{33}$
22	8,9,10,11,12,1	$V_{22}$	41	2,3,4,5,6,7	$V_{41}$
	2,3,4,5,6,7	$V_{50}$		8,9,10,11,12,1	$V_{13}$

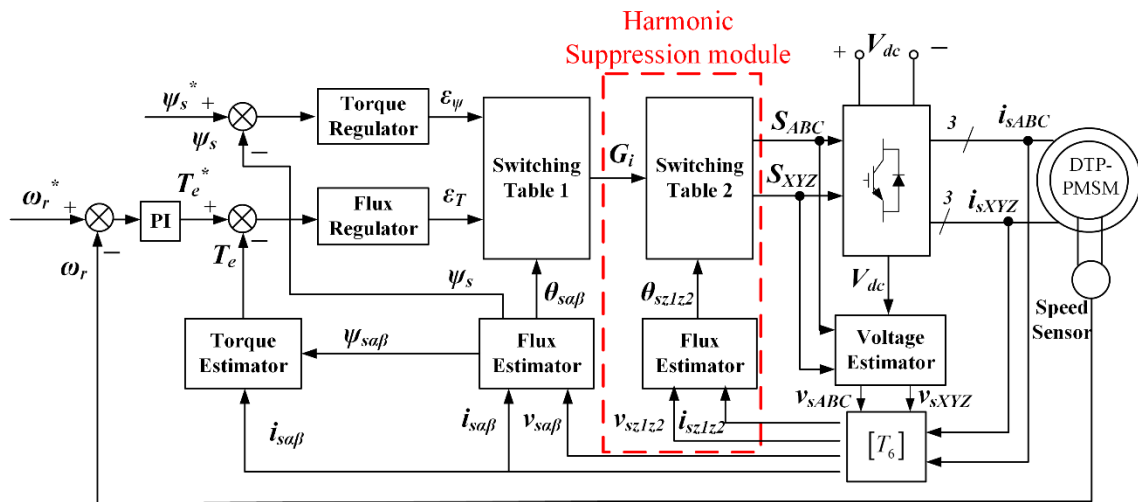


Fig. 5.3. Block diagram of proposed ST-DTC strategy.

In general, the proposed ST-DTC strategy is simple because only the position information of the stator flux vector  $\psi_{sz1z2}$  is required, as shown in Fig. 5.3. As in the  $\alpha\beta$  reference frame, the problem

of flux drifting still exists in the  $z_1z_2$  reference frame. Flux drift will cause the controller to fail to reduce the harmonic currents, and also lead to a decrease in the average torque. Therefore, a low pass filter is employed to replace the pure integrator. A slight reduction of the utilization rate of the DC supply will inevitably occur because of the difference in magnitude between voltage vectors in  $D_3$  and  $D_4$ . Specifically, the amplitude of the vectors in  $D_3$  and  $D_4$  can be calculated according to Fig. 1.17(a). Taking  $V_9$  and  $V_{43}$  as example,

$$D_4: |V_9| = 2A \cos 15^\circ = \frac{\sqrt{6} + \sqrt{2}}{2} A \quad (5.3)$$

$$D_3: |V_{43}| = 2A \cos 45^\circ = \sqrt{2} A \quad (5.4)$$

where  $A = 2/3V_{dc}$  is the amplitude of the synthesized vector of one set of three phases in the dual three-phase drive.

Given a vector group selected from Table 5.1, the applicability of selecting a vector from  $D_3$  or  $D_4$  in Table 5.2 is the same. Therefore, the utilization rate of DC supply of the proposed ST-DTC strategy compared to that of classical ST-DTC strategy can be estimated as

$$\eta = \frac{|V_9| \cdot T_s / 2 + |V_{43}| \cdot T_s / 2}{|V_9| \cdot T_s} \cdot 100\% = \frac{\frac{\sqrt{6} + \sqrt{2}}{2} A + \sqrt{2} A}{2 \cdot \frac{\sqrt{6} + \sqrt{2}}{2} A} \cdot 100\% = 86.60\% \quad (5.5)$$

In summary, this proposed ST-DTC strategy only slightly changes the average amplitude of the applied voltage vector. Therefore, the torque performance, simple structure and desirable dynamic performance have been preserved, which results in the similar robustness to external disturbances. This is verified by the experimental results described shortly.

Note that the hysteresis band does have an important effect on the steady-state performance of torque. Since this chapter focuses on the reduction of harmonic currents and the hysteresis band has limited effect on the harmonic currents, this analysis is not expanded upon here. The detailed analysis of hysteresis band can be found in the literature [MAT13]. However, we have reduced the steady-state error of torque by using a band-shifted method which has been successfully applied

on the ST-DTC running a three-phase drive in Chapter 3 and [ZHU14].

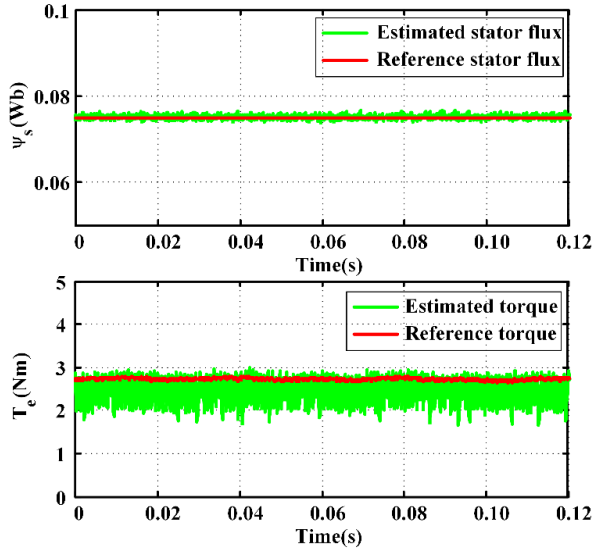
There are many factors that cause harmonic currents in a real-time system including, for example, the harmonic supply voltage, dead-time, and inverter nonlinearity. However, the harmonic supply voltage is the most dominant cause of the large harmonic currents in ST-DTC. By employing this modified ST-DTC strategy, the majority of the harmonic currents have been suppressed. The merits of the classical direct torque control, i.e. simple structure and good dynamic performance, are still preserved. For the sake of simplicity and parameter independence, other factors are not compensated in this chapter.

## 5.5. Experimental Results

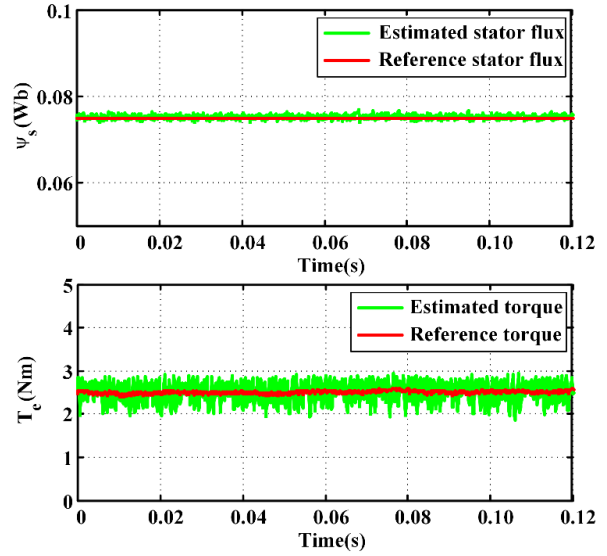
The overall control schemes with classical and proposed DTC strategies are shown in Fig. 1.19 and Fig. 5.3, respectively. Various experiments are implemented on the laboratory prototype dual three-phase PMSM machine II shown in Appendices A. The sample frequency is 10 kHz, and the DC-Bus voltage is set to 40 V. All the results were captured using dSPACE software, and then plotted using Matlab.

### 5.5.1. Steady-state Performance of Different ST-DTC Strategies

Fig. 5.4 - Fig. 5.6 shows the experimental results of the classical and proposed ST-DTC strategies for dual three-phase PMSM drives. The rotor speed reference and stator flux reference are set to 300 rpm, 0.075 Wb, respectively, while the load torque is approximately 2.5 Nm. From Fig. 5.4, the torque and stator flux can be controlled well both in the classical and proposed DTC strategies. The torque ripple is slightly reduced due to the decrease of the average amplitude of the applied voltage in one sampling period. The steady-state error of torque has been significantly reduced by using the band-shifted torque regulator of chapter 3 and [ZHU14]. However, the phase currents of the classical DTC strategy are non-sinusoidal, Fig. 5.5(a). This is because the components in the  $z_1z_2$  subspace are not controlled in the classical ST-DTC strategy, hence, the stator flux in the  $z_1z_2$  subspace  $\psi_{sz_1z_2}$  is not negligible any more, as shown in Fig. 5.5(d), resulting in the large harmonic currents, Fig. 5.5(b), (c). By using the proposed two-step process to choose the appropriate voltage vector, the stator flux in the  $z_1z_2$  subspace  $\psi_{sz_1z_2}$  is reduced compared to that in the classical strategy, Fig. 5.6(d). Therefore, the harmonic currents are significantly reduced, and consequently much more sinusoidal phase currents are achieved, Fig. 5.6(a), (b), (c).

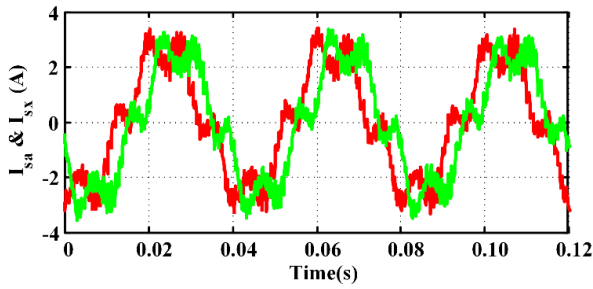


(a)

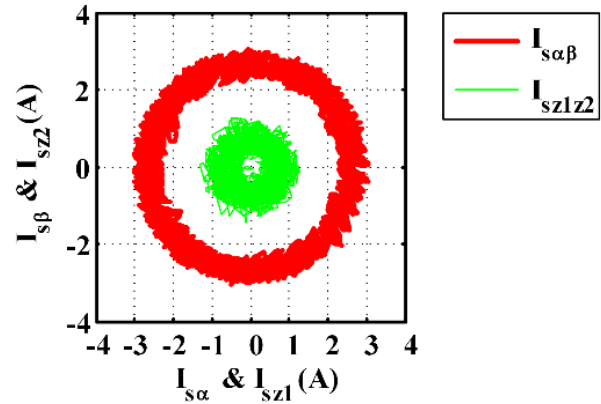


(b)

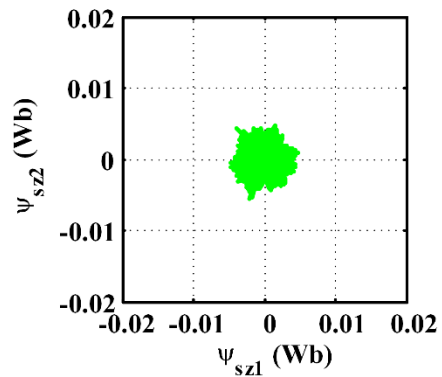
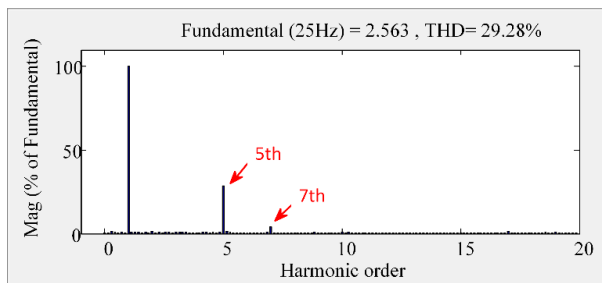
Fig. 5.4. Steady-state performance of torque and stator flux using different DTC strategies. (a) Classical ST-DTC strategy. (b) Proposed ST-DTC strategy.



(a)



(b)



(c)

(d)

Fig. 5.5. Steady-state performance of classical ST-DTC strategy. (a) Phase currents. (b)  $\alpha\beta$  and  $z1z2$  current circles. (c) Phase current harmonic spectrum. (d)  $z1z2$  stator flux circle.

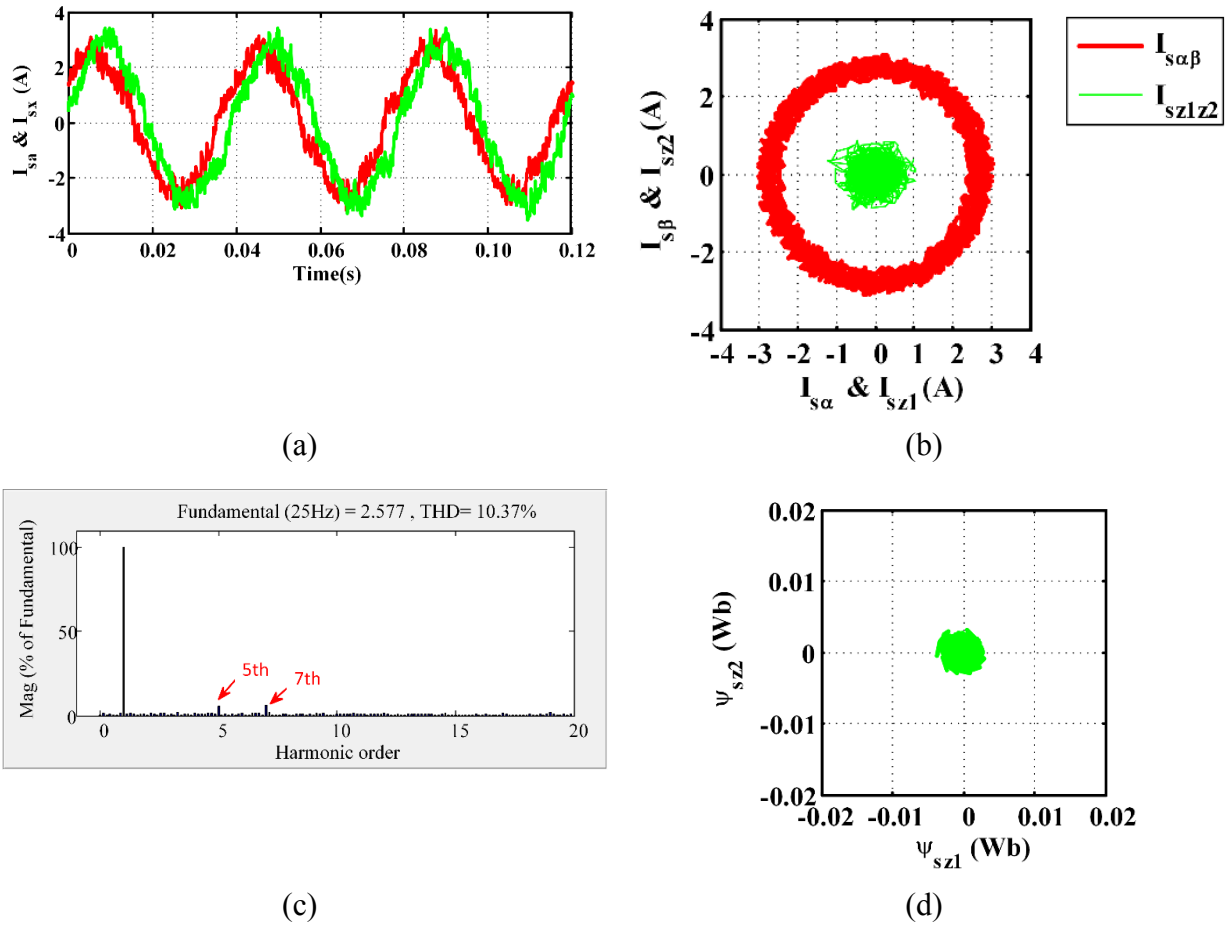


Fig. 5.6. Steady-state performance of proposed ST-DTC strategy. (a) Phase currents. (b)  $\alpha\beta$  and  $z1z2$  current circles. (c) Phase current harmonic spectrum. (d) Stator flux circle.

Since the harmonic components do not contribute the electromechanical energy conversion, both the stator flux ripple in the  $\alpha\beta$  subspace and the torque ripple are almost equal to those using classical ST-DTC strategy. Detailed quantitative results are given in Table 5.3, where the torque and stator flux ripples are calculated as (3.17) and (3.18).

In switching-table-based DTC strategies, the switching frequency changes with the operating conditions. Therefore, the average commutation frequency  $f_{av}$ , which is calculated by counting the total commutation instants of one phase leg over a fixed period, is used to indicate the switching

losses [ZHA11a].

Table 5.3 Experimental Results of Classical and Proposed ST-DTC Strategies

300 rpm, 2.5 Nm	Classical ST-DTC	Proposed ST-DTC
Ripple of stator flux, $\psi_{s\_ripple}$ (Wb)	$5.4279 \times 10^{-4}$	$4.9134 \times 10^{-4}$
Torque ripple, $T_{e\_ripple}$ (Nm)	0.3106	0.2392
THD of phase-a current, $i_{a\_THD}$ (%)	29.28	<b><u>10.37</u></b>
Average commutation frequency, $f_{av}$ (kHz)	2.7572	3.5472

From Table 5.3, both the stator flux and torque ripple of the proposed ST-DTC strategy slightly decreases compared to the classical ST-DTC. This is due to the decrease of the average amplitude of applied voltage vectors. The THD of phase current has been decreased by 18.91%, from 29.28% to 10.37%, due to the significant reduction of harmonic currents in the  $z_1z_2$  subspace, Fig. 5.6(b). One drawback of the proposed method is that the average commutation frequency will increase a little, 0.79 kHz in this case, which results in a small increase of the switching losses. In the proposed strategy, two switching tables are needed to choose the most appropriate voltage vector. This makes the voltage vectors change more frequently compared to the classical approach. It is desirable to obtain a significant reduction of harmonic currents with only a small penalty of increasing the average commutation frequency slightly.

Table 5.4 shows the THD of phase-a current for classical and proposed ST-DTC strategies at the same rotor speed (400 rpm, the rated speed) and at various load torque from 1 Nm to 3 Nm. From Table 5.4 the proposed ST-DTC strategy can significantly reduce the THD of phase currents under a wide range of load conditions.

Table 5.4 THD of Phase-A Current for Classical and Proposed ST-DTC Strategies.

400 rpm	Classical ST-DTC	Proposed ST-DTC
1 Nm	52.14%	26.22%
2 Nm	33.84%	14.65%
3 Nm	26.06%	9.83%

### **5.5.2. Dynamic Performance of Inner Torque Loop Control for Conventional and Proposed DTC**

As mentioned above, the utilization rate of DC supply is slightly reduced in the proposed DTC strategy. Therefore, it is necessary to check whether the dynamic performance of torque control will deteriorate accordingly.

Fig. 5.7 shows the dynamic response of torque when the torque reference changes from 1 Nm to 3 Nm, with open-loop speed control, i.e. with inner torque control only, for both conventional and improved DTC strategies. The torque can reach the reference torque in less than 1 ms, which is similar to that of the conventional DTC strategy. Hence, the proposed strategy will not deteriorate the dynamic torque performance.

### **5.5.3. Dynamic Response to External Load Disturbance for Proposed DTC Strategy**

The response to external load disturbance is compared between the conventional DTC and the proposed method. The motor is initially operated under steady-state at 400 rpm with no load. The external load of approximately 2.5 Nm is suddenly added at 1.0 s in Fig. 5.8. The torque generated with the proposed method can follow the reference produced by the speed regulator as similarly to the conventional controller. The speeds in both the conventional and the proposed strategy return to the original value in less than 0.3 s.

These experimental results show that the proposed ST-DTC method can preserve the robustness against external load disturbances of the conventional ST-DTC.

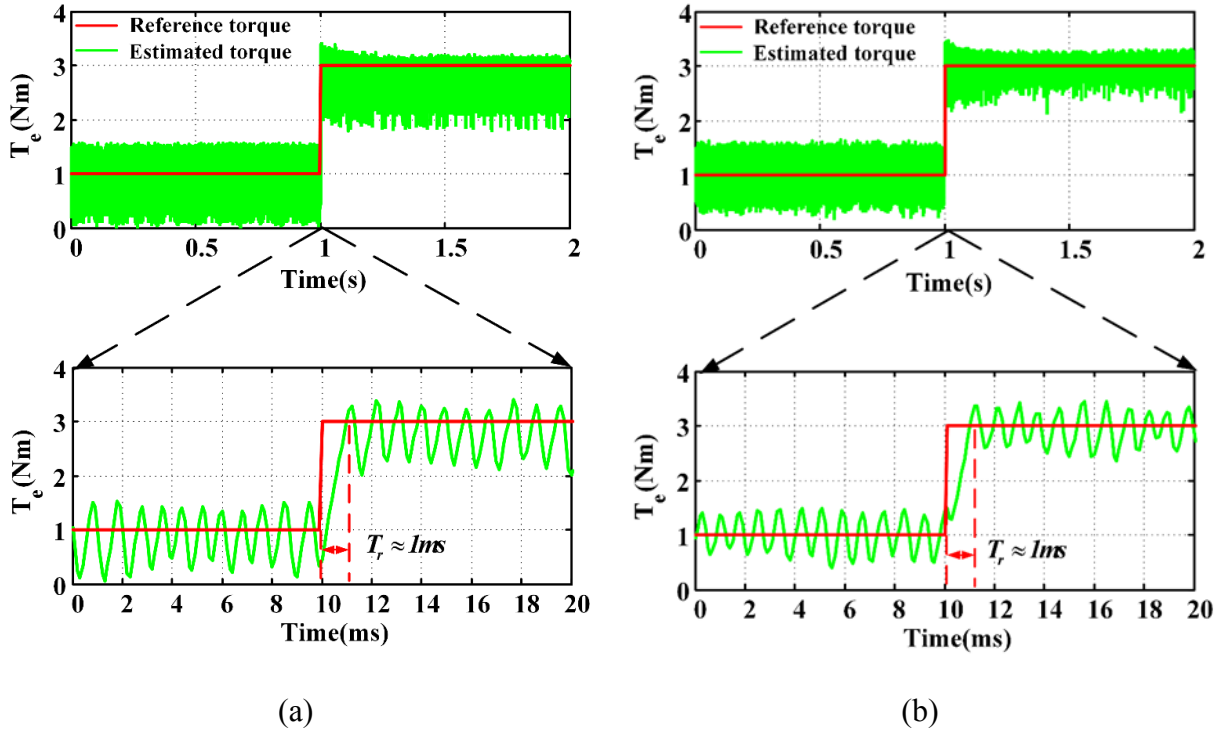


Fig. 5.7. Dynamic performance of inner torque loop control using different DTC methods: reference torque: 1 Nm to 3 Nm. (a) Classical ST-DTC strategy. (b) Proposed ST-DTC strategy.

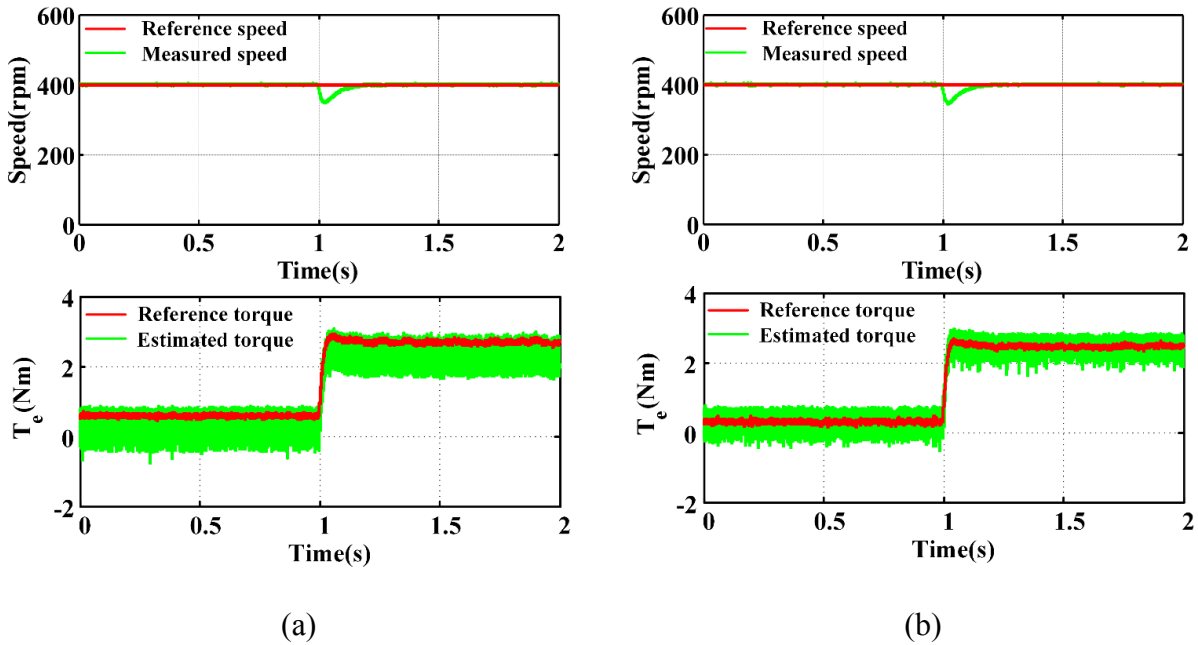


Fig. 5.8. Responses to external disturbance of different DTC strategies. (a) Classical ST-DTC strategy. (b) Proposed ST-DTC strategy.

## 5.6. Conclusion

This chapter presents the application of ST-DTC to a dual three-phase PMSM drive using a vector space decomposition technique. To minimize the undesirable large stator harmonic currents, a two-step process voltage vector selection scheme has been proposed. The classical ST-DTC strategy only controls the variables in the  $\alpha\beta$  subspace relating to the torque production, so the uncontrolled flux space vector in the other subspace results in substantial stator harmonics currents. The proposed ST-DTC strategy not only controls the variables in the  $\alpha\beta$  subspace, but also significantly reduces the magnitude of the flux space vector in the  $z_1z_2$  subspace, which results in considerably lower harmonic stator currents. The experimental results verify that the proposed methods can significantly reduce the stator current harmonics. Since only a single harmonic suppression module, consisting of the flux estimator in the  $z_1z_2$  subspace and a switching table is added, the merits of the classical direct torque control, i.e. simple structure and good robustness are preserved.

## **6. Enhancement of Steady-state Performance in Direct Torque Controlled Dual Three-phase Permanent Magnet Synchronous Machine Drives with Modified Switching Table**

### **6.1. Introduction**

Dual three-phase PMSM suffers from the large harmonic currents when the classical DTC is utilized. Chapter 5 presents a two-step process voltage vector selection scheme. However, the harmonic currents in this situation can only be reduced to some extent. Furthermore, two switching tables and an additional flux observer are required, which compromises the simplicity of the ST-DTC scheme.

This chapter presents an improved ST-DTC strategy to reduce the stator current harmonics, suppress the torque ripple and reduce steady-state error of torque. Based on the analysis of the influence of the inverter vectors on torque production and stator flux in different subspaces, a modified switching table consisting of twelve new synthetic voltage vectors is proposed, and the most suitable switching sequence for the implementation in a real-time system is presented, as well as the modified torque regulator. The proposed strategy preserves the advantages of ST-DTC including, simple structure and desirable dynamic performance. Experimental results are provided to substantiate the effectiveness of the proposed strategy.

### **6.2. Proposed ST-DTC Strategy**

#### **6.2.1. Principle of Proposed ST-DTC Strategy**

As mentioned above, only using the outermost dodecagon ( $D_4$ ) of the  $\alpha\beta$  subspace is not enough to obtain sufficient steady-state performance as current harmonics will inevitably exist. The increased number of the voltage vectors allows the possibility to generate a more elaborate switching table in which the selection of the voltage vectors will meet not only the flux and torque regulation requirements, but also the demand of eliminating the current harmonics.

As discussed in Chapter 5, by employing the vectors in the  $D_3$  and  $D_4$  dodecagons together, it is possible that the amplitude of  $\psi_{sz1z2}$  can be reduced, and that the corresponding harmonic currents will be decreased. Based on this principle, a two-step process is proposed to use the vectors of  $D_3$  and  $D_4$  dodecagons together depending on the position of  $\psi_{sz1z2}$ , as discussed in chapter 5. In this

method, the two vectors, one from  $D_3$  and the other from  $D_4$ , which point to the same direction in the  $\alpha\beta$  subspace, will be considered as one group. The classical switching table decides which group to choose, and then according to the position of  $\psi_{sz1z2}$ , the most suitable vector will be picked to decrease the stator flux  $\psi_{sz1z2}$ , Fig. 6.1(a). This method is shown to be effective to reduce the stator current harmonics [HOA15]. However, two switching tables and one additional flux observer for  $\psi_{sz1z2}$  are required in this method, which will increase the complexity of the DTC strategy. Moreover, the utilization rate of DC supply is also reduced by approximately 13.40% due to the use of vectors in the  $D_3$  dodecagon.

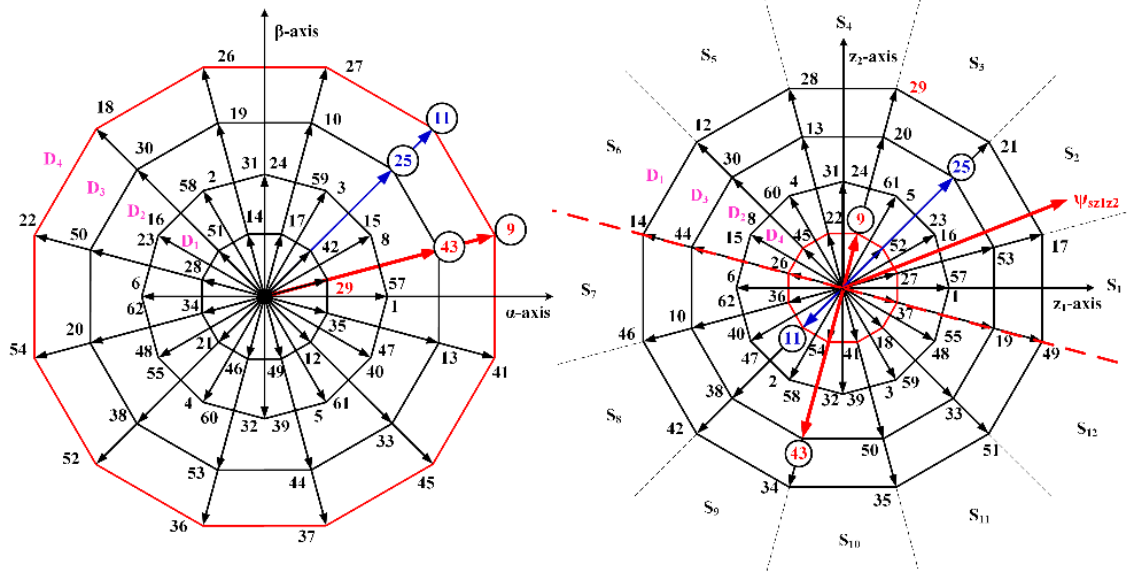
In this chapter, 12 new synthetic voltage vectors are employed to replace the 12 vectors of  $D_4$  which are used in the classical DTC. The block diagram of the proposed ST-DTC strategy is shown in Fig. 1.19. It is instructive to compare the block diagram of classical ST-DTC strategy shown in Fig. 1.19 with Fig. 6.2. The control structures are almost the same, only the switching table is modified, i.e., the new layer  $D_{\text{new}}$  consisting of 12 new synthetic voltage vectors is employed to replace the classical one ( $D_4$ ) used in the classical DTC strategy, to reduce the stator harmonic currents, Fig. 6.1(b). Therefore, the merits of the classical DTC strategy, i.e. simple structure, and robustness, are preserved.

In order to minimize the stator harmonic currents, 12 new synthetic voltage vectors are obtained by a weighted-sum approach using the vectors of  $D_3$  and  $D_4$  together to minimize the flux in  $z_1z_2$  subspace.

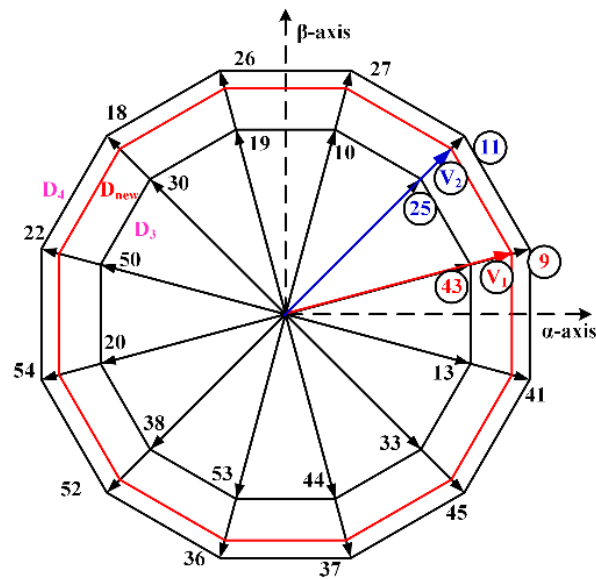
The amplitude of the vectors in  $D_3$  and  $D_4$  in  $z_1z_2$  subspace can be calculated according to Fig. 5(b), as follows:

$$D_4: |V_{D4}|_{-z_1z_2} = 2A \cos 75^\circ = \frac{\sqrt{6} - \sqrt{2}}{2} A \quad (6.1)$$

$$D_3: |V_{D3}|_{-z_1z_2} = 2A \cos 45^\circ = \sqrt{2} A \quad (6.2)$$



(a)



(b)

Fig. 6.1. Improved voltage vector selection strategies: (a) Two-step selection strategy. (b) Proposed selection strategy.

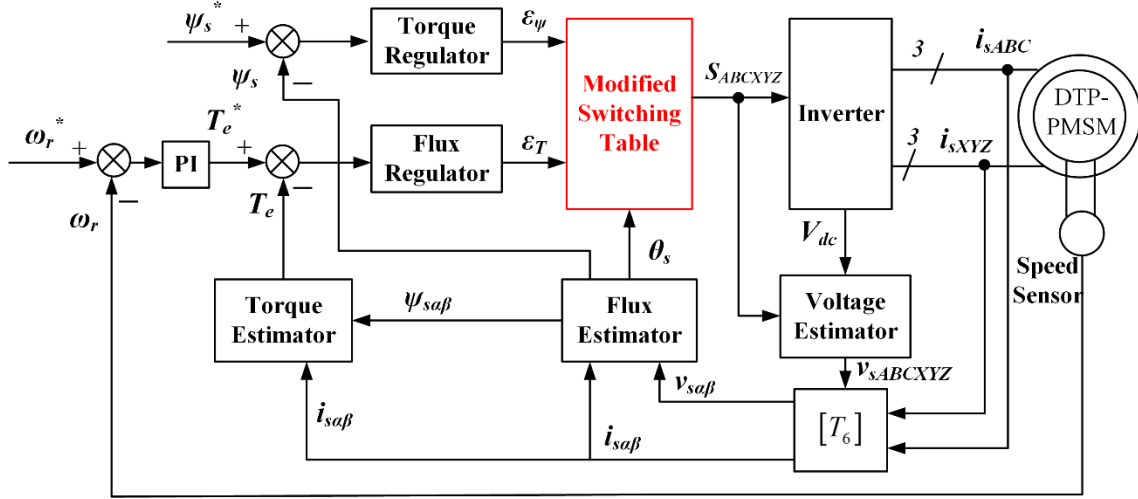


Fig. 6.2. Block diagram of proposed ST-DTC strategy.

Therefore, to minimize the amplitude of the stator flux in  $z_{1Z2}$  subspace, the relationship of the action times of the vectors in  $D_3$  and  $D_4$ ,  $T_{D3}$  and  $T_{D4}$ , can be expressed as

$$\begin{cases} \frac{\sqrt{6}-\sqrt{2}}{2} A \cdot T_{D4} = \sqrt{2} A \cdot T_{D3} \\ T_{D4} + T_{D3} = T_s \end{cases} \quad (6.3)$$

According to (6.3), the action times of the vectors in  $D_3$  and  $D_4$  can be calculated as

$$\begin{cases} T_{D4} = (\sqrt{3}-1)T_s \\ T_{D3} = (2-\sqrt{3})T_s \end{cases} \quad (6.4)$$

Hence, by applying the vectors of  $D_3$  and  $D_4$  with the appropriate time durations  $T_{D3}$  and  $T_{D4}$ , the stator current harmonics can be minimized.

Slight reduction of the utilization rate of DC supply will still occur due to the difference in magnitudes between voltage vectors in  $D_3$  and  $D_4$  in the  $\alpha\beta$  subspace.

The amplitudes of the vectors in the  $D_3$  and  $D_4$  dodecagons can be calculated according to Fig. 6.1(a), as follows

$$D_4: |V_{D4}|_{-\alpha\beta} = 2A \cos 15^\circ = \frac{\sqrt{6}+\sqrt{2}}{2} A \quad (6.5)$$

$$D_3: |V_{D3}|_{-\alpha\beta} = 2A \cos 45^\circ = \sqrt{2}A \quad (6.6)$$

Therefore, the amplitude of the synthetic vector in the  $\alpha\beta$  subspace is

$$|V_{\alpha\beta}| = |V_{D4}|_{-\alpha\beta} * T_{D4} + |V_{D3}|_{-\alpha\beta} * T_{D3} = (3\sqrt{2} - \sqrt{6})A \quad (6.7)$$

The utilization rate of DC supply of proposed ST-DTC strategy compared to that of classical ST-DTC scheme will be

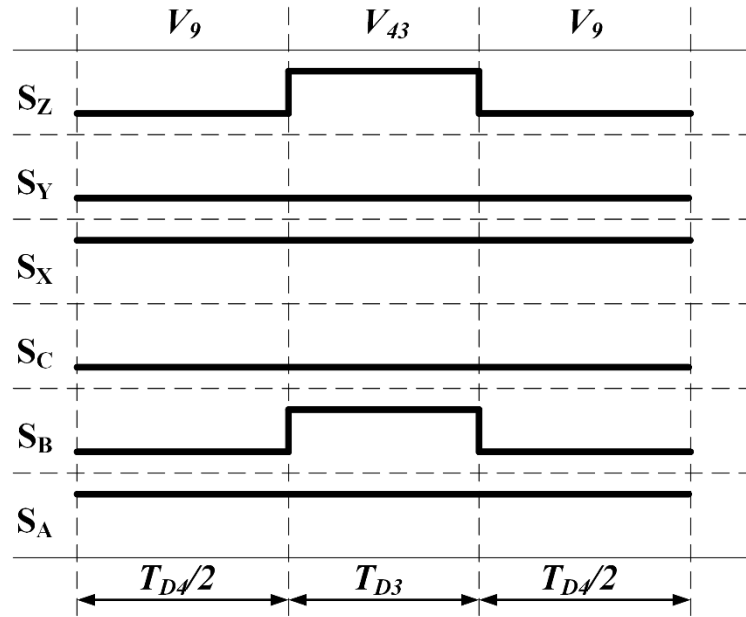
$$\eta_{V_{dc}} = \frac{|V_{\alpha\beta}|}{|V_{D4}|_{-\alpha\beta}} * 100\% = \frac{(3\sqrt{2} - \sqrt{6})A}{\frac{\sqrt{6} + \sqrt{2}}{2} A} * 100\% = 92.82\% \quad (6.8)$$

which is higher than that of the two-step ST-DTC method in chapter 5.

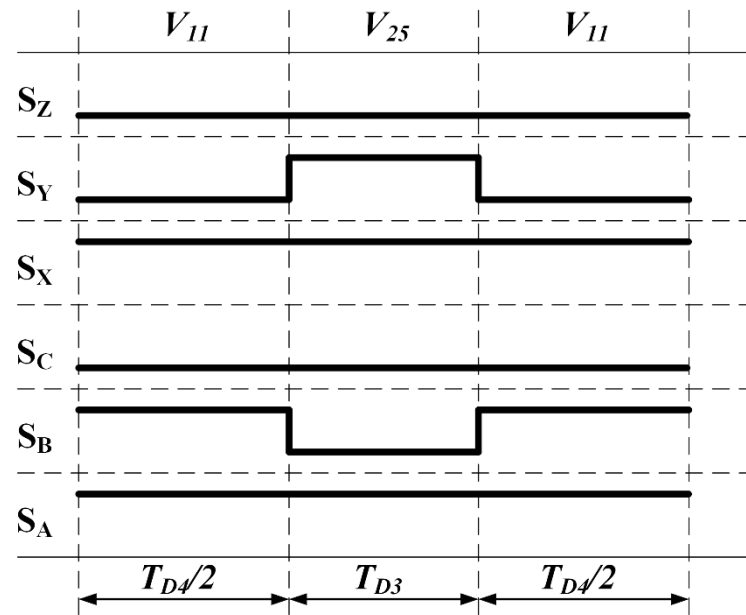
### 6.2.2. Switching Sequence and Implementation

Since there are two vectors within one sampling period, a suitable switching sequence should be devised. Taking  $V_9-V_{43}$  and  $V_{11}-V_{25}$  as examples, the switching sequences for them are shown in Fig. 6.3(a) and (b), respectively. The most commonly used PWM generation technique produces a signal in which the inverted and non-inverted signals are symmetrical around the middle of the PWM period, and the level of the signals in the middle of the PWM period are high. This can be considered as a standard switching sequence for real-time systems such as DSP and dSPACE systems. Therefore, it is easy to implement the standard switching sequence  $V_9-V_{43}$ , while difficult for non-standard switching sequence  $V_{11}-V_{25}$  because the levels of  $S_Y$  and  $S_B$  are always different in the middle of the PWM period. It requires specific PWM generation techniques to implement these kinds of non-standard waveforms, which increases the computation burden and abates the simplicity of ST-DTC strategies.

In order to keep the merit of ST-DTC strategies, the switching sequences need to be modified. For instance, by reassigning the PWM levels of  $S_B$  in Fig. 6.3(b), the standard switching sequence can be obtained as shown in Fig. 6.3(c), which is easy to implement. However, the actual applied voltage vectors have been changed from  $V_{11}-V_{25}$  to  $V_9-V_{11}-V_{27}$ , and the action time of each vector has been modified accordingly, Fig. 6.3(c). The combination of this new synthetic vector and its amplitudes in two subspaces can be calculated from Fig. 6.4:



(a)



(b)

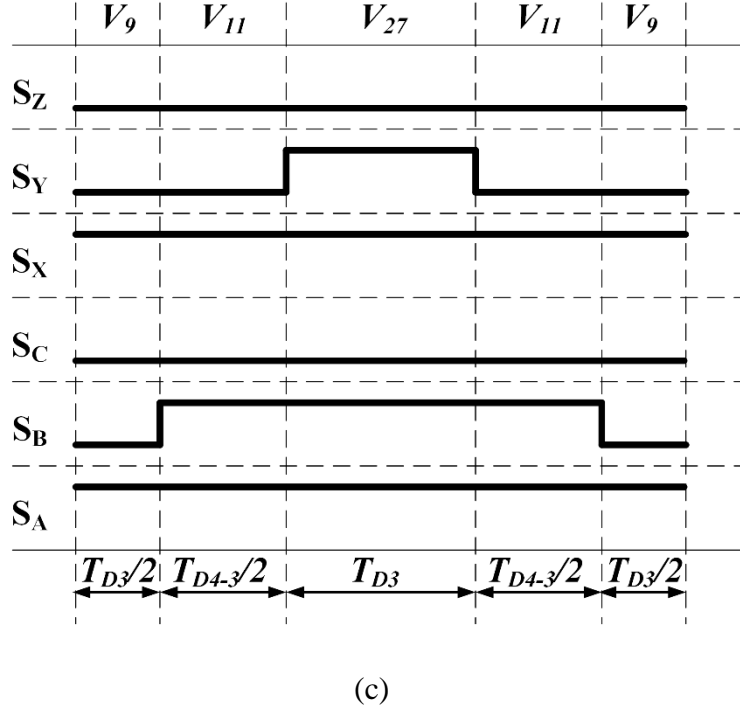


Fig. 6.3. Switching sequences of the synthetic vectors. (a)  $V_9$ - $V_{43}$ . (b)  $V_{11}$ - $V_{25}$ . (c)  $V_9$ - $V_{11}$ - $V_{27}$ .

$$T_{D4-3} = T_{D4} - T_{D3}.$$

$$\begin{aligned} |V_{\alpha\beta}|_{-new} &= \left[ |V_{D4}|_{-\alpha\beta} * \cos(\pi/6) * T_{D3} * 2 + |V_{D4}|_{-\alpha\beta} * (T_{D4} - T_{D3}) \right] / T_s \\ &= (3\sqrt{2} - \sqrt{6})A \end{aligned} \quad (6.9)$$

$$\begin{aligned} |V_{z1z2}|_{-new} &= \left[ |V_{D4}|_{-\alpha\beta} * \cos(\pi/6) * T_{D3} * 2 - |V_{D4}|_{-\alpha\beta} * (T_{D4} - T_{D3}) \right] / T_s \\ &= 0 \end{aligned} \quad (6.10)$$

From (6.7), (6.9) and (6.10) the amplitude of the new synthetic vector is given by  $V_9$ - $V_{11}$ - $V_{27}$ . In both the  $\alpha\beta$  subspace and the  $z_1z_2$  subspace, this is the same as that of the synthetic vector consisting of  $V_{11}$ - $V_{25}$ . The modification of switching sequence keeps the influences on torque and stator flux in  $\alpha\beta$  subspace the same. Therefore the amplitude of the stator flux in  $z_1z_2$  subspace still can be minimized.

Similar results can be obtained for the rest of the synthetic vectors in Fig. 6.1(b). All the synthetic vectors, which have standard switching sequences, are listed in Table 6.1. In summary, six

synthetic vectors can be obtained by two vectors, and the other six synthetic vectors should adopt three vectors to meet the requirement of the standard switching sequences.

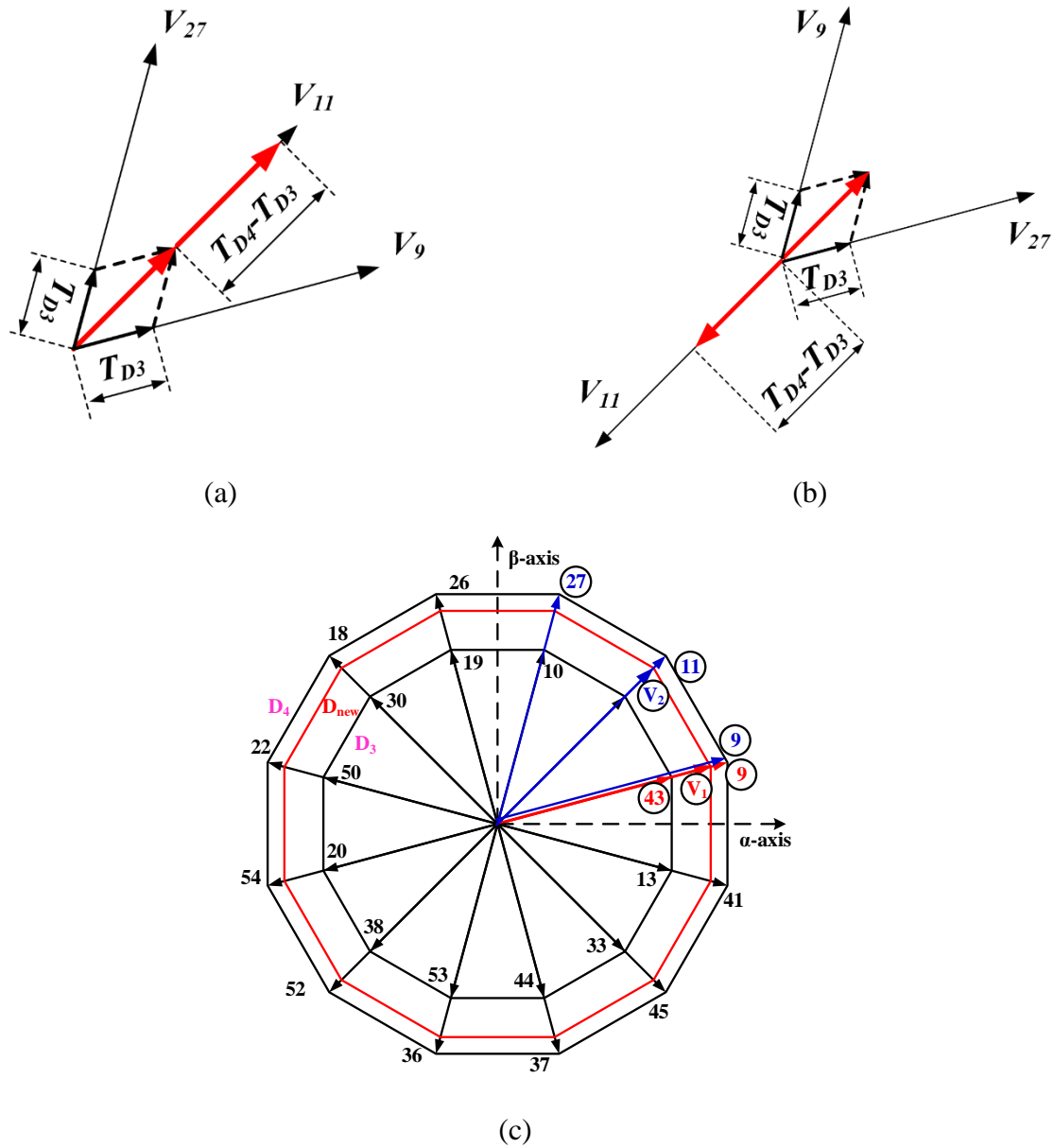


Fig. 6.4. Calculation of amplitudes of new synthetic vector in different subspaces. (a)  $\alpha\beta$  subspace. (b)  $z_1z_2$  subspace. (c) Combination of new synthetic vector.

The duty cycle of each switching component for the proposed strategy is presented in Table 6.2. It is convenient to implement the proposed strategy in the real-time system: select the vectors from Table 5.1 just like the classical ST-DTC scheme, and then change the duty cycle of each vector according to Table 6.2.

Table 6.1 Selection of Synthetic Vectors for Proposed ST-DTC Strategy

Vectors for classical ST-DTC strategy	Synthetic vectors for proposed ST-DTC strategy
$V_9$	$V_9 \cdot T_{D4} + V_{43} \cdot T_{D3}$
$V_{11}$	$V_9 \cdot T_{D3} + V_{11} \cdot T_{D4-3} + V_{27} \cdot T_{D3}$
$V_{27}$	$V_{27} \cdot T_{D4} + V_{10} \cdot T_{D3}$
$V_{26}$	$V_{27} \cdot T_{D3} + V_{26} \cdot T_{D4-3} + V_{18} \cdot T_{D3}$
$V_{18}$	$V_{18} \cdot T_{D4} + V_{30} \cdot T_{D3}$
$V_{22}$	$V_{18} \cdot T_{D3} + V_{22} \cdot T_{D4-3} + V_{54} \cdot T_{D3}$
$V_{54}$	$V_{54} \cdot T_{D4} + V_{20} \cdot T_{D3}$
$V_{52}$	$V_{54} \cdot T_{D3} + V_{52} \cdot T_{D4-3} + V_{36} \cdot T_{D3}$
$V_{36}$	$V_{36} \cdot T_{D4} + V_{53} \cdot T_{D3}$
$V_{37}$	$V_{36} \cdot T_{D3} + V_{37} \cdot T_{D4-3} + V_{45} \cdot T_{D3}$
$V_{45}$	$V_{45} \cdot T_{D4} + V_{33} \cdot T_{D3}$
$V_{41}$	$V_{45} \cdot T_{D3} + V_{41} \cdot T_{D4-3} + V_9 \cdot T_{D3}$

Table 6.2 Duty Cycle of Each Switching Component for Proposed ST-DTC Strategy

Vectors and switching state for classical ST-DTC strategy	Duty cycle of each switching component for proposed ST-DTC strategy					
	$S_Z$	$S_Y$	$S_X$	$S_C$	$S_B$	$S_A$
$V_9(001001)$	$T_{D3}$	0	1	0	$T_{D3}$	1
$V_{11}(001011)$	0	$T_{D3}$	1	0	$T_{D4}$	1
$V_{27}(011011)$	0	$T_{D4}$	1	0	1	$T_{D4}$
$V_{26}(011010)$	0	1	$T_{D4}$	0	1	$T_{D3}$
$V_{18}(010010)$	0	1	$T_{D3}$	$T_{D3}$	1	0
$V_{22}(010110)$	$T_{D3}$	1	0	$T_{D4}$	1	0
$V_{54}(110110)$	$T_{D4}$	1	0	1	$T_{D4}$	0
$V_{52}(110100)$	1	$T_{D4}$	0	1	$T_{D3}$	0
$V_{36}(100100)$	1	$T_{D3}$	0	1	0	$T_{D3}$
$V_{37}(100101)$	1	0	$T_{D3}$	1	0	$T_{D4}$
$V_{45}(101101)$	1	0	$T_{D4}$	$T_{D4}$	0	1
$V_{41}(101001)$	$T_{D4}$	0	1	$T_{D3}$	0	1

### 6.2.3. Modification of Torque Regulator to Improve the Steady-state Performance of Torque Response

By employing the new synthetic vectors, harmonic stator currents can be suppressed significantly. However, the steady-state error and ripple of torque which always exist are also very important metrics of performance. They cannot be reduced due to the similar influence on torque of the classical vectors and proposed vectors. A modified torque regulator has been employed to reduce the steady-state error of torque for three-phase drives [ZHU14]. Similar principles can be extended to dual three-phase drives. However, as noted in [ZHU14], torque ripple still exists at the same level. Although introducing zero vectors within one sampling period can significantly reduce the torque ripple, high computational burden would exist because of the complicated calculation of the duration of active vectors. Also, high switching frequency cannot be avoided using this method.

The aim of this chapter is to improve the steady-state performance of classical ST-DTC when the switching frequency is limited. Simple structure and parameter dependence are also required. Hence, a very simple modified torque regulator is needed here. Since the decreasing variation of torque is usually larger than the increasing variation, especially under medium and high speed conditions [REN14], [ZHU14], the active vectors which increase the torque should be treated differently from the ones which decrease the torque. That means the classical torque regulator, which deals with active vectors equally, should be modified. In order to clearly explain the modification of torque regulator, the actual torque curves have been divided into several segments, as shown in Fig. 6.5. Considering the effect of the one-step delay, an effective torque regulator should ensure that the applied vector which is supposed to be employed in very segment (if no delay has been considered) could also be adopted in the next segment. According to this rule, the active vector in the FG segment, which will reduce the torque significantly, is not a good choice since the actual torque would drop below the torque reference too much if that active vector is applied on segment GH. This would result in large torque ripple. Therefore, it is preferred to apply zero vectors which also reduce torque but with small variation, rather than to apply that active vector with larger decreasing variation. Similarly, zero vectors applied in segment GH should be replaced by an active vector to increase torque, as shown in Fig. 6.5(b). Therefore, by using this modified torque regulator combined with the method proposed in Chapter 3 and in [ZHU14] together, both the steady-state error and ripple of torque can be reduced.

In summary, compared to the two-step selection DTC method in chapter 5, the proposed method not only keeps the merit of simple structure of classical ST-DTC, but also achieves higher utilization rate of DC supply. Even compared to the classical DTC strategy, the proposed strategy only has about 7% reduction, according to (6.8), in the utilization rate of DC supply. There is also a significant reduction of stator current harmonics, torque ripple and steady-state torque error.

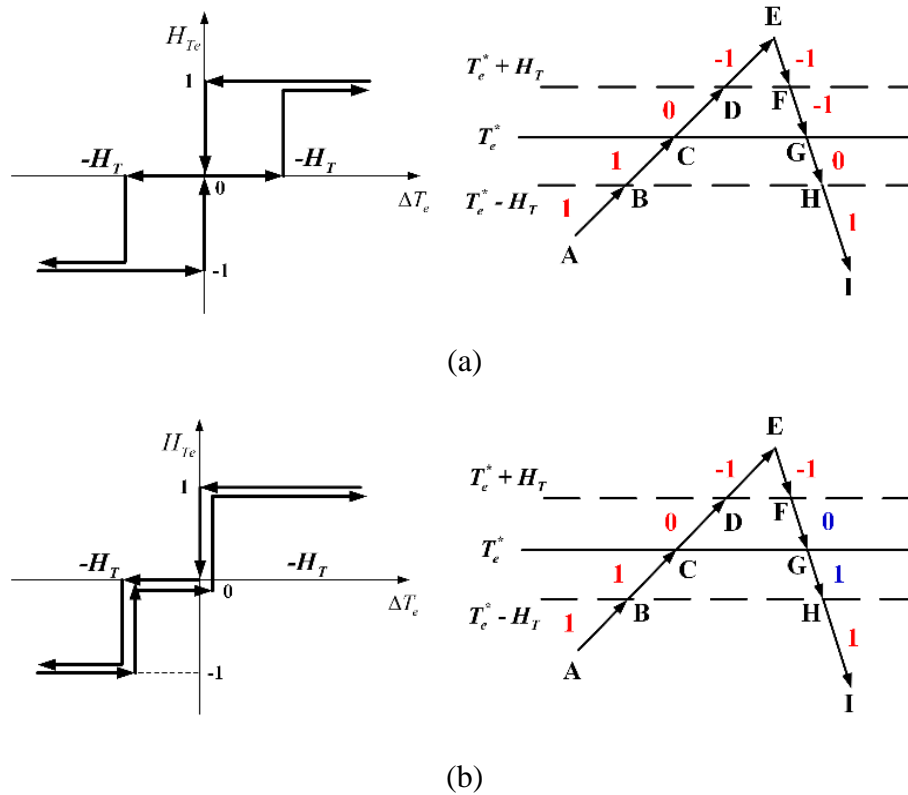


Fig. 6.5. Illustration of classical and proposed torque regulators. (a) Classical torque regulator.  
 (b) Proposed torque regulator.

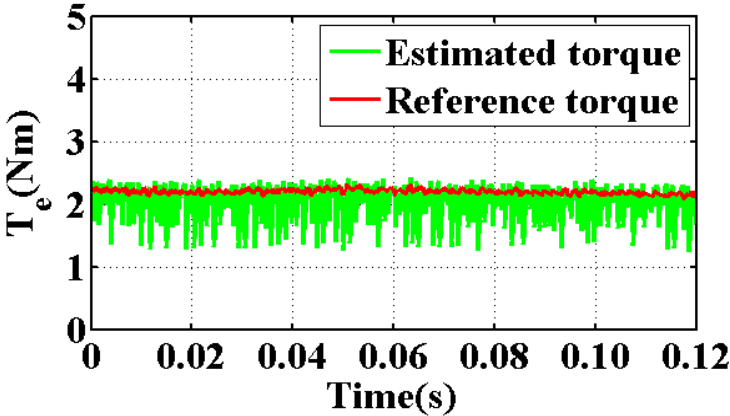
### 6.3. Experimental Results

Experiments are carried out on a dSPACE DS1005 platform with a laboratory prototype of dual three-phase PMSM machine II. The overall control schemes with classical and proposed ST-DTC strategies are shown in Fig. 1.19 and Fig. 6.2, respectively. The sample frequency is 10 kHz unless otherwise stated and the DC-link voltage is 40 V. The torque and flux hysteresis bands are set as 0.1 Nm and 0.0002 Wb, respectively. A model which combines the voltage model and the current model is employed to estimate the stator flux and torque [LEE11]. All the results were captured using dSPACE software, and then plotted using MATLAB M files.

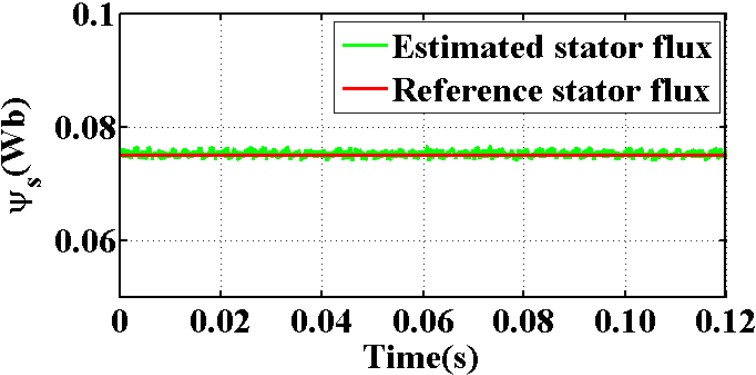
#### 6.3.1. Steady-state Performance of Different ST-DTC Strategies

Fig. 6.6-Fig. 6.9 show the experimental results of the classical, two-step (Chapter 5) and proposed ST-DTC strategies for dual three-phase PMSM drives, respectively. The rotor speed reference is set to 400 rpm, and the load torque is about 2 Nm. The steady-state error of torque has

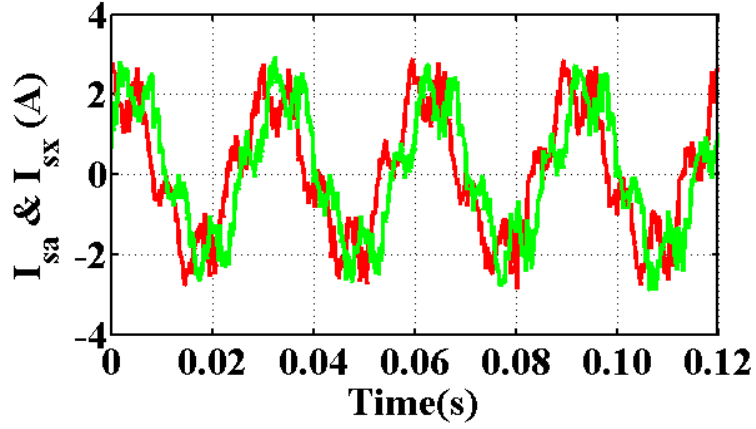
been considerably reduced in the proposed methods, Fig. 6.6(a)-Fig. 6.9(a). The phase currents of the classical DTC are non-sinusoidal, Fig. 6.6(c)-(e). By using the two-step method, the harmonic currents become much smaller and a lower THD value is achieved, Fig. 6.7(c)-(e). Compared to these two methods, the proposed strategy can achieve the lowest level of stator current harmonics, Fig. 6.8(c)-(e), and the least torque ripple and steady-state error of torque.



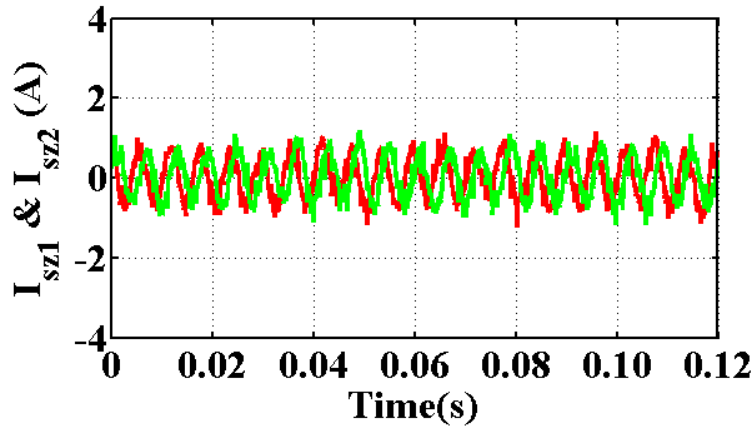
(a)



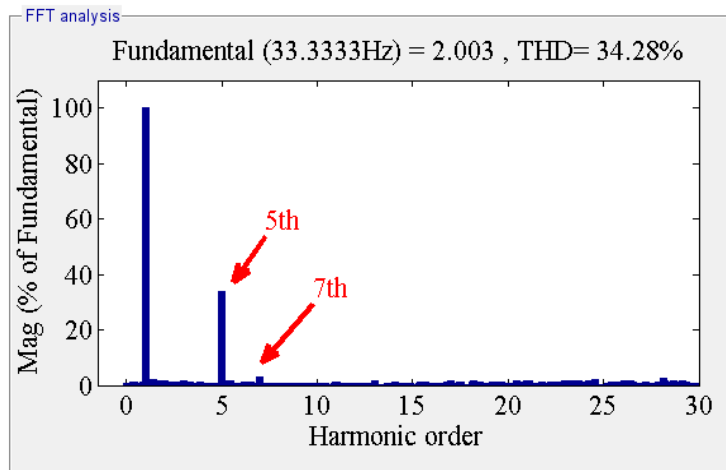
(b)



(c)

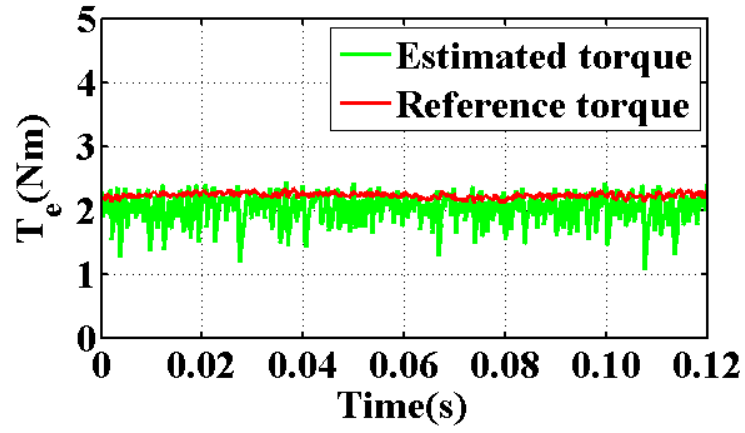


(d)

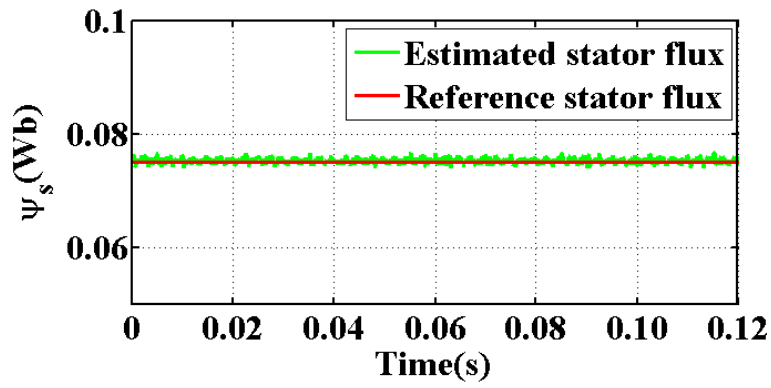


(e)

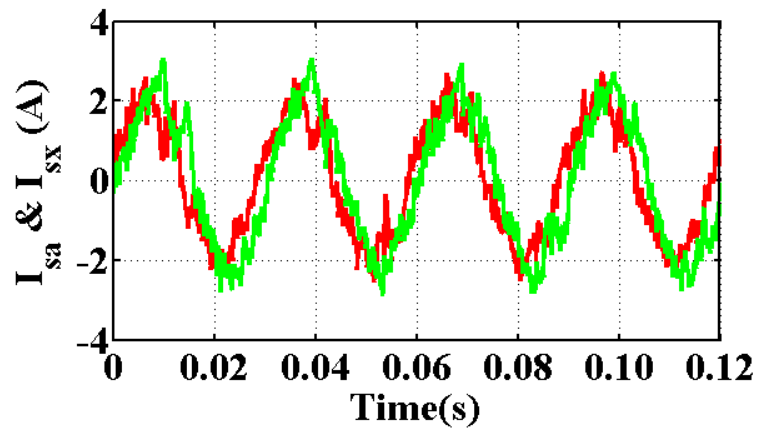
Fig. 6.6. Experimental results of classical ST-DTC strategy ( $f_s = 10$  kHz). (a) Electromagnetic torque. (b) Stator flux. (c) Phase currents. (d)  $z_1z_2$  currents. (e) Phase current harmonic spectrum.



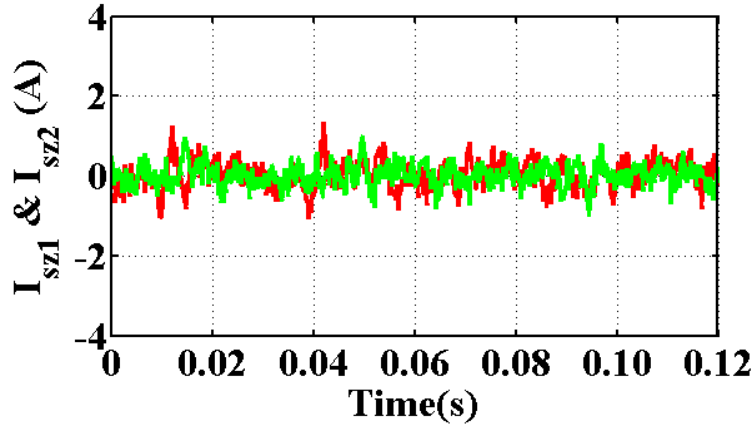
(a)



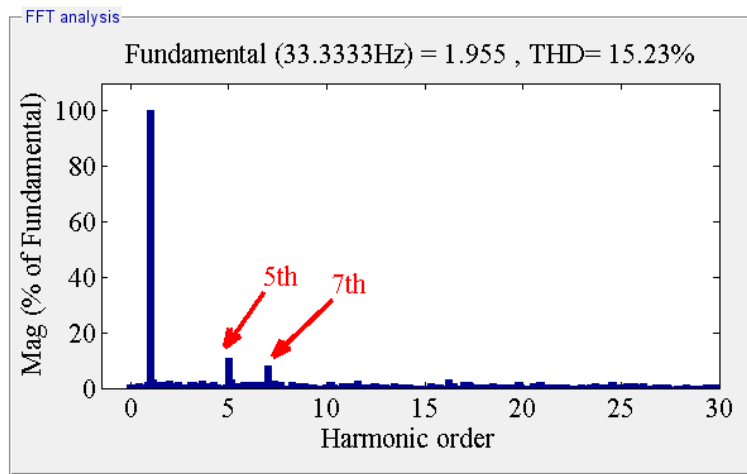
(b)



(c)

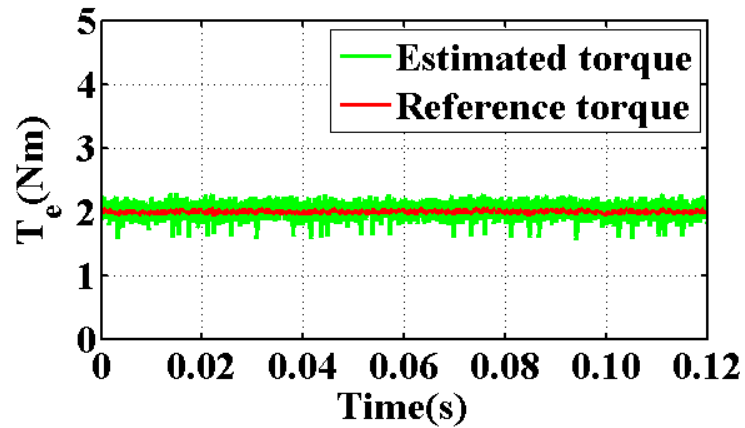


(d)

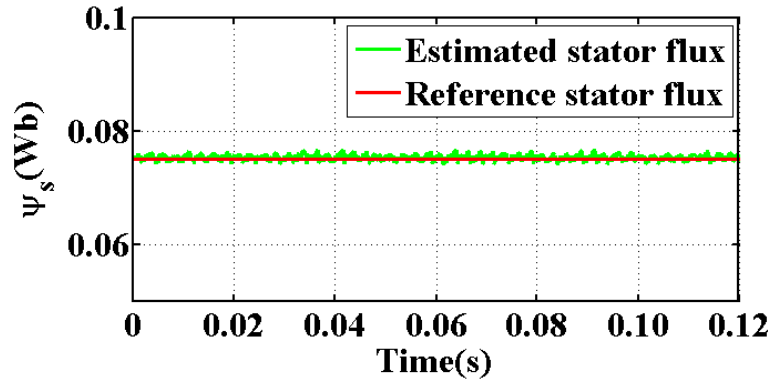


(e)

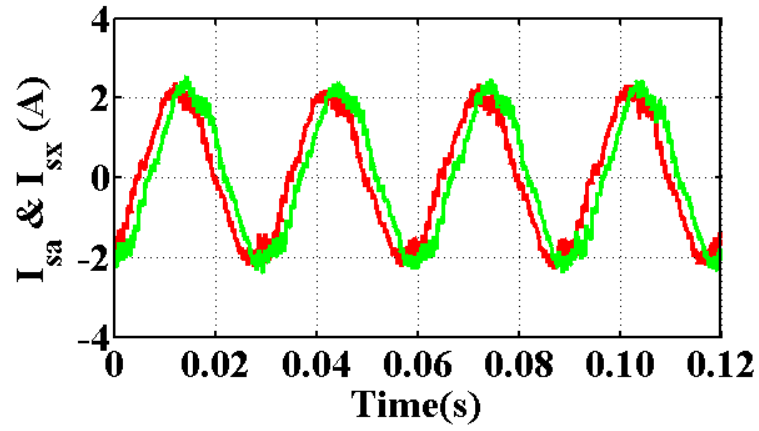
Fig. 6.7. Experimental results of two-step ST-DTC strategy ( $f_s = 10$  kHz). (a) Electromagnetic torque. (b) Stator flux. (c) Phase currents. (d)  $z_1z_2$  currents. (e) Phase current harmonic spectrum.



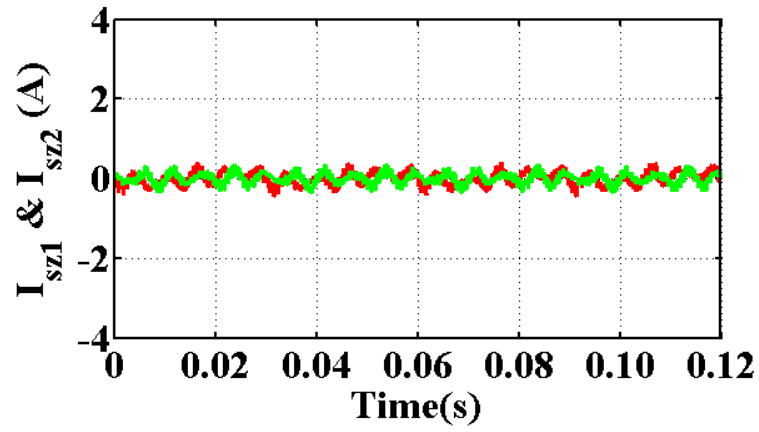
(a)



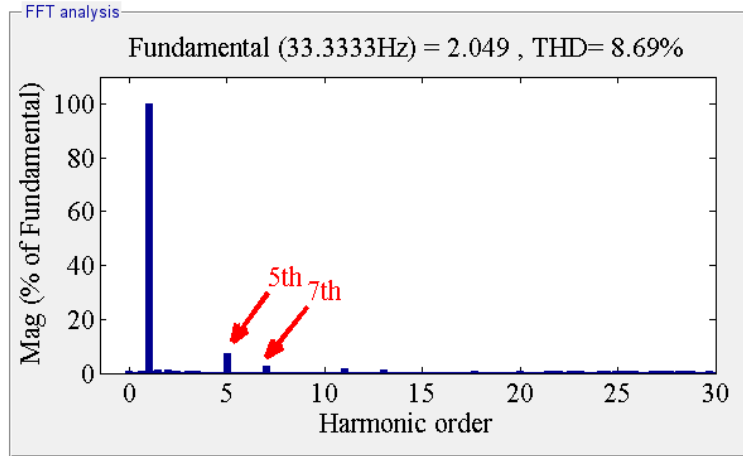
(b)



(c)

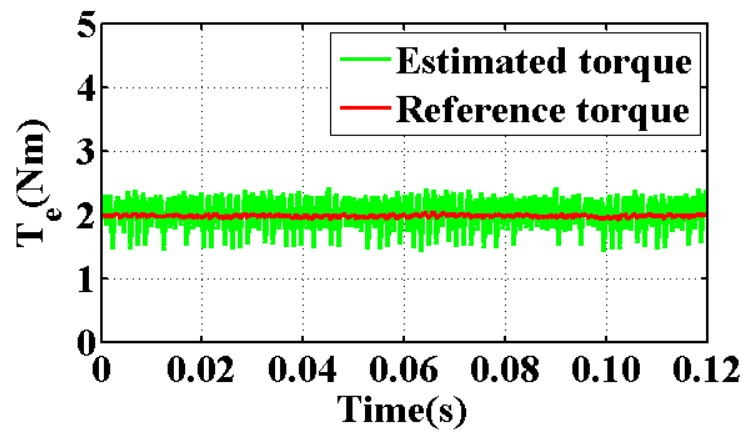


(d)

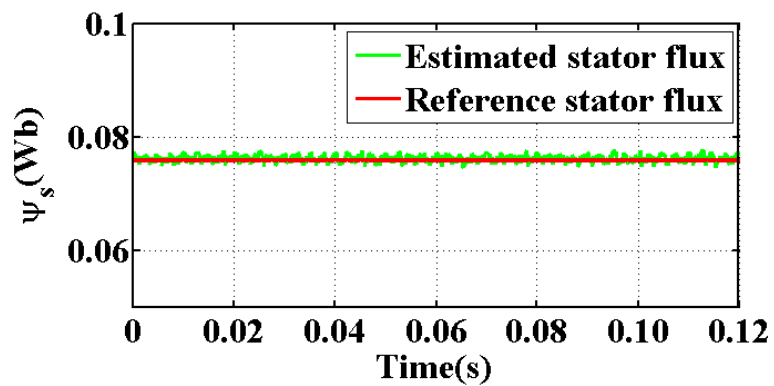


(e)

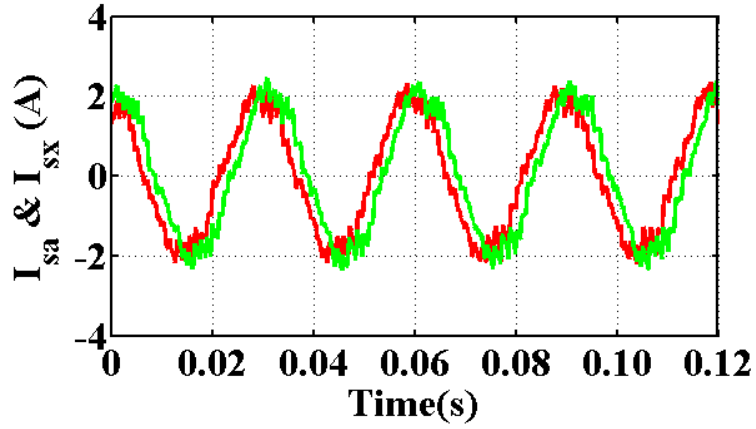
Fig. 6.8. Experimental results of proposed ST-DTC strategy ( $f_s = 10$  kHz). (a) Electromagnetic torque. (b) Stator flux. (c) Phase currents. (d)  $z1z2$  currents. (e) Phase current harmonic spectrum.



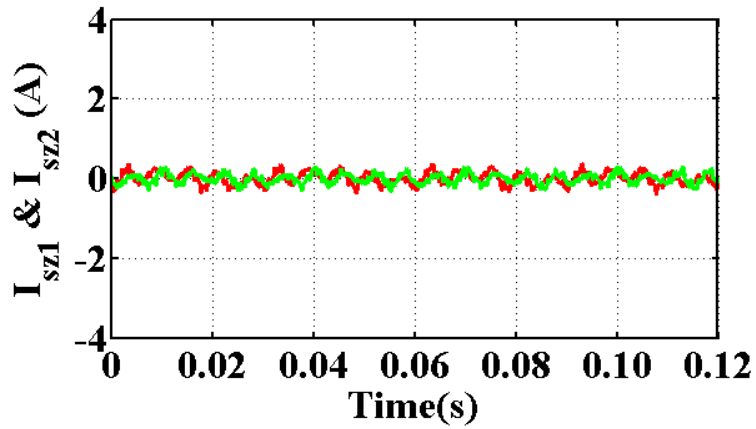
(a)



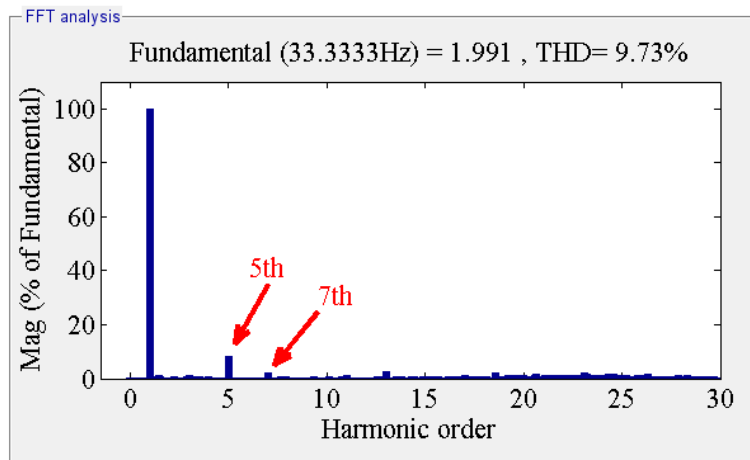
(b)



(c)



(d)



(e)

Fig. 6.9. Experimental results of proposed ST-DTC strategy ( $f_s = 8$  kHz). (a) Electromagnetic torque. (b) Stator flux. (c) Phase currents. (d)  $z_1z_2$  currents. (e) Phase current harmonic spectrum.

Detailed quantitative results are given in Table 6.3, where the torque and stator flux ripple is calculated as

Table 6.3 Steady-state Performance of Different ST-DTC Strategies

400 rpm, 2 Nm	Classical ( $f_s = 10$ kHz)	Two-step ( $f_s = 10$ kHz)	Proposed ( $f_s = 10$ kHz)	Proposed ( $f_s = 8$ kHz)
$\Delta \psi_s$ (%)	0.3679	0.3799	0.4235	0.4131
$\Delta T_e$ (%)	4.2332	4.5177	0.0322	0.0249
$\psi_s$ ripple (Wb)	5.455e-4	4.833e-4	5.159e-4	6.229e-4
$T_e$ ripple (Nm)	<b><u>0.2786</u></b>	0.2366	<b><u>0.1609</u></b>	<b><u>0.2401</u></b>
THD $I_a$ (%)	34.28	15.13	<b><u>8.69</u></b>	<b><u>9.73</u></b>
$f_{av}$ (kHz)	<b><u>2.555</u></b>	3.353	3.459	<b><u>2.719</u></b>

From Table 6.3, all the methods can achieve good steady-state performance of stator flux. Due to the use of the modified torque regulator, the torque ripple of the proposed ST-DTC strategy have been reduced by 42.25% compared to the classical ST-DTC strategy The steady-state error of torque has almost been eliminated. Both the two-step method and the proposed DTC strategy can reduce the current harmonics significantly. The proposed DTC strategy achieves more reduction of harmonic currents than the two-step method. The THD of phase current is 57.44% of that in the two-step method, and 25.35% of that in the classical DTC, while only incurring a slight increase of average switching frequency. In calculating the THD of stator current, the maximum frequency is 1000 Hz, in this case when the machine speed is 400 rpm, the maximum harmonic order is 29<sup>th</sup>.

Since more than one active vector is working during a sampling period, the average switching frequency will inevitably increase, from 2.555 kHz to 3.459 kHz (Table 6.3). This results in higher switching loss. To achieve similar average switching frequency, the results of the proposed control method using a sampling frequency of 8 kHz are shown in Fig. 6.9 and Table 6.3. With the reduced sampling frequency, the switching frequency of the proposed method decreases to a similar level as that of classical method, while the reduction of steady-state error of torque and THD of currents are similar to those obtained with a 10 kHz sampling frequency. Furthermore, the torque ripple is still smaller than that of the classical method.

The performance of DTC strategies with the classical and proposed torque regulators are also compared under different operating conditions. Fig. 6.10 shows the THD of phase-a current and the torque ripple for different ST-DTC strategies under the condition of same rotor speed which is 400 rpm and a range of load torque from 20% of rated load to full load. Fig. 6.12 shows the THD of phase-a current and the torque ripple for different ST-DTC strategies under the condition of same load which is 2 Nm and different speed from 10% to 100% of rated speed. Fig. 6.10-Fig. 6.11 show that both the two-step method and the proposed ST-DTC methods can significantly reduce the THD of phase currents and the torque ripple under a wide range of operating conditions, whilst the proposed strategy exhibits better performance, when the sampling frequency is the same.

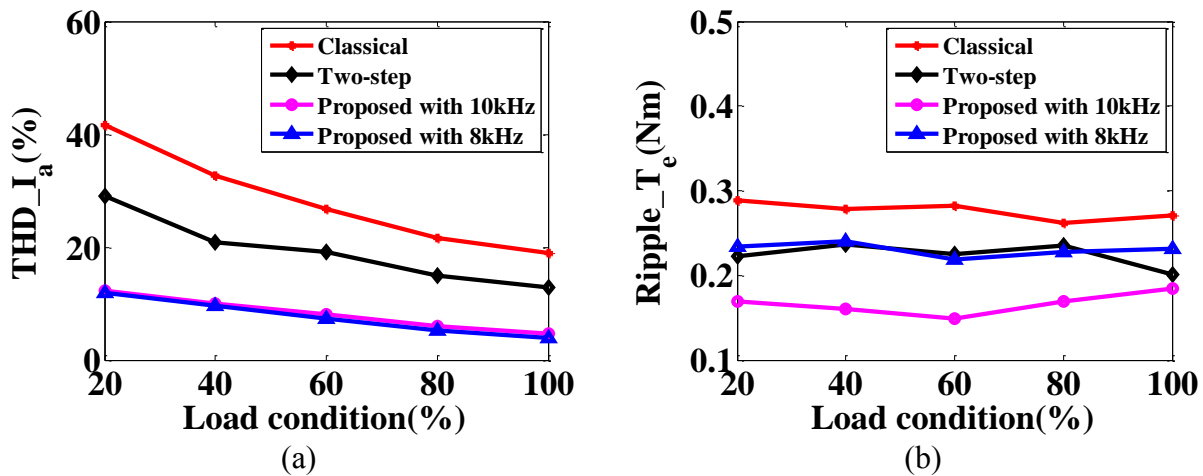


Fig. 6.10. Comparison of steady-state performances for different ST-DTC strategies under different load conditions, machine speed: 400 rpm. (a) THD of phase current. (b) Torque ripple.

When the sampling frequency decreases from 10 kHz to 8 kHz, the THD of phase currents of the proposed method almost remains at the same level, whilst the torque ripple is similar to that of two-step method with 10 kHz sampling frequency, but is still slightly smaller than that of classical method.

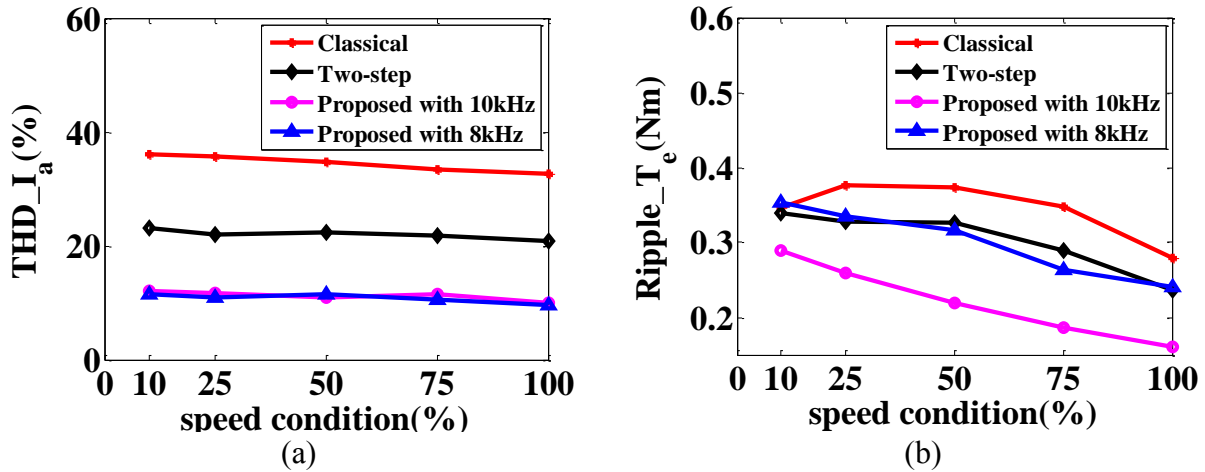
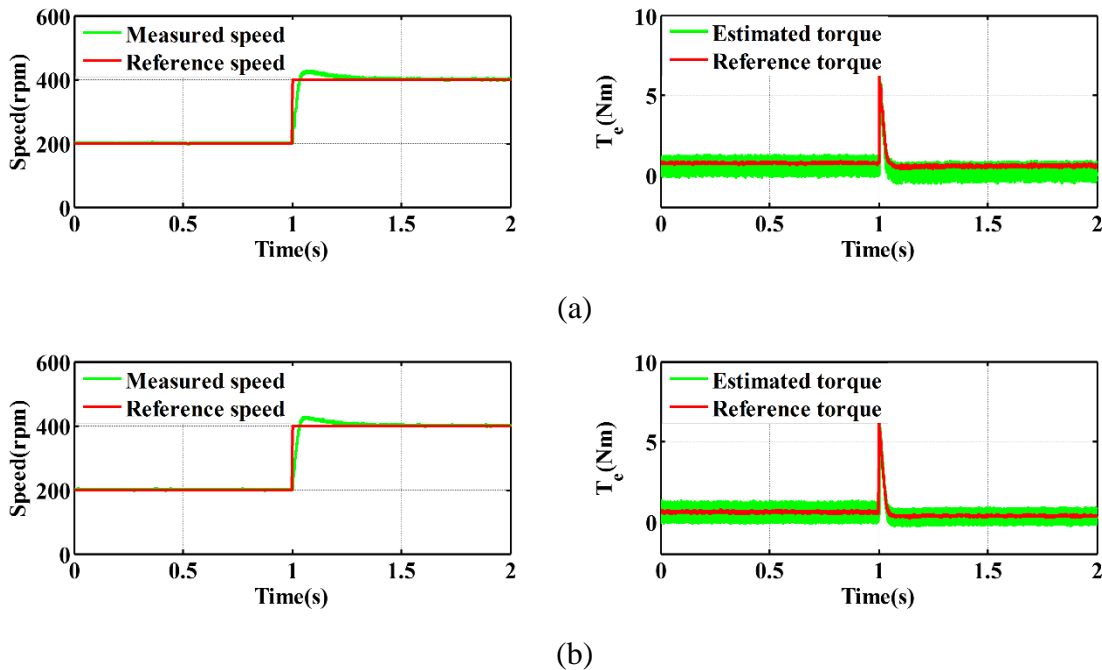


Fig. 6.11. Comparison of steady-state performances for different ST-DTC strategies under different speed conditions, load torque: 2 Nm. (a) THD of phase current. (b) Torque ripple.

### 6.3.2. Dynamic Performance of Speed Response

One of the merits of classical ST-DTC is the dynamic performance. Therefore, it is necessary to check whether the dynamic performance of the proposed method will deteriorate compared to the classical method.



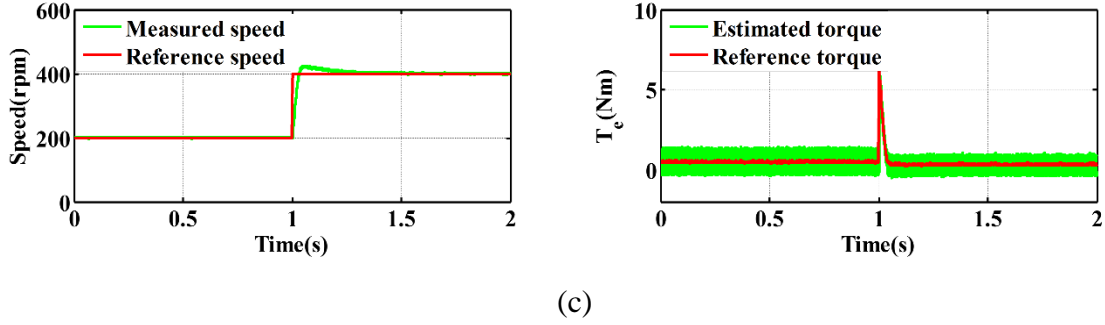


Fig. 6.12. Dynamic performance of speed response using different ST-DTC strategies: reference speed: 200 rpm to 400 rpm. (a) Classical ST-DTC strategy. (b) Proposed ST-DTC strategy with  $f_s = 10$  kHz. (c) Proposed ST-DTC strategy with  $f_s = 8$  kHz.

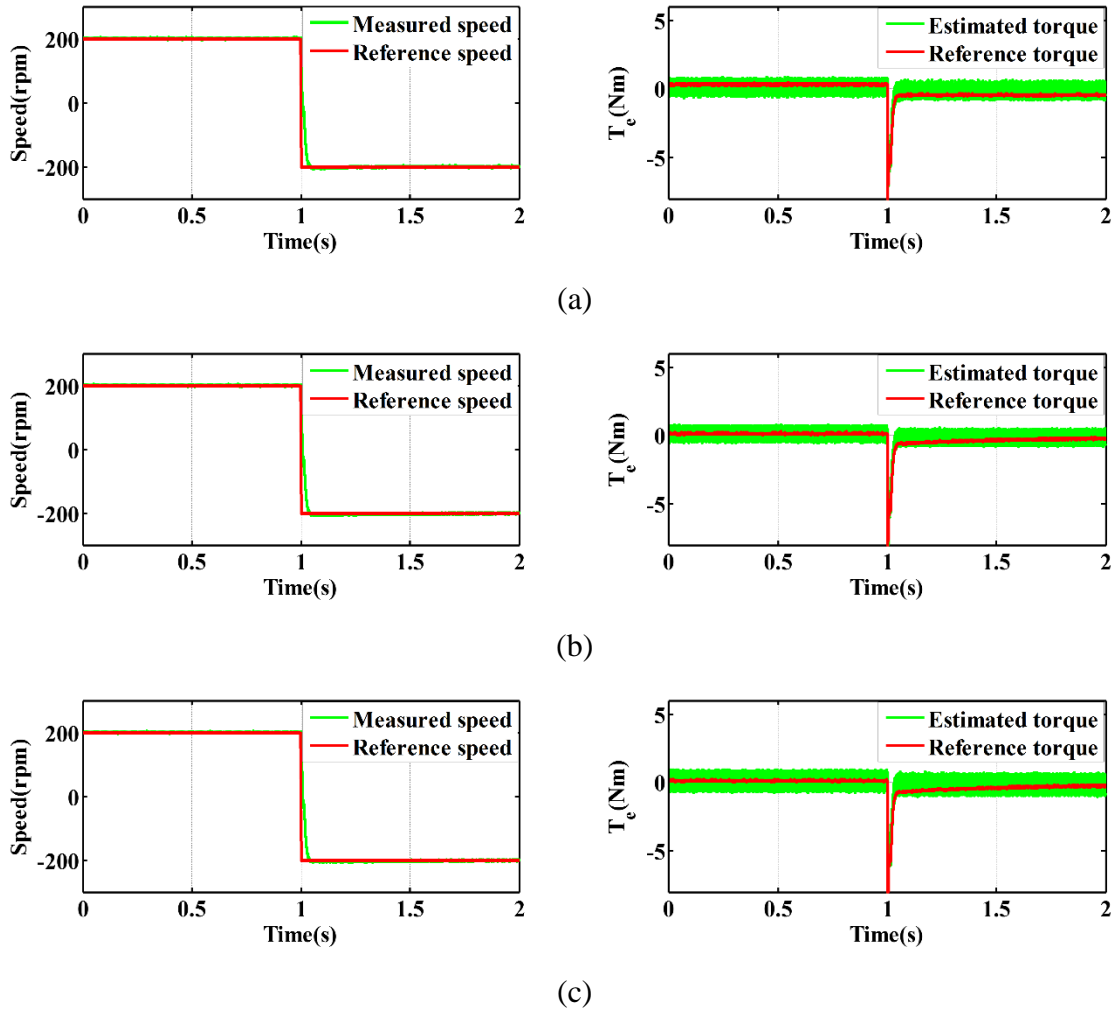
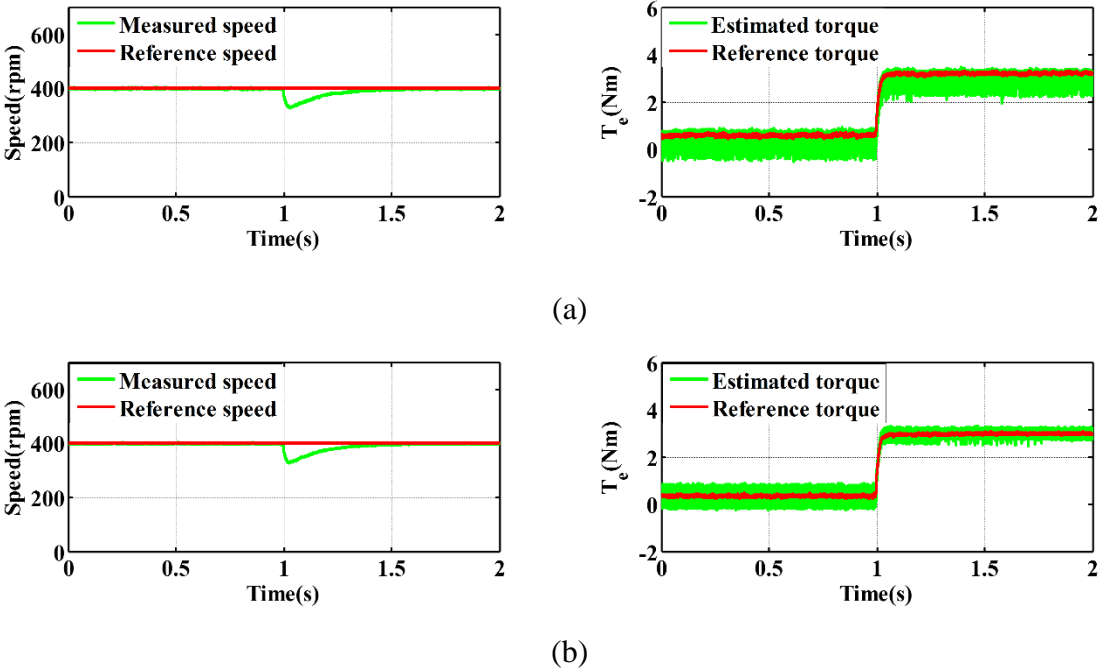


Fig. 6.13. Dynamic performance of speed reversal using different ST-DTC strategies: reference speed: 200 rpm to -200 rpm (a) Classical ST-DTC strategy. (b) Proposed ST-DTC strategy with  $f_s = 10$  kHz. (c) Proposed ST-DTC strategy with  $f_s = 8$  kHz.

Fig. 6.12-Fig. 6.13 shows the dynamic performance of the classical and proposed ST-DTC methods when the reference speed changes from 200 rpm to 400 rpm and when the direction of rotation is reversed, without load, respectively. From Fig. 6.12-Fig. 6.13, the proposed strategy has the similar dynamic performance to the classical DTC when the reference speed experiences a step change or reverses, even with the reduced sampling frequency.

### 6.3.3. Dynamic Response to External Load Disturbance for the Proposed DTC Strategy

The response to external load disturbance is compared between the classical DTC and the proposed method. Initially, the motor is operated under steady-state of 400 rpm without load. The external load of approximately 3 Nm is suddenly added by connecting the load resistance to the machine windings at 1.0s the result of this event is shown in Fig. 6.14.



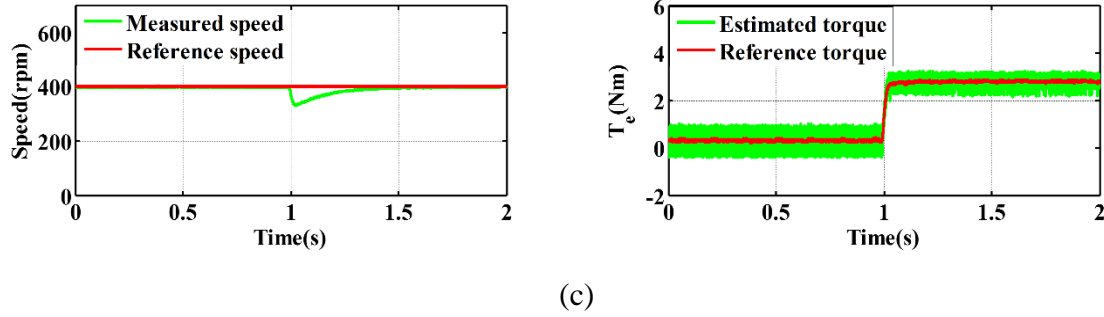


Fig. 6.14. Responses to external disturbance using different DTC strategies: external load (3 Nm) is added at the instant of 1.0s. (a) Classical ST-DTC strategy. (b) Proposed ST-DTC strategy with  $f_s = 10$  kHz. (c) Proposed ST-DTC strategy with  $f_s = 8$  kHz.

The torque generated with the proposed method follows the reference produced by the speed regulator similarly to the classical strategy. The speed in both the classical and the proposed strategy returns to its original value in less than 0.3 s.

The experimental results show that the proposed ST-DTC method can preserve the robustness against external load disturbance of the classical ST-DTC.

## 6.4. Conclusion

The classical ST-DTC scheme for dual three-phase drives suffers from significant current harmonics. This chapter introduced a modified switching table consisting of 12 new synthetic voltage vectors. The switching sequences have been discussed, and the most suitable one for the implementation on a real-time system has been proposed to minimize the computational burden. Considering the difference of decreasing and increasing variation and the influence of one-step delay in a real-time system, a simple modified torque regulator is proposed to improve the torque response performance. The proposed ST-DTC strategy has the following features:

- 1) Simple structure. Compared to classical ST-DTC, it is only necessary slight modification of the switching table and torque regulator.
- 2) Simple to implement in real-time systems.
- 3) Desirable steady-state performance (reduction of harmonic currents, torque ripple and steady-state error of torque) over a wide range of operating speed, with slight reduction of the utilization of DC supply and an increase of average commutation frequency (with same sampling frequency).

- 4) Significant reduction of harmonic currents and steady-state error of torque. A slight decrease of torque ripple over a wide range of operating speed, while experiencing only a modest reduction of the utilization rate of DC supply (with similar average switching frequency).
- 5) Desirable torque transient response and robustness against external load disturbance to the classical ST-DTC.

Although the analysis and experiments in this chapter are outlined on a hysteresis-based ST-DTC of dual three-phase PMSM drives, the concept of the synthetic voltage vectors and its simplified implementation for real-time system can also be extended for general use and applied to the other various modifications of switching table-based direct torque and power control methods of dual three-phase AC machines.

## **7. Reduction of Harmonic Current and Torque Ripple for Dual Three-phase Permanent Magnet Synchronous Machines Using a Modified Switching-table-based Direct Torque Controller**

### **7.1. Introduction**

The dual three-phase drive system has attracted increasing interest during the past few decades. Stator harmonic currents occur in the classical ST-DTC of dual three-phase PMSM drives due to the lack of control of the variables which relate to the harmonic currents in the VSD technique. Fortunately, there are 64 inverter states in the two-level dual three-phase inverters, many more than in their three-phase counterparts. This provides more potential for the application of DTC techniques, but also requires a more elaborate voltage vector selection criterion and switching sequence arrangement method.

In the current vector control technique for multiphase drives, specified SVM is usually adopted to eliminate harmonic current by controlling the average voltages in the harmonic-related subspace. According to this principle, virtual voltage vectors, whose average amplitudes of voltage vectors are zero, have been introduced in the ST-DTC of five-phase drives to suppress the harmonic currents [LIL11], [ZHE11]. However, they either require complicated switching tables and lack a proper switching sequence [LIL11], or fail to mention the torque ripple [ZHE11] and steady-state error of torque [LIL11], [ZHE11]. The design of the only controllable variables in the ST-DTC — the flux and torque hysteresis regulators have not be mentioned in detail in these reports. Similar methods have been adopted in dual three-phase drives with a two-step process, as discussed in Chapter 5 and in [HOA15], where the torque performance is similar, and an additional flux observer and a switching table are required. Synthetic vectors are introduced together with a modified torque regulator to improve the current and torque performance for dual three-phase drives, as discussed in Chapter 6 and in [REN15]. However, the reduction of torque ripple is limited since the amplitude of the synthetic vectors is similar to that of the vectors in the classical ST-DTC, because similar amplitude of vectors means similar effects on torque performance.

This chapter aims to deal with the problems the ST-DTC faces in dual three-phase drive systems. Firstly, in order to suppress the harmonic currents, two groups of synthetic vectors are introduced to replace the traditional vectors. Then, the switching sequences for each group are arranged to

make them suitable for the implementation in a real-time system. After that, one five level torque regulator is introduced to improve the torque performance. Finally, based on the analysis of the variation of flux and torque for different synthetic vectors, a design method for the flux and torque regulators is provided. A simple dead-time compensator is used to further improve the current performance.

This modified ST-DTC strategy can considerably reduce the stator current harmonics, and simultaneously, reduce the steady-state error and ripple of torque at the low cost of an increase in average switching frequency. The advantages of classical ST-DTC such as, simple structure and excellent dynamic performance are preserved. Experimental results are provided to substantiate the effectiveness of the proposed strategy.

## **7.2. Proposed ST-DTC Strategy of DTP PMSM System**

### **7.2.1. Selection of Applied Vectors**

ST-DTC of the dual three-phase PMSM has three major problems: torque ripple, steady-state error of torque and harmonic currents. Classical ST-DTC of the dual three-phase PMSM does not take harmonic currents into consideration since it is only an extension of the ST-DTC of a single three-phase PMSM where the harmonic current problem does not exist. Fortunately, the increased number of the voltage vectors permits a more elaborate switching table to obtain fine flux and torque control, as well as the considerable reduction of current harmonics.

According to (1.14), the harmonic current is proportional to the value of stator flux  $\psi_{sz1z2}$ . Hence, the influence of the vectors on flux in  $z1z2$  subspace should be investigated first.

By considering all of the non-null vectors, it can be shown that some vectors in dodecagons  $D_1$ ,  $D_3$ , and  $D_4$  have the same directions in the  $\alpha\beta$  subspace, which means they have similar effects on flux and torque response. The vectors with greater amplitudes provide a faster response [REN15]. For instance, Fig. 5.2 shows,  $V_{43}$  of  $D_3$  and  $V_{29}$  of  $D_1$  point in the same direction with  $V_9$  of  $D_4$  in the  $\alpha\beta$  subspace while  $V_{43}$  points in the opposite direction to  $V_9$  and  $V_{29}$  in the  $z1z2$  subspace, and hence causes the opposite effect on the flux  $\psi_{sz1z2}$ .

By employing vectors in the  $D_1$ ,  $D_3$  and  $D_4$  dodecagons together, the corresponding harmonic currents can be reduced when the amplitude of  $\psi_{sz1z2}$  is controlled. Based on this principle, a two-

step process has been proposed to use the vectors of  $D_3$  and  $D_4$  dodecagons together [HOA15]. This work confirmed the effectiveness of reducing the harmonic currents. However, two switching tables and one additional flux observer for  $\psi_{sz1z2}$  are required, which increases the complexity of the DTC strategy. Moreover, the steady-state error and ripple of torque remain similar to the classical ST-DTC. To preserve the merit of the simple structure, synthetic voltage vectors utilizing the vectors of the  $D_3$  and  $D_4$  dodecagons together by a weighted-sum approach in each sampling period, are introduced to reduce the harmonic currents to an insignificant level, as discussed in Chapter 6 and in [REN15]. It is shown experimentally that the use of synthetic vectors, instead of the traditional vectors from the  $D_4$  dodecagon, reduces the harmonic currents to a magnitude where they have no significant effect on machine operation. However, due to the similar amplitude of the synthetic vectors compared to that of the vectors from the  $D_4$  dodecagon, the reduction of the torque ripple is moderate.

Another group of synthetic vectors (designated as synthetic vectors II), which are a combination of vectors from the  $D_1$  and  $D_3$  dodecagons, are also employed to further improve the torque performance. Similar to the synthetic vectors with larger amplitudes (designated as synthetic vectors I), the calculation process of obtaining action times of the vectors in the  $D_1$  and  $D_3$  dodecagons is:

The amplitude of the vectors in  $D_1$  and  $D_3$  in  $z_1z_2$  subspace can be obtained from Table 7.1:

$$D_1: |V_{D1}|_{-z_1z_2} = V_{\max} = (\sqrt{6} + \sqrt{2}) / 3 \cdot V_{dc} \quad (7.1)$$

$$D_3: |V_{D3}|_{-z_1z_2} = V_{mid1} = 2\sqrt{2} / 3 \cdot V_{dc} \quad (7.2)$$

In order to minimize the amplitude of the stator flux in the  $z_1z_2$  subspace, the equation of the action times of the vectors in  $D_1$  and  $D_3$ ,  $T_{D1}$  and  $T_{D3}$ , can be expressed as

$$\begin{cases} (\sqrt{6} + \sqrt{2}) / 3 \cdot V_{dc} \cdot T_{D1\_II} = 2\sqrt{2} / 3 \cdot V_{dc} \cdot T_{D3\_II} \\ T_{D1\_II} + T_{D3\_II} = T_s \end{cases} \quad (7.3)$$

According to (7.3), the action times of the vectors in  $D_1$  and  $D_3$  is

$$\begin{cases} T_{D1\_II} = (1 - \sqrt{3}/3) \cdot T_s \\ T_{D3\_II} = \sqrt{3}/3 \cdot T_s \end{cases} \quad (7.4)$$

Then the amplitude of the synthetic vectors II in the  $\alpha\beta$  subspace is

$$\begin{aligned} |V_{\alpha\beta}| &= (|V_{D1}|_{-\alpha\beta} \cdot T_{D1\_II} + |V_{D3}|_{-\alpha\beta} \cdot T_{D3\_II}) / T_s \\ &= (\sqrt{6} - \sqrt{2}) \cdot 2/3 \cdot V_{dc} \end{aligned} \quad (7.5)$$

A comparison of the two groups of synthetic vectors and classical vectors is given in Table 7.1.

Table 7.1 Comparison of Different Vectors

	Classical	Synthetic I (Chapter 6)	Synthetic II (This chapter)
Groups of Vectors	D <sub>4</sub>	D <sub>4</sub> , D <sub>3</sub>	D <sub>1</sub> , D <sub>3</sub>
Action times	$T_{D4} = T_s$	$T_{D4\_I} = (\sqrt{3} - 1) \cdot T_s$	$T_{D1\_II} = (1 - \sqrt{3}/3) \cdot T_s$
Amplitude	$(\sqrt{6} + \sqrt{2}) / 3 \cdot V_{dc}$ $\approx 1.29V_{dc}$	$\frac{2\sqrt{3}}{3} V_{dc} = (2\sqrt{6}\sqrt{3}) / 3 \cdot V_{dc}$ $\approx 1.20V_{dc}$	$(\sqrt{6} - \sqrt{2}) / 3 \cdot V_{dc}$ $\approx 0.69V_{dc}$

From Table 7.1, the amplitude of synthetic vectors I is very similar to the classical vectors from D<sub>4</sub>, while the amplitude of synthetic vectors II is only about half of that. These two groups of synthetic vectors have their own merits and drawbacks. The synthetic vectors I have larger torque and flux variation, which means greater maximum rate of change of torque in torque dynamic performance, but also imply larger steady-state error of torque and larger torque ripple. On the other hand, the synthetic vectors II can reduce torque ripple more than synthetic vectors I but are not suitable for the large torque transient process when the torque are expected to change quickly.

### 7.2.2. Switching Sequence and Implementation

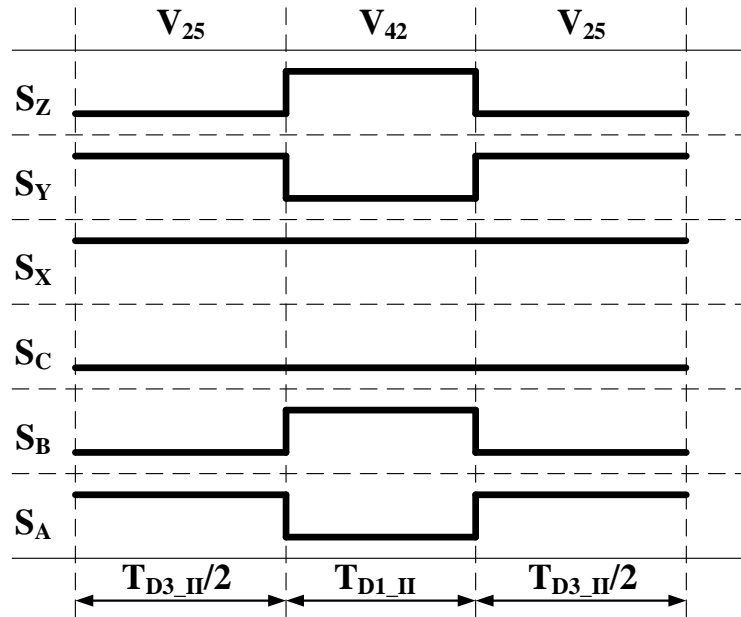
In order to preserve the simplicity of the classical ST-DTC, the switching sequences need to be modified. Not only the synthetic vectors I as analysed in chapter 6, but also the synthetic vectors II require optimal arrangement of the switching sequence.

As mentioned in chapter 6, for the most commonly used PWM generation technique, the inverted and non-inverted signals are symmetrical to the middle of the PWM period, where the level of the signal is high. This type of PWM signal can be considered as the standard switching sequence for

the real-time systems. All the switching sequences for the vectors in the synthetic vectors II group are non-standard signals. Taking  $V_{25}$ - $V_{42}$  as an example, the levels of  $S_Y$  and  $S_A$  are always different with  $S_Z$  and  $S_B$  in the whole PWM period, Fig. 7.1(a). A specific PWM generation technique is usually required which inevitably increases the computation burden and erodes the simplicity of the ST-DTC strategy. To avoid this, the PWM levels of  $S_Y$  and  $S_A$  have been rearranged, then the standard switching sequence can be achieved as illustrated in Fig. 7.1 (b). Thus, the actual applied voltage vectors have been changed from  $V_{25}$ - $V_{42}$  to  $V_8$ - $V_{25}$ - $V_{59}$ , and the action time of each vector has been recalculated accordingly, Fig. 7.1(b). The amplitude of the modified synthetic vector for  $V_{25}$ - $V_{42}$  in two subspaces can be calculated from Fig. 7.2.

$$\begin{aligned} |V_{\alpha\beta}|_{-new-II} &= [V_{mid2} \cdot \cos(\pi/12) \cdot T_{D1\_II} \cdot 2 + V_{mid1} \cdot (T_{D3\_II} - T_{D1\_II})] / T_s \\ &= (2\sqrt{6} - 2\sqrt{2})/3 \cdot V_{dc} \end{aligned} \quad (7.6)$$

$$\begin{aligned} |V_{z1z2}|_{-new-II} &= [V_{mid2} \cdot \cos(5\pi/12) \cdot T_{D1} \cdot 2 - V_{mid1} \cdot (T_{D3} - T_{D1})] / T_s \\ &= 0 \end{aligned} \quad (7.7)$$



(a)



Table 7.2 Duty Cycle of Each Switching Component for the Proposed ST-DTC Strategy.

Vectors and switching state for classical ST-DTC strategy	Duty cycle of each switching component for proposed ST-DTC strategy					
	S <sub>Z</sub>	S <sub>Y</sub>	S <sub>X</sub>	S <sub>C</sub>	S <sub>B</sub>	S <sub>A</sub>
V <sub>9</sub> (001001) →Synthetic I	T <sub>D3_I</sub>	0	1	0	T <sub>D3_I</sub>	1
V <sub>9</sub> (001001) →Synthetic II	T <sub>D3_II</sub>	T <sub>D1_II</sub>	1	T <sub>D1_II</sub>	T <sub>D3_II</sub>	1
V <sub>11</sub> (001011) →Synthetic I	0	T <sub>D3_I</sub>	1	0	T <sub>D4_I</sub>	1
V <sub>11</sub> (001011) →Synthetic II	T <sub>D1_II</sub>	T <sub>D3_II</sub>	1	0	T <sub>D1_II</sub>	T <sub>D3_II</sub>

From (7.5), (7.6) and (7.7), the amplitudes of the new synthetic vector consisting of  $V_8$ - $V_{25}$ - $V_{59}$  are the same that of the synthetic vector which is composed of  $V_{25}$ - $V_{42}$  in both the  $\alpha\beta$  subspace and the  $z_1z_2$  subspace. This means the modified synthetic vectors can still minimize the amplitude of the stator flux in  $z_1z_2$  subspace, and simultaneously, obtain the same influence on torque and stator flux in  $\alpha\beta$  subspace.

Similar results can be obtained for the rest of the synthetic vectors II. Combined with the results given in [REN15], the duty cycle of each switching component for the proposed strategy can be simply summarized in Table 7.2. A diagram of two synthetic vectors in the  $\alpha\beta$  subspace is shown in Fig. 7.3, taking vector  $V_9$  and  $V_{11}$  as examples.

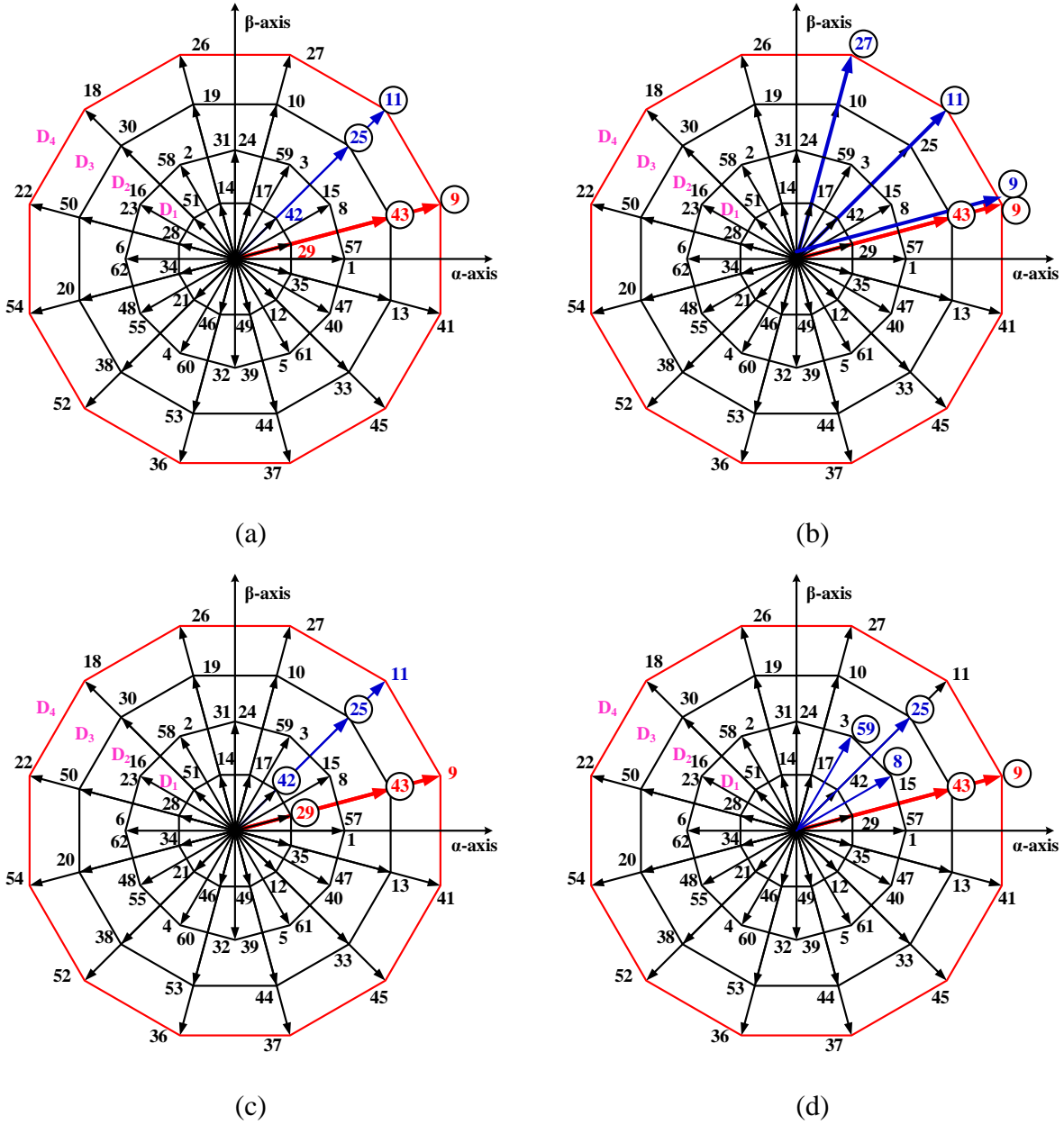


Fig. 7.3. Diagrams of two synthetic vectors in the  $\alpha\beta$  subspace: (a) Synthetic vectors I. (b) Synthetic vectors I after rearrangement for optimal switching sequence. (c) Synthetic vectors II. (d) Synthetic vectors II after rearrangement for optimal switching sequence.

### 7.2.3. Design of Torque Regulator to Enhance the Steady-state Performance of Torque Response

Both of two groups of synthetic vectors can considerably reduce the stator harmonic currents. The synthetic vectors II group can effectively reduce the torque ripple, while synthetic vectors I can maintain similar dynamic performance to classical vectors from D<sub>4</sub>.

In order to utilise these advantages of these two groups of synthetic vectors, one 5-level torque regulator is employed instead of the classical 3-level torque regulator.

The conventional 5-level torque regulator is implemented in the five-phase system [LIL11], where zero vectors are employed within inner bands, and small synthetic vectors are adopted between inner bands and outer bands, whereas the large synthetic vectors will be applied when the torque exceeds the outer bands. However, neither analysis of the influence of vectors on torque or discussion of the design of the 5-level torque regulator is provided.

To make the two types of vectors operate more effectively, the analysis of the torque variation for different vectors are presented first. Then detailed design of the torque regulator is presented in the following subsections.

#### Analysis of Torque Variation for Different Vectors:

The torque generation only involves the variables in  $\alpha\beta$  subspace. Therefore, the analysis about the torque variation for the three-phase PMSM can be extended to the dual three-phase PMSM. The torque variation can be expressed as [REN14]

$$\frac{dT_e}{dt} = -\frac{R_s}{L_s} T_{e0} + \frac{3P}{L_s} (-\psi_{r\beta} V_{s\alpha} + \psi_{r\alpha} V_{s\beta} - \omega_1 |\psi_{r\alpha\beta}| |\psi_{s\alpha\beta}| \cos \delta) \quad (7.8)$$

where  $T_{e0}$  is the instant values of torque, and  $\delta$  is the angle between stator flux and rotor flux.

It may be shown that, with suitable assumptions, the instantaneous value of torque has minimal effect on the torque ripple, as discussed in Chapter 3 and in [REN14]. Then, the torque variation due to individual vectors obeys the principle of superposition. The amplitude of the first term is proportional to the amplitude of the applied vector. The second term can be regarded as a negative offset in which the value is proportional to the machine speed. Therefore, all utilized vectors in the

proposed method can be classified into five types according to their values of torque variation.

Two types of vectors that increase torque:

(1)  $\mathbf{V}_{I+}$ : Synthetic vectors I which increase torque

(2)  $\mathbf{V}_{II+}$ : Synthetic vectors II which increase torque

The absolute value of increasing variation of torque:

$$\sigma_{V_{I+}} > \sigma_{V_{II+}} \quad (7.9)$$

Three types of vectors that decrease torque:

(1)  $\mathbf{V}_{I-}$ : Synthetic vectors I which decrease torque;

(2)  $\mathbf{V}_{II-}$ : Synthetic vectors II which decrease torque;

(3)  $\mathbf{V}_{zero}$ : Zero vectors which always decrease torque.

The absolute value of decreasing torque variation:

$$|\sigma_{V_{I-}}| > |\sigma_{V_{II-}}| > |\sigma_{V_{zero}}| \quad (7.10)$$

The absolute value of torque variation:

$$|\sigma_{V_{I-}}| > |\sigma_{V_{I+}}| \quad (7.11)$$

$$|\sigma_{V_{II-}}| > |\sigma_{V_{II+}}| \quad (7.12)$$

It should be noted that if the machine speed is high,  $\sigma_{V_{II+}}$  will become negative because of the large back-EMF and the torque would not increase as expected, which means only using synthetic vectors II cannot ensure the machine operates at the reference speed. Therefore, synthetic vectors I which has larger amplitude is an essential part of the torque regulator.

To clearly express how the machine speed affects the torque variation for different types of vectors, Fig. 7.4 presents the experimental results of torque responses caused by synthetic vectors I and II when dual three-phase PMSM operates at the speed of 100 rpm and 300 rpm without a load. From Fig. 7.4, the absolute values of decreasing torque variation are similar to the increasing

ones for both synthetic vectors I and II when the machine works in the low speed region, while they are much larger than the increasing torque variations on the high speed region. The absolute value of torque variation for synthetic vectors II is smaller than the corresponding values for synthetic vectors I, which indicates lower torque ripple. The results shown in Fig. 7.4 are consistent with (7.9)-(7.12).

These features point to two empirical rules which need to be applied in the design of torque regulator:

**Rule1:** The vectors decreasing and increasing torque should be treated differently to avoid the steady-state error and large ripple of torque [ABA08], [REN14].

**Rule2:** The synthetic vectors II should be employed for as long as possible to reduce torque ripple.

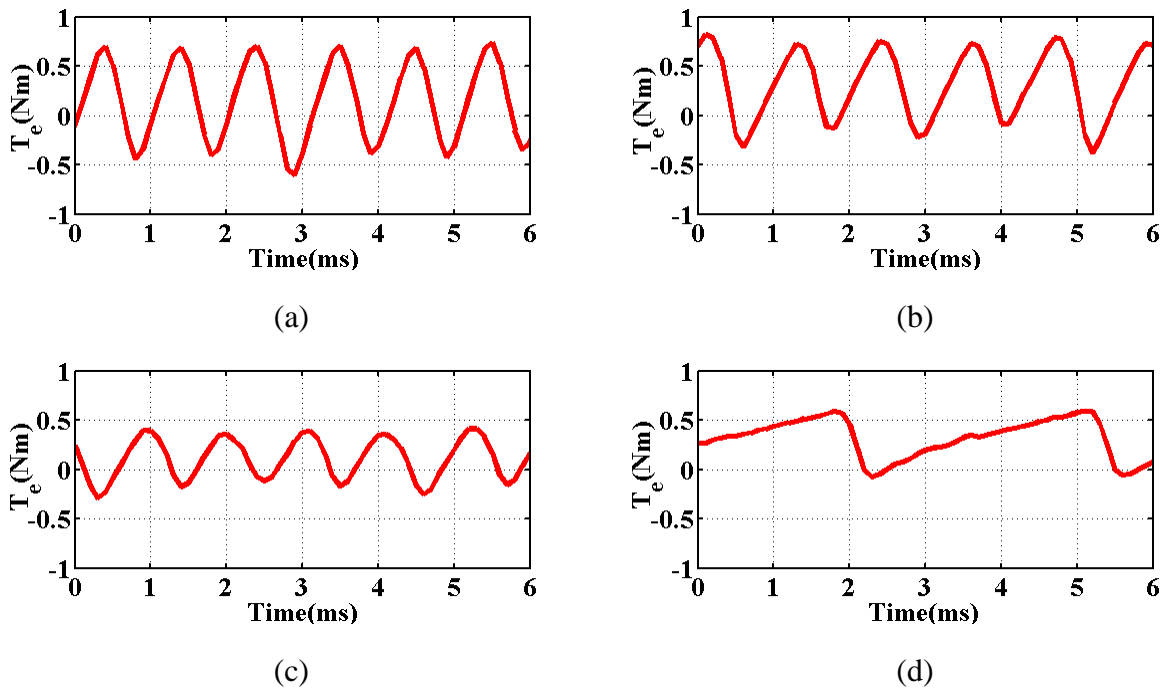


Fig. 7.4. Experimental results of torque responses using different types of vectors (sampling frequency: 10 kHz). (a) Synthetic vectors I: 100 rpm. (b) Synthetic vectors I: 300 rpm. (c) Synthetic vectors II: 100 rpm. (d) Synthetic vectors II: 300 rpm.

For the same type of synthetic vectors and at each operating point, the increasing and decreasing variation of flux is almost identical [REN14].  $\mathbf{V}_{I+}$  and  $\mathbf{V}_{II+}$  both point in the same direction in the  $\alpha\beta$  subspace, as shown in Fig. 7.5(a). Both  $\mathbf{V}_{I+}$  and  $\mathbf{V}_{II+}$  meet the requirement of flux control for

normal operation. This is confirmed by the following experimental results. Therefore, a classical flux regulator is employed here, Fig. 7.5(b), which means that the modified torque regulator is the only change in the control structure.

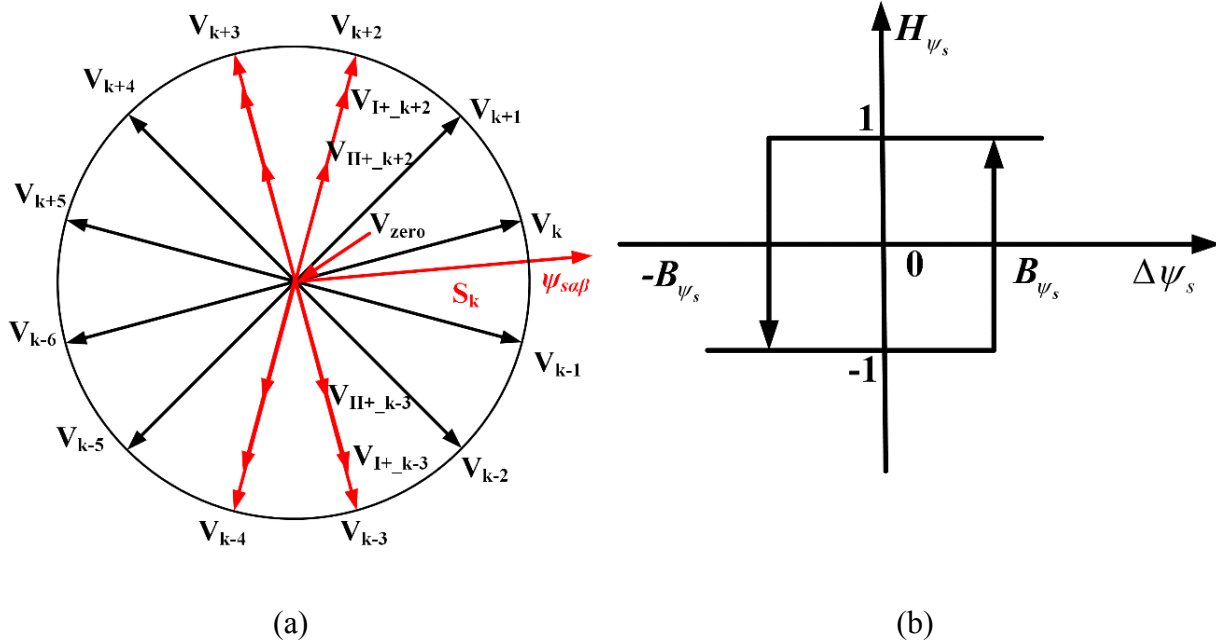


Fig. 7.5. Illustration of the classical flux regulator and selection of vectors. (a) Selection of vectors when the stator flux lies in sector  $k$ . (b) Classical flux regulator.

### Design of Torque Regulator Bands

For the 5-level torque regulator, the main objectives of the two bands are different: the aim of the outer bands is to guarantee the dynamic performance and the stability of system at high speed, while the objective of the inner bands is to reduce the torque ripple.

The bandwidth is determined by the torque variation within one sampling period. As shown in Fig. 7.4, for the same type of vectors, e.g.,  $V_I$  has different torque variations when machine operates under different speed conditions. Even for the same speed, torque variations of  $V_I$  still slightly changes due to the different position the stator flux is located. Therefore, calculating the bandwidth according to every instant torque variation is not a desirable method. For the sake of the simplicity and parameter independence, it is preferred to determine the proper bandwidths according to the average absolute values of increasing and decreasing variation rates of synthetic vectors, named  $B_{T_I}$  and  $B_{T_{II}}$ , respectively. According to (7.8), torque variation is proportional to

the amplitude of the applied vectors. Table 7.1 shows the ratio of the amplitude of synthetic vectors II to that of synthetic vectors I is around

$$\rho_{V_{II}/V_I} \approx 0.69/1.20 \approx 0.575 \quad (7.13)$$

Therefore, the ratio of the bandwidths of synthetic vectors II (inner bands) to that of synthetic vectors I (outer bands) can be set as the value of 0.575, as provided in (7.13).

The outer bandwidth should be large enough, otherwise, the synthetic vectors II would be barely used because the torque would always exceed the outer bands, which is against Rule 2. It also results in larger torque ripple. On the other hand, the outer bandwidth is not the larger the better, because it would take too much time to let the actual torque reach the hysteresis bands if the outer bandwidth is too large. Consequently, according to Fig. 7.4, the outer bands can be set as

$$\pm B_{T\_I} = \pm 0.3 \text{Nm} \quad (7.14)$$

which is approximately the average absolute value of decreasing and increasing torque variations obtained from Fig. 7.4(a).

By using these bands, in most cases, the torque changes only once within the outer bands, which can ensure the utilization of synthetic vectors II (which means small torque ripple) and good dynamic performance. Then the bands of synthetic vectors II can be easily obtained

$$\pm B_{T\_II} = \pm B_{T\_I} \cdot \rho_{V_{II}/V_I} = \pm 0.173 \text{Nm} \quad (7.15)$$

Although the bands can be further optimized by considering the effect of machine speed, the aim of this chapter is to improve the torque and current performance, and to keep the merit of simple controller structure. Therefore, the method with rough band values, which is simple and exhibits desirable torque performance, is implemented in the real-time system.

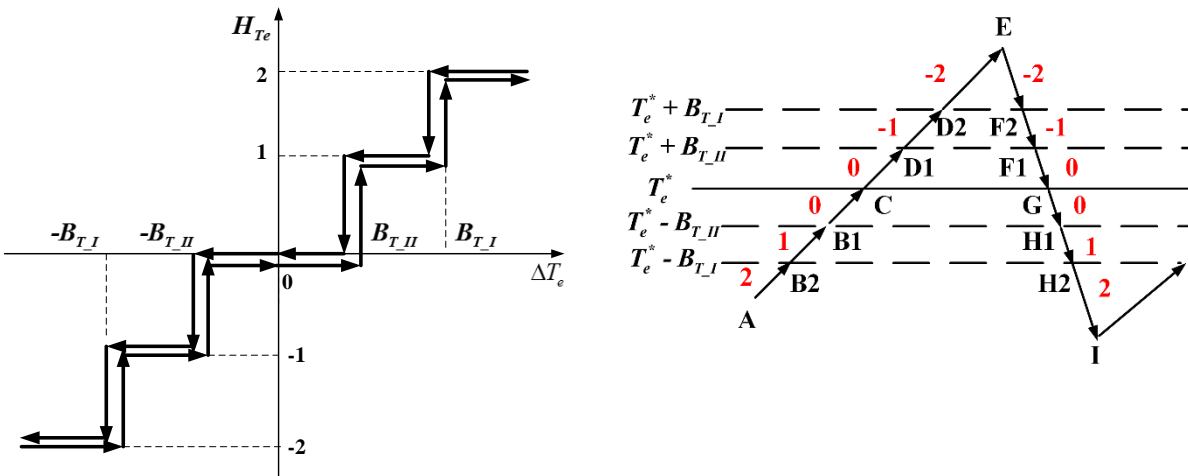
### **Design of Output Setting for Proposed Torque Regulator**

Treating the vectors having increasing variation and decreasing variation equally results in steady-state error and ripple of torque. Hence, the classical 5-level torque regulator, which is

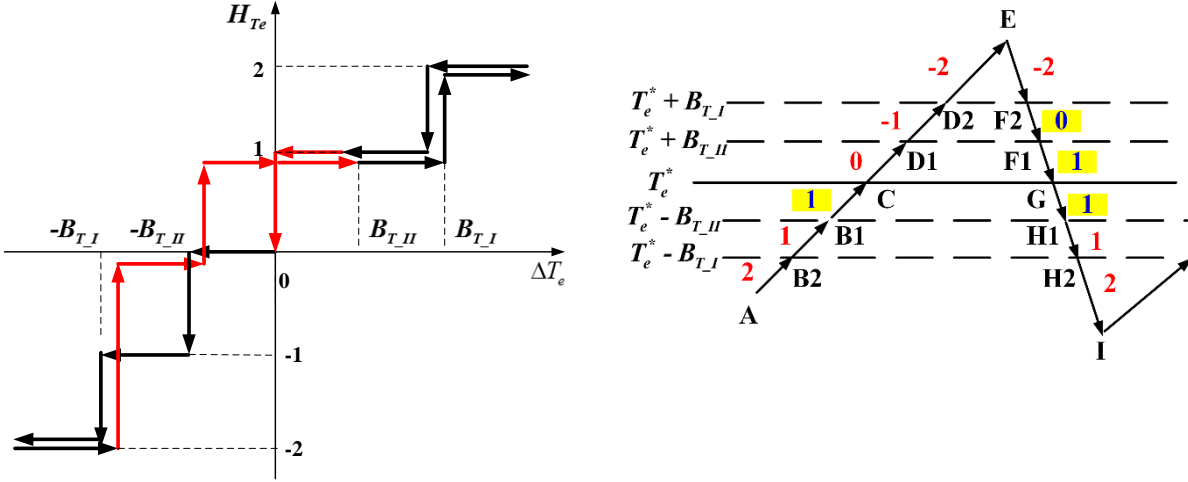
symmetrical along the torque reference, needs to be modified to improve the torque performance, Fig. 7.6(a). The relationship between  $H_{Te}$  in Fig. 7.6 and five types of utilized vectors is shown in Table 7.3.

Table 7.3 Selection Criterion of Utilized Vectors

$H_{Te}$	Function of $H_{Te}$	Utilized vectors
2	Increase torque greatly	$V_{I+}$
1	Increase torque slightly	$V_{II+}$
0	Keep torque	0
-1	Decrease torque slightly	$V_{II-}$
-2	Decrease torque greatly	$V_{I-}$



(a)



(b)

Fig. 7.6. Illustration of classical and proposed torque regulators. (a) Classical 5-level torque regulator. (b) Proposed 5-level torque regulator.

To enable a clear description, the torque track trajectories have been divided into several segments, as shown in Fig. 7.6. Considering the influence of the one-step delay which exists in every real-time system, the qualified torque regulator should guarantee that the output of the torque regulator in the current segment should still be suitable for the next segment. Accordingly, zero vectors, which decrease the torque, are not a good choice on segment F1G since the torque will continue drop in segment GH1 where the torque is already smaller than its reference, which will increase the torque ripple. Therefore, it is preferred to apply  $V_{II+}$  to increase the torque somewhat. The same principle can be applied on segment F2F1, where  $V_{II-}$  should be replaced with  $V_{zero}$  which has a smaller absolute value of decreasing torque variation. The zero vectors in segment GH1 are not appropriate for the same reason, they should also be replaced with  $V_{II+}$  which increase the torque a bit. Lastly,  $V_{II+}$  should be utilized in segment B1C instead of zero vectors because torque in segment B1C needs to be increased rather than decreased.

With the modified torque regulator having appropriate bands as well as the modification which has been employed to reduce the steady-state error of torque for three-phase drives [ZHU14], the three main problems of ST-DTC of dual three-phase machines, i.e. current harmonics, steady-state error and ripple of torque, can be considerably ameliorated, while the merits of classical ST-DTC, such as simple structure, have been preserved.

#### 7.2.4. Compensation of Inverter Non-linearity

The use of synthetic vectors can considerably reduce the harmonic currents from the PWM side. However, in the real-time system, inverter non-linearity also introduces harmonic voltages [CHE14], [JON09], [PAR12], [SEU91]. The dominant inverter non-linearity harmonic voltages in dual three-phase machines appear in the  $z_1z_2$  subspace, which results in non-negligible harmonic currents due to the low impedance in  $z_1z_2$  subspace. Thus, a resonant controller in the harmonic-related ( $z_1z_2$ ) reference frame is utilized to reduce the dead-time effect [CHE14]. However, coordinate transformation and one additional resonant controller are required, which erodes the merit of simple structure of ST-DTC. Consequently, a much simple compensation method which does not need the coordinate transformation and additional controllers is required. As the dead-time effect can be presented as a square wave [CHE14], [SEU91], a simple method has been presented in [CHO07], [GON11]. It estimates the disturbance voltage by measuring current and using the inverter physical characteristics, and then feedback to the terminal voltage command, as shown in Fig. 7.7. This simple method has been employed in this chapter. Although the effects of inverter non-linearity may not be fully suppressed, this simple compensation method achieves considerable improvement without deteriorating the structure of the ST-DTC methods. This is confirmed by the experimental results, and hence is suitable for the proposed control strategies.

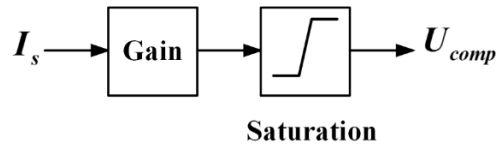


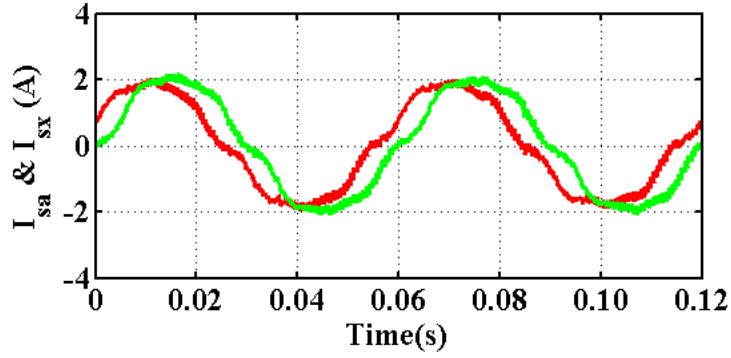
Fig. 7.7. Simple dead-time compensator.

### 7.3. Experimental Results

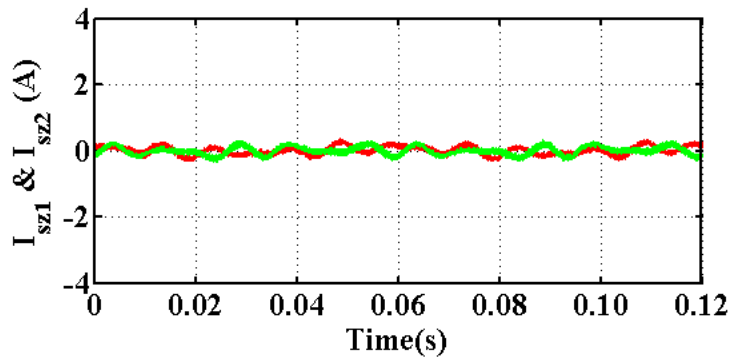
Experimental tests are conducted on the laboratory prototype of dual three-phase PMSM machine II. The overall control schemes of the proposed ST-DTC strategies are given in Fig. 7.8. A model which combines the voltage model and the current model is employed to estimate the stator flux and torque [LEE11]. All the results were captured using dSPACE 1005 software, and then plotted using MATLAB.

Four types of ST-DTC strategies are compared:

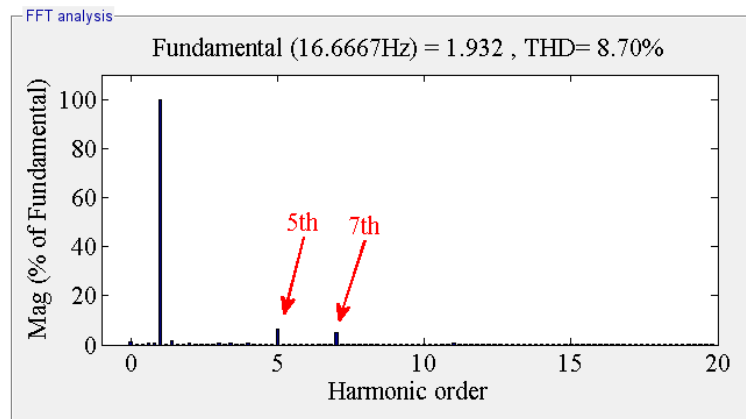




(a)

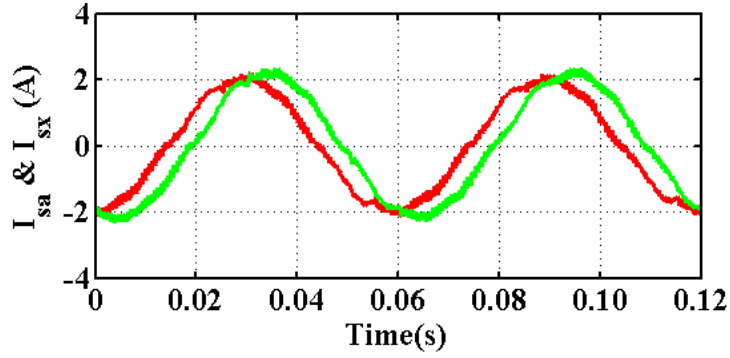


(b)

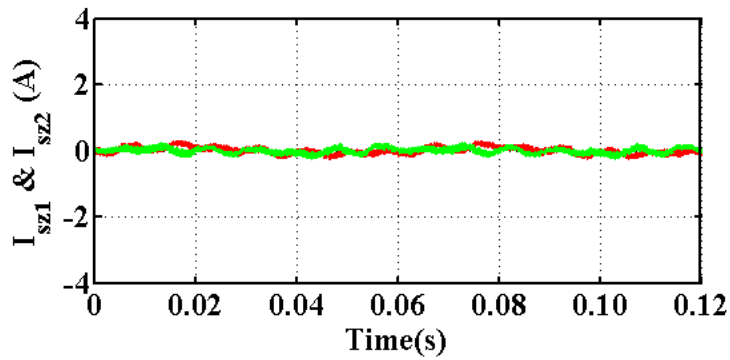


(c)

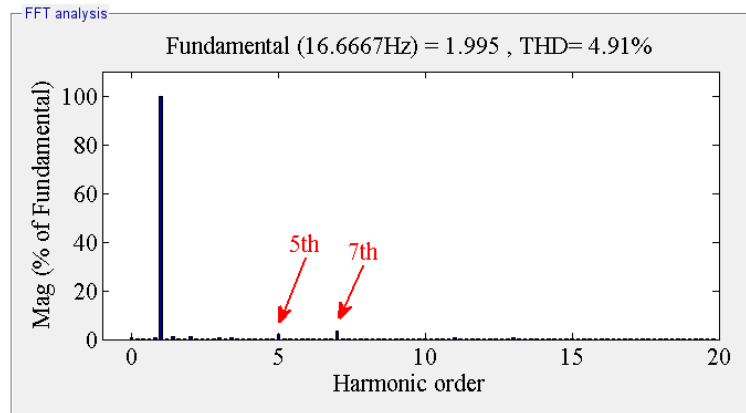
Fig. 7.9. Steady-state performance of proposed ST-DTC strategy without dead-time compensator. (a) Phase currents. (b) Currents in  $z_1z_2$  subspace. (c) Phase current harmonic spectrum.



(a)



(b)



(c)

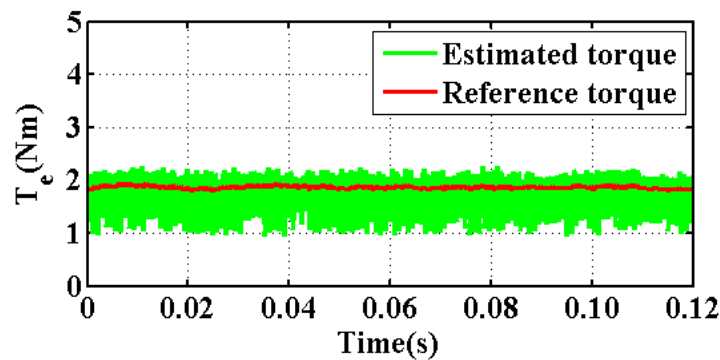
Fig. 7.10. Steady-state performance of the proposed ST-DTC strategy with dead-time compensator. (a) Phase currents. (b) Currents in  $z_1z_2$  subspace. (c) Phase current harmonic spectrum.

The effect of inverter non-linearity causes harmonic currents, mainly 5<sup>th</sup> and 7<sup>th</sup>. The use of a simple dead-time compensator reduces the harmonic currents considerably, as can be seen from

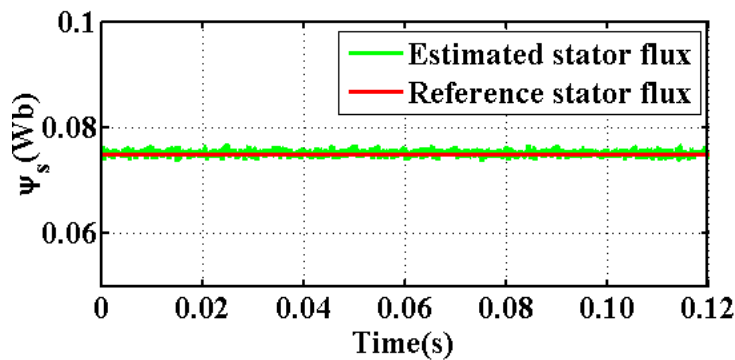
waves of phase currents, currents in  $z_1z_2$  subspace and phase current harmonic spectrum, Fig. 7.10.

### 7.3.2. Steady-state Performance of Different ST-DTC Strategies

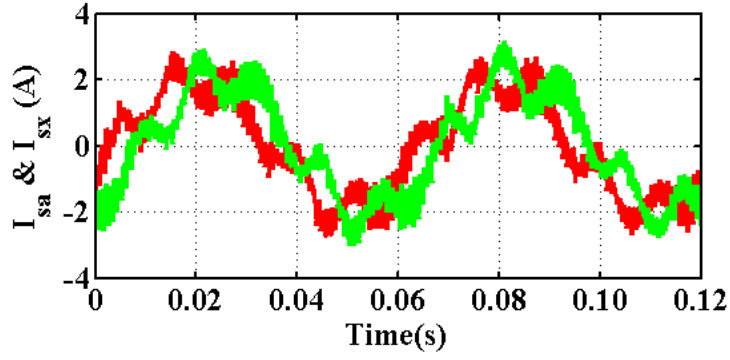
Fig. 7.11-Fig. 7.14 show the steady-state performance of different ST-DTC strategies when the machine speed is 200 rpm and the load torque is approximately 1.5 Nm. It is clear that the classical ST-DTC suffers from steady-state error and ripple of torque, as well as large harmonic currents which mainly exist in the  $z_1z_2$  subspace, as shown in Fig. 7.11. With the use of synthetic vectors I introduced in Chapter 6 and in [REN15], large harmonic currents can be considerably suppressed as well as the steady-state error of torque, but the reduction of the torque ripple is modest, Fig. 7.12. By introducing synthetic vectors II and a 5-level torque regulator, the torque ripple and harmonic currents can be further decreased, and between the two proposed methods, the proposed method with the modified 5-level torque regulator exhibits better performance both in terms of harmonic currents and torque ripple.



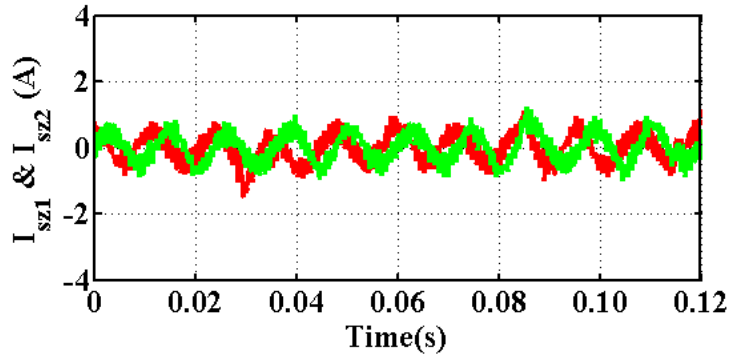
(a)



(b)

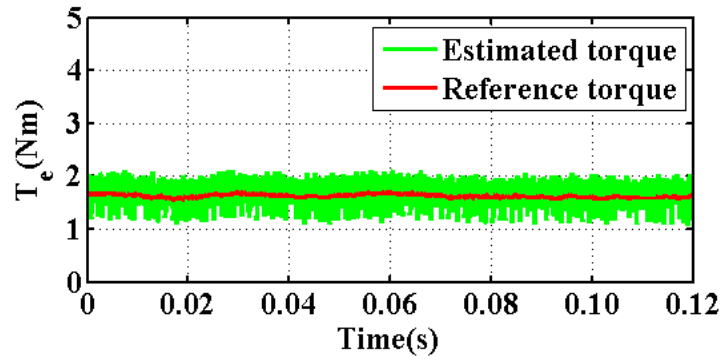


(c)

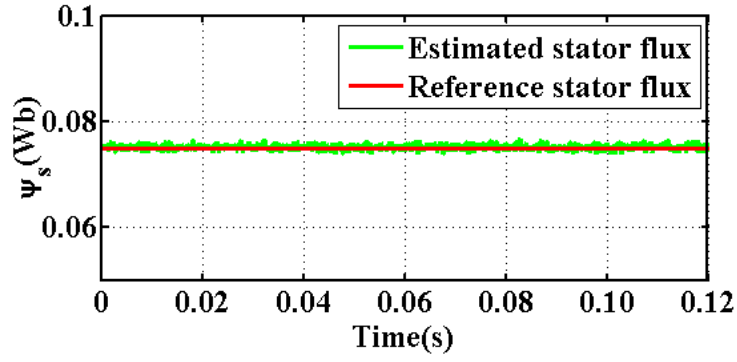


(d)

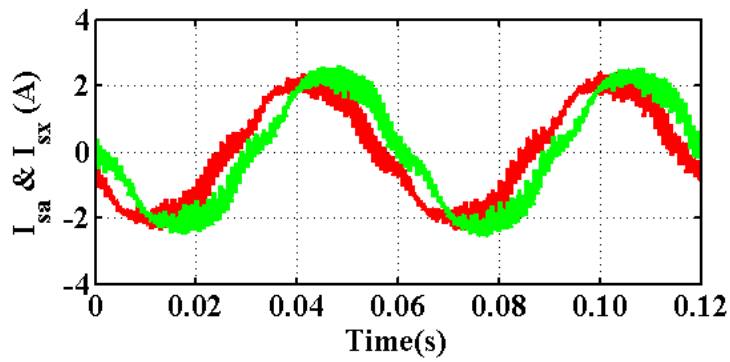
Fig. 7.11. Steady-state performance of classical ST-DTC strategy. (a) Electromagnetic torque. (b) Stator flux. (c) Phase currents. (d) Currents in  $z_1z_2$  subspace.



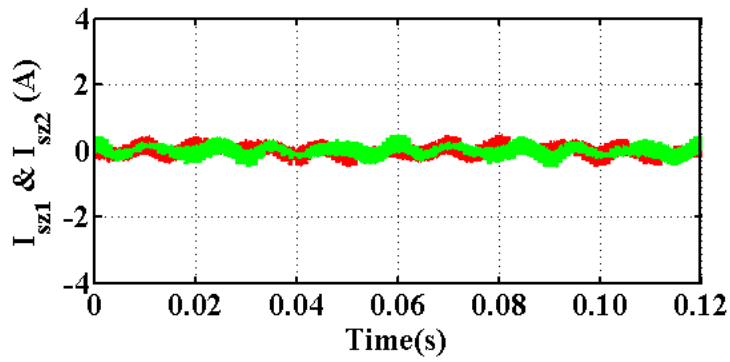
(a)



(b)

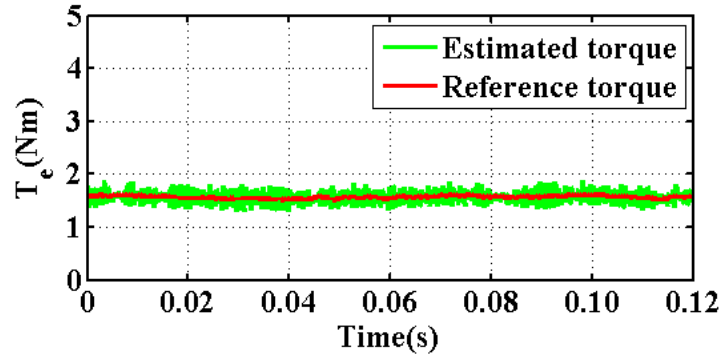


(c)

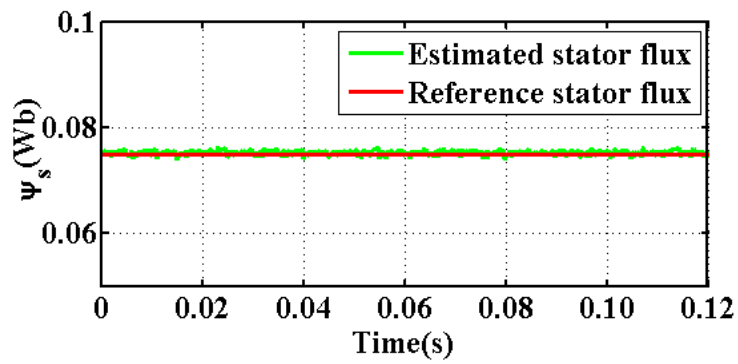


(d)

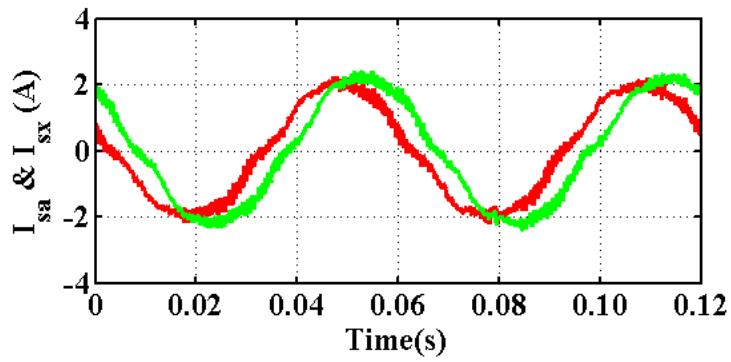
Fig. 7.12. Steady-state performance of synthetic ST-DTC strategy. (a) Electromagnetic torque. (b) Stator flux. (c) Phase currents. (d) Currents in  $z_1z_2$  subspace.



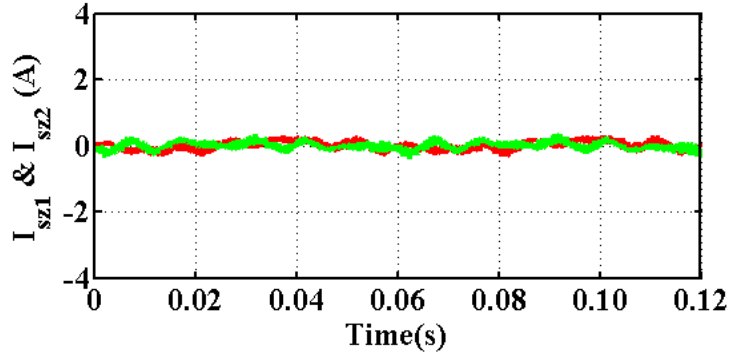
(a)



(b)

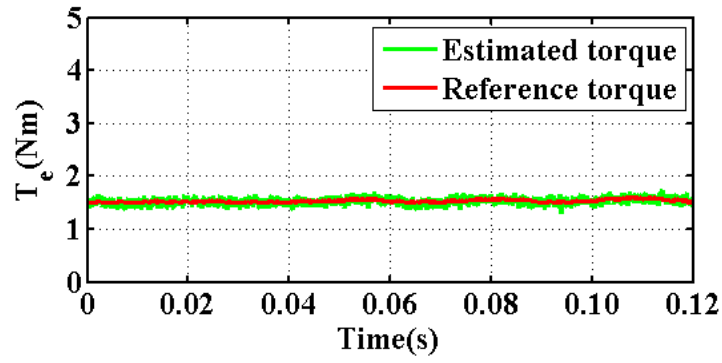


(c)

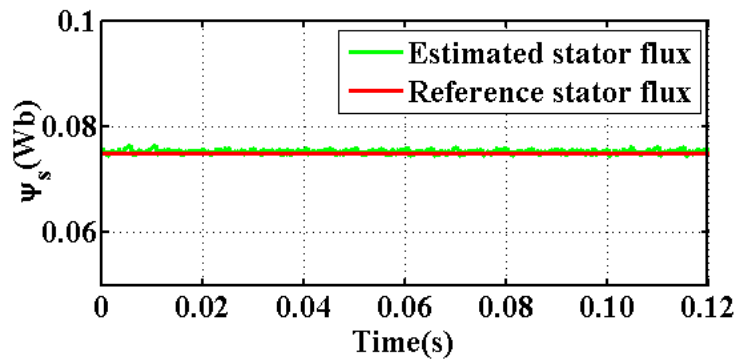


(d)

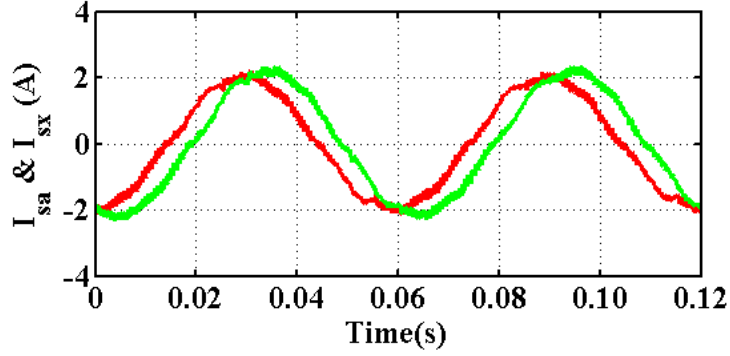
Fig. 7.13. Steady-state performance of proposed I ST-DTC strategy. (a) Electromagnetic torque. (b) Stator flux. (c) Phase currents. (d) Currents in  $z_1z_2$  subspace.



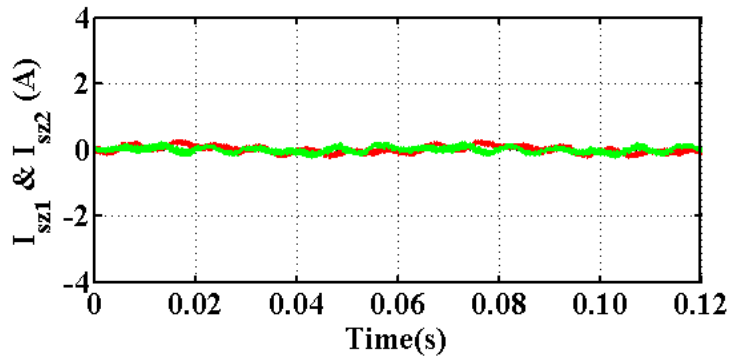
(a)



(b)



(c)



(d)

Fig. 7.14. Steady-state performance of proposed II ST-DTC strategy. (a) Electromagnetic torque. (b) Stator flux. (c) Phase currents. (d) Currents in  $z_1z_2$  subspace.

Table 7.4 Comparison Results of Steady-state Performance for Different ST-DTC Strategies

200 rpm,	Classical	Synthetic	Proposed I	Proposed II
$\Delta \psi_s(\%)$	0.1939	0.2215	0.2355	0.2474
$\Delta T_e(\%)$	4.2864	0.0195	0.0644	0.0162
$\psi_{s\_ripple} (Wb)$	5.7930e-4	5.4751e-4	4.0512e-4	3.6678e-4
$T_{e\_ripple} (Nm)$	0.3673	0.2766	<b><u>0.1215</u></b>	<b><u>0.0714</u></b>
$THD_{I_a}(\%)$	33.89	11.20	<b><u>6.33</u></b>	<b><u>4.91</u></b>
$f_{av} (kHz)$	2.904	4.773	4.895	4.790

From Table 7.4, the steady-state torque error is almost eliminated in the synthetic method and

proposed strategies. Desirable steady-state performance of stator flux can be obtained for all the ST-DTC strategies, i.e. both the steady-state error and ripple of flux are less than 1% of the reference flux. This confirms that the classical flux regulator is capable of flux control for all of the four ST-DTC strategies. By introducing synthetic vectors II and a 5-level torque regulator, the proposed method achieves a considerable reduction of torque ripple, which is only 43.93% of that in synthetic method, and 33.08% of that in classical ST-DTC. By modifying the 5-level torque regulator, further reduction for torque ripple can be obtained, from 0.1215 Nm to 0.0714 Nm. For the harmonic currents, the synthetic method can significantly reduce them to around one third of that in classical ST-DTC. Using a dead-time compensator, the proposed ST-DTC strategies achieve further reduction of harmonic currents over the synthetic method, and the THD of phase current is less than one fifth of that in the classical ST-DTC. The average switching frequency slightly increase from 2.904 kHz to 4.790 kHz, which is inevitable because all the synthetic vectors no matter synthetic vectors I or synthetic vectors II can be considered as more than one vectors applied on each sampling period. Both the proposed I and proposed II exhibit similar average switching frequency to the synthetic strategy, but yield better torque and current performance.

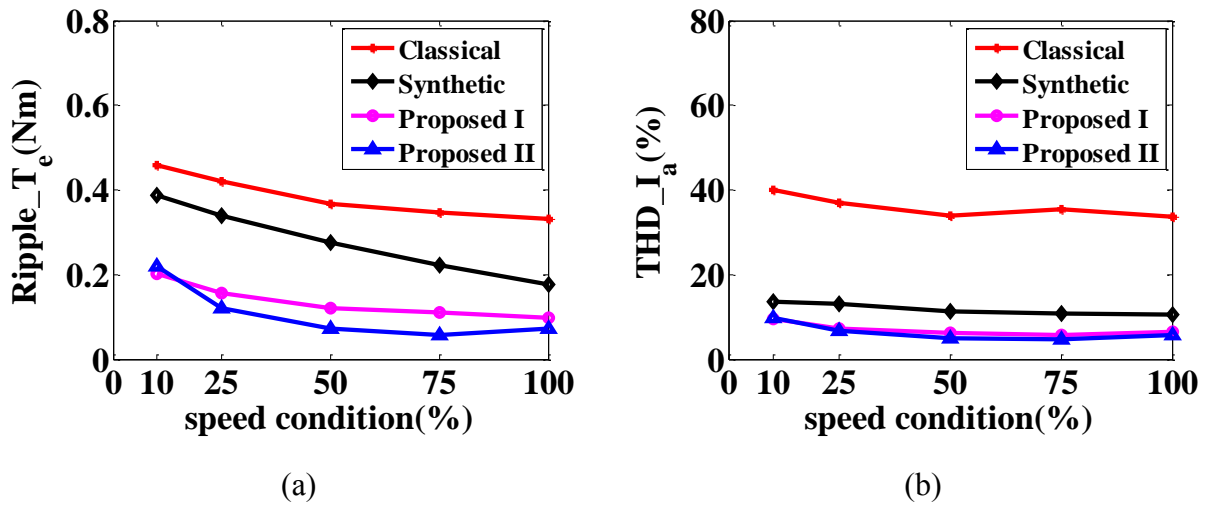
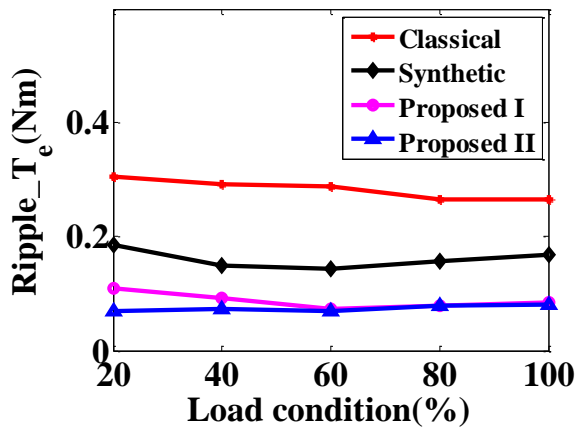
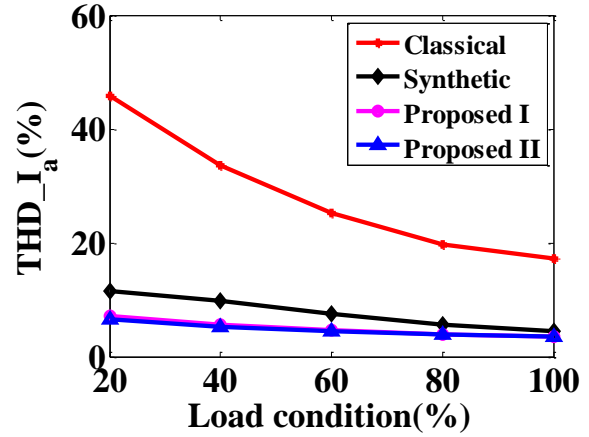


Fig. 7.15. Comparison of steady-state performance for different ST-DTC strategies under different speed conditions, load torque: 1.5 Nm. (a) Torque ripple. (b) THD of phase current.



(a)



(b)

Fig. 7.16. Comparison of steady-state performance for different ST-DTC strategies under different load conditions, machine speed: 400 rpm. (a) Torque ripple. (b) THD of phase current.

The performance of the four ST-DTC methods are also compared under different operating regions. Fig. 7.15 shows the torque ripple and the THD of phase-a current for different ST-DTC strategies under the condition of same load, 1.5 Nm, and at different speeds from 10% to 100% of rated speed. Fig. 7.16 expresses the torque ripple and the THD of phase-a current for different ST-DTC strategies under the condition of same rotor speed which is 400 rpm and at various load torque from 20% of rated load to full load. From Fig. 7.15-Fig. 7.16, both the synthetic method and the proposed ST-DTC method can significantly reduce the THD of phase currents over a wide range of operating conditions. The proposed methods exhibit better current performance due to the dead-time compensators. Moreover, a considerable reduction in torque ripple is achieved by the proposed method over the wide range of working regions, due to the introduction of synthetic vectors II having smaller torque variation. Further reduction of torque ripple can be achieved at medium and high speed with partial load by the use of a modified 5-level torque regulator with the proposed I method. When the machine works on the region of high speed and heavy load, the torque ripple of the two proposed methods are similar. This is because synthetic vectors I, whose torque variation is much larger than that of synthetic vectors II, are utilized for majority of the time. Nevertheless, both proposed methods still exhibit much better performance in terms of torque ripple.

### 7.3.3. Dynamic performance of Different ST-DTC Strategies

Fig. 7.17 shows the dynamic performance of classical and proposed ST-DTC methods when the reference speed changes from 200 rpm to 400 rpm without load. From Fig. 7.17, both the proposed strategies have similar dynamic performance to the classical DTC when the reference speed jumps.

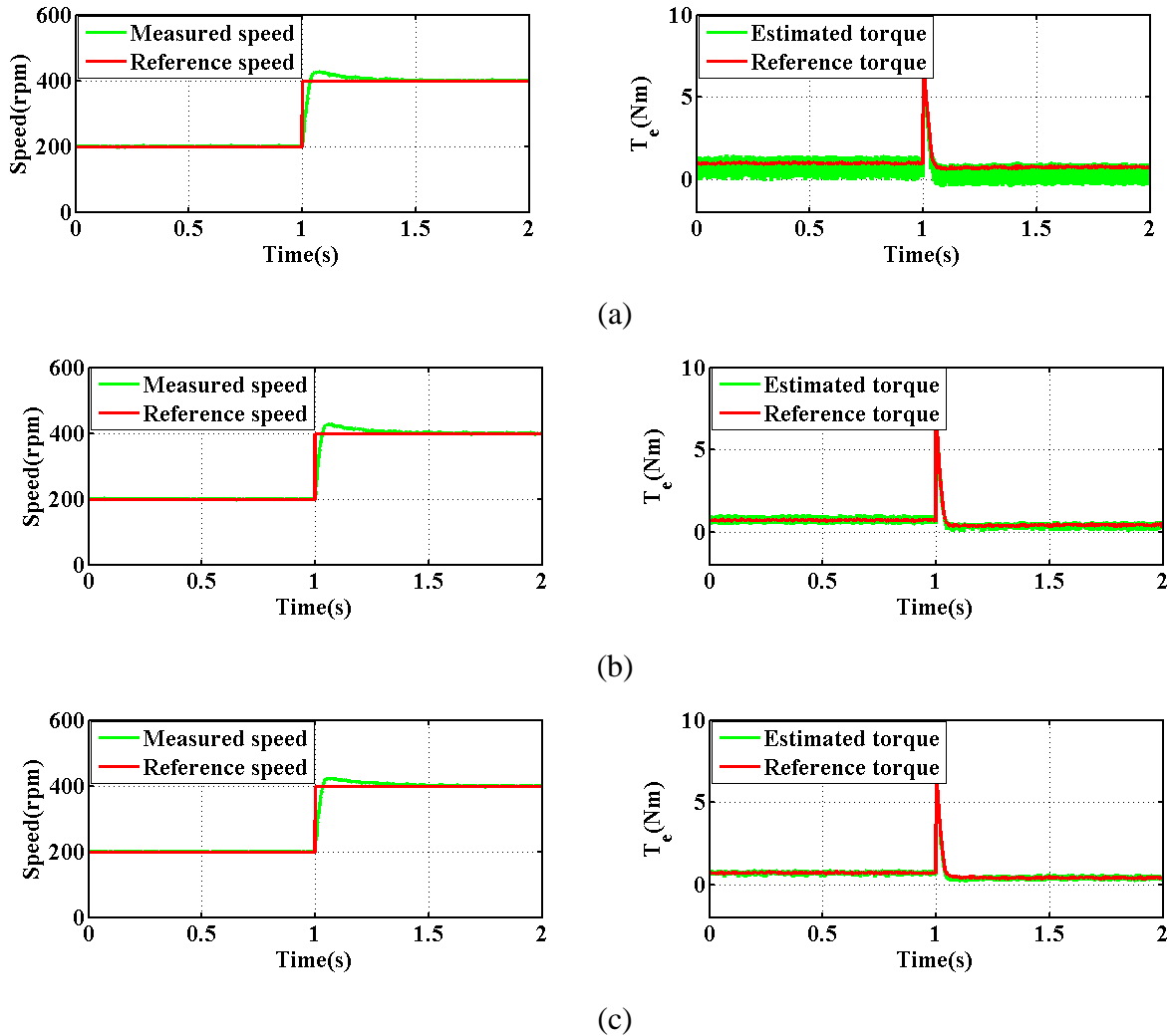


Fig. 7.17. Dynamic performance of speed response using different ST-DTC strategies (reference speed: 200 rpm to 400 rpm). (a) Classical strategy. (b) Proposed I strategy. (c) Proposed II strategy.

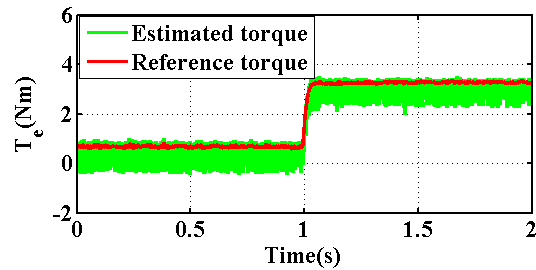
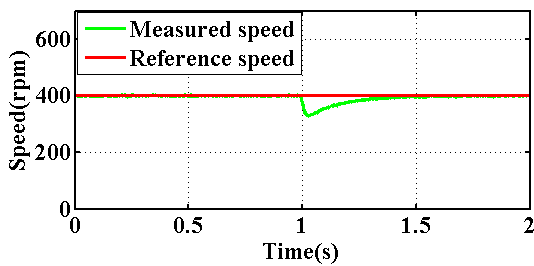
It also should be noted that, although the torque regulators of the two proposed strategies are partly different, they exhibit similar dynamic performance since only one type of synthetic vectors (type I) are employed during almost the whole transient process, where the torque error is always

large enough to exceed the outer bands, in order to track the reference torque as quickly as possible.

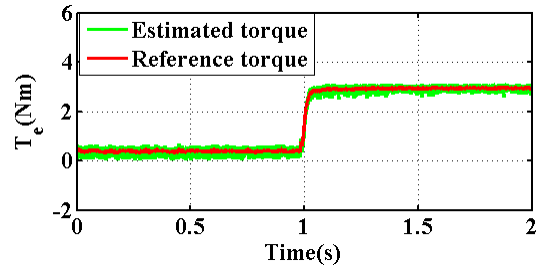
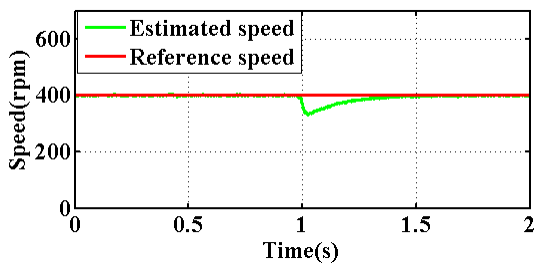
### 7.3.4. Dynamic Response to External Load Disturbance for the Proposed DTC Strategy

The responses to external load disturbance are compared between the classical ST-DTC and the proposed methods. The motor is initially operated under steady-state at 400 rpm with no load. Then the external load of approximately 3 Nm is added at 1.0 s, Fig. 7.18.

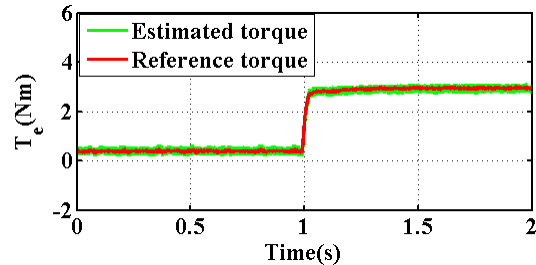
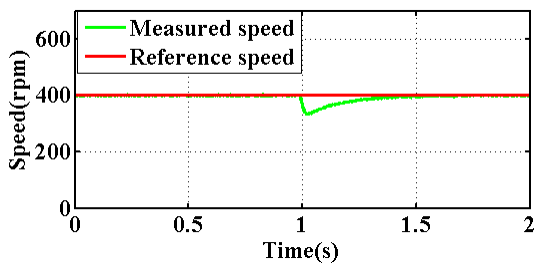
The torque generated with both the proposed methods and the classical method follow the reference equally well. This leads to similar speed tracking performance for the proposed and classical strategies, i.e. both speeds return to their original values in less than 0.3 s. Therefore, the proposed DTC method can preserve the robustness against external load disturbance of the classical DTC.



(a)



(b)



(c)

Fig. 7.18. Responses to external disturbance using different DTC strategies: external load (3 Nm) is added at the instant of 1.0 s. (a) Classical strategy. (b) Proposed I strategy. (c) Proposed II strategy.

#### 7.4. Conclusion

This chapter proposes a simple modified ST-DTC method for dual three-phase PM machine drives to greatly reduce harmonic currents, steady-state error and ripple of torque, without compromising the simplicity of structure and excellent dynamic performance. Two groups of synthetic vectors which can minimize the harmonic currents within one sampling period have been introduced, along with their most optimal switching sequences for implementation in a real-time system. The torque variations for both large and small synthetic vectors and zero vectors in different operating regions have been analysed, and then the function of outer and inner bands of torque regulator has been discussed. Consequently, a simple modified torque regulator is proposed to further improve the steady-state performance of torque.

Following features are obtained with the proposed ST-DTC strategy:

- (1) Simple structure. Only the switching table and torque regulator are slightly modified compared to the classical ST-DTC.
- (2) Easy to implement for real-time systems. The most appropriate switching sequences are given.
- (3) Considerable reduction of steady-state error and ripple of torque, as well as the harmonic currents at the price of slightly increasing average switching frequency.
- (4) Excellent dynamic performance and robustness against external load disturbance similar to the classical ST-DTC.

The analysis and experiments in this chapter are based on the ST-DTC of dual three-phase PMSM drives. However, the concept of employing synthetic vectors to reduce the harmonic currents, and the design of a modified torque regulator according to the amplitudes of different types of synthetic vectors, can be extended for general use. For instance, they can be applied to the other multiphase machines of switching table-based direct torque, power control methods which

may exhibit aforementioned three issues of harmonic currents, ripple and steady-state error of torque or power.

## **8. Space-vector PWM Based Direct Torque Control of Dual Three-phase Permanent Magnet Synchronous Machine Drives**

### **8.1. Introduction**

As discussed in Chapter 1, various kinds of current control methods using PWM techniques have been presented for dual three-phase machine drives. As an alternative solution to the current control strategies, DTC strategy is extended from three-phase drives to dual three-phase drives, thanks to its simple structure, excellent transient response. The existing ST-DTC methods cannot avoid the problem of current harmonics [BOJ05] [HAT05]. Therefore, based on the VSD technique, the two-step ST-DTC method (Chapter 5), synthetic-vector-based ST-DTC strategies (Chapter 6) and combined-synthetic-vector-based ST-DTC strategies (Chapter 7) have been developed in the previous chapters. Consequently, the torque performance can be improved and the harmonic currents can be greatly reduced. However, since the switching-table is used, all of the ST-DTC methods inevitably suffer from the problem of variable switching frequency, which is not suitable for some industry applications. To achieve constant switching frequency, a specific PWM strategy is required. For dual three-phase drives, carrier-based PWM with double zero-sequence injection and specific SVPWM are the two commonly used techniques [LEV08a], [ZHA95]. According to the machine model, based on a VSD technique, the torque production of dual three-phase machines is similar to that of three-phase machines. Therefore, the PWM-based DTC for three-phase machine drives can be easily extended to dual three-phase machine drives, as shown in Fig. 1.21.

In principle, all the reference voltage calculators used for the three-phase cases can be employed for the PWM-based DTC of dual three-phase drives. Bojoi [BOJ05] discusses this kind of solution, where a deadbeat algorithm is employed with the carrier-based PWM using a double zero-sequence strategy for dual three-phase drives. Although constant switching frequency can be obtained using this method, the current harmonics cannot be eliminated. As discussed in Chapter 1, proper PWM technique is not enough for the elimination of current harmonics. This is because besides the voltage harmonic of improper PWM technique, inverter non-linearity and the possible machine/inverter asymmetries result in the current harmonic as well [CHE14].

This chapter aims to provide an improved DTC strategy based on the deadbeat algorithm for the

dual three-phase machine drives, using a special SVPWM technique and harmonic currents controllers, as well as the suitable simple dead-time compensator. The proposed method improves current performance, provides a constant switching frequency, and enhances the steady-state performance of flux and torque.

## 8.2. Deadbeat DTC Algorithm

### 8.2.1. Deadbeat Algorithm

The deadbeat-DTC schemes can be implemented in a stationary reference frame [HAB92], synchronous reference frame aligned with the rotor flux vector [WES09], [LEE11], [XU14], and the synchronous reference frame aligned with the stator flux vector [BOJ05]. The three types of reference frames of PMSM are depicted in Fig. 1.7. To keep the DTC scheme sensorless and also simplify the computational effort, the deadbeat-DTC strategy implemented in the synchronous reference frame aligned with the stator flux vector is discussed in this chapter.

As noted already, the electromagnetic torque produced by the dual three-phase surface-mounted PMSM can be described as

$$T_e = 3P(\boldsymbol{\psi}_s \otimes \mathbf{I}_s) \quad (8.1)$$

Therefore, the instantaneous torque variation can be expressed as

$$\frac{dT_e}{dt} = 3P\left(\frac{d\boldsymbol{\psi}_s}{dt} \otimes \mathbf{I}_s + \boldsymbol{\psi}_s \otimes \frac{d\mathbf{I}_s}{dt}\right) \quad (8.2)$$

Discretizing(8.2), using a first-order approximation, results in

$$\frac{T_e(k+1) - T_e(k)}{T_s} = 3P\left(\frac{\boldsymbol{\psi}_s(k+1) - \boldsymbol{\psi}_s(k)}{T_s} \otimes \mathbf{I}_s(k) + \boldsymbol{\psi}_s \otimes \frac{\mathbf{I}_s(k+1) - \mathbf{I}_s(k)}{T_s}\right) \quad (8.3)$$

The deadbeat algorithm aims at obtaining the reference values of torque and stator flux in one sampling time, therefore,

$$\begin{cases} T_e^* = T_e(k+1) \\ \psi_s^* = \psi_s(k+1) \\ I_s^* = I_s(k+1) \end{cases} \quad (8.4)$$

Substituting (8.4) into (8.3), yields

$$\frac{\Delta T_e}{T_s} = 3P \left( \frac{\Delta \psi_s}{T_s} \otimes I_s + \psi_s \otimes \frac{\Delta I_s}{T_s} \right) \quad (8.5)$$

The deadbeat algorithm addressed here is implemented in the  $MT$  synchronous reference frame aligned with the stator flux vector, which means

$$\begin{cases} \psi_M = \psi_s \\ \psi_T = 0 \end{cases} \quad (8.6)$$

Therefore, by ignoring the effect of stator resistance on the variation of stator flux [REN14], the  $M$ -axis reference value of voltage can be expressed as

$$V_M^* = \frac{\Delta \psi_{sM}}{T_s} = \frac{\psi_s^* - \psi_s}{T_s} = \frac{\Delta \psi_s}{T_s} \quad (8.7)$$

Then, the  $T$ -axis reference voltage can be obtained from (8.5) and (8.7)

$$V_T^* = \frac{\frac{L_s \Delta T_e}{3PT_s} - L_s V_M^* I_{sT} + \psi_s e_{sT}}{\psi_s - L_s I_{sM}} \quad (8.8)$$

Consequently, the reference voltage vector in the stationary reference frame can be written as

$$V_{s\alpha\beta}^* = V_{sMT}^* e^{j\theta_s} + R_s I_{s\alpha\beta} \quad (8.9)$$

### 8.2.2. Specific PWM Technique for Dual Three-phase Drives

For the three phase machine system, the classical SVPWM technique is usually employed to implement the reference voltage vector. For the dual three-phase machine, a specific SVPWM approach [ZHA95], [HAD06], [MAR08] is commonly used. By using the VSD technique, each

vector in the  $\alpha\beta$  and the  $z_1z_2$  subspace is shown in Fig. 1.18. As discussed in Chapter 1, to gain the maximum DC link voltage utilization, the outermost 12 vectors are commonly used, as shown in Fig. 1.18. Unlike the three-phase drives, where only two nearest vectors are needed to construct the reference voltage vectors, since the dual three-phase drive system can be regarded as a four-dimensional system, four nearest vectors out of the outermost 12 vectors in the  $\alpha\beta$  subspace will be selected along with the zero vectors, where the dwell time of each vector is given in section 1.3.3 of Chapter 1.

The conventional deadbeat-PWM-DTC only controls the variables in the  $\alpha\beta$  subspace, while the reference voltage in the  $z_1z_2$  subspace is set to zero [BOJ05]. Therefore, this specific SVPWM technique can successfully force the average voltage in the  $z_1z_2$  subspace to zero in principle, which can greatly reduce the harmonic currents caused by the PWM harmonics. However, as discussed in chapter 1, voltage harmonics caused by improper PWM techniques are not the only reason for the existence of current harmonics, other factors include inverter non-linearity and the possible machine/inverter asymmetries results [CHE14]. Therefore, the PWM-based DTC strategies which are simply extended from three-phase machine drives cannot minimize the harmonic currents in the real-digital dual three-phase drive systems [BOJ05].

Different types of current control methods in the  $z_1z_2$  subspace are presented, and a resonant controller is presented for dead-time compensation in [CHE14]. Although the current performance is shown to be desirable for current control strategies, lots of coordinate transformations and additional controllers are required. For the sake of simplicity, the PI controllers in a synchronous reference frame are employed for currents in the  $z_1z_2$  subspace, and the much simpler dead-time (which dominates inverter non-linearity) compensator has been employed in this chapter [CHO07], [GON11], [REN15].

### **8.3. Experimental Results**

Experimental tests are conducted on the laboratory prototype of dual three-phase PMSM machine II. The specification of the machine is given in Appendix I. All the results were captured using dSPACE 1005 software, and then plotted using MATLAB. A block diagram of the deadbeat-SVPWM-DTC strategy is depicted in Fig. 8.1.

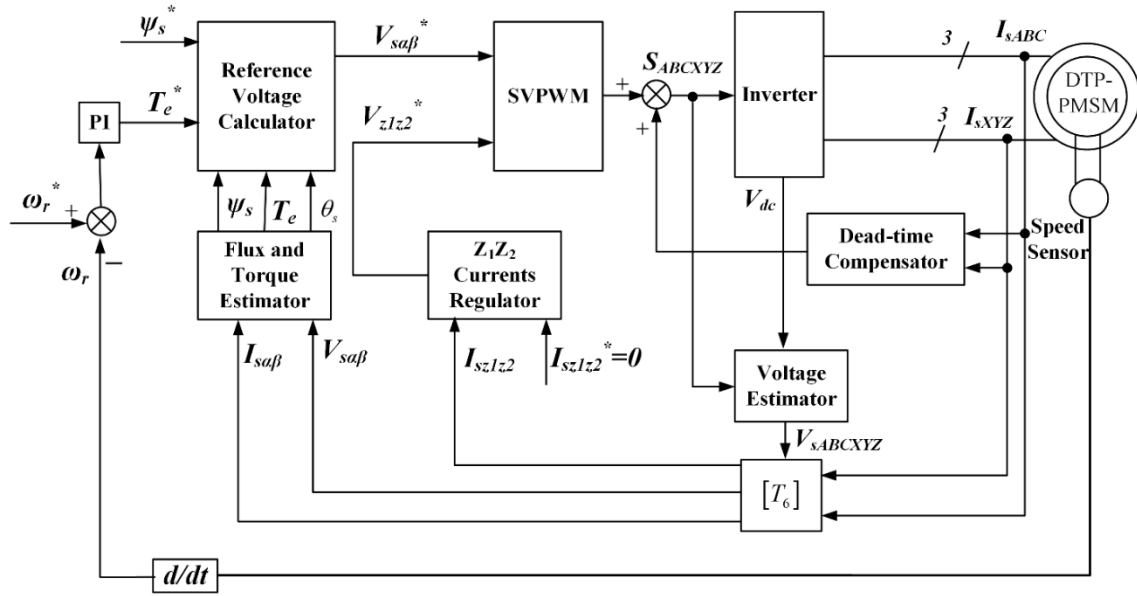


Fig. 8.1. Block diagram of deadbeat-SVPWM-DTC strategy.

Four types of ST-DTC strategies are compared:

- (a) Classical ST-DTC, named classical method;
- (b) Modified ST-DTC with modified 5-level torque regulator and two types of synthetic vectors, named combined-synthetic method (Chapter 7).
- (c) Deadbeat SVM-DTC method without  $z_1z_2$  current controllers or dead-time compensator, named deadbeat-PWM-DTC I;
- (d) Deadbeat SVM-DTC method with  $z_1z_2$  current controllers and the dead-time compensator, named deadbeat-PWM-DTC II;

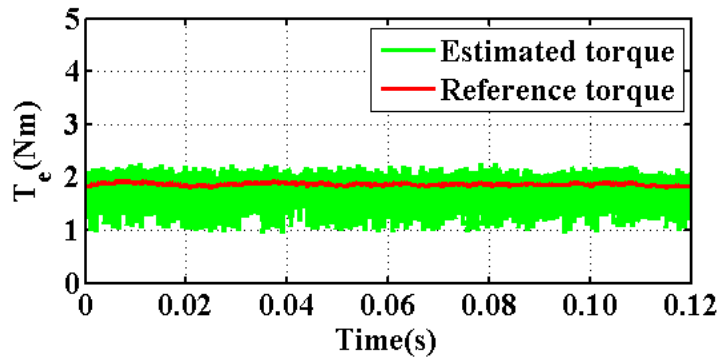
The torque and flux hysteresis bands for the classical method are set as 0.173 Nm and 0.0002 Wb, respectively, while for combined-synthetic method, the outer and inner bands are set to 0.3 Nm and 0.173 Nm, respectively, the same as that in the chapter 7. The switching frequency of the deadbeat SVM-DTC is set to 10 kHz.

### 8.3.1. Steady-state Performance of Different ST-DTC Strategies

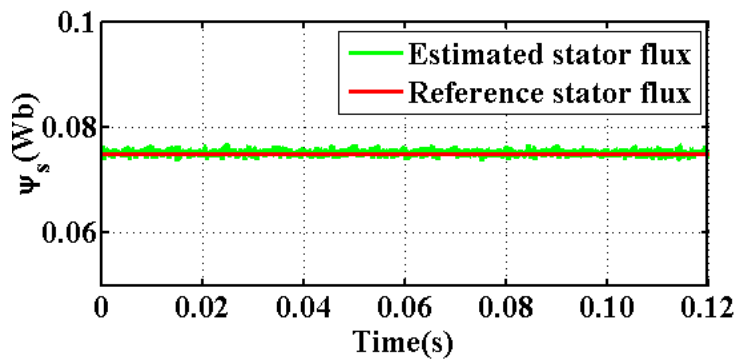
Fig. 8.2-Fig. 8.5 show the steady-state performance of the different ST-DTC strategies when the

machine speed is 200 rpm and the load torque is about 1.5 Nm. The classical ST-DTC suffers from steady-state error and ripple of torque as well as large harmonic currents which mainly exist in the  $z_{1z2}$  subspace, as shown in Fig. 8.2. The use of the combined-synthetic method as proposed in chapter 7, considerably decreases the torque ripple and harmonic currents. The torque ripple can be further reduced by using the deadbeat-PWM-DTC strategies, Fig. 8.4-Fig. 8.5. The phase currents in the deadbeat-PWM-DTC I are less sinusoidal, and the harmonic currents can be clearly observed in  $z_{1z2}$  subspace, Fig. 8.4 (c)-(d), where the main harmonic order is 5<sup>th</sup> and 7<sup>th</sup>, Fig. 8.4(f). After the use of current controllers in  $z_{1z2}$  subspace and the simple dead-time compensator, the current harmonics can be significantly reduced, Fig. 8.5.

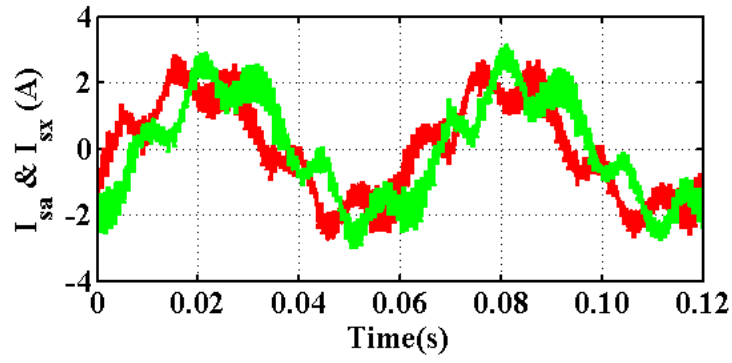
For the ST-DTC strategies, since the switching frequency is variable, the current harmonics can occur across a wide range of frequencies, which means lots of noise in the system, Fig. 8.2(e) and Fig. 8.3(e). When the SVPWM technique is employed, the current harmonics are mainly located in the area near to the switching frequency, which means the noise can be considerably reduced, Fig. 8.4(e) and Fig. 8.5(e).



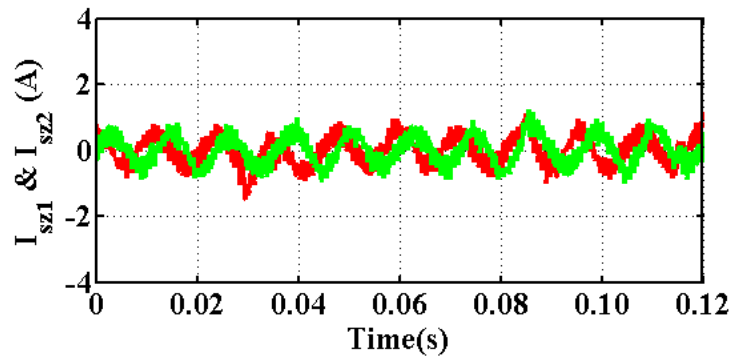
(a)



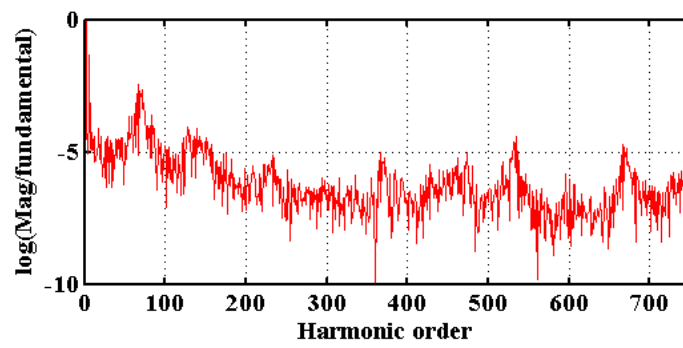
(b)



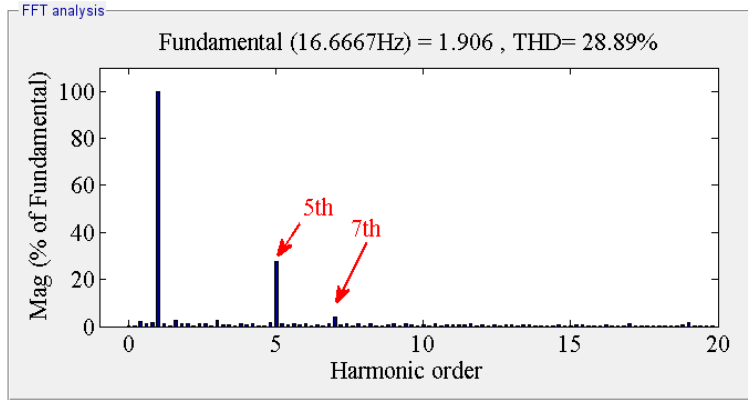
(c)



(d)

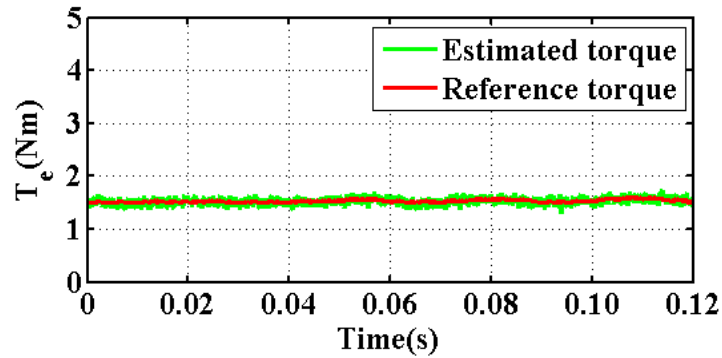


(e)

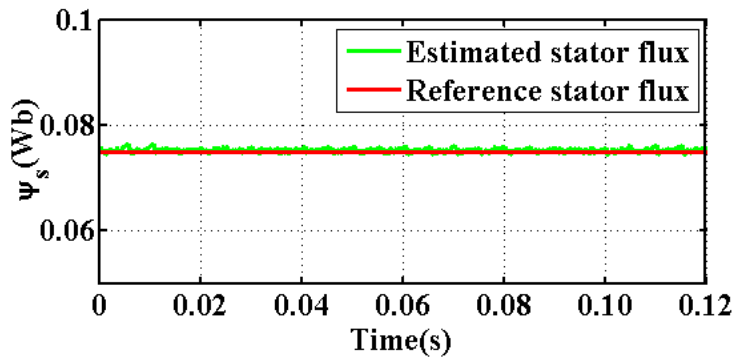


(f)

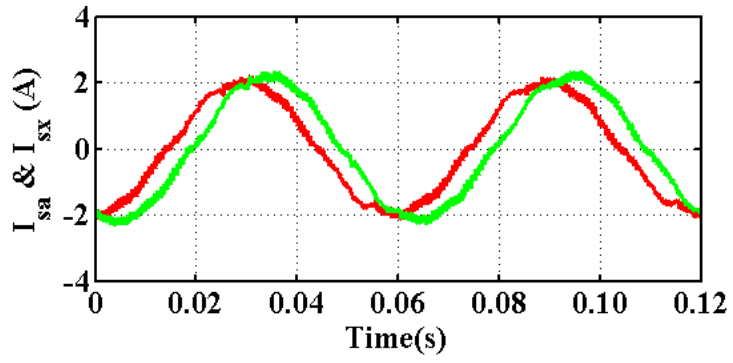
Fig. 8.2. Steady-state performance of classical ST-DTC strategy. (a) Electromagnetic torque. (b) Stator flux. (c) Phase currents. (d) Currents in the  $z1z2$  subspace. (e) Phase current harmonic spectrum including high and low harmonics. (f) Phase current harmonic spectrum in the range of low harmonics.



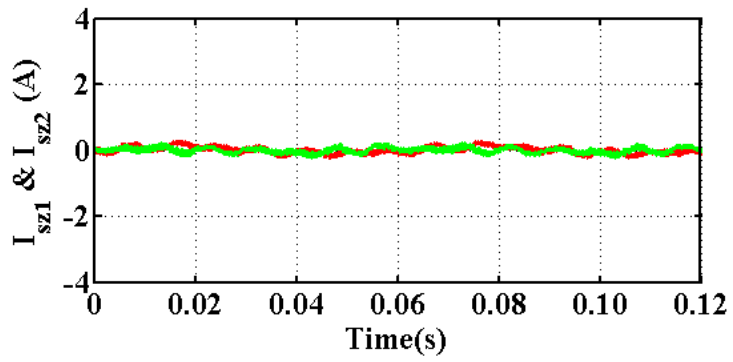
(a)



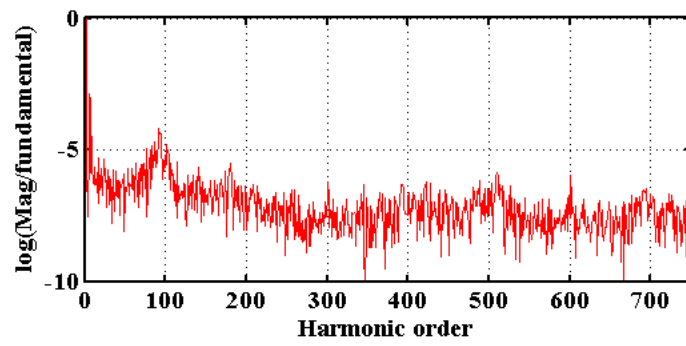
(b)



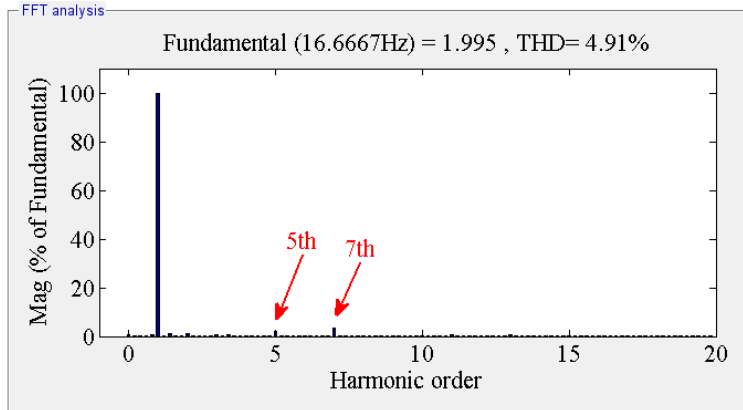
(c)



(d)

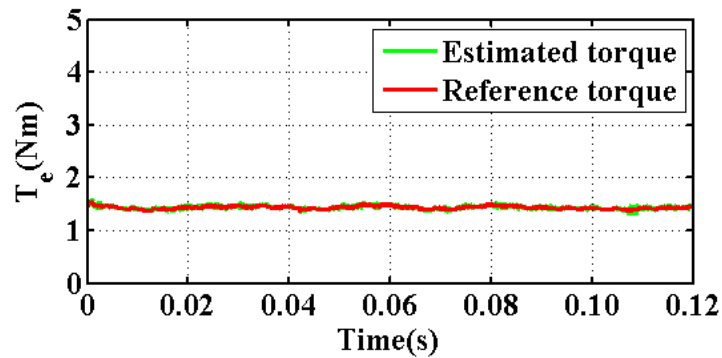


(e)

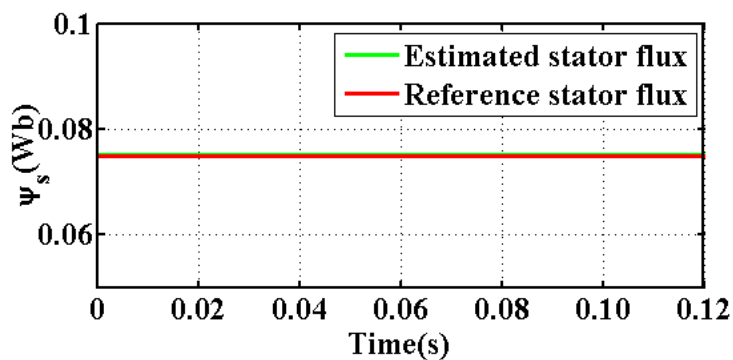


(f)

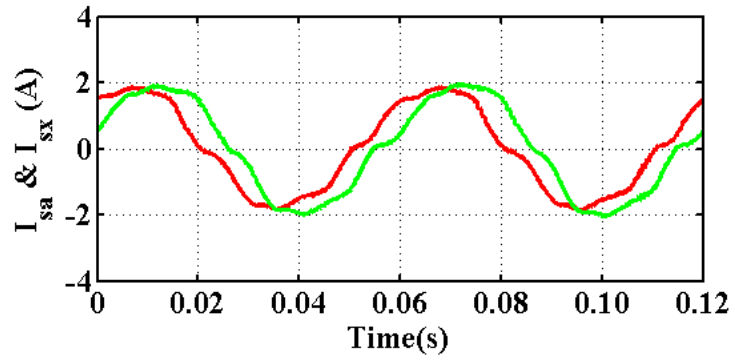
Fig. 8.3. Steady-state performance of Combined-synthetic method strategy. (a) Electromagnetic torque. (b) Stator flux. (c) Phase currents. (d) Currents in the  $z_1z_2$  subspace. (e) Phase current harmonic spectrum including high and low harmonics. (f) Phase current harmonic spectrum in the range of low harmonics.



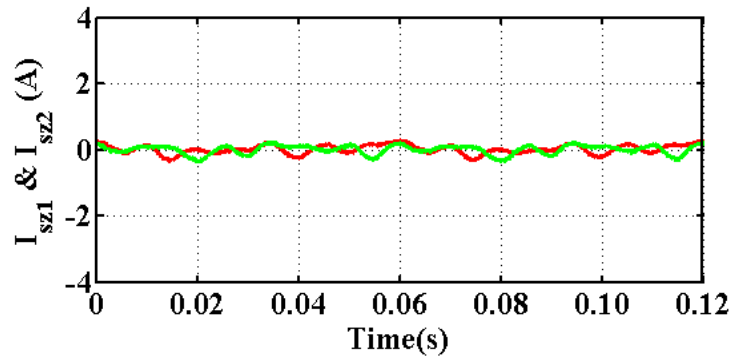
(a)



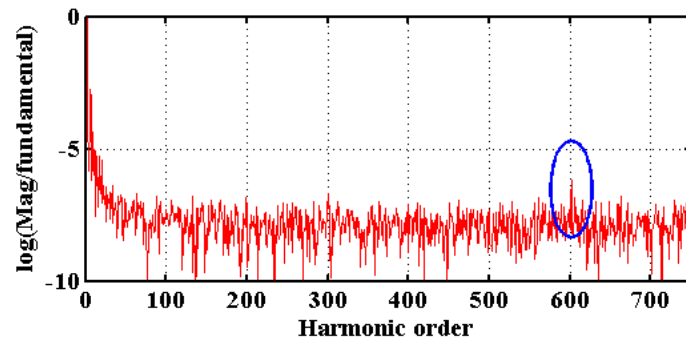
(b)



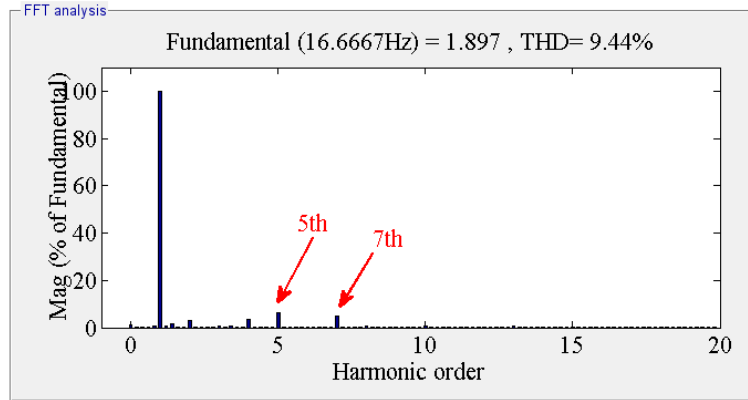
(c)



(d)

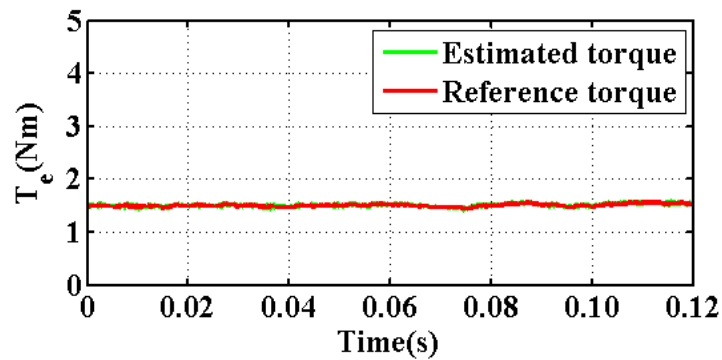


(e)

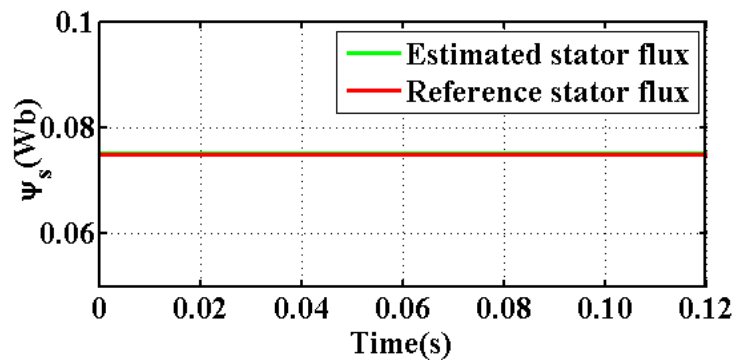


(f)

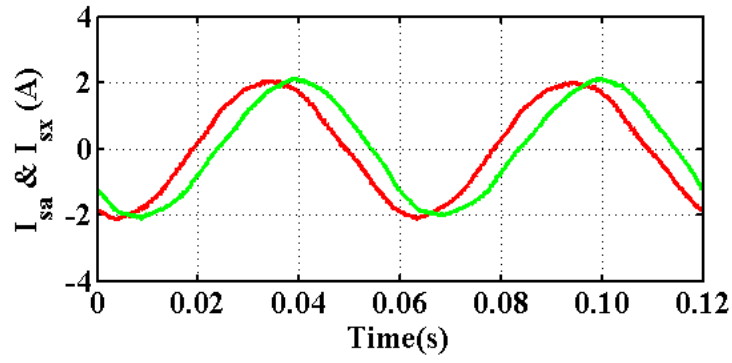
Fig. 8.4. Steady-state performance of Deadbeat-PWM-DTC I strategy. (a) Electromagnetic torque. (b) Stator flux. (c) Phase currents. (d) Currents in the  $z_1z_2$  subspace. (e) Phase current harmonic spectrum including high and low harmonics. (f) Phase current harmonic spectrum in the range of low harmonics.



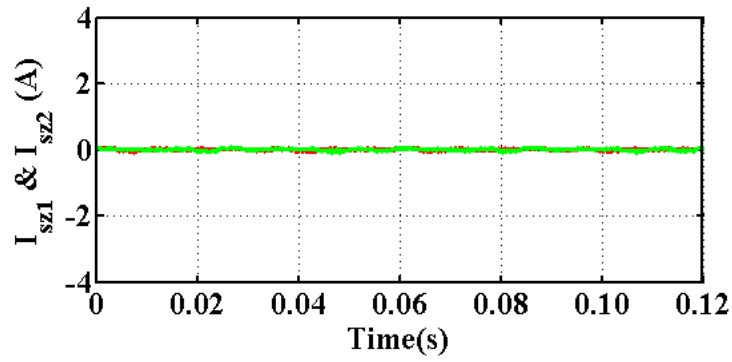
(a)



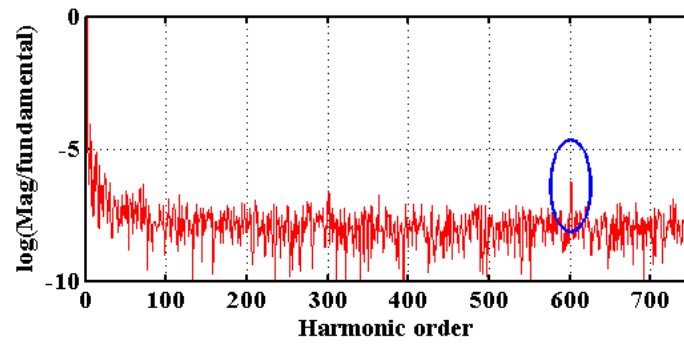
(b)



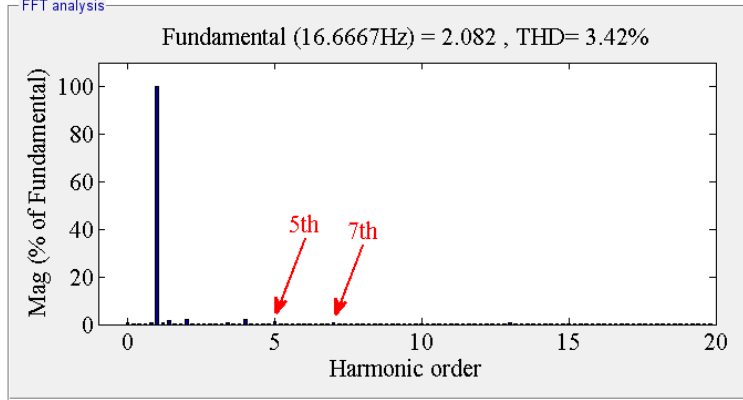
(c)



(d)



(e)



(f)

Fig. 8.5. Steady-state performance of deadbeat-PWM-DTC II strategy. (a) Electromagnetic torque. (b) Stator flux. (c) Phase currents. (d) Currents in the  $z_1z_2$  subspace. (e) Phase current harmonic spectrum including high and low harmonics. (f) Phase current harmonic spectrum in the range of low harmonics.

To permit a clear comparison, detailed quantitative results are presented in Table 8.1.

Table 8.1 Comparison Results of Steady-state Performance for Different DTC Strategies

200 rpm 1.5 Nm	Classical	Combined-Synthetic	Deadbeat-SVM I	Deadbeat-SVM II
$\Delta \psi_s(\%)$	0.1939	0.2474	0.0895	0.1072
$\Delta T_e(\%)$	4.2864	0.0162	0.0176	0.0244
$\psi_{s\_ripple} (Wb)$	5.7930e-4	3.6678e-4	0.0976e-4	0.0892e-4
$T_{e\_ripple} (Nm)$	0.3673	<b><u>0.0714</u></b>	<b><u>0.0351</u></b>	<b><u>0.0304</u></b>
$THD_{I_a}(\%)$	33.89	<b><u>4.91</u></b>	<b><u>9.44</u></b>	<b><u>3.42</u></b>

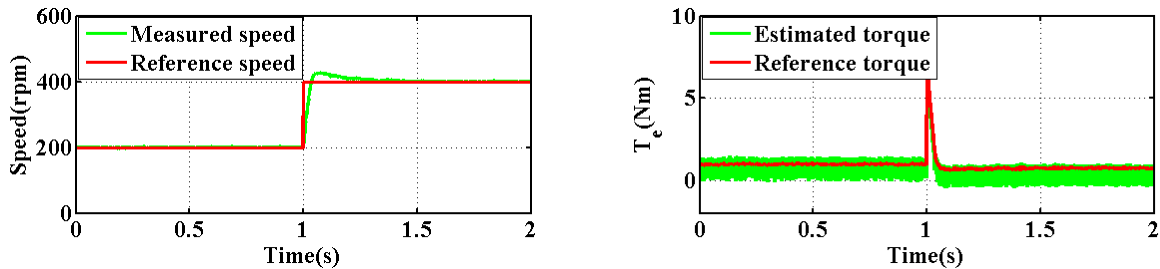
From Table 8.1, desirable steady-state performance of stator flux can be obtained for all the DTC strategies, i.e. both the steady-state error and ripple of flux are less than 1% of the reference flux. The steady-state error of torque which is apparent in the classical ST-DTC, is almost eliminated in other three strategies. By using the combined-synthetic ST-DTC method, the torque ripple can be considerably reduced to only 19.44% of that in classical ST-DTC. By the introduction of the deadbeat algorithm and the SVPWM technique, further reduction of torque ripple can be obtained by both of the deadbeat-PWM-DTC methods. The reduction of torque ripple of the proposed

method is only 42.58% - 49.16% of that in combined-synthetic method, and 8.28% - 9.56% of that in classical ST-DTC.

For the harmonic currents, the combined synthetic ST-DTC achieves significant reduction of harmonic currents, and the THD of phase current is less than one fifth of that in the classical ST-DTC. The deadbeat-SVM DTC I achieves better current performance compared to that of classical ST-DTC, the THD of phase current is reduced from 33.89% to 9.44%. However, since this method only eliminates the effect on harmonic currents from the PWM technique side, the inverter non-linearity and the machine/inverter asymmetries still cause harmonic currents. After considering these two factors into the strategy, the deadbeat-SVM DTC II obtains the best current performance among all the implemented methods, where the THD of phase current is only 3.42%.

### 8.3.2. Dynamic Performance of Different ST-DTC Strategies

Fig. 8.6 shows the dynamic performance of different DTC methods when the reference speed changes from 200 rpm to 400 rpm without load. From Fig. 8.6, both the combined-synthetic method and deadbeat-PWM-DTC methods have similar dynamic performance to the classical DTC when the reference speed instantly changes. Although PI regulators are employed for controlling harmonic currents in the  $z_{1z2}$  subspace in the deadbeat-PWM-DTC methods, the variables in the  $z_{1z2}$  subspace do not contribute the torque production. It is unsurprising that dynamic performance is undiminished compared to the classical controller. Similarly, for the control of flux and torque in  $\alpha\beta$  subspace, no PI regulators are used in any of the DTC methods.



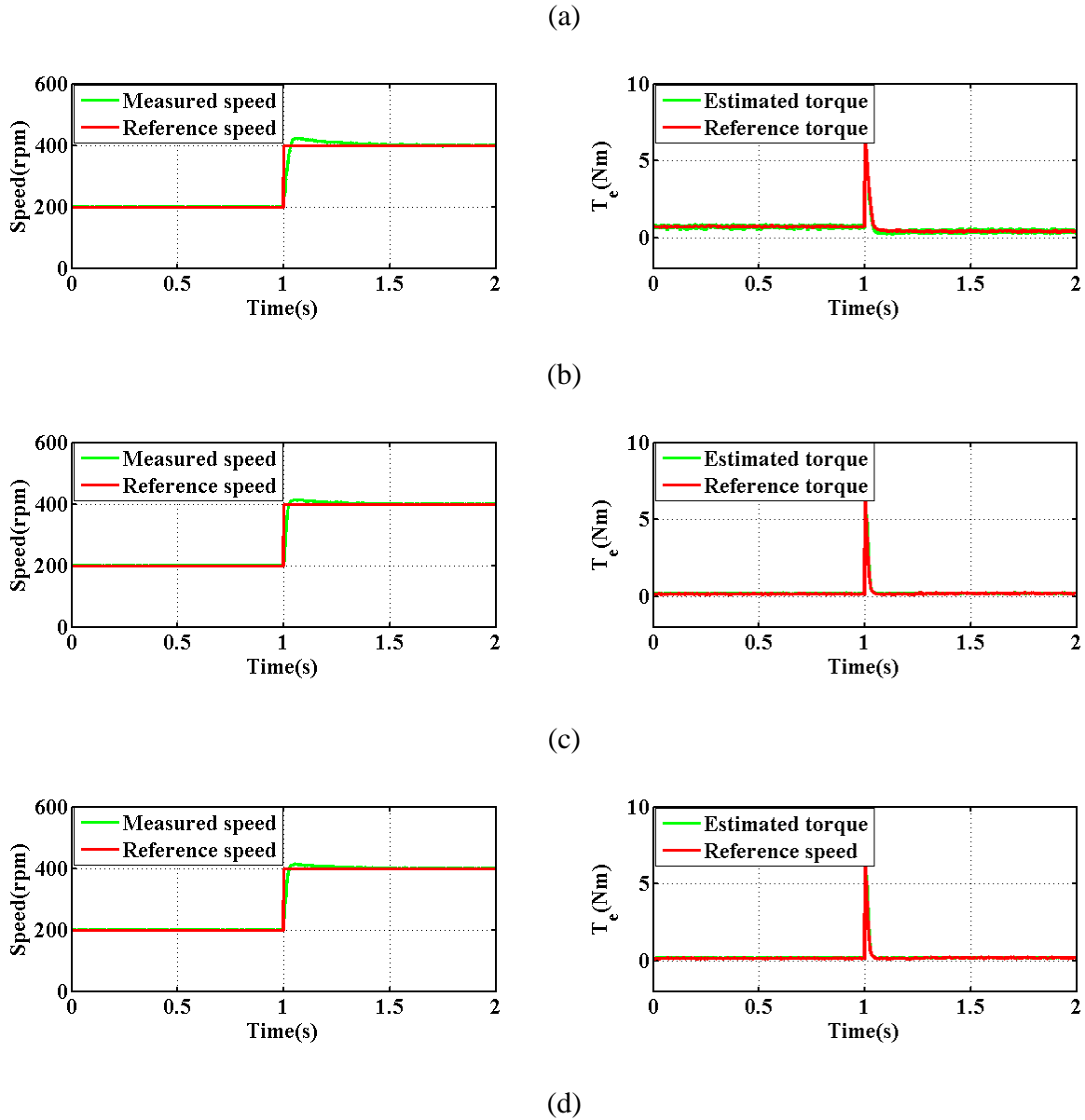


Fig. 8.6. Dynamic performance of speed response using different ST-DTC strategies: reference speed: 200 rpm to 400 rpm. (a) Classical strategy. (b) Combined-synthetic strategy. (c) Deadbeat-PWM-DTC I strategy. (d) Deadbeat-PWM-DTC II strategy.

#### 8.4. Conclusion

This chapter proposed a modified deadbeat-based PWM-DTC strategy for dual three-phase machine drives. PWM-DTC strategies are suitable solutions where constant switching frequency is required. Among them, deadbeat-PWM-DTC is featured for its good dynamic performance since no PI regulators are employed in the flux or torque control loop. However, conventional deadbeat-

PWM-DTC has neither harmonic current controllers nor inverter-nonlinearity compensator, and hence, the harmonic currents cannot be eliminated. This chapter proposed the improved deadbeat-PWM-DTC, where PI controllers in a synchronous reference frame for currents in the  $z_{1Z2}$  subspace are employed together with the deadbeat-based reference voltage calculator. Then specific SVPWM techniques were adopted to implement the reference voltage vectors. Thereafter, a simple dead-time compensator is utilized to reduce the effect of inverter non-linearity on harmonic currents.

The proposed deadbeat-PWM-DTC has achieved considerable reduction of steady-state error and ripple of torque, as well as the harmonic currents, while maintaining the merit of excellent dynamic performance of ST-DTC. However, since the machine parameters are required in this strategy, accurate machine parameters or on-line machine parameter estimation are usually necessary.

## 9. General Conclusions and Discussions

This thesis focuses on the DTC of single and dual three-phase PMSM drives, with particular reference to the reduction of steady-state errors, torque ripple, and current harmonics in ST-DTC.

### 9.1. Switching-table-based Direct Torque Control of Three-phase PMSM

FOC and DTC are the two most widely used strategies for AC machine drives. Compared to the FOC scheme, DTC does not require current regulators, coordinate transformations or specific modulation. Hence, DTC has the features of simple structure, excellent transient response and robustness against rotor parameters. However, although the flux performance is acceptable, AC machine drives using ST-DTC usually suffer from steady-state error and ripple of torque.

According to the machine model and the basic principle of ST-DTC, the instantaneous variation rates of stator flux and torque of each converter output voltage vector in each sector are detailed and analysed. It is found that the absolute value of increasing variation rates and decreasing variation rates are usually quite different. Hence, large steady-state error of torque and torque ripple occur since only one vector operates for the whole sampling period. To minimise the steady-state error of torque response, a new band-shifted torque regulator is proposed. This proposed method can significantly reduce the steady-state error of torque response over a wide range of operating conditions, whilst the merits of the conventional DTC such as simple structure and excellent transient response, are preserved.

The so-called duty-based DTC method, which applies the active vector for the appropriate dwell time instead of the whole sampling period, is another solution to reduce torque ripple. Considering the existing duty-based DTC methods are always time-consuming and machine parameter dependent, a simple and effective method for determining the appropriate duty ratio in DTC three-phase PMSM drives accounting for the influence of machine angular velocity is proposed. An estimation method is given to obtain the range of the key control parameters. Compared to the existing duty-based DTC methods, the proposed method can achieve desirable performance of torque and flux at the lower cost of increased average commutation frequency.

Although the analyses and experiments are based on the DTC of three-phase PMSM drives, the new band-shifted torque regulator and the proposed duty ratio determination can also be extended for general use and applied to the other machines of switching table-based direct torque, and power

control methods which may exhibit the same problem of ripple and/or steady-state error.

## **9.2. Switching-table-based Direct Torque Control of Dual Three-phase PMSM**

Dual three-phase machine is one of the most popular kinds of multiphase machines. It has two sets of three-phase windings spatially shifted by 30 electrical degrees and, hence, dual three-phase machine is featured as its inherent advantage of suppression of the sixth harmonic of torque pulsation, in addition to common merits of multiphase such as power segmentation, lower torque pulsations, high reliability at the system level, and lower dc-link voltage requirement. The current control of dual three-phase machines has been researched for decades, and effective current control schemes have been presented as well as PWM techniques, i.e. carrier-based PWM with double zero-sequence injection and the specific SVPWM designed for dual three-phase drives. These current control methods exhibit acceptable steady-state current performance. However, they are usually complicated and machine parameter dependent, and the torque dynamic performance is limited due to the use of PI current regulators. Therefore, ST-DTC strategies are the potential alternative solution when the torque dynamic performance is vital.

Besides the steady-state error and ripple of torque, the large harmonic currents is the other problem that should be considered during the design of ST-DTC strategies for dual three-phase systems. According to a VSD technique, the dual three-phase system consists of two subspaces where the  $\alpha\beta$  subspace is related to the torque production and the  $z_1z_2$  subspace is an additional one which is responsible for the harmonic currents, which means that the harmonic currents can be reduced if the flux in the additional subspace is minimized. Therefore, a two-step process to determine the most appropriate inverter voltage vector is proposed to reduce the stator harmonic currents. This method requires an additional flux estimator in the  $z_1z_2$  subspace, and one additional switching table, which make the method complicated.

To keep the merit of simple structure of the ST-DTC, synthetic vectors are employed to replace the conventional vectors. The concept of synthetic vectors are inspired by the space vector PWM (SVPWM) for dual three-phase machine drives, which can minimize the voltage components in the additional subspace within one control period. The switching sequence which is most suitable for the implementation of real-time systems has been proposed to minimize the computational burden. The synthetic method achieves better current performance while keeping the advantages

of the classical ST-DTC. However, the reduction of torque ripple is limited since the amplitude of the synthetic vectors is similar to that of the vectors used in classical ST-DTC.

To reduce the torque ripple and current harmonics at the same time for ST-DTC, two types of synthetic vectors, which can reduce the harmonic currents effectively, are first introduced, together with the most suitable switching sequences. Then, a modified five-level torque regulator has been proposed to improve the torque performance. With the proposed method, the harmonic currents can be suppressed, and the steady-state error and ripple of torque can be considerably reduced. Furthermore, the merits of classical ST-DTC such as simple structure and excellent dynamic performance are preserved.

### **9.3. PWM-based Direct Torque Control of Dual Three-phase PMSM**

The modified ST-DTC strategies discussed so far are suitable for most applications since they obtain desirable torque and currents performance and maintain the merits of classical ST-DTC methods, such as simple structure, good dynamic performance and parameter independence. However, due to the use of switching tables, the switching frequencies of the modified ST-DTC strategies are variable. Therefore, they cannot be employed on some applications where the constant switching frequency is required. As a result, PWM techniques such as carrier-based PWM with double zero-sequence injection and the specific SVPWM are incorporated into the DTC strategies, which are then named PWM-DTC strategies. There are many ways to obtain the reference voltage vector, which can be divided into two main types: PI-regulators-based methods and machine-model-based methods. Among them, deadbeat DTC scheme, is taken as an example to implement the PWM-based DTC for dual three-phase machine drives. Deadbeat DTC scheme is lauded for its desirable dynamic performance, since no PI regulators are employed in the flux or torque control loop, The steady-state torque and current performance are further improved due to the use of specific PWM techniques for dual three-phase machine drives at the cost of increased computational burden and machine parameter dependence.

The comparison of the discussed five DTC strategies for dual-three phase PMSM drives is given in Table 9.1.

Table 9.1 Comparison of different ST-DTC strategies for dual-three phase PMSM drives

	Classical (Chapters 5-8)	Two-step (Chapter 5)	Synthetic (Chapter 6)	Combined- synthetic (Chapter 7)	Deadbeat- PWM-DTC (Chapter 8)
Steady-state flux	Acceptable	Acceptable	Acceptable	Acceptable	Acceptable
Harmonic currents	High	Medium	Low	Lower	Lowest
Steady-state error of torque	High	Low	Low	Low	Low
Torque ripple	High	Medium	Medium	Low	Lowest
Dynamic performance	Good	Good	Good	Good	Good
Algorithm complexity	Lowest	Medium	Low	Medium	High
Switching frequency	Variable	Variable	Variable	Variable	Constant

#### 9.4. Future Work

This thesis has studied ST-DTC of dual three-phase PMSM drives, and also introduced deadbeat-based SVM-PWM. For the DTC of dual three-phase drives, the number of existing papers are still limit. For the future work, the following contents can be further studied:

(1). For the ST-DTC, the algorithms are only studied when the machine operates in linear region. To fully utilize the DC power supply, the DTC strategies should also be capable for the operation in over modulation region as well. Therefore, how to achieve desirable performance for ST-DTC strategies in over modulation region is also an interesting topic.

(2). For the DTC without PWM modulators, the duty-ratio-based DTC is another kind of strategy which will employ active vectors and zero vectors together within one sampling period. The synthetic vectors presented in this thesis can be utilized as active vectors in the duty-ratio-based DTC strategies. The existing methods to obtain duty ratio for the three phase drives, and the simple duty-ratio method proposed in Chapter 4 can be potentially employed to get the duty ratio of active vectors. The stator current harmonic currents should be considered into the modification of the

aforementioned methods.

(3). The thesis mainly focuses on the modified ST-DTC strategies of dual three-phase PMSM drives. In some areas where there are machine/inverter asymmetries, current harmonics cannot be minimized by any ST-DTC strategies. Due to the structural limitation of ST-DTC, the harmonic current cannot be directly controlled by a closed-loop controller, only the average amplitude of voltage components in the additional  $z_1z_2$  subspace is controlled to zero in ST-DTC to ensure that the harmonic currents are minimized. The current harmonics can be successfully eliminated if both the machine and inverter are balanced. However, when there are machine/inverter asymmetries, the required voltage components in  $z_1z_2$  subspace are not zero, as discussed in relation to current control schemes. Therefore, in such kinds of applications, two current regulators for the harmonic currents are usually required. Then the output switching state cannot be easily obtained from a switching table. Instead, the suitable PWM techniques such as carrier-based PWM or SVPWM are usually required. Then, the hysteresis regulators should also be replaced by the reference voltage calculator in the  $\alpha\beta$  subspace. Therefore, the specific PWM scheme should be employed to implement the obtained reference voltages in  $\alpha\beta$  subspace and  $z_1z_2$  subspace. In this thesis, only deadbeat algorithm implemented in the synchronous reference frame aligned with the stator flux vector is discussed. The deadbeat algorithm can be implemented in the synchronous reference frame aligned with the rotor flux vector. The investigation of the other sorts of PWM-based DTC for dual three-phase machine drives can be implemented in the future. For instance, PI regulators and resonant regulators can be used together to generate the required phase voltage commands. Other machine-model-based methods, such as predictive-DTC (P-DTC) can be employed to obtain required voltage reference.

(4) For the machine-model-based methods, the machine parameter estimation methods can be applied to avoid the effect of machine parameter variation.

(5). The limitation of stator currents would affect the performance of DTC strategies. To address this issue, the appropriate methods to get the reference stator flux and the modification of torque reference are required. Different control methods of flux weakening, such as feedforward method which is based on the machine model and feedback method which utilized a PI regulator, can be applied for the dual three-phase PMSM drives. The efficiency of the machine can be compared and optimized by utilizing different strategies. The stator current harmonic should be considered

in the design of the appropriate strategies.

(6). As the inherent sensorless method, DTC based on sensorless methods for dual three-phase PMSM drives is also one very interesting topic.

## References

- [ABA08] G. Abad, M. A. Rodriguez, and J. Poza, "Two-level VSC based predictive direct torque control of the doubly fed induction machine with reduced torque and flux ripples at low constant switching frequency," *IEEE Trans. Power Electron.*, vol. 23, no. 3, pp. 1050-1061, May 2008.
- [ABB84] M. A. Abbas, R. Christen, and T. M. Jahns, "Six-phase voltage source inverter driven induction motor," *IEEE Trans. Ind. Appl.*, vol. IA-20, no. 5, pp. 1251-1259, Sep. 1984.
- [AMB04] V. Ambrozic, G. S. Buja, and R. Menis, "Band-constrained technique for direct torque control of induction motor," *IEEE Trans. Ind. Electron.*, vol. 51, no. 4, pp. 776-784, Aug. 2004.
- [BEE10] J. Beerten, J. Verwekken, and J. Driesen, "Predictive direct torque control for flux and torque ripple reduction," *IEEE Trans. Ind. Electron.*, vol. 57, no. 1, pp. 404-412, Jan. 2010.
- [BOJ03] R. Bojoi, M. Lazzari, F. Profumo, and A. Tenconi, "Digital field-oriented control for dual three-phase induction motor drives," *IEEE Trans. Ind. Appl.*, vol. 39, no. 3, pp. 752-760, May/June 2003.
- [BOJ03C] R. Bojoi, F. Profumo, A. Tenconi, Ieee, and Ieee, "Digital synchronous frame current regulation for dual three-phase induction motor drives," in *PESC'03: 2003 IEEE 34th Annual Power Electronics Specialists Conference, Conference Proceedings*, New York: IEEE, 2003, pp. 1475-1480.
- [BOJ05] R. Bojoi, F. Farina, G. Griva, F. Profumo, and A. Tenconi, "Direct torque control for dual three-phase induction motor drives," *IEEE Trans. Ind. Appl.*, vol. 41, no. 6, pp. 1627-1636, Nov./Dec. 2005.
- [BOJ06] R. Bojoi, E. Levi, F. Farina, A. Tenconi, and F. Profumo, "Dual three-phase induction motor drive with digital current control in the stationary reference frame," *IEE Proc.-Electr. Power Appl.*, vol. 153, no. 1, pp. 129-139, Jan. 2006.

- [CAP13] R. Morales-Caporal, E. Bonilla-Huerta, M. A. Arjona, and C. Hernandez, "Sensorless predictive DTC of a surface-mounted permanent-magnet synchronous machine based on its magnetic anisotropy," *IEEE Trans. Ind. Electron.*, vol. 60, no. 8, pp. 3016-3024, Aug. 2013.
- [CAS00] D. Casadei, G. Serra, and K. Tani, "Implementation of a direct control algorithm for induction motors based on discrete space vector modulation," *IEEE Trans. Power Electron.*, vol. 15, no. 4, pp. 769-777, Jul. 2000.
- [CAS02] D. Casadei, F. Profumo, G. Serra, and A. Tani, "FOC and DTC: Two viable schemes for induction motors torque control," *IEEE Trans. Power Electron.*, vol. 17, no. 5, pp. 779-787, Sep 2002.
- [CHE14] H. S. Che, E. Levi, M. Jones, W. P. Hew, and N. Abd Rahim, "Current control methods for an asymmetrical six-phase induction motor drive," *IEEE Trans. Power Electron.*, vol. 29, no. 1, pp. 407-417, Jan 2014.
- [CHO07] C. H. Choi and J. K. Seok, "Compensation of zero-current clamping effects in high-frequency-signal-injection-based sensorless PM motor drives," *IEEE Trans. Ind. Appl.*, vol. 43, no. 5, pp. 1258-1265, Sept./Oct. 2007.
- [DEP88] M. Depenbrock, "Direct self-control (DSC) of inverter-fed induction machine," *IEEE Trans. Power Electron.*, vol. 3, no. 4, pp. 420-429, Oct. 1988.
- [DSP10] Dspace, "Hardware installation and configuration reference," Release 6.6, May 2010.
- [DUR11] M. J. Duran, J. Prieto, F. Barrero, S. Toral, "Predictive current control of dual three-phase drives using restrained search techniques," *IEEE Trans. Ind. Electron.*, vol. 58, no. 8, pp. 3253-3263, Aug. 2011.
- [FAR06] F. Farina, R. Bojoi, A. Tenconi, and F. Profumo: 'Direct torque control with full order stator flux observer for dual three-phase induction motor drives', *IEEE Trans. Ind. Appl.*, vol. 126, no 4, pp. 412-419, 2006.

- [GAO11] L. L. Gao, J. E. Fletcher, L. B. Zheng, "Low-speed control improvements for a two-level five-phase inverter-fed induction machine using classic direct torque control," *IEEE Trans. Ind. Electron.*, vol. 58, no. 7, pp. 2744-2754, Jul. 2011.
- [GEY09] T. Geyer, G. Papafotiou, and M. Morari, "Model predictive direct torque control-part I: concept, algorithm, and analysis," *IEEE Trans. Ind. Electron.*, vol. 56, no. 6, pp. 1894-1905, Jun. 2009.
- [GON11] L. M. Gong and Z. Q. Zhu, "A novel method for compensating inverter nonlinearity effects in carrier signal injection-based sensorless control from positive-sequence carrier current distortion," *IEEE Trans. Ind. Appl.*, vol. 47, no. 3, pp. 1283-1292, May/Jun. 2011.
- [GOP84] K. Gopakumar, S. Sathiakumar, S. K. Biswas, and J. Vithayathil, "Modified current source inverter fed induction-motor drive with reduced torque pulsations," *IEE Proceedings-B Electric Power Appl.*, vol. 131, pp. 159-164, Jul. 1984.
- [GOP93] K. Gopakumar, V. T. Ranganathan, and S. R. Bhat, "Split-phase induction motor operation from PWM voltage source inverter," *IEEE Trans. Ind. Appl.*, vol. 29, pp. 927-932, Sep./Oct. 1993.
- [HAB92] T. G. Habetler, F. Profumo, M. Pastorelli, and L. M. Tolbert, "Direct torque control of induction machines using space vector modulation," *IEEE Trans. Ind. Appl.*, vol. 28, no. 5, pp. 1045-1051, Sep-Oct 1992.
- [HAD06] D. Hadiouche, L. Baghli, and A. Rezzoug, "Space-vector PWM techniques for dual three-phase AC machine: analysis, performance evaluation, and DSP implementation," *IEEE Trans. Ind. Appl.*, vol. 42, no. 4, pp. 1112-1122, Jul./Aug. 2006.
- [HAO12] Z. Hao, X. Xi, and L. Yongdong, "Torque ripple reduction of the torque predictive control scheme for permanent-magnet synchronous motors," *IEEE Trans. Ind. Electron.*, vol. 59, no. 2, pp. 871-877, Feb. 2012.
- [HOA12C] K. D. Hoang, Z. Q. Zhu, and M. Foster, "Optimum look-up table for reduction of current harmonics in direct torque controlled dual three-phase permanent magnet brushless

- AC machine drives," in *Power Electronics, Machines and Drives (PEMD 2012), 6th IET International Conference on*, 2012, pp. 1-6.
- [HOA15] K. D. Hoang, Y. Ren, Z. Zhu, and M. Foster, "Modified switching-table strategy for reduction of current harmonics in direct torque controlled dual three-phase permanent magnet synchronous machine drives," *IET Electr. Power Appl.*, vol. 9, no. 1, pp. 10-19, Jan. 2015.
- [HAT05] K. Hatua and V. T. Ranganathan, "Direct torque control schemes for split-phase induction machine," *IEEE Trans. Ind. Appl.*, vol. 41, no. 5, pp. 1243-1254, Sep./Oct. 2005.
- [HIN03] M. Hinkkanen and J. Luomi, "Modified integrator for voltage model flux estimation of induction motors," *IEEE Trans. Ind. Electron.*, vol. 50, no. 4, pp. 818-820, Aug. 2003.
- [HOU03C] L. Hou, Y. Su, and L. Chen, "DSP-based indirect rotor field oriented control for multiphase induction machines," in *Electric Machines and Drives Conference, 2003. IEMDC'03. IEEE International*, pp. 976-980, 2003.
- [HU11] J. Hu and Z. Q. Zhu, "Investigation on switching patterns of direct power control strategies for grid-connected DC-AC converters based on power variation rates," *IEEE Trans. Power Electron.*, vol. 26, no. 12, pp. 3582-3598, Dec. 2011.
- [HU14] Y. Hu, Z. Q. Zhu, and K. Liu, "Current Control for Dual Three-Phase Permanent Magnet Synchronous Motors Accounting for Current Unbalance and Harmonics," *Emerging and Selected Topics in Power Electronics, IEEE Journal of*, vol. 2, no. 2, pp. 272-284, Jun. 2014.
- [ISH05] D. Ishak, Z. Q. Zhu, and D. Howe, "Permanent-magnet brushless machines with unequal tooth widths and similar slot and pole numbers," *IEEE Trans. Ind. Appl.*, vol. 41, no. 2, pp. 584-590, Mar./Apr. 2005.
- [JON09] M. Jones, S. N. Vukosavic, D. Dujic, and E. Levi, "A synchronous current control scheme for multiphase induction motor drives," *IEEE Trans. Energy Convers.*, vol. 24, no. 4, pp. 860-868, Dec 2009.

- [JUN04] J. Jung, G. Jeong, and B. Kwon, "Stability improvement of V/f-controlled induction motor drive systems by a dynamic current compensator," *IEEE Trans. Ind. Electron.*, vol. 51, no. 4, pp. 930-933, Aug. 2004.
- [KAN99] J.-K. Kang and S.-K. Sul, "New direct torque control of induction motor for minimum torque ripple and constant switching frequency," *IEEE Trans. Ind. Appl.*, vol. 35, no. 5, pp. 1076-1082, Sep./Oct. 1999.
- [KAN01] J. W. Kang and S. K. Sul, "Analysis and prediction of inverter switching frequency in direct torque control of induction machine based on hysteresis bands and machine parameters," *IEEE Trans. Ind. Electron.*, vol. 48, no. 3, pp. 545-553, Jun. 2001.
- [KAR14] J. Karttunen, S. Kallio, P. Peltoniemi, P. Silventoinen, and O. Pyrhonen, "Decoupled vector control scheme for dual three-phase permanent magnet synchronous machines," *IEEE Trans. Ind. Electron.*, vol. 61, no. 5, pp. 2185-2196, May 2014.
- [KEL03] J. W. Kelly, E. G. Strangas, and J. M. Miller, "Multiphase space vector pulse width modulation," *IEEE Trans. Energy Convers.*, vol. 18, no. 2, pp. 259-264, Jun. 2003.
- [KEN03] B. H. Kenny and R. D. Lorenz, "Stator- and rotor-flux-based deadbeat direct torque control of induction machines," *IEEE Trans. Ind. Appl.*, vol. 39, no. 4, pp. 1093-1101, Jul-Aug 2003.
- [KLI83] E. A. Klingshirn, "High phase order induction motors - part I-description and theoretical considerations," *IEEE Trans. Power Apparatus and Systems* vol. PAS-102, no. 1, pp. 47-53, Jan. 1983.
- [LAI01] Y.-S. Lai and J.-H. Chen, "A new approach to direct torque control of induction motor drives for constant inverter switching frequency and torque ripple reduction," *IEEE Trans. Energy Convers.*, vol. 16, no. 3, pp. 220-227, Sep. 2001.
- [LAS04a] C. Lascu and A. M. Trzynadlowski, "Combining the principles of sliding mode, direct torque control, and space-vector modulation in a high-performance sensorless AC drive," *IEEE Trans. Ind. Appl.*, vol. 40, no. 1, pp. 170-177, Jan./Feb. 2004.

- [LAS04b] C. Lascu, I. Boldea, and F. Blaabjerg, "Variable-structure direct torque control - a class of fast and robust controllers for induction machine drives," *IEEE Trans. Ind. Electron.*, vol. 51, no. 4, pp. 785-792, Aug. 2004.
- [LEE11] J. S. Lee, C. H. Choi, J. K. Seok, and R. D. Lorenz, "Deadbeat-direct torque and flux control of interior permanent magnet synchronous machines with discrete time stator current and stator flux linkage observer," *IEEE Trans. Ind. Appl.*, vol. 47, pp. 1749-1758, Jul-Aug. 2011.
- [LEV07] E. Levi, R. Bojoi, F. Profumo, H. A. Toliyat, and S. Williamson, "Multiphase induction motor drives - a technology status review," *IET Electr. Power Appl.*, vol. 1, no. 4, pp. 489-516, Jul 2007.
- [LEV08a] E. Levi, "Multiphase electric machines for variable-speed applications," *IEEE Trans. Ind. Electron.*, vol. 55, no. 5, pp. 1893-1909, May 2008.
- [LEV08b] E. Levi, D. Dujic, M. Jones, and G. Grandi, "Analytical determination of DC-bus utilization limits in multiphase VSI supplied AC drives," *IEEE Trans. Energy Convers.*, vol. 23, no. 2, pp. 433-443, Jun. 2008.
- [LEV15] E. Levi, "Advances in converter control and innovative exploitation of additional degrees of freedom for multiphase machines," *IEEE Trans. Ind. Electron.*, vol. PP, no. 99, pp. 1-1, 2015.
- [MAR08] K. Marouani, L. Baghli, D. Hadiouche, A. Kheloui, and A. Rezzoug, "A new PWM strategy based on a 24-sector vector space decomposition for a six-phase VSI-fed dual stator induction motor," *IEEE Trans. Ind. Electron.*, vol. 55, no. 5, pp. 1910-1920, May 2008.
- [MAT13] S. Mathapati and J. Boecker, "Analytical and offline approach to select optimal hysteresis bands of DTC for PMSM," *IEEE Trans. Ind. Electron.*, vol. 60, no. 3, pp. 885-895, Mar. 2013.

- [MIR09] H. Miranda, P. Cortes, J. I. Yuz, and J. Rodriguez, "Predictive torque control of induction machines based on state-space models," *IEEE Trans. Ind. Electron.*, vol. 56, no. 6, pp. 1916-1924, Jun. 2009.
- [PAC05] M. Pacas and J. Weber, "Predictive direct torque control for the PM synchronous machine," *IEEE Trans. Ind. Electron.*, vol. 52, no. 5, pp. 1350-1356, Oct. 2005.
- [PAR07] L. Parsa and H. A. Toliyat, "Sensorless direct torque control of five-phase interior permanent-magnet motor drives," *IEEE Trans. Ind. Appl.*, vol. 43, no. 4, pp. 952-959, Jul./Aug. 2007.
- [PAR12] Y. Park and S. K. Sul, "A novel method utilizing trapezoidal voltage to compensate for inverter nonlinearity," *IEEE Trans. Power Electron.*, vol. 27, no. 12, pp. 4837-4846, Dec 2012.
- [PER03] P. D. C. Perera, F. Blaabjerg, J. K. Pedersen, and P. Thogersen, "A sensorless, stable V/f control method for permanent-magnet synchronous motor drives," *IEEE Trans. Ind. Appl.*, vol. 39, no. 3, pp. 783-791, May/Jun. 2003.
- [PRE13] M. Preindl and S. Bolognani, "Model predictive direct torque control with finite control set for PMSM drive systems, part 1: maximum torque per ampere operation," *IEEE Trans. Ind. Inf.*, vol. 9, pp. 1912-1921, Nov 2013.
- [REN14] Y. Ren, Z. Q. Zhu, J. M. Liu, "Direct torque control of permanent-magnet synchronous machine drives with a simple duty ratio regulator," *IEEE Trans. Ind. Electron.*, vol. 61, no. 10, pp. 5249-5258, Oct. 2014.
- [REN15] Y. Ren and Z. Q. Zhu, "Enhancement of steady-state performance in direct torque controlled dual three-phase permanent magnet synchronous machine drives with modified switching table," *IEEE Trans. Ind. Electron.*, vol. 62, no. 6, pp. 3338-3350, Jun. 2015.
- [ROM03] L. Romeral, A. Arias, E. Aldabas, and M. G. Jayne, "Novel direct torque control (DTC) scheme with fuzzy adaptive torque-ripple reduction," *IEEE Trans. Ind. Electron.*, vol. 50, no. 3, pp. 487-492, Jun. 2003.

- [SEU91] J. Seung-Gi and M. H. Park, "The analysis and compensation of dead-time effects in PWM inverters," *IEEE Trans. Ind. Electron.*, vol. 38, no. 2, pp. 108-114, Apr. 1991.
- [SHY10] K.-K. Shyu, J.-K. Lin, V.-T. Pham, M.-J. Yang, and T.-W. Wang, "Global minimum torque ripple design for direct torque control of induction motor drives," *IEEE Trans. Ind. Electron.*, vol. 57, no. 9, pp. 3148-3156, Sep. 2010.
- [YOO09] A. Yoo and S.-K. Sul, "Design of Flux Observer Robust to Interior Permanent-Magnet Synchronous Motor Flux Variation," *IEEE Trans. Ind. Appl.*, vol. 45, no. 5, pp. 1670-1677, Sep.-Oct. 2009.
- [TAH12] A. Taheri, A. Rahmati, and S. Kaboli, "Efficiency improvement in DTC of six-phase induction machine by adaptive gradient descent of flux," *IEEE Trans. Power Electron.*, vol. 27, no. 3, pp. 1552-1562, Mar. 2012.
- [TAK86] I. Takahashi and T. Noguchi, "A new quick-response and high-efficiency control method of an induction-motor," *IEEE Trans. Ind. Appl.*, vol. 22, no. 5, pp. 820-827, Sep./Oct. 1986.
- [TAN04] L. Tang, L. Zhong, M. F. Rahman, and Y. Hu, "A novel direct torque controlled interior permanent magnet synchronous machine drive with low ripple in flux and torque and fixed switching frequency," *IEEE Trans. Power Electron.*, vol. 19, no. 2, pp. 346-354, Mar. 2004.
- [TAN16] Z. Tang, X. Li, S. Dusmez, and B. Akin, "A new V/f-based sensorless MTPA control for IPMSM drives," *IEEE Trans. Power Electron.*, vol. 31, no. 6, pp. 4400-4415, Jun. 2016.
- [WES09] N. T. West and R. D. Lorenz, "Digital implementation of stator and rotor flux-linkage observers and a stator-current observer for deadbeat direct torque control of induction machines," *IEEE Trans. Ind. Appl.*, vol. 45, no. 2, pp. 729-736, Mar./Apr. 2009.
- [XIA14] C. L. Xia, J. X. Zhao, Y. Yan, and T. N. Shi, "A novel direct torque control of matrix converter-fed PMSM drives using duty cycle control for torque ripple reduction," *IEEE Trans. Ind. Electron.*, vol. 61, no. 6, pp. 2700-2713, Jun 2014.

- [XU14] W. Xu and R. D. Lorenz, "Dynamic loss minimization using improved deadbeat-direct torque and flux control for interior permanent-magnet synchronous machines," *IEEE Trans. Ind. Appl.*, vol. 50, no. 2, pp. 1053-1065, Mar-Apr 2014.
- [ZHA95] Y. Zhao and T. A. Lipo, "Space vector PWM control of dual three-phase induction machine using vector space decomposition," *IEEE Trans. Ind. Appl.*, vol. 31, no. 5, pp. 1100-1109, Sep./Oct. 1995.
- [ZHA11a] Y. Zhang and J. Zhu, "Direct torque control of permanent magnet synchronous motor with reduced torque ripple and commutation frequency," *IEEE Trans. Power Electron.*, vol. 26, no. 1, pp. 235-248, Jan. 2011.
- [ZHA11b] Y. Zhang and J. Zhu, "A novel duty cycle control method to reduce both torque and flux ripples for DTC of permanent magnet synchronous motor drives with switching frequency reduction," *IEEE Trans. Power Electron.*, vol. 26, no. 10, pp. 3055-3067, Oct. 2011.
- [ZHA11c] Y. Zhang, J. Zhu, W. Xu, and Y. Guo, "A simple method to reduce torque ripple in direct torque-controlled permanent-magnet synchronous motor by using vectors with variable amplitude and angle," *IEEE Trans. Ind. Electron.*, vol. 58, no. 7, pp. 2848-2859, Jul. 2011.
- [ZHA12] Y. C. Zhang, J. G. Zhu, Z. M. Zhao, W. Xu, and D. G. Dorrell, "An improved direct torque control for three-level inverter-fed induction motor sensorless drive," *IEEE Trans. Power Electron.*, vol. 27, no. 3, pp. 1502-1513, Mar 2012.
- [ZHE11] L. B. Zheng, J. E. Fletcher, B. W. Williams, and X. N. He, "A novel direct torque control scheme for a sensorless five-phase induction motor drive," *IEEE Trans. Ind. Electron.*, vol. 58, no. 2, pp. 503-513, Feb. 2011.
- [ZHO15] C. Zhou, G. Yang, and J. Su, "PWM strategy with minimum harmonic distortion for dual three-phase permanent-magnet synchronous motor drives operating in the overmodulation region," *IEEE Trans. Power Electron.*, in press.

[ZHU14] Z. Q. Zhu, Y. Ren, and J. M. Liu, "Improved torque regulator to reduce steady-state error of torque response for direct torque control of permanent magnet synchronous machine drives," *IET, Electr. Power Appl.*, vol. 8, no. 3, pp. 108-116, 2014.

## APPENDICES

### Appendix A: Specification of Prototype Machines

#### Test Machine I: Three-phase PM Machine

Parameters	Values
Rated speed	400 rpm
Rated torque	5.5 Nm
Supply DC voltage	40 V
Slot number	12
Pole number	10
Stator outer radius	50 mm
Stator inner radius	28.5 mm
Rotor outer radius	27.5 mm
Yoke height	3.7 mm
Tooth body width	7.1 mm
Slot opening	2 mm
Stack length	50 mm
Airgap length	1 mm
Magnet thickness	3 mm
Magnet remanence	1.2 T
Number of series turns per phase	132
Permanent magnet flux	0.707 Wb
Stator resistance	0.32 $\Omega$
$\alpha$ -axis and $\beta$ -axis inductance	3.366 mH

Test Machine II: Dual three-phase PM Machine

Parameters	Values
Rated speed	400 rpm
Rated torque	5.5 Nm
Supply DC voltage	40 V
Slot number	12
Pole number	10
Stator outer radius	50 mm
Stator inner radius	28.5 mm
Rotor outer radius	27.5 mm
Yoke height	3.7 mm
Tooth body width	7.1 mm
Slot opening	2 mm
Stack length	50 mm
Airgap length	1 mm
Magnet thickness	3 mm
Magnet remanence	1.2 T
Number of series turns per phase	132
Permanent magnet flux	0.734 Wb
Stator resistance	1.096 $\Omega$
$\alpha$ -axis and $\beta$ -axis inductance	2.142 mH
$z_1$ -axis and $z_2$ -axis inductance	0.875 mH

## Appendix B: The stator flux and torque estimators

Two types of stator flux estimators are utilized in this thesis.

### B.1. Stator flux estimator based on voltage model [HIN03], [ZHA11a].

The surface-mounted PMSM can be modelled in a stationary reference frame as

$$\mathbf{V}_{s\alpha\beta} = R_s \mathbf{I}_{s\alpha\beta} + p\boldsymbol{\Psi}_{s\alpha\beta} \quad (\text{B.1})$$

Therefore, the stator flux can be obtained as

$$\boldsymbol{\Psi}_{s\alpha\beta} = \int (\mathbf{V}_{s\alpha\beta} - R_s \mathbf{I}_{s\alpha\beta}) dt \quad (\text{B.2})$$

In practical implementation, the pure integration is sensitive to DC drift. A low-pass filter (LPF) is usually used instead of pure integration. The effect of DC drift can be eliminated by the introduction of LPF, however, it brings errors in both magnitude and phase. To compensate the magnitude and phase errors, the following modified voltage model is used in Chapters 3 and 4.

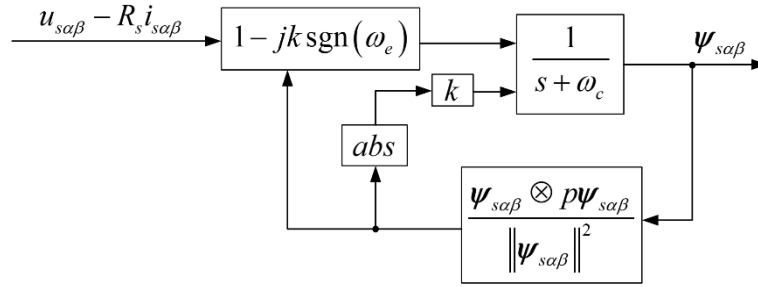


Fig. B.1. Modified voltage model [HIN03], [ZHA11a]

In Fig. B.1,  $k$  is the coefficient from 0.1 to 0.5 [HIN03],  $\omega_c$  is the cutoff frequency of LPF,  $\omega_e$  is the synchronous frequency of stator flux.

B.2. Stator flux estimator based on the combination of the voltage model and the current model [LEE11], [SUL09].

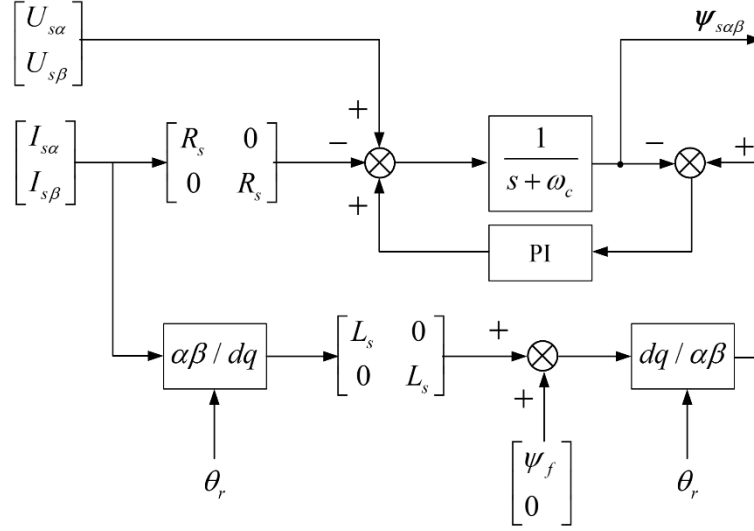


Fig. B.2. Stator flux estimator based on the combination of the voltage model and the current model [LEE11], [SUL09].

The current model is combined with the voltage model to increase the accuracy of the estimation of stator flux. The drawback is that the model require the machine parameters and rotor position. These parameters can be estimated for the sake of parameter independence, although the computational burden is enviably increased [LEE11], [SUL09].

Note that these two models can be applied for both three phase PMSM and dual three-phase PMSM since the machine model in a stationary reference frame are similar.

This stator flux estimator is employed in Chapters 5-7.

For the estimation of flux in  $z_1z_2$  subspace for the dual three-phase machine, the classical voltage model flux model in utilized.

### B.3. Stator flux estimator based on voltage model [HIN03], [ZHA11a].

The torque can be estimated based on the measured currents and estimated stator flux.

Three phase PMSM:

$$T_e = \frac{3}{2} P (\psi_{s\alpha} i_{s\beta} - \psi_{s\beta} i_{s\alpha}) \quad (\text{B.3})$$

Dual three-phase PMSM:

$$T_e = 3P(\psi_{s\alpha}i_{s\beta} - \psi_{s\beta}i_{s\alpha}) \quad (\text{B.4})$$

## Appendix C: The method to identify parameters of the machines

### 1. Measurement of stator resistance:

All the stator resistances are measured by the multimeter.

### 2. Measurement of stator inductance:

Take dual three-phase PMSM as an example:

Disconnect the neutral point, connect phase A with AC voltage ( $U_A$  is the amplitude of terminal voltage, and the frequency  $\omega=400\text{Hz}$ ), then measure current of phase A with amplitude of  $I_A$  and induced voltage on other phases with amplitude  $U_{AB}$ ,  $U_{AC}$ ,  $U_{AX}$ ,  $U_{AY}$ ,  $U_{AZ}$ . The stator resistance can be ignored, therefore, the self-inductance and mutual-inductance can be obtained.

$$L_A = U_A / (\omega I_A) \quad (\text{C.1})$$

$$M_{AB} = U_{AB} / (\omega I_A) \quad (\text{C.2})$$

$$M_{AC} = U_{AC} / (\omega I_A) \quad (\text{C.3})$$

$$M_{AX} = U_{AX} / (\omega I_A) \quad (\text{C.4})$$

$$M_{AY} = U_{AY} / (\omega I_A) \quad (\text{C.5})$$

$$M_{AZ} = U_{AZ} / (\omega I_A) \quad (\text{C.6})$$

Then the inductance matrix can be obtained:

$$L_{ss} = \begin{bmatrix} L_A & M_{AB} & M_{AC} & M_{AX} & M_{AY} & M_{AZ} \\ M_{BA} & L_B & M_{BC} & M_{BX} & M_{BY} & M_{BZ} \\ M_{CA} & M_{CB} & L_C & M_{CX} & M_{CY} & M_{CZ} \\ M_{XA} & M_{XB} & M_{XC} & L_X & M_{XY} & M_{XZ} \\ M_{YA} & M_{YB} & M_{YC} & M_{YX} & L_Y & M_{YZ} \\ M_{ZA} & M_{ZB} & M_{ZC} & M_{ZX} & M_{ZY} & L_Z \end{bmatrix} \quad (\text{C.7})$$

By using VSD technique [ZHA95], the conventional six-dimensional system can be transformed to a new six-dimensional composed of three mutually orthogonal subspaces, by using a transformation matrix  $[T_6]$ , which is given in (1.9). Therefore, the inductance in the stationary reference frame can be obtained [ZHA95]:

$$[L_{s6}] = [T_6][L_{ss}][T_6]^{-1} \quad (C.8)$$

where

$$[L_{s6}] = [L_{s\alpha} \quad L_{s\beta} \quad L_{z1} \quad L_{z2} \quad L_{o1} \quad L_{o2}]^{-1} \quad (C.9)$$

where  $L_{s\alpha}$ ,  $L_{s\beta}$  are the  $\alpha$ -axis and  $\beta$ -axis inductance, respectively,  $L_{z1}$ ,  $L_{z2}$  are the  $z_1$ -axis and  $z_2$ -axis inductance, respectively,  $L_{o1}$ ,  $L_{o2}$  are the  $o_1$ -axis and  $o_2$ -axis inductance, respectively.